Evaluation and Application of Leaf Anatomical Links to Climate in *Metasequoia* (Cupressaceae)

by

Molly Ng

A dissertation submitted in partial fulfillment
of the requirements for the degree of
Doctor of Philosophy
(Earth and Environmental Sciences)
in the University of Michigan
2020

Doctoral Committee:

Assistant Professor Selena Y. Smith, Chair
Emeritus Professor Robyn Burnham
Associate Professor Naomi E. Levin
Professor Nathan Sheldon

Molly Ng
mollyng@umich.edu
ORCID ID: 0000-0002-3070-0513

This is dedicated to my sister Karen and my brother Stephen who have shaped who I am and continue to love and support me. Especially Karen who helped with my third grade science project on photosynthesis, bought me my first plant, took me to my first botanical garden, birthday flowers, homemade linzer cookies, and for doing my dishes when she visited.

ACKNOWLEDGMENTS

There are many people to thank for the work I have accomplished. First, I thank my advisor Selena Smith, for converting my science thoughts to cohesive written products, and committee members Robyn Burnham, Naomi Levin, and Nathan Sheldon. My professors at UCLA—Arthur Gibson, Charles Taylor, Jared Diamond, Paul Barber, & Lawren Sack—who have shaped how I think and see the world, especially Charles Taylor & Lawren Sack for their encouragement. I thank the former Specht Lab at UC Berekely for being inclusive, fostering, and introducing me to Selena. I thank students Jessie Agee, Kaylie Charland, & Daniel Wu for assistance with photography and data collection. For modern samples, I thank Joanne Baggs, Steve Baumann, Joe Bishop, Caren Briscoe, Ole Byrgesen, Jason Drake, Doris Fanelli, Sherry Gaston, Cody Haynes, Jesper Kårehed, Taylor La Val, Sean Lahmeyer, Darren Loomis, Chris Maldonado, Karen Mangan, David Michener, Valencia Morris, Kathy Musial, David Riskind, Steve Schulze, Alexandra Sotkovsky, Jennifer Stafford, PJ Walker, Tao Su, & Larry Westcott. For access and assistance to collections at the University of Alberta Paleobotany Collection, I thank Eva Koppelhus and Stefan Little. I also thank Judy Poore and Carol Whitinger for technical support with histology. My work was supported by the NSF Graduate Research Fellow Program, U of M Rackham Graduate School, Ronald and Eileen Weiser Center for Europe and Eurasia at U of M International Institute, a Winifred B. Chase award from Matthaei Botanical Gardens, and Department of Earth and Environmental Sciences Scott Turner Awards. The support I receive from family and friends has been extremely valuable. I thank the best friends I have—Karen Ng, Karin Jackson, Emily Forscher, Jenny Hyunh, and Kelsie Morioka—, friends and colleagues I made while a graduate student, especially PEPPR Lab members, Kathryn I. Rico, Katherine M. Loughney, Margaret Veitch, Jenny C. Bowen, Matthew Medina, Derek Smith, Phoebe Aron, Nikita La Cruz, Sarah Brehm, XiaoJing Du, Yi Wang, I would especially like to thank Amy Yu for laughing, eating, and being angry with me.

TABLE OF CONTENTS

LIST OF FIGURES

LIST OF TABLES

LIST OF APPENDICES

ABSTRACT

Plant response to climate is valuable in understanding many aspects of evolution and ecology, including climate and biogeochemical processes. The close relationship between plants and climate has been extensively studied in eudicot angiosperms (woody flowering plants), showing links between climate and leaf shape. However angiosperms only represent a small portion of plant life on land, ~125 of 425 Ma (millions of years). In contrast, non-angiosperm approaches tend to be qualitative or semi-quantitative, limiting implications that could potentially be derived. Exploring other methods, like plant anatomy, which has been shown to reflect their growing environment, has the potential to expand our knowledge of non-angiosperm response to climate.

In this dissertation, I focus on conifers within Cupressaceae because of their diverse morphology and habitats, and extensive fossil record. I investigate anatomical links to climate across gradients in the modern world and apply these data to answer questions about their evolution and ecology. I focus on *Metasequoia glyptostroboides* Hu and Cheng (Cupressaceae), the dawn redwood, a deciduous conifer that naturally inhabits a small valley in central China. *Metasequoia* has an extensive fossil record (~100 Ma) across the Northern Hemisphere from mid- to high-latitudes. First, I collected leaves from *Metasequoia glyptostroboides* and its close relatives, *Sequoia sempervirens* and *Taxodium distichum*, across their natural and cultivated ranges across North America, Asia, and Europe. Then, I made leaf cross-sections and measured the following traits: cross-sectional area, vascular bundle area, resin canal area, leaf width and thickness.

In Chapter 2, I focused on how modern leaf anatomy within *M. glyptostroboides* relates to climate across a gradient. I use canonical correlation analysis (CCA), a multivariate ordination method, to link anatomy and 19 Bioclim climate variables. I found leaf width

and cross-sectional area were associated with cold-season precipitation, vascular bundle area with warm-season precipitation, leaf thickness with mild cold-season temperatures and mean annual temperature, and resin canal area with daily temperature fluctuations and mild cold-season temperatures. To test how these relationships held across time, I applied it to the fossil record by measuring the same anatomical traits in *Metasequoia milleri*, an anatomically preserved fossil from the Princeton Chert Locality (Allenby Formation, BC, Canada) from the early Eocene ($\sim$55 Ma). These estimated climate variables were compared to previously reconstructed climates of nearby fossil localities. My estimates were within these previous independently derived estimates of climate, demonstrating that anatomy is linked to climate and that these relationships held over geologic time.

Whether the leaf anatomical links to climate I found in Chapter 2 are also true among other conifers was investigated in Chapter 3. I included taxa closely related to *Metasequoia*, *S. sempervirens* and *T. distichum*, and added physiological proxies related to photosynthesis (carbon/nitrogen content; δ^{13}C calculate photosynthetic discrimination (Δ_{leaf}), water use efficiency (WUE), and internal cellular:atmospheric pCO_2 (c_i/c_a)). These data were combined with 19 Bioclim variables and I found relationships were different across and within species. Most significantly, I found *Metasequoia* and *Sequoia* independently showed a strong association between cross-sectional area and precipitation of the driest quarter, suggesting a shared or conserved climatic response. Further, I was able to show that while anatomy between taxa are distinct, their physiologies converge, implying different strategies to achieve a similar physiology.

Chapter 4 uses the modern trait-climate relationships I established in Chapter 3 to test whether past traits could be reconstructed using climate. I combine modern anatomy-climate relationships of *M. glyptostroboides*, published fossil localities of *M. occidentalis* and *M. sp.*, and early Eocene ($\sim$50 Ma) climate simulations at 3x and 6x pre-industrial CO_2 to create, test, and apply generalized linear models with fossil leaf measurements. Generally, cross-sectional area, leaf width, and leaf thickness decrease with

increased CO_2, while resin canal area increase. These responses to warming climate most likely reflect cooling strategies to offload heat. Leaf width measured from fossils match 3x reconstructed traits, showing promising potential for applications to test evolutionary hypotheses.

By studying conifer adaptations, or traits, we can deepen our understanding of conifer evolution. This thesis demonstrated how conifer leaves were linked to climate and how I applied these relationships to uncover evolutionary implications within conifers. Conifer leaves are reflective of their growing environment and expanding research into conifer response to climate has valuable significance for understanding evolutionary history within conifers.

CHAPTER 1

Introduction

Studying how plants respond to climate and how climate has shaped plant evolutionary history will deepen our knowledge about different aspects on the evolution of plant response, historical biogeography, and traits. Plants have adaptations that are linked to their growing conditions, which results in a close relationship between plants and climate. Thus, exposure to abiotic stressors require plants to respond through adaptations in order to mitigate stress and survive (Sultan, 1987; Ackerly et al., 2000; Ackerly, 2003). Many of these adaptations are preserved in the plant fossil record, providing an opportunity to understand past conditions of plants. By investigating plant response to environmental changes then applying these relationships to the fossil record, we can test hypotheses of plant evolution and ecology.

The relationship between plants and climate has been studied extensively (Bailey and Sinnott, 1915; Wolfe, 1994; Mosbrugger and Utescher, 1997; Wilf et al., 1998; Huff et al., 2003; Royer et al., 2005; Greenwood et al., 2005; Mosbrugger, 2009; Peppe et al., 2011; Harris et al., 2017). These links are predominately based on non-monocot angiosperms (flowering plants), providing both qualitative and quantitative estimates of climate variables that have been used to reconstruct past climates (further discussed in section 1.1). Methods limited to eudicots only cover a small portion of plant evolutionary history on land (the most recent $\sim$125 Myr of a $\sim$450 Myr history; Crane and Lidgard, 1989; Smith et al., 2010b; Magallón et al., 2013) and focus on leaf shape and size, which assumes anatomical

and physiological uniformitarianism across evolutionary history.

Non-angiosperm seed plants, such as conifers (*e.g.*, pines, firs, cedars, redwoods), have a much longer history than and dominated terrestrial landscapes prior to angiosperms (Miller, 1977; Taylor et al., 2009). The origin of conifers has been traced back to the late Paleozoic (∼300 Ma; Clayton, 1996; Taylor et al., 2009; Leslie et al., 2012), where non-plant based climatic proxies are sometimes compromised due to the diagenesis of carbonates and paleosols. Expanding research on plant-climate links to include conifers may provide insights into the evolution of plant lineages and plant response to climate, such as studying how modern climate has been shaped by the global floral transition from conifers to angiosperms in the Late Cretaceous. This is especially relevant to understanding how modern ecosystems have formed by angiosperm ecological dominance and how larger processes, such as biogeochemical cycles, have evolved.

Across the globe, there are a total of six modern conifer families from three orders that can be traced back to the Mesozoic: Araucariales, with Araucariaceae (strictly Southern Hemisphere) and Podocarpaceae (predominately Southern Hemisphere), Cupressales, with Cupressaceae (predominately Northern Hemisphere), Sciadopityaceae (strictly Northern Hemisphere), and Taxaceae (Northern and Southern Hemisphere), and Pinales, with only Pinaceae (Northern Hemisphere; Miller, 1977; Taylor et al., 2009; Leslie et al., 2012, 2018). Relationships are still unresolved but recent research suggests Araucariales and Cupressales share a common ancestor. Pinales are found paraphyletic to sister taxa Araucariales and Cupressales. Within Cupressales, Cupressaceae and Taxaceae are more closely related to each other than with Sciadopityaceae (Leslie et al., 2012, 2018). Conifers are also diverse in their habitat, ranging from temperate forests to floodplains (Farjon, 2005). The widespread diversity of conifers provide an additional source of data to understanding the relationships between leaf traits and environment. By studying the leaf response of conifers to climate, we can apply this relationship to test evolutionary and ecological hypotheses. Conifers are generally overlooked and considered insensitive to climate because they do not exhibit

similar changes in leaf physiognomy as angiosperms. The application of eudicot leaf metrics such as shape and size to conifer needles is an unfair assessment of plant response to climate in this group. Thus, when investigating non-angiosperm links to climate, different metrics must be used.

Cupressaceae in particular are an interesting and compelling conifer family to study, with many well-known and iconic trees such as junipers, *Juniperus* spp., and the coastal redwood, *Sequoia sempervirens*. This widespread conifer family inhabits a broad range of environments, from dense swamps to arid deserts (Farjon, 2005). Their physiological shift in drought tolerance is hypothesized to have helped them inhabit new environments as Cenozoic climate cooled and became arid (Pittermann et al., 2012). Moreover, the leaf morphologies of Cupressaceae are highly diverse, showing variations of flattened needle and scale-like leaves (Farjon, 2005). Studies investigating conifer leaf response within an individual to their environment have shown connections between leaf anatomy, physiology, and growing conditions (Niinemets and Kull, 1995; Niinemets et al., 1998, 2007; Oldham et al., 2010). By investigating how leaf anatomy and physiology responds to climate across both a gradient and species, we can further understand how conifers respond to their environments and more broadly, climate. These links can be used to study plant evolution, and ultimately, understand the implications and mechanisms behind the terrestrial landscape transition from a conifer to angiosperm dominated world.

This thesis sets out to establish leaf anatomical and physiological response to climate variables within Cupressaceae across broad climatic gradients, focusing on *Metasequoia glyptostroboides* Hu and Cheng (dawn redwood). Specifically, I aim to answer 1) if conifers alter their leaf anatomy and physiology to adapt to their growing conditions, how do these traits change over broad climatic gradients? And 2) do closely related conifers alter their leaf anatomy and physiology similarly? *Metasequoia glyptostroboides* is a modern deciduous conifer occurring naturally in a small valley within Hubei Province in central China (Farjon, 2005). Its fossil record extends back to ca. 100 Ma across the Northern

Hemisphere from mid- to high latitudes (LePage et al., 2005), providing opportunities to test hypotheses of plant-climate links in conifers over geologic time and further deepening our knowledge of how this once widespread conifer underwent extreme range contraction. By studying and applying links between leaves and climate, I answer questions about the evolutionary stasis of leaf anatomy and climatic niche, and address the effects of climate on leaf traits. In this chapter, I will explain in more detail the current state of research into plant links to climate, why leaves are valuable in studying plant-climate links especially leaf anatomy in conifers, and why I chose to focus on *M. glyptostroboides*.

1.1 Plant links to climate

Understanding how plants are linked to climate offers insights into how plants respond to environmental change, which is crucial for their survival. Different plant-based methods to infer past climate fall into two main categories: taxonomy-dependent and leaf physiognomy. Taxonomy-dependent approach can be used for all taxa, so long as modern climatic tolerances are known. In contrast, leaf physiognomy is strictly limited to woody eudicots (wood producing angiosperms). I introduce leaf anatomy in section 1.1.3 as a prospective method to investigate correlations to climatic variables in conifers. Leaf anatomy has been shown to link anatomical traits to environment, and has potential for broader applications.

1.1.1 Taxonomy-dependent approaches to reconstructing paleoclimate

Taxonomic-dependent approaches, as the name implies, require and depend on correct taxonomic identification of fossils. The Nearest Living Relative method (NLR; Mosbrugger, 2009) relies on correct taxonomic identification and assumes climatic tolerances have remained the same through time, often at a high taxonomic rank. Presence

or absence of specific taxa within fossil assemblages would suggest the general climate at the time of growth and the minimum and maximum tolerances of the taxa present. A number of environmental parameters can be estimated from the NLR approach, such as cold month mean temperature (CMMT), mean annual precipitation (MAP), etc. For example, because modern cycads are frost intolerant, a fossil cycad at a locality would indicate a warm climate and CMMT > 5°C (Greenwood and Wing, 1995; Greenwood et al., 2005).

The Coexistence Approach (CoA) and Bioclimatic Analysis (BA) builds upon NLR by collectively analyzing the climatic tolerances of the entire fossil assemblage. These semi-quantitative approaches reconstruct paleoclimate by finding a climatic interval of tolerance where all plants preserved in an assemblage could survive (Mosbrugger and Utescher, 1997). CoA is applied to Paleogene and Neogene plants, limiting the analytical scope to the Cenozoic, and, like NLR, relies on correct taxonomic identification. A few examples of climatic variables that can be reconstructed includes: seasonal temperature and precipitation estimate, relative humidity and potential evaporation. This approach can be problematic if outliers exist in the data, which is a problem addressed by BA (Greenwood et al., 2003, 2005; Reichgelt et al., 2013). BA is similar to CoA in that it uses climatic envelopes of micro- and macrofloras, but only retains the 10^{th} and 90^{th} percentile of the modern climatic range.

Both CoA and BA assumes conservation of climatic envelopes between related species through time, like NLR. This climatic conservation assumption remain untested until recently. Harris et al. (2017) assessed how well climatic tolerances of select taxonomic ranks (species, genus, family) were able to accurately reflect climate variables (mean annual temperature (MAT), MAP, and CMMT). They found that genera and families performed well when measured for accuracy and precision of temperature variables. Precipitation estimates remain difficult to link with taxonomy, often over- and under-predicting such that estimates occasionally have negative annual precipitation (Harris et al., 2017). Overall, these semi-quantitative approaches are reliant on correct

taxonomic assignment of fossils (which may undergo revisions), and sometimes require a certain number of species to constrain and increase confidence of estimates. So long as climate tolerances of modern relatives are obtained, these methods can be applied to all species.

1.1.2 Leaf physiognomy approaches to reconstructing paleoclimate

Unlike taxonomic-dependent approaches, leaf physiognomy relies on qualitative and quantitative characters of woody non-monocot angiosperm leaves, independent of taxonomic identification. These characters and measurements have been linked to climate using either univariate or multivariate approaches.

Bailey and Sinnott (1915) were the first to discover a relationship between leaf structure and climate by showing MAT correlated with the proportion of non-monocot angiosperms with toothed to non-toothed (entire) leaf margins in an assemblage or ecosystem, termed Leaf Margin Analysis (LMA). This univariate relationship showed that as MAT decreased, we would observe more toothed leaved species within a system. When sampling bias is minimized, LMA has been demonstrated to predict MAT well (Wolfe, 1985; Wilf, 1997). However, not all toothed margins are the same nor do they respond similarly. Royer et al. (2001) examined the toothed margins across the distribution of both *Acer rubrum* L. (red maple; Sapindaceae) and *Quercus kelloggii* Newb. (California black oak; Fagaceae) and found that response to MAT varied between species; *Q. kelloggii* showed little response to MAT but responded to changes in elevation. This is further complicated by significant ($p<0.001$) phylogenetic signal found between MAT and leaf margin type which demonstrates an inherent evolutionary pattern linked to historical biogeography (Little et al., 2010). Overall, how leaf traits or morphology reflect climate, and are linked to plant evolutionary history highlight the importance of understanding intraspecific patterns of leaf traits and the historical biogeography of lineages, further demonstrating the complexity of plant-climate relationships.

Another univariate method, Leaf Area Analysis (LAA; Wilf et al., 1998), was developed using the link between moisture availability and leaf area to develop and demonstrated a strong, predictive relationship between MAP and leaf area within an assemblage (r^2 = 0.76). Leaves in areas with high MAP had larger leaves than areas with lower MAP. This method was developed in response to taxonomy-dependent approaches and CLAMP (discussed next), which often under- or over- predicted MAP (Wilf et al., 1998).

Climate Leaf Analysis Multivariate Program (CLAMP; Wolfe, 1994), a multivariate analysis, captures the complexity of relating leaf to climate variables within woody non-monocot angiosperms. CLAMP scores 29 leaf traits based on physiognomy in order to estimate 11 climate variables such as MAT and CMMT. This approach requires a minimum of 20 woody dicot species. Initially CLAMP was calibrated using both warm and cool temperate floras in North America. Over the years, CLAMP has improved its calibrations for different forests such as those in east Asia and Europe (Spicer et al., 2004, 2009, 2011; Jacques et al., 2011; Kennedy et al., 2014). These calibrations stress that response to climate variables can differ between seemingly similar biomes. Collecting leaf characters for CLAMP can be time consuming. Automating leaf measurements has long been an area of study in part to increase accuracy and decrease errors made by fatigue or inconsistent scoring (MacLeod, 2002; Macleod, 2005; Cope et al., 2012; Corney et al., 2012; MacLeod and Steart, 2015). Recent methods by MacLeod and Steart (2015) show high rates of accuracy, between 87 and 100%.

Another multivariate approach, Digital Leaf Physiognomy (DiLP; Huff et al., 2003; Royer et al., 2005; Peppe et al., 2011), aimed to reduce the uncertainty of scored traits in CLAMP by employing a digital standard and added physiologically informative traits (total 21 traits, 8 climate variables), such as shape factor, ratio of feret diameter, and teeth count and area. Generally, DiLP has demonstrated leaves in colder climates were highly dissected and had larger teeth compared to leaves in warmer climates that were less dissected and rounder in shape (Huff et al., 2003). In toothed leaves, tooth area

correlates negatively with leaf mass per area and positively with nitrogen content (Royer et al., 2005). These different approaches of linking plant traits to climate demonstrate how researchers are continuously testing and improving methods over time. Leaf physiognomic approaches have been incredibly valuable in reconstructing past climates and environments. Because it is limited to non-monocot angiosperm leaves, these methods are restricted to their evolution.

1.1.3 The potential of leaf anatomy to help reconstruct past climates

Leaf anatomy will expand the way in which we understand plant-climate response beyond the evolution of angiosperms and especially in conifers. The focus of quantitative methods so far are based on angiosperms. By shifting our focus from angiosperms to conifers and away from leaf physiognomy, we can improve how plants are used to reconstruct climates and deepen our understanding of plant-climate response to shifts in global climate through time. Current methods to reconstruct climate in conifers rely on climatic tolerances of modern taxa especially since leaf physiognomic approaches are only calibrated for woody eudicots. Conifers have needle-like or scale-like leaves that are structurally and physiologically constrained, as they have not developed an efficient hydraulic system like angiosperms (De Boer et al., 2012). Although at a hydraulic disadvantage, modern conifers are able to tolerate and inhabit extreme environments, such as arid deserts, boreal and subalpine conditions, deep shade, and floodplains subject to saline influxes (Farjon, 2005; Pittermann et al., 2012). Adaptations to such habitats should encourage research on conifer links to climate in order to better understand their implications for conifer evolution and function.

Connecting conifer leaf anatomy to climate is one way to circumvent the structural and physiological constraints of needle-like and scale-like leaves. Anatomical features, such as stomata/cuticle morphology and the size or density of stomata, have proved valuable in understanding taxonomy and reflective of physiological links to climate (Alvin and Boulter,

1974; Woodward and Woodward, 1987). Photosynthesis in plants is directly linked to their physiology. When plants open their stomata to take in CO_2, water that is needed for photosynthesis is lost in the process. One way plants minimize water loss is by altering their stomatal size and numbers (Woodward and Woodward, 1987; Bettarini et al., 1998). Because stomata control gas exchange, the link between stomata and gases is expected to be strong. This was demonstrated by McElwain and Chaloner (1995) who showed an inverse relationship between leaf stomatal density and atmospheric [CO_2]. Leaves with fewer stomata are operating in higher levels of CO_2 while leaves with more stomata, in lower levels of CO_2 (McElwain and Chaloner, 1995). Royer et al. (2001) further refined this relationship by developing the stomatal index, which accounts for environmental effects that alter epidermal cells, such as water stress resulting in smaller epidermal cells compared to non-water-stressed plants. These methods are limited in their reconstructive abilities as stomata become insensitive above $\sim$450 ppm CO_2 levels, and $\sim$12% of species tested reflects a relationship between stomata and CO_2 (Royer, 2001; Barclay and Wing, 2016). Two lineages most often used to reconstruct past CO_2 levels are *Ginkgo* (Ginkgoaceae) and *Metasequoia* (Cupressaceae), both non-angiosperms, that exhibit sensitivity to different levels of CO_2 and have an extensive fossil record (Beerling et al., 1998; Royer et al., 2001; Beerling and Royer, 2002; Smith et al., 2010a; Maxbauer et al., 2014; Wang et al., 2015; Barclay and Wing, 2016).

Several studies have shown intraspecific variation of leaf anatomy within conifers is linked to their growing environment and biophysics (Niinemets and Kull, 1995; Apple et al., 2002; Oldham et al., 2010; Gebauer et al., 2011). Within a leaf, cellular anatomical characters are linked to photosynthesis. Thicker leaves, for example, are an indicator of the amount of tissue available for photosynthesis, and thus positively correlated to productivity (Sharkey, 2012). Cell layers are differentiated depending on environment, *e.g.* in sun and shade leaves: elongated columnar palisade cells and higher levels of chloroplasts are found in sun leaves, in contrast to short square palisade cells of shade leaves, to tolerate high

irradiation (Vogelmann, 1993; Terashima and Hikosaka, 1995; Sharkey, 2012; Gotoh et al., 2018).

1.2 Leaves as a tool to study conifer–climate links

Leaf anatomy generally reflects environmental conditions. Functional traits of Pinaceae, such as wood density, needle nutrient composition, and specific leaf area, have shown variability across populations, reflecting local adaptations and economic strategies (Laforest-Lapointe et al., 2014). Physiological response to climate can translate into anatomical response. Drought stress response in *Pinus sylvestris* L. (Scots pine; Pinaceae) resulted in restricted cambial wood growth (less xylem) and higher stomatal control in leaves to regulate water loss (Fernández-de Uña et al., 2017). Fernández-de Uña et al. (2017) showed that water stress is linked to xylem production and size, which affected photosynthesis through increased stomatal response to regulate carbon uptake and minimize water loss.

Leaf anatomy in conifers has been previously tied closely with physiology and climate. Variation within a tree has often been explained by light gradient (sun vs shade leaf), but has been shown to reflect physiology (Niinemets and Kull, 1995; Oldham et al., 2010). Within *Picea abies* (L.) H. Karst. (Norway spruce; Pinaceae), needle width decreased with increased light availability, and results showed that needle dimensions were not correlated with light nor height, but with changing leaf mass per area, a measure of relative growth rate and productivity (Niinemets and Kull, 1995). A study of *Sequoia sempervirens* (D. Don) Endl. (coastal redwood; Cupressaceae) showed that leaf dimorphism between the upper and lower canopy is the result of a hydraulic, not light gradient, evident in xylem and transfusion tissue sizes (Oldham et al., 2010). By further exploring leaf anatomy and applying these relationships over broad geographic ranges, we can investigate how leaf anatomical links broadly reflect climate.

1.3 *Metasequoia* (Cupressaceae) as a focal taxon

In this dissertation, *Metasequoia glyptostroboides*, the dawn redwood, was chosen as a focal taxon because of its widespread past distribution and extensive fossil record dating back ∼100 Ma. *Metasequoia* is a deciduous conifer that currently inhabits a seasonally warm and humid temperate climate inclined to riparian habitats subject to periodic flooding (Farjon, 2005; Tang et al., 2011). In its natural range, *Metasequoia* either dominates or inhabits a mixed forest. Within the mixed forest, *Metasequoia* forms the top canopy, *Cryptomeria* (Cupressaceae) in the mid canopy, and herbaceous plants in the understory. *Metasequoia* is suggested to have remained in evolutionary stasis based on static gross morphology (∼70 Ma to present; Liu et al., 1999). This hypothesis was further supported with genetic studies that showed lower genetic variability, and even lower when restored populations were compared to wild *Metasequoia* populations (Li et al., 2012). Overall, the static gross morphology of *Metasequoia* provides an interesting perspective to test hypotheses of evolutionary stasis and plant climatic response through time.

Metasequoia was thought to be extinct until 1941 when *M. glyptostroboides* was discovered living in a small valley of the Hubei Province in central China (Hendricks and Søndergaard, 1998; Farjon, 2005). Natural and wild stands are rare since anthropogenic inhabitance and activity have negatively affected its range over time (Farjon, 2005; LePage et al., 2005; Tang et al., 2011; Wang et al., 2019). In comparison, the fossil record of *Metasequoia* shows it once occupied an extensive geographic range across the Northern Hemisphere in the early Cenozoic, contracting and expanding with changes in climate through time (LePage et al., 2005).

Its discovery ignited an effort to study and grow *Metasequoia* outside of its natural habitat throughout North America and Europe. Although this effort was met with geopolitical conflicts with World War II and the Bamboo curtain, it resulted in two expeditions thirty-three years apart in 1946 and 1979 and *Metasequoia* seeds sent to 76 institutions to grow (Hendricks and Søndergaard, 1998). These efforts tested the

climatic tolerance of *Metasequoia* as well as its ecology and morphology. Access to living specimens clarified the fossil record of *Metasequoia*, which was often incorrectly assigned to *Taxodium* (L.) Rich. (cypress) or *Sequoia* (Cupressaceae; Chaney, 1950).

Research into the physiology and ecology of *Metasequoia* has remained popular and provided a foundation for studying links to climate. Cretaceous and Paleogene Arctic Circle occurrences of *Metasequoia* forests are especially curious for scientists (Irving et al., 1991; McKenna, 1980; Basinger et al., 1994; Greenwood and Basinger, 1994). Plants face challenges growing at high latitudes regardless of global climate, such as seasonally continuous light and dark growing conditions. Arctic forests in the Mesozoic and Paleogene have led some scientists to hypothesize that the origin of the deciduous habitat at high latitudes was an adaptation to avoid losing carbon through respiration during dark months (Axelrod, 1966, 1983; Read and Francis, 1992; Royer et al., 2003). Growth experiments conducted with *Metasequoia*, *Taxodium*, and *Sequoia* attempted to recreate ancient polar conditions, testing variables such as light and CO_2 levels in order to gain insight into their physiology (Beerling and Royer, 2002; Osborne and Beerling, 2003; Royer et al., 2003; Jagels and Equiza, 2007; Equiza et al., 2006; Llorens et al., 2009). These experiments were able to reject the hypothesis that deciduous habit prevented carbon losses from respiration, showing no physiological advantages. Although the reasons for the deciduous habit remains a mystery, these studies have offered valuable data on the ecology and physiology of *Metasequoia*.

1.3.1 Morphology and leaf anatomy of *Metasequoia glyptostroboides*

The morphology of *M. glyptostroboides* has also been well studied, further making it an ideal taxon to investigate links to climate. The extensive fossil record shows that the gross morphology of *Metasequoia* has remained relatively static over geologic time. Generally, this refers to leaf shape and arrangement on a branchlet as these are most often preserved. *Metasequoia glyptostroboides* is easily distinguishable from other conifer species. It can

reach a height of up to 50 m tall, however, most individuals today are ∼35 m tall, with a maximum of 2.2 m diameter at breast height (Farjon, 2005). Different branch and trunk forms are observed in individuals. Branches are known to grow straight outwards or curve upwards, whereas tree trunks are either constant in size from base to diameter at breast height, or swollen at the base and tapering upwards (Farjon, 2005).

Leaves are oppositely arranged on a deciduous branchlet. *Metasequoia* leaves are thin and elongated, with a rounded apex and base, ranging from 8–15 mm long, 1.5–2.5 mm wide, and 0.7–1 mm thick (Farjon, 2005). Leaves attach to the branchlet by a decurrent leaf base, with branchlets ranging from ∼5–15 cm long. The ovulate and pollen cones are both opposite-decussate arranged cone scales. Ovulate cones are approximately 20–25 mm in length with a peduncle (Basinger, 1981; Farjon, 2005). The wood is characterized by lacking in aroma, being composed primarily of tracheid/parenchyma cells with resin cysts present, rare separation of ray cells that have single horizontal rows of crossfield pits, sparse longitudinal parenchyma cells, and usually smooth parenchyma wall (Basinger, 1981; Visscher and Jagels, 2003).

A transverse (cross) section of a *Metasequoia* leaf is elliptical in shape, with one central vascular bundle and three resin canals (one central and adaxial to the vascular bundle, and one at each tip of the leaf margin). Epidermal cells are papillate and mesophyll cells are considered underdeveloped because chloroplasts levels are low (Basinger, 1981; Jagels and Day, 2004).

1.3.2 Fossil record and biogeography of *Metasequoia*

The first appearance of *Metasequoia* is in the Cenomanian (Late Cretaceous, estimated ∼100–93.9 Ma) represented by fossils found in Russia, Canada, and Alaska (Chaney, 1950; Florin, 1963; Liu et al., 1999; Yang and Jin, 2000). *Metasequoia* was widespread in its geographic distribution from the Late Cretaceous to the end of the Eocene (∼33.9 Ma), found from mid-latitudes to the Arctic Circle, 34–82 ºN (Liu et al., 2007). From the

early Oligocene (∼33.9–27.8 Ma) to Plio-Pleistocene (∼5–0.01 Ma), the distribution of *Metasequoia* gradually contracted as climate cooled, with a brief expansion during the warm Middle Miocene Climatic Optimum (17–15 Ma; LePage et al., 2005; Liu et al., 2007). Three extinct species are recognized within *Metasequoia*: *M. milleri* (Rothwell and Basinger, 1979), *M. foxii* (Stockey et al., 2001), and *M. occidentalis* (Chaney, 1950; Liu et al., 1999). *Metasequoia occidentalis* was formerly several species that are now considered by Liu et al. (1999) to represent a single species. These fossils are the most common *Metasequoia* found and are predominately preserved as compression/impression fossils represented by branchlets, leaves, cones, and seeds at numerous localities across the Northern Hemisphere. *Metasequoia foxii* is known from over 10,000 compression fossils of leaves, cones, seeds, seedlings, and permineralized wood from the Paleocene Munce's Hill and Gao Mine localities (Paskapoo Formation) in Alberta, Canada (Falder et al., 1999; Stockey et al., 2001). *Metasequoia milleri* is based on cones, wood, and leaves that are anatomically preserved in the early Eocene Princeton Chert locality (Allenby Formation) in British Columbia, Canada (Rothwell and Basinger, 1979; Basinger, 1981, 1984).

The historical biogeography of *Metasequoia* has been determined partly by global climate and sea levels. Climate throughout the Late Cretaceous to Eocene was warm, reaching its warmest in the early Eocene (Zachos et al., 2001). Throughout the Late Cretaceous *Metasequoia* was found in Asia and western North America, connected by the Beringian Corridor. The fossil record shows *Metasequoia* occupied paleolatitudes ∼55–80º N at the beginning of the Late Cretaceous (∼100–90 Ma), and expanded to 30–70º N by end Late Cretaceous (∼89–65 Ma), with fossil localities found in western Asia (LePage et al., 2005; Liu et al., 1999). By the Paleocene, the retreat of the Western Interior Seaway permitted *Metasequoia* to spread eastward across North America into Greenland, then Europe, maintaining mid- to high paleolatitude distribution throughout the Eocene (LePage et al., 2005).

During the Eocene-Oligocene Transition, as global climate cooled dramatically (Zachos

et al., 2001), the range of *Metasequoia* contracted from lower latitudes, resulting in a latitudinal range of 64–82 ºN (Liu et al., 1999; LePage et al., 2005; Liu et al., 2007). By the Miocene, the range was thought to have expanded again, to 55–80 ºN latitude, however a recent fossil discovery from middle Miocene deposits in Sanzhangtian, located in Yunnan (∼24 ºN, Southwest China) provides evidence for the southernmost recorded finding of *Metasequoia* fossils in its history (Liu et al., 2007; Wang et al., 2019). *Metasequoia* is represented in the Late Miocene by fossils from Japan and mainland China (LePage et al., 2005; Yamakawa et al., 2017). The Pliocene Kobiwako Group of central Japan represents our earliest record of habitat shift, where it was no longer found in hydric peat-forming layers but in mesic habitats (Yamakawa et al., 2017). *Metasequoia* persisted in what is now Japan, contracting and expanding until the early Pleistocene, the most recent fossil documented. Its disappearance from the fossil record led scientists to believe it was extinct until its rediscovery in 1941.

1.4 Thesis structure

In this thesis, I aim to address how leaf anatomy and physiology are modified to their environment across a wide climatic gradient in *Metasequoia glyptostroboides*, and whether similar responses are observed in closely related taxa, *Sequoia sempervirens* and *Taxodium distichum*. Once this link was established, I investigated trait and climatic niche shifts within *Metasequoia*. Anatomically preserved fossils were used to infer climate in order to test whether anatomy-climate links held through time. In order to infer the effects of climate on plants, I used early Eocene climate models with fossil localities to estimate anatomical traits and trait selection in plants over time, using compressed fossil measurements to validate my estimates.

Chapter 2 establishes links between leaf anatomy and climate in *Metasequoia glyptostroboides* and tests whether this relationship holds over geological time by

estimating climate in the past and comparing with independent climatic reconstructions of nearby fossil localities. I measured cross-sectional area, vascular bundle area, resin canal area, leaf width, and leaf thickness of leaves from living *Metasequoia* collected along an environmental gradient, and for the anatomically preserved fossils of *Metasequoia* milleri from the early Eocene Princeton Chert (Allenby Formation; British Columbia, Canada). The relationship between anatomy and climate was established in modern *Metasequoia*, then used to determine whether this relationship has remained the same through time. The inferred past climate of *M. milleri* was compared with independent paleoclimatic reconstructions of the surrounding areas. I found leaf width and cross-sectional area were associated with cold-season precipitation, vascular bundle area with warm-season precipitation, leaf thickness with mild cold-season temperatures and mean annual temperature, and resin canal area with daily temperature fluctuations and mild cold-season temperatures. Estimated climate for *M. milleri* matched published independent climate estimates of nearby fossil localities, demonstrating my model accurately predicted leaf-climate relationships through geologic time.

Whether the leaf anatomical links to climate found in Chapter 2 apply to conifers more broadly is tested using closely related taxa in Chapter 3. *Metasequoia glyptostroboides* and closely related taxa *Sequoia sempervirens* and *Taxodium distichum* were sampled across broad climatic gradients. Both leaf anatomy (using the same variables as in Chapter 2) and physiological traits related to photosynthesis (carbon/nitrogen content; δ^{13}C to calculate photosynthetic discrimination (Δ_{leaf}), water use efficiency (WUE), and internal cellular:atmospheric pCO_2 (c_i/c_a)) were collected. I focus on interspecific variation across climate gradients to understand whether links to anatomy and physiology are the same across taxa. I found relationships between traits and climate were different across taxa. Strong associations were found in cross-sectional area with temperature seasonality, leaf width with mean annual precipitation, and leaf thickness with temperature evenness. Further, analysis showed that while anatomy between taxa was distinct, they have similar

physiological function.

The relationships established between anatomy and climate in Chapter 3 were applied in Chapter 4 to investigate how climate might have affected leaf traits, and therefore physiological functioning/photosynthetic performance, of *Metasequoia* in the early Eocene. Generalized linear models of modern trait-climate relationships were created. These models were tested for fit and then used with published early Eocene climate model and fossil localities to infer the distribution of past traits. Leaf widths of fossil leaves were used to validate the models. I demonstrated that trait response depends on the magnitude of CO_2 warming, highlighting how climatic constraints influence past—and future—response to climates.

CHAPTER 2

Evaluating stasis in *Metasequoia* (Cupressaceae): testing the relationship between leaf traits and climate. *

Abstract

Plant response to climate through time is commonly investigated with leaf physiognomy, but anatomical response has not been well studied. Here, I use *Metasequoia* (Cupressaceae) to investigate leaf anatomical response to climate over geologic time. I establish the link between leaf anatomy and climate for extant *Metasequoia* and apply the results to the fossil *Metasequoia milleri* to examine climatic niche shift through time. Leaves of extant *Metasequoia glyptostroboides* collected across climate gradients in North America, Asia, and Europe and leaves of extinct *M. milleri* from the Eocene Princeton Chert locality were studied. Leaf anatomical traits—cross-sectional area, resin canal area, vascular bundle area, and leaf thickness and width—of extant and extinct *Metasequoia* were measured, analyzed using principal components analysis (PCA), and tested for relationships with 19 bioclimatic variables in a canonical correlation analysis (CCA). Fossil climate variables estimated from CCA results were compared with independent paleoclimate proxy estimates. All

*A version of Chapter 2 is published in *International Journal of Plant Sciences: Ng, M and Smith, SY. 2020. Int. J. Plant Sci. 181(2); DOI: 10.1086/706994*

measured anatomical traits statistically differ between extinct and extant *Metasequoia*, and the two species do not overlap in leaf anatomical morphospace. Measured traits of extant *Metasequoia* were found to correlate with several climate variables grouped into six climate groupings. Leaf width and cross-sectional area correlated with high cold-season precipitation, vascular bundle area with high warm-season precipitation, leaf thickness with mild cold-season temperatures and high mean annual temperatures, and resin canal area with daily temperature fluctuations and mild cold-season temperatures. Estimated paleoclimates based on the leaf anatomy–climate model were similar to independent proxy estimates. A relationship between leaf traits and climate was found that supports different leaf anatomical morphospaces and climatic niches for both species of *Metasequoia* that were tested, despite previous hypotheses of static morphology within *Metasequoia*. Testing interactions between climate and anatomy could improve paleoenvironmental inferences from fossil conifers.

2.1 Introduction

Changes in climate over geologic time are one of many influences that have shaped plant evolutionary history. Water availability, for example, shifts with climate and alters the landscape, creating potentially unsuitable habitats for plants. In response to limited water availability, plants alter their distribution through contraction or expansion of their range and consequently may experience extinction/extirpation (*e.g.*, Carboniferous arborescent lycopods; Falcon-Lang and DiMichele, 2010) or speciation (*e.g.*,allopatric speciation of *Quercus* (Fagaceae) in the Quaternary; Axelrod, 1983). In order to evade extinction as a result of climatic selection, lineages must shift at a rate matching climate change or find refugia. Plants still experience and undergo selection, ultimately influencing modern day climatic tolerances. Identifying this selection, and its effects, in the fossil record will improve our understanding of plant response to climate.

Leaves are the most abundant plant organ and are susceptible to abiotic stress (Coleman, 1986; Chartzoulakis et al., 2002; Diefendorf et al., 2010; Webb, 1968), but changes in morphoanatomical traits can optimize their function. These traits may be plastic or stable. Plastic traits respond to and reflect abiotic factors yet retain their integral morphology, such as changes in leaf area with precipitation (Sultan, 1987; Ackerly, 2003; Wilf et al., 1998), while stable traits are conserved within lineages and are more strongly linked to biology than to environment. For example, leaves with non-entire margins, which are conserved in lineages, are more abundant in climates with higher seasonality (Bailey and Sinnott, 1915). Leaves of *Acer rubrum* (Sapindaceae) show both plastic (*e.g.*, leaf area) and stable (*e.g.*, leaf margin and general venation pattern) traits along the species' geographic range: leaf area of plants grown in Vermont is four times larger than that of plants grown in Florida; however, all *A. rubrum* leaves have non-entire margins and palmate leaf venation (Royer et al., 2008).

Since Bailey and Sinnott (1915), the link between plant morphology and climate has been studied extensively and applied to the fossil record (Wolfe, 1994; Wilf, 1997; Wilf et al., 1998; Mosbrugger, 2009). Leaf physiognomy—the general shape of leaves—has been demonstrated to reflect climate and, for several decades, was used to quantitatively reconstruct climate; however, this method is limited to eudicots, covering only a small portion of plant evolutionary history since angiosperm macrofossils have been present for 125 of 420 Myr (Bailey and Sinnott, 1915; Wolfe, 1979; Wilf et al., 1998; Yang et al., 2011; Khan et al., 2014; Lowe et al., 2018). One way to expand our understanding of plant response to climate within other groups is to investigate leaves at the anatomical (cellular) level, including stomata, mesophyll cell layers, and xylem. Leaf anatomy has been shown to reflect abiotic stressors in the plant's environment and general climate, yet the precise nature of leaf anatomical response to abiotic factors remains poorly understood (Ashton and Berlyn, 1994; McElwain and Chaloner, 1995; Royer, 2001; Oldham et al., 2010; Schubert et al., 2012; Jordan et al., 2013). Similar to leaf physiognomy, anatomical

variation with climate is either known from within certain plant groups or documented for various plant groups along climate gradients by sampling across species' entire geographic range (Ashton and Berlyn, 1994; Jordan et al., 2013; Ranjbar and Hajmoradi, 2016). For example, the anatomy of sun and shade leaves of different *Quercus* species was variable, demonstrating variability in structure responses (thickness of leaf, epidermis cell, palisade cell, and cuticle; stomatal density and index; and stomatal length measurements), and anatomy in some species (*e.g.*, *Quercus velutina* Lam.) was highly responsive, while in others (*e.g.*, *Quercus rubra* L.), it was less responsive to abiotic factors (Ashton and Berlyn, 1994). In conifers, scale-like leaves of juvenile plants in *Thuja plicata* Donn ex D. Don and *Platycladus orientalis* (L.) Franco (Cupressaceae) were studied for leaf anatomy. Dörken (2013) found a "superimposed bifacial" condition in *T. plicata* leaves in which internal leaf anatomy was rearranged: sun-exposed shoots had a high density of palisade cells (light capturing), while shade-exposed shoots had a high density of spongy mesophyll cells (high ratio of surface area to volume for gas exchange). Comparable scale-like leaves in *P. orientalis* retained the conventional cellular layer, with development of palisade cells toward the adaxial and spongy mesophyll cells toward the abaxial leaf (Dörken, 2013). Across different species within Proteaceae, xylem cell size increased with mean annual precipitation at both a regional scale and a global scale (Jordan et al., 2013).

Thus, variation of leaf anatomy across climate gradients should reflect a response to the environment in which the plant grew. When applied over geologic time, plant response to changing environments can inform how plants responded to past global and regional climate shifts. Understanding how plants have responded to climate shifts in the past will provide insights into the evolution of species' climate niche, the existence of species in multidimensional climate space or bioclimatic envelopes (Pearson and Dawson, 2003) over time, and whether that encompasses changes in realized or fundamental climatic tolerance or habitat tracking, ultimately providing insights into the effects of climate within a lineage. Shifts in climatic tolerance are important to our current comprehension of

plant response to climate because they influence how past climates and paleoenvironments are reconstructed. Paleoclimatic reconstruction methods such as "nearest living relative" are built on the premise that climate tolerance is conserved through time within lineages (physiological uniformitarianism; *e.g.,* Mosbrugger, 2009). A common application is seen with palms: modern palms grow in frost-free climates; thus, the presence of palms in a fossil flora indicates a frost-free climate (Larcher and Winter, 1981; Sakai and Larcher, 2012; Reichgelt et al., 2018). However, to improve our understanding of extinct species' paleoecology, and improve paleoclimate reconstructions, we need to explicitly test whether a species' climate tolerance has changed over time, and leaf anatomy could be a useful tool with which to do this.

Metasequoia glyptostroboides (Cupressaceae), the dawn redwood, is a deciduous conifer found in the Hubei Province of central China (Chaney, 1950; LePage et al., 2005; Liu et al., 2007). The fossil record of *Metasequoia* shows widespread distribution across the Northern Hemisphere (fig. 2.1) from middle to high latitudes (Chaney, 1950; LePage et al., 2005; Liu et al., 2007). Its range expanded and contracted over the Cenozoic as global climate cooled, with fossils found only in Asia by the late Pliocene (Chaney, 1950; LePage et al., 2005; Liu et al., 2007). Pittermann et al. (2012) hypothesized that within Cupressaceae drought tolerance increased with Cenozoic climate change; whether drought tolerance in *Metasequoia* increased is unknown. What makes *Metasequoia* compelling as a study system is that while the gross morphology of leaves appears unchanged since its first appearance in the fossil record, its habitat has shifted significantly (Liu et al., 1999; Stockey et al., 2001; LePage et al., 2005). This provides an opportunity to investigate anatomical changes while gross morphology is static.

Here, I test leaf anatomical response to climate gradients in *Metasequoia* to evaluate whether there was anatomical stasis despite environmental habitat shifts in the past. Extant *Metasequoia* resides naturally in riparian lowland habitats in temperate deciduous forests of eastern Asia, while its extensive fossil record, including the depositional environments

and preservation quality of fossils, suggests that extinct species inhabited swamp-type ecosystems, demonstrating a clear shift in its habitat (LePage et al., 2005; Tang et al., 2011). The fossil record of *Metasequoia* comprises three species: *M. foxii*, *M. occidentalis*, and *M. milleri*. *Metaseqoia occidentalis* and *M. foxii* are known from leaf/branchlet and cone compression/impression fossils (LePage et al., 2005; Stockey et al., 2001). Anatomically preserved *M. milleri* is represented by cones, wood, and leaves and is found only from the early Eocene Princeton Chert locality (Allenby Formation) British Columbia, Canada (Rothwell and Basinger, 1979; Basinger, 1981, 1984). In this study, I combine leaf anatomy data from fossil *M. milleri* and extant *M. glyptostroboides* with climate data to test for anatomical responses to climate and, from an evolutionary perspective, anatomical changes over time within the genus.

Figure 2.1: Fossil record of *Metasequoia* from the Cretaceous to Pliocene. Each site marked by time period. Locality data from LePage et al. (2005) and Wang et al. (2019).

2.2 Methods

2.2.1 Sample Collection and Preparation

To test variability of anatomical traits along a climate gradient, samples of *Metasequoia glyptostroboides* from cultivation were collected across North America (2016), Asia (2017), and Europe (2017; Appendix table A.1; fig. 2.2).

These sites were selected based on published accounts, climatic gradient, and permissions granted from national parks, state parks, and botanical gardens. Latitude and

longitude for each sampling location were recorded with a handheld GPS device (Garmin eTrex Venture HC, WGS84). Three branchlets (about 1–3 m from the ground) from up to three trees per site were collected and stored in formalin propionic acid (FPA; only North American sites, six trees total) or 100% ethanol for at least 24 h before transferring to 70% ethanol for long-term storage. Samples were in 70% ethanol at least 1 wk before they were embedded in paraffin. Potential effects from fixation by FPA versus 100% ethanol were tested on three branchlets and showed that samples in ethanol had ∼3% shrinkage for traits measured (thickness, width, and cross-sectional area) compared with samples in FPA. Because this is minimal, I treated all samples the same. Voucher specimens were also collected for each site. Vouchers and prepared slides are accessioned at MICH (Appendix table A.1). A total of 24 sites and 64 trees were sampled. Some of these trees are grown by gardens and cities with an added watering regime that raises concerns about whether these leaves reflect their local precipitation regime; however, I treat this effect as nonsignificant. To examine the amount of variation within a single tree, leaves were also sampled in 2018 from two trees of *M. glyptostroboides*: one from the University of Michigan, Ann Arbor Matthaei Botanical Gardens (Matthaei) and the other from the Nichols Arboretum (Nichols). Twenty branchlets were sampled from the inner (IC) and outer (OC) canopy at three heights (Appendix table A.1) and preserved in FPA. Samples from Matthaei (n=12 branchlets, 31 leaves) were taken from heights of 3 m (IC, n = 9 leaves; OC, n = 4), 5 m (IC, n = 4; OC, n = 6), and 6.5 m (IC, n = 8); samples from Nichols (n = 8 branchlets, 20 leaves) were taken from heights of 1 m (IC, n = 5; OC, n = 6), 6.5 m (OC, n = 2), and 8 m (OC, n = 7).

For each collection, the middle portions of three leaves from three branchlets (n = 9) were embedded in paraffin (after Johansen et al., 1940) using an automated paraffin tissue processor (Leica ASP 300) and tissue embedding station (Sakura FineTek Tissue-Tek) at the University of Michigan Microscope and Imaging analysis Laboratory (MIL; now Orthopedic Research Laboratory, ORL).

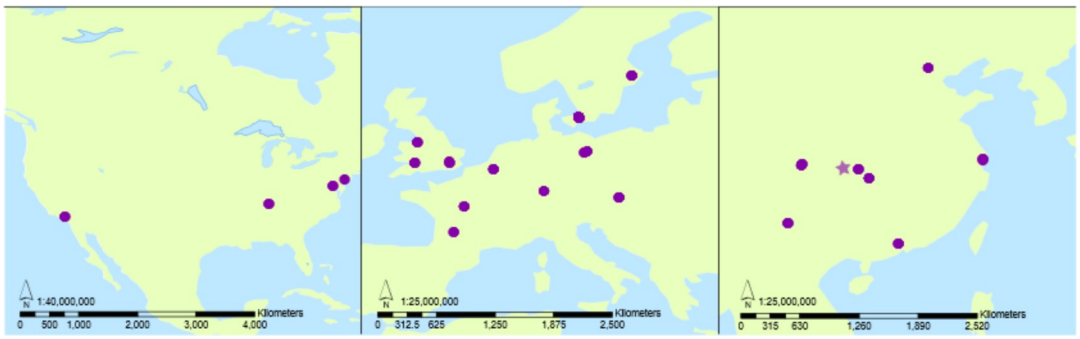

Figure 2.2: Map of sampling sites for *Metasequoia glyptostroboides* (circles) in North America (A), Europe (B), and Asia (C) in 2016 and 2017. Note protected natural distribution (star) in central China.

Once embedded, samples were sectioned at 10 μm thick using a Leica RM2235 or RM2255 rotary microtome (available at MIL/ORL) and adhered to slides using Mayer's albumen adhesive (one part egg white, one part glycerin, and 1g sodium benzoate) or Haupt adhesive (gelatin, glycerin, and phenolbased adhesive). Then slides were stained with 0.1% toluidine blue O solution in 0.1 M benzoate buffer, pH 4.4 (Yeung, 1998), in a xylene and ethanol series and mounted with Eukitt mounting medium (O. Kindler).

Photographs of cellulose acetate peels of *Metasequoia milleri* from the Princeton Chert locality were obtained from the University of Alberta Paleontology Collection (UAPC, n = 26). The following are specimens observed (n = 1 unless otherwise noted; bot = bottom): SL2613 (P1060 Cbot, n = 2), SL2615 (P1060 Dbot), SL5008 (P1060 Etop), SL2617 (P1060 Ftop, n = 2), SL5010 (P1089 Btop), SL5011 (P1095 Bbot), SL2622 (P1095 Cbot-A), SL2623 (P1095 Cbot-B, n = 2). SL2632 (P1095 Btop), SL2631 (P1095 Bbot, n = 2), SL5012 (P1095 Bbot), SL2627 (P1095 Eb), SL2628 (P1095 Ec), SL2629 (P1095 Ed), SL2618 (P1096 A), SL2633 and SL2634 (P1102 Etop), SL2635 (P1102 Ftop), and SL5463 (P1181 Gtop, n = 4).

2.2.2 Anatomy

Photographs of prepared sections were taken on Nikon Eclipse LV100-ND microscope with a NikonDS-Fi2/DS-U3 camera unit. Five anatomical features were measured:

cross-sectional area, vascular bundle area, resin canal area, leaf thickness at vascular bundle, and leaf width (fig. 2.3), using Nikon Imaging Software Elements version 4.30 for each sample.

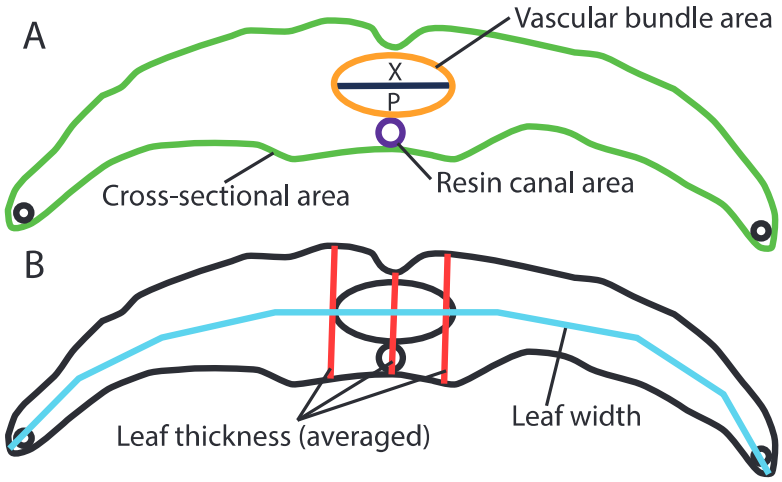

Figure 2.3: Diagram showing trait measurements taken for each cross section. A, Cross-sectional area (green), vascular bundle area (orange), and resin canal area (purple). B, Leaf width (light blue) and average leaf thickness (pink).

2.2.3 Climate

2.2.3.1 Modern samples.

Bioclimatic (Bioclim) climate data were extracted from GPS sampling locations using 19 Bioclim variables from WorldClim version 2.0 at 30-s resolution (Fick and Hijmans, 2017). For the samples collected to test variation within a tree, Bioclim variables were the same; however, Matthaei was exposed to full sun growing in seasonally wet soil, and Nichols was growing next to another *Metasequoia* and surrounded by tall trees on a slope.

2.2.3.2 Fossil samples.

Paleoclimate estimates of mean annual temperature (MAT), mean annual precipitation (MAP), and cold month mean temperature (CMMT) for the Allenby Formation (table 2.1) were extracted from previous studies by (Wolfe, 1994; Wolfe et al., 1998; Wing

and Greenwood, 1993) and (Greenwood et al., 2005). These studies used various methods to reconstruct paleoclimate. Climate-leaf analysis multivariate program (CLAMP; wolfe1994) and leaf margin analysis (LMA; Bailey and Sinnott, 1915) rely on global relationships between leaf traits from all eudicot species in an assemblage. Bioclimatic analysis used by Greenwood et al. (2005) is similar to the coexistence approach (Mosbrugger, 2009), which uses the overlap of climate profiles from the "nearest living relatives" of all species in a fossil assemblage. The CLAMP and LMA-derived estimates, based on only eudicots and no conifer data, are therefore estimates independent of paleoclimate.

2.2.4 Analysis and Statistics

Each leaf was treated as a separate sample. Principal components analysis (PCA) was performed to analyze anatomical variation for three separate data sets—variation within a tree, across all *M. glyptostroboides* (climate gradient and variation within a tree), and between *M. glyptostroboides* (climate gradient) and *M. milleri*—by standardizing data using z-scores ($x - \overline{x} \times \mathrm{SD}(x)^{-1}$), then running analyses in PAST version 3.19 (Hammer et al., 2001). Next, anatomical measurements across climate gradients (*M. glyptostroboides*) were combined with climate data for canonical correspondence analysis (CCA), also conducted in PAST. Boxplots, correlations, ANOVAs, and pairwise t-tests with Bonferroni adjustment on raw data were conducted in RStudio (Team et al., 2015).

The functions cca() and predict() from R package "vegan" version 2.5-2 (Oksanen et al., 2018) were used together to estimate Bioclim variables from raw measurements of *M. milleri*. Cca() used both standardized anatomy measurements of extant *M. glyptostroboides* and modern climate data to create a model of anatomy-climate. Predict() combined my CCA results (multivariate linear model) and fossil anatomical measurements to determine Bioclim variables for each fossil leaf measured. These estimates were averaged and compared with independently derived paleoclimate data from Allenby Formation (table

Table 2.1: Paleoclimate estimates from Princeton Chert Locality and surrounding area

Locality	MAT (° C)	Method	CMMT (° C)	Method	MAP (cm yr^{-1})	Method
One Mile Creek	13.1 ± 3.1^{A}	BA	5.3 ± 2.8^{A}	BA	114 ± 2^{A}	CLAMP
	9.3^{B}	CLAMP				
	8.3^{C}	CLAMP				
	3.5 ± 2.0^{D}	LMA				
	5.1 ± 2.0^{D}	LMA[1]				
Quilchena	15.0 ± 0.6^{A}	BA	5.8 ± 2.0^{A}	BA	114 ± 2^{A}	CLAMP
	15.3 ± 2.1^{E}	LMA				
	14.8 ± 2.0^{E}	LMA[1]				
Princeton Chert	11.8 ± 1.7	CCA	3.5	CCA[2]	83.6 ± 14	CCA

These estimated climate data for One Mile Creek and Quilchena came from different studies. Princeton Chert is from this study.

^{B} (Wolfe, 1994)

^{C} Wolfe et al. (1998)

^{D} Wing and Greenwood (1993)

^{E} Greenwood and Wing (1995)

^{A} Greenwood et al. (2005)

NOTE.–CLAMP = Climate Leaf Analysis Multivariate Programme (Wolfe, 1994), LMA = Leaf Margin Analysis (Bailey and Sinnott, 1915), BA = Bioclimatic Analysis; similar to coexistence analysis (Mosbrugger, 2009), and CCA = this study.

[1] LMA calibrated via CLAMP

[2] estimate derived from CCA estimated variable, subtracting Bio 7 from Bio 5 (see methods under climate)

2.1; see "Climate"). Finally, I performed a sensitivity analysis by increasing one anatomical trait at a time by 25% and testing for predicted Bioclim equivalents of MAT (Bio 1), MAP (Bio 12), CMMT (Bio 11), and warm-month mean temperature (WMMT; Bio 10). I performed an ANOVA and pairwise t-test with Bonferroni adjustment on all models against my estimated climate reconstruction model.

2.3 Results

2.3.1 Variation within a Tree

Anatomical traits of 51 leaves from two trees sampled from Matthaei and Nichols in Ann Arbor, Michigan, were measured and found to vary both in canopy height and between trees (table 2.3; fig. 2.4 and 2.5). Generally, samples from Nichols had a larger cross-sectional area and were wider and thicker than samples from Matthaei (fig. 2.5). ANOVAs showed Matthaei and Nichols were statistically different ($p<0.05$) in cross-sectional area ($p<0.001$), vascular bundle area ($p = 0.02$), leaf width ($p<0.001$), and leaf thickness ($p = 0.04$). Pairwise t-tests using Bonferroni adjustment showed Matthaei and Nichols were statistically different from one another ($p<0.05$) in cross-sectional area ($p<0.001$), vascular bundle area ($p = 0.02$), leaf width ($p<0.001$), and leaf thickness ($p = 0.04$). Pairwise t-tests using Bonferroni adjustment within each tree showed statistically different paired samples ($n = 13$, $p<0.05$; table 2.7) across four traits: cross-sectional area ($n = 1$), vascular bundle area ($n = 5$), leaf width ($n = 3$), and leaf thickness ($n = 4$). These differences were predominantly in Matthaei samples, with Nichols showing differences in leaf thickness between lower and higher OC leaves (table 2.7). Correlations between height and anatomy were weak; height and leaf thickness had the strongest correlation ($n = 21$, $r = 0.52$, $r^2 = 0.27$).

PCA of leaf anatomy variation within a tree showed 81.5% of variation is explained by the first two axes (fig. 2.6; table 2.2). Principal component (PC) 1 (59.2% of the variation)

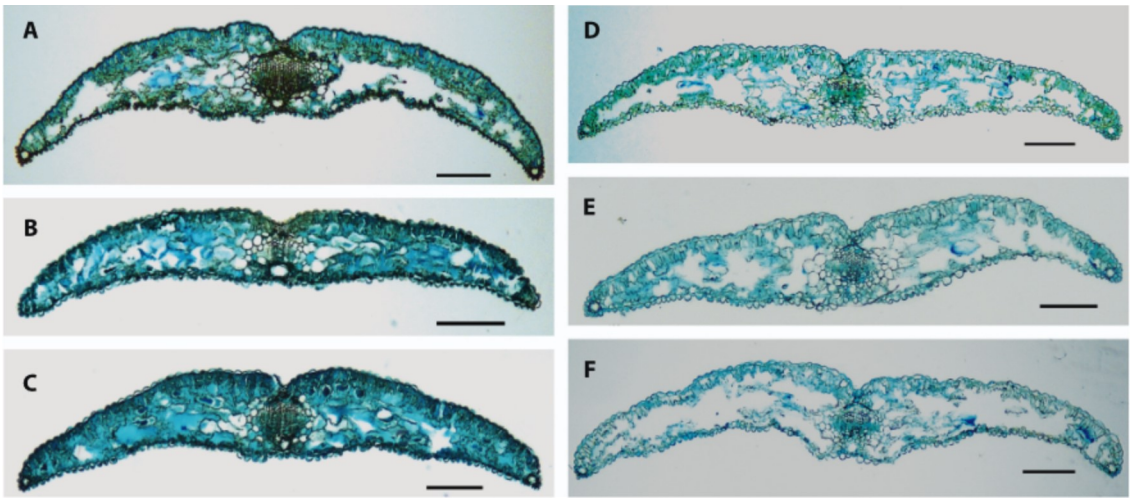

Figure 2.4: Leaf anatomy variation within two individuals of *Metasequoia glyptostroboides*. A–C, Matthaei Botanical Garden. A, MN18-27, height ca. 7 m, inner canopy (IC). B, MN18-10, height ca. 5 m, outer canopy (OC). C, MN18-13, height ca. 1 m, OC. D–F, Nichols Arboretum. D, MN18-23, height ca. 8 m, OC. E, MN18-22, height ca. 6 m, OC. F, MN18-21, height ca. 1 m, IC. Scale bars = 200 μ m.

Table 2.2: PCA Eigenvalues and percent variance for each model

PC	Variation within a tree		$M.glyptostroboides$ (all)		Fossil and Modern $Metasequoia$	
	Eigenvalue	Percent variance	Eigenvalue	Percent variance	Eigenvalue	Percent variance
1	2.95819	59.164	3.15405	63.081	2.16344	43.269
2	1.11568	22.314	0.897085	17.942	1.99074	39.815
3	0.642238	12.845	0.534753	10.695	0.443692	8.8738
4	0.217217	4.3443	0.302802	6.056	0.337007	6.7401
5	0.066679	1.3336	0.111311	2.2262	0.06512	1.3024

correlates with cross-sectional area, while PC 2 (22.3%) is most strongly correlated with resin canal area. While the morphospaces of Matthaei and Nichols overlap (fig. 2.6), there are no clear trends or indications that this is related to differences in height.

2.3.2 Modern *Metasequoia* across Climate Gradients

Anatomical traits for 490 leaves were measured for *M. glyptostroboides* across a climatic gradient of 24 sites and 64 trees (fig. 2.7 and 2.8A-D; table 2.3). Combined analysis of all anatomical measurements of *M. glyptostroboides* (fig. 2.7; table 2.3), including variation in canopy height, resulted in a PC axis 1 (63.1%) with the strongest correlation with cross-sectional area and PC 2 (17.9%) strongly correlating with leaf width. Samples

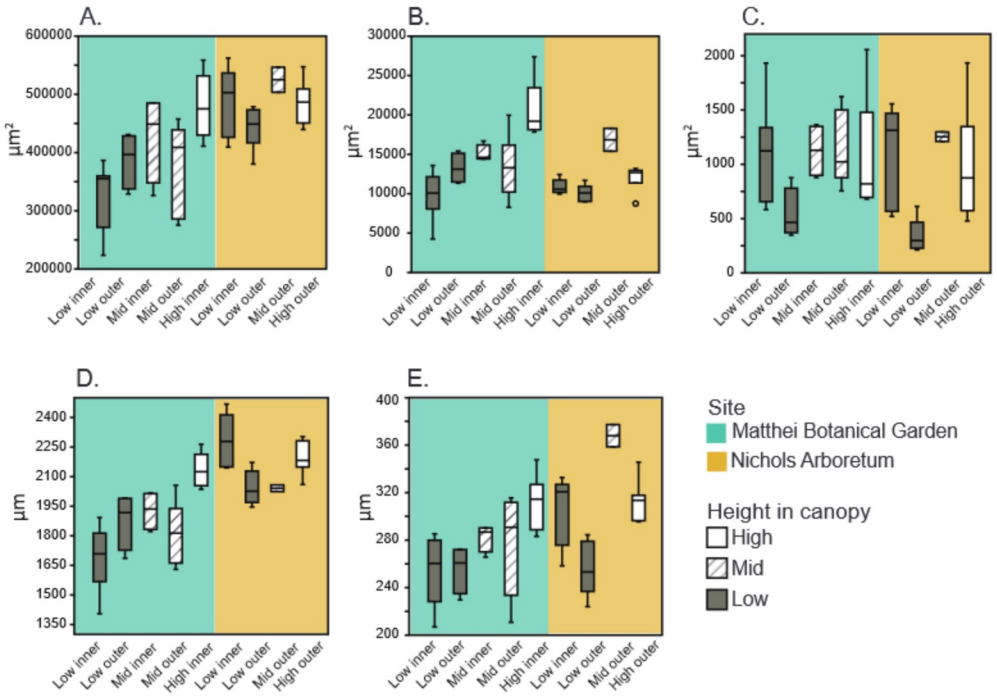

Figure 2.5: Boxplots of *Metasequoia glyptostroboides* leaf anatomical traits sampled from Matthaei Botanical Garden and Nichols Arboretum. A, Cross-sectional area. B, Vascular bundle area. C, Resin canal area. D, Leaf thickness. E, Leaf width. Grouped by height (low, mid, and high) and canopy positions (inner, outer). Outliers indicated by open circles. All traits except resin canal area are statistically significant ($p<0.05$).

from varying canopy heights are nested within samples from across climatic gradients (fig. 2.9).

In CCA of *M. glyptostroboides*, the first two axes showed 85% of the variation in the data (fig. 2.10; table 2.4, Appendix table A.3). The first axis (59.0%) correlated strongly with annual precipitation (Bio 12), while the second axis (26.0%) correlated strongly with mean temperature of coldest period (Bio 6 and 11). Clusters of climate vectors (Bioclim climate variables with similar vectors in CCA) were identified and interpreted collectively, resulting in six separate climate groupings (table 2.3.2): daily temperature fluctuations, mild cold-season temperatures, high mean annual temperature, high warm-season precipitation, high temperature seasonality, and high cold-season precipitation. CCA showed anatomical traits correlated with climate groupings (table

Table 2.3: *Metasequoia* anatomical traits measurements

	Cross-sectional area (μm^2) mean ± sd, min–max	Vascular bundle area (μm^2) mean ± sd, min–max	Resin canal area (μm^2) mean ± sd, min–max	Leaf width (μm) mean ± sd, min–max	Leaf thickness (μm) mean ± sd, min–max
Metasequoia glyptostroboides					
Climate gradient	422385.1 ± 118642.4, 140944.4–970908.3	13192.3 ± 7314.2, 844.9–63069.9	1446.7 ± 1024.6, 135.8–9792.7	1941.0 ± 216.3, 1202.0–2531.3	258.7 ± 56.4, 133.0–531.1
Matthaei Botanical Garden	393546.1 ± 76623.6, 223529.8–558503.5	14903.0 ± 4826.6, 4251.2–27367.4	1055.2 ± 404.0, 347.89–2055.6	1892.0 ± 197.8, 1404.6–2264.1	278.0 ± 29.9, 206.9–347.5
Nichols Arboretum	480638.4 ± 36336.2, 380281.6–562210.5	12014.4 ± 2185.7, 8749.8–18296.9	950.1 ± 442.0, 211.54–1933.7	2156.9 ± 129.4, 1946.1–2468.1	309.6 ± 41.6, 224.0–377.2
Metasequoia milleri					
Princeton Chert Locality	265329.9 ± 151559.2, 114095.5–764190.0	9879.9 ± 5249.4, 3398.6–23240.6	3028.5 ± 2033.5, 898.7–8688.9	1133.1 ± 401.5, 629.6–2122.5	332.7 ± 67.0, 221.9–486.1

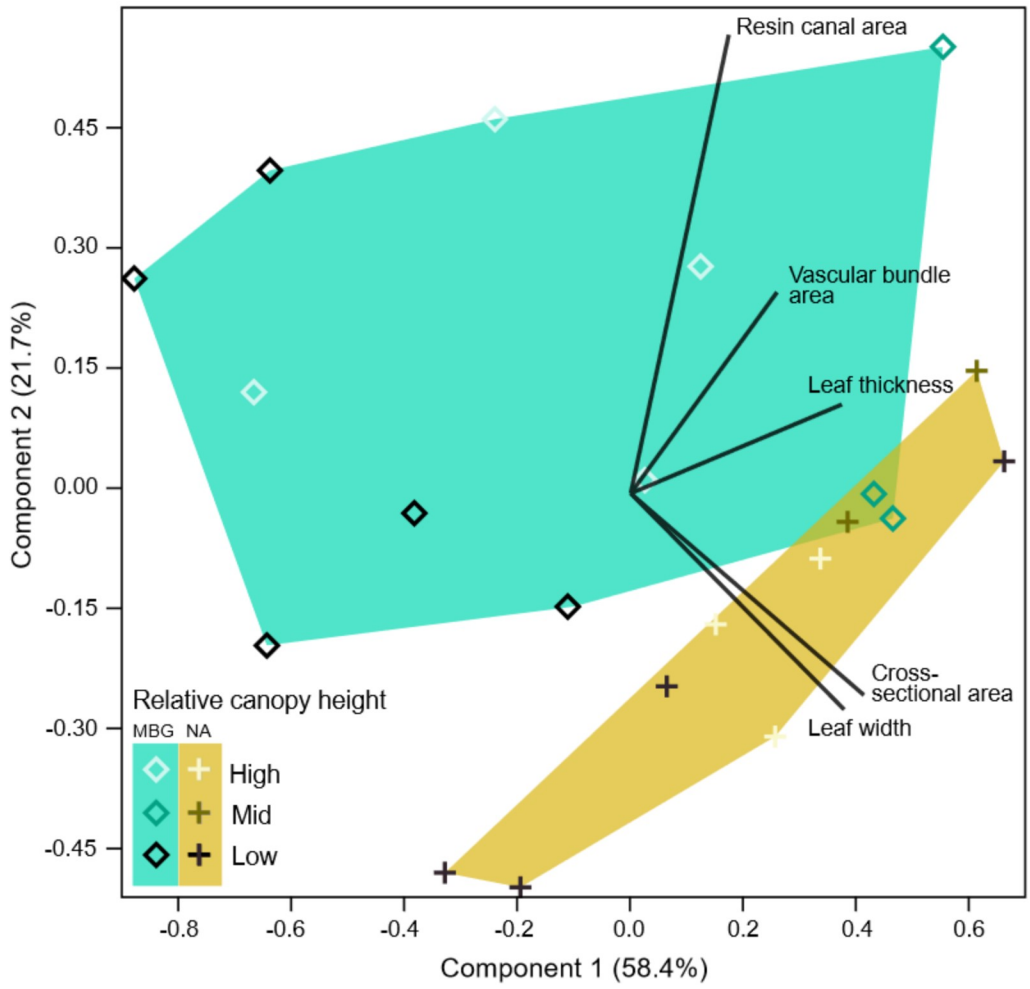

Figure 2.6: Principal components analysis (PCA) of leaf anatomical traits of two individuals of *Metasequoia glyptostroboides*. PC 1 (59.2%) correlates most with cross-sectional area and PC 2 (22.3%) with resin canal area. MBG = Matthaei Botanical Gardens; NA = Nichols Arboretum.

2.3.2): leaf width and cross-sectional area correlate with high cold-season precipitation, vascular bundle area correlates with high warm season precipitation, leaf thickness correlates with mild cold season temperatures and high mean annual temperatures, and resin canal area correlates with daily temperature fluctuations and mild cold-season temperatures. Bivariate correlations of anatomy and climate were weak but statistically significant ($r<0.5$, $p<0.05$; Appendix table A.2).

Table 2.4: CCA Eigenvalues and percent variance

Axis	Eigenvalue	% variance
1	0.013965	58.97
2	0.006159	26.01
3	0.002822	11.91
4	0.000735	3.103

Table 2.5: Bioclim variable and inferred climate groupings based on CCA with anatomical traits of modern *Metasequoia*

	Bioclim Variables	Daily temp variation	High MAT	High cold season precip	High warm season precip	High temp seasonality	Mild cold season temp
Bio 1	Mean annual temp		x				
Bio 2	Mean diurnal range			x			
Bio 3	Isothermality	x					
Bio 4	Temp annual range					x	
Bio 5	Max Temp of Warmest Month				x		
Bio 6	Min Temp of Coldest Month						x
Bio 7	Temp seasonality					x	
Bio 8	Mean Temp of Wettest Quarter				x		
Bio 9	Mean Temp of Driest Quarter			x			
Bio 10	Mean Temp of Warmest Quarter				x		
Bio 11	Mean Temp of Coldest Quarter						x
Bio 12	Annual Precipitation				x		
Bio 13	Precipitation of Wettest Month				x		
Bio 14	Precipitation of Driest Month			x			
Bio 15	Precipitation seasonality				x		
Bio 16	Precipitation of Wettest Quarter				x		
Bio 17	Precipitation of Driest Quarter			x			
Bio 18	Precipitation of Warmest Quarter				x		
Bio 19	Precipitation of Coldest Quarter			x			

Note: temp = temperature, precip = precipitation

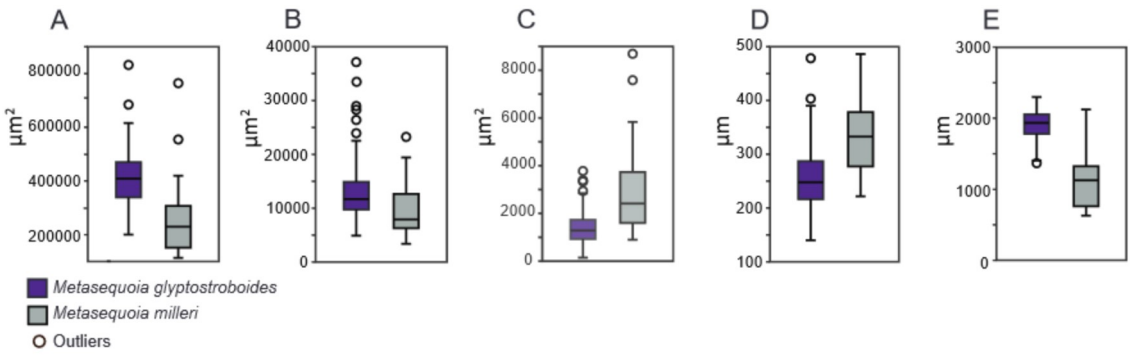

Figure 2.7: Boxplots of measured leaf anatomical traits for *Metasequoia glyptostroboides* and *Metasequoia milleri*. A, Cross-sectional area. B, Vascular bundle area. C, Resin canal area. D, Leaf thickness. E, Leaf width. All measurements significant ($p<0.05$).

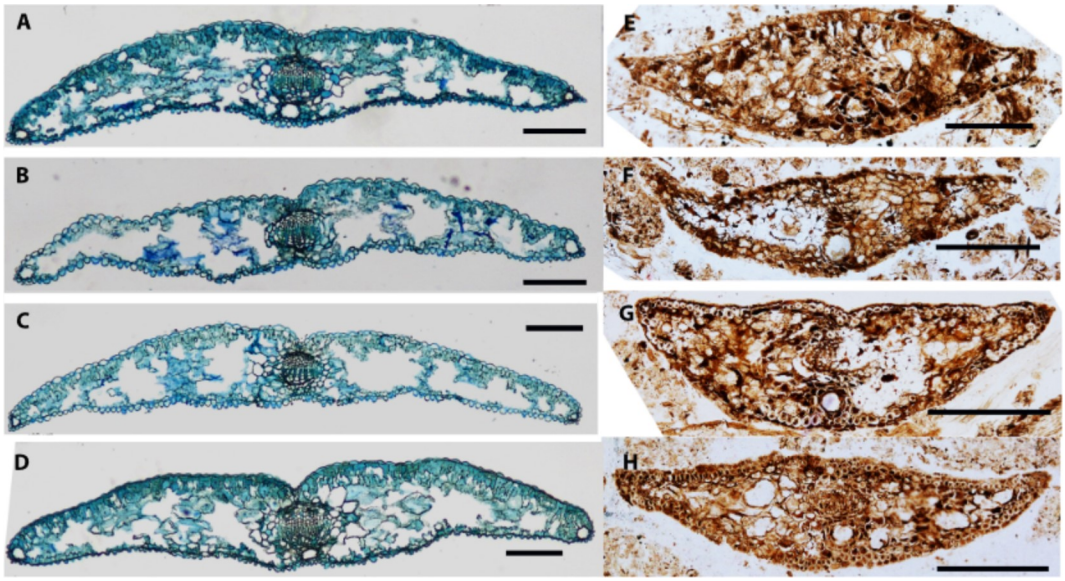

Figure 2.8: Cross sections of leaves of *Metasequoia glyptostroboides* and *M. milleri*. A–D, *Metasequoia glyptostroboides*. A, Cardiff (Wales, UK), MN17-53. B, Jiangjiajie (Hunan Province, China), MN17-24. C, Shanghai (China), MN17-31. D, Copenhagen (Denmark), MN17-35. E–H, *Metasequoia milleri*. E, UAPC SL2623. F, UAPC SL2617. G, UAPC SL2617. H, UAPC SL2613. Scale bars=200 μm (A–D), 25 μm (E–H).

2.3.3 Incorporating Fossils

Anatomical traits were measured for *M. milleri* (n = 19; figs. 7, 8E–8H; table 2.3). In comparison with *M. glyptostroboides*, cross-sectional area, vascular bundle area, and leaf width measurements were smaller. my measurements also showed leaf thickness and resin canal area were larger in *M. milleri* than in *M. glyptostroboides*. Pairwise t-tests using

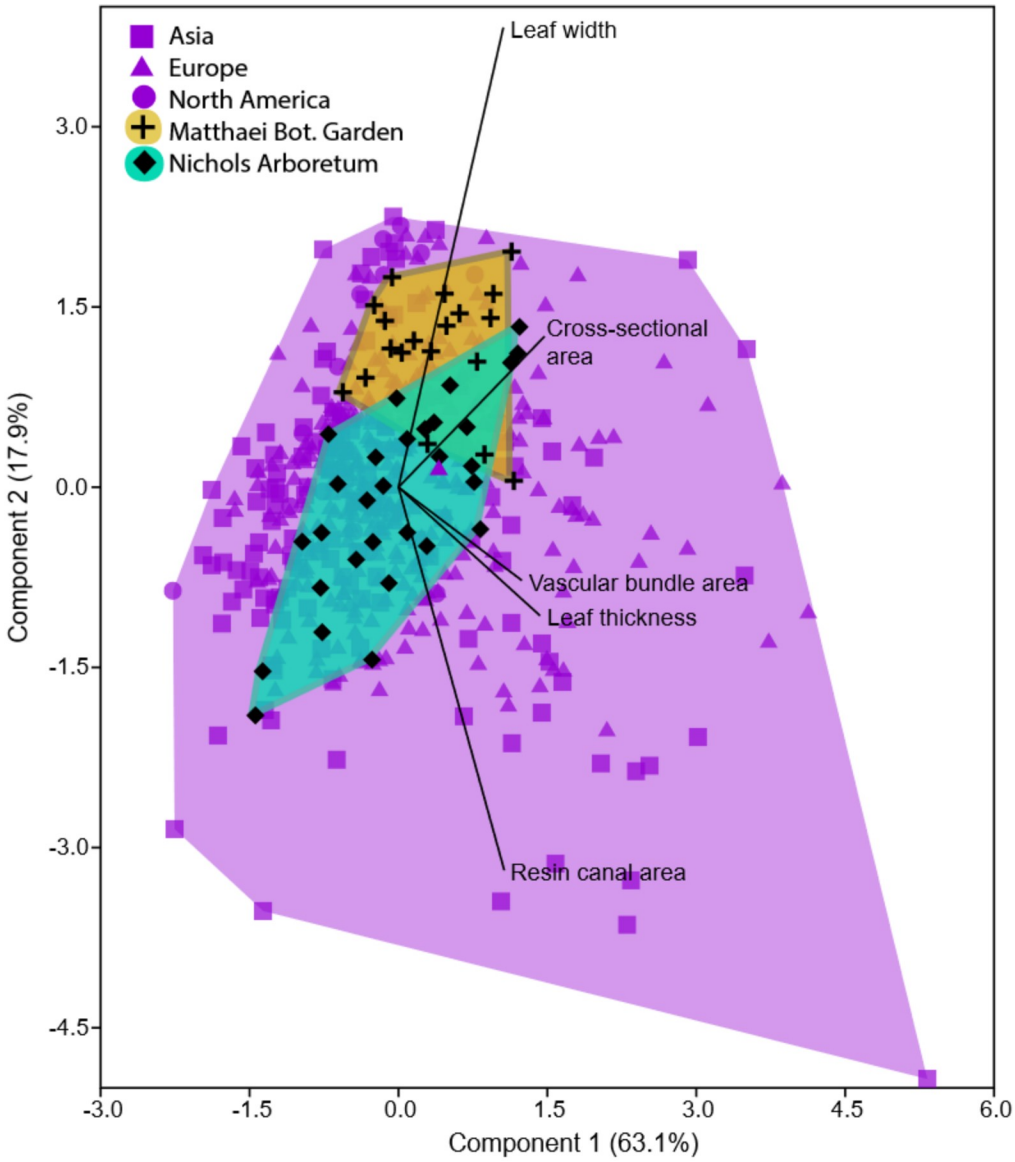

Figure 2.9: Principal components analysis (PCA) of leaf anatomical traits of *Metasequoia glyptostroboides* across sampled climate gradient in North America, Europe, and Asia. PC 1 (63.5%) showed most correlation with cross-sectional area and PC 2 (17.7%) with leaf width. Note Matthaei and Nichols samples nested within broader climatic gradient.

Bonferroni adjustment showed fossil and modern *Metasequoia* were significantly different, where $p<0.001$ for all measured traits except form vascular bundle area, which had a p value of 0.03.

PCA of fossil and modern *Metasequoia* shows PC 1 (43.3%) is most strongly correlated with cross-sectional area, and PC 2 (39.8%) is most strongly correlated with leaf width (fig.

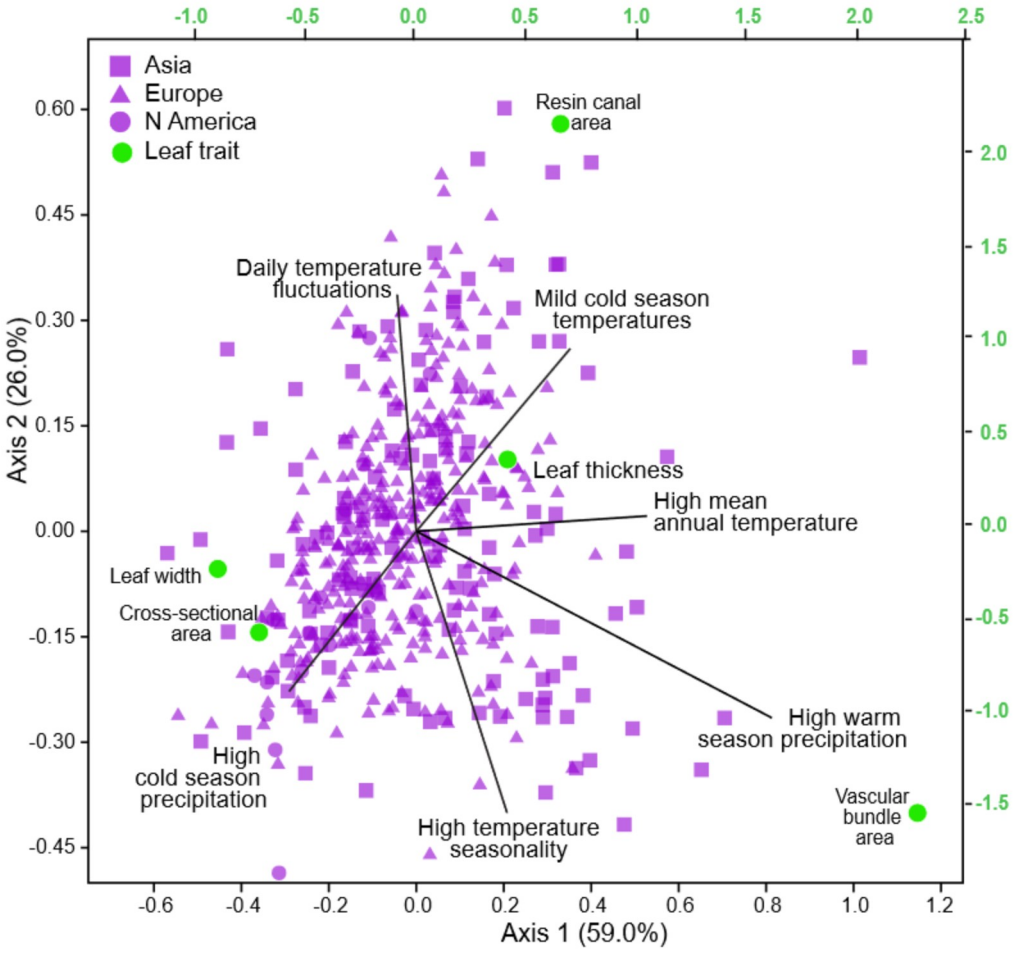

Figure 2.10: Canonical correspondence analysis of *Metasequoia glyptostroboides* leaf anatomy and climate data. Bioclimatic (Bioclim) climate variables grouped into six climate groupings. Axis 1 (59.0%) showed highest variability with high warm-season precipitation and axis 2 (26.0%) with high temperature seasonality.

2.11). Each taxon occupies a separate morphospace, with *M. glyptostroboides* showing larger vascular bundle area, cross-sectional area, and leaf width, and *M. milleri* showing larger resin canal area and leaf thickness.

Using the R package "vegan" version 2.5-2, I input the anatomical traits of *M. milleri* into my CCA model in order to predict Bioclim climate variables for *M. milleri* (table 2.3.3). These predicted variables were then compared with independently derived estimates of paleoclimatic data from the Allenby Formation (table 2.1). Examining the climate of modern and predicted fossil species shows that Bioclim variables were comparable for

Table 2.6: Bioclim climate variable for *Metasequoia glyptostroboides* and estimates derived for *M. milleri* from CCA

Bioclim variable	*Metasequoia glyptostroboides*		*Metasequoia milleri*	
	Mean ± SE	Range	Mean ± SE	Range
Bio 1 (ºC)	11.6 ± 0.7	6.0–16.9	11.8 ± 0.3	9.9–15.2
Bio 2 (ºC)	7.7 ± 0.3	5.5–11.7	4.5 ± 0.2	2.5–7.6
Bio 3 (%)	30.3 ± 1.0	23.2–39.6	26.3 ± 1.1	19.7–41.1
Bio 4 (ºC)1	668.8 ± 32.8	441.4–1121.2	450.3 ± 19.5	288.8–730.3
Bio 5 (ºC)	24.0 ± 1.0	18.4–32.1	19.9 ± 0.5	16.1–24.3
Bio 6 (ºC)	-2.0 ± 0.7	-10–3.2	3.52	Not Available[2]
Bio 7 (ºC)	25.9 ± 1.1	18.4–42.1	16.5 ± 0.7	10.2–26.9
Bio 8 (ºC)	15.5 ± 1.5	4.8–26.6	9.5 ± 0.4	7.2–13.9
Bio 9 (ºC)	6.2 ± 1.1	-2.1–19.8	5.0 ± 0.1	4.0–6.2
Bio 10 (ºC)	19.8 ± 0.8	15.5–26.6	17.6 ± 0.5	14.5–21.5
Bio 11 (ºC)	3.5 ± 0.6	-2.8–9.0	6.6 ± 0.4	2.3–10.3
Bio 12 (mm)	839.4 ± 58.5	542–1461	835.8 ± 28.7	646.2–1117.9
Bio 13 (mm)	119.7 ± 13.7	61–240	88.9 ± 5.0	28.8–137.8
Bio 14 (mm)	35.2 ± 3.5	2–71	39.9 ± 1.7	27.8–58.6
Bio 15 (%)	37.9 ± 6.5	11.1–136.0	1.96 ±2.6	-21.4–30.3*
Bio 16 (mm)	322.4 ± 34.2	169–652	267.7 ± 13.2	112.7–368.5
Bio 17 (mm)	119.2 ± 11.1	7–249	136.4 ± 6.4	89.4–205.7
Bio 18 (mm)	292.7 ± 34.4	140–632	262.6 ± 11.6	106.0–368.5
Bio 19 (mm)	142.8 ±15.9	7–313	128.3 ± 7.1	75.6–202.9

Note: Refer to table 2.3.2 for each Bioclim climate variable.
SE = standard error.
[1] Bio 4 calculated using standard deviation multiplied by 100 (Fick and Hijmans, 2017).
[2] derived from CCA estimated variable, subtracting Bio 7 from Bio 5 (see methods).
Value not possible, cannot have negative precipitation.

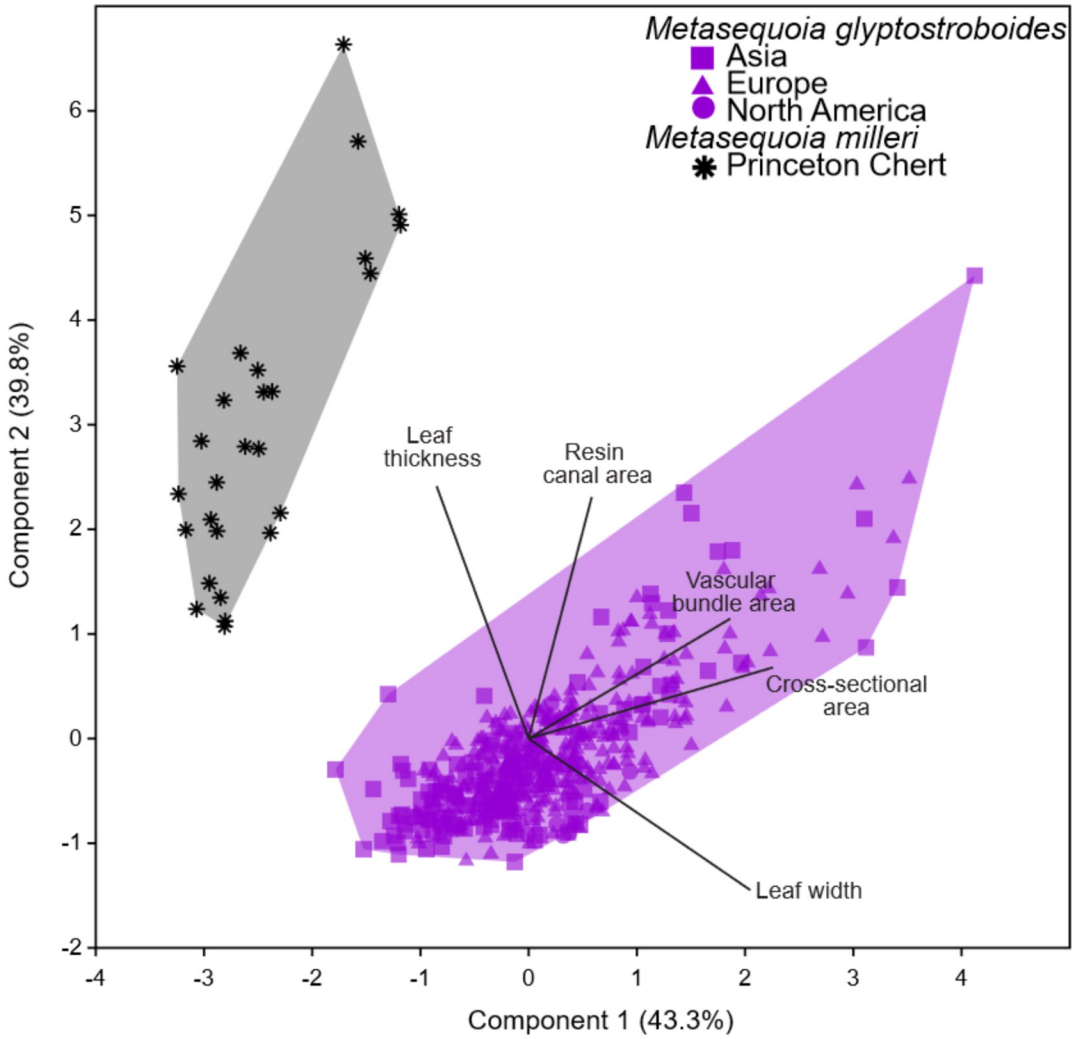

Figure 2.11: Principal components analysis (PCA) of leaf anatomical traits between *Metasequoia glyptostroboides* and*Metasequoia milleri*. PC 1 explains 52.8% of the variance and most correlated with cross-sectional area. PC 2 (31.5%) is most correlated with leaf width.

MAT and MAP, isothermality (Bio 3), maximum temperature of the warmest month (Bio 5), mean temperature of the warmest quarter (Bio 10), and precipitation of the coldest quarter (Bio 19; table 2.3.3). Mean (temperature) diurnal range (Bio 2), temperature seasonality (Bio 4), temperature range (Bio 7), mean temperature of the wettest quarter (Bio 8), and mean temperature of the driest quarter (Bio 9) were lower for *M. milleri* than for *M. glyptostroboides*. Two variables were out of range: precipitation seasonality (Bio 15) was very low and mean temperature of coldest quarter (Bio 11) was about double that of *M.*

glyptostroboides. Minimum temperature of the coldest month (Bio 6) was not estimated for *M. milleri* but was calculated by subtracting the estimated temperature range (Bio 7) from the maximum temperature of warmest month (Bio 5).

My climate estimates for *M. milleri* are comparable to previous studies (tables 1, 7). LMA-derived estimates of MAT in Quilchena (MAT 15.0º ± 0.6º C) and One Mile Creek (13.1º ± 3.1º C; Greenwood et al., 2005) are warmer than the estimated MAT of 11.8º ± 0.3º C, but the estimated value falls within the range of error for One Mile Creek. CLAMP-based estimates of MAP (Greenwood et al., 2005) for One Mile Creek (1140 ± 20 mm yr^{-1}) and Quilchena (1260 ± 280 mm yr^{-1}) are higher than the estimate of 836 ±29 mm yr^{-1} (tables 1, 7). Bioclimatic analysis estimated CMMT of 5.3º ± 2.8º C at One Mile Creek and 5.8º ± 2.0º C at Quilchena. Estimates of minimum temperature of the coldest month (Bio 6) and mean temperature of the coldest quarter (Bio 11), the Bioclim variables closest to CMMT, were within range, calculated at 3.5º and 6.6º ± 0.4º C,respectively. Sensitivity analysis showed that for each trait, ANOVA was not statistically significantly different among groups except for Bio 11, where $p<0.05$. However, pairwise t-tests showed that each model that was increased one trait at a time by 25% was not statistically different ($p>0.05$) from estimated climate of *M. milleri*.

2.4 Discussion

From the Eocene to present, the climatic niche and habitat of *Metasequoia* shifted to its modern state. The fossil occurrences of *Metasequoia* recorded changing forests in the Cenozoic, possibly as a result of cooling climate and increased aridity (fig. 2.1; LePage, 2007; Tang et al., 2011; Pittermann et al., 2012). From the Paleogene to Neogene, *Metasequoia* transitioned from inhabiting diverse ecosystems with other conifers, such as *Glyptostrobus* (Cupressaceae), in lowland swamps to occupying mesic forests with *Cunninghamia* (Cupressaceae; LePage, 2007; Tang et al., 2011). Similar to its

fossil relatives, extant *Glyptostrobus* grows in floodplain habitats of southeast China and northern Vietnam (Farjon, 2005). The fossil record also demonstrates that *Glyptostrobus*, like *Metasequoia*, was found throughout the Northern Hemisphere and contracted its distribution during the late Miocene with global change (LePage et al., 2005; LePage, 2007; Liu et al., 2007). By the late Pliocene, both these taxa were found only in eastern Asia. A paleoenvironment analysis of the late Pliocene Kobiwako Group of central Japan showed evidence of habitat partitioning between *Glyptostrobus* and *Metasequoia*. *Metasequoia* was not found with *Glyptostrobus* in the hydric peat-forming layers but with species that are mesic inhabiting (Yamakawa et al., 2017). This mesic habitat is more similar to its modern habitat, consisting of an herbaceous understory and mixed forest with other deciduous angiosperms (Tang et al., 2011). By investigating leaf anatomy within a tree and across climate gradients in *M. glyptostroboides*, I test modern plant response with fossils and have shown changes in leaf anatomy over time and estimated past climate using a multivariate method that closely matches published studies. This approach could be applied more generally to other fossil conifers to improve paleoclimate and paleoenvironmental inferences.

2.4.1 Variation Within and Between Trees

Leaves analyzed from a single tree showed the most variance in cross-sectional area and resin canal area, whereas across many trees, variation was best explained by cross-sectional area and leaf width. Differences observed in leaf anatomy between Matthaei and Nichols samples likely reflect differences in physiology, such as hydrostatic gradient, or environment, such as photosynthetic ability due to the amount of light. PCA of individual trees at varying heights combined with samples from a climatic gradient show that while the morphospace of individual trees is substantial, it is nested within the morphospace of all modern *Metasequoia* sampled across climate gradients (fig. 2.9). Thus, the variation between trees, and along climate gradients, was interpreted as more important. I observe

Table 2.7: Variation within a tree showing significant pairs of pairwise t-test using Bonferroni Adjustment

Trait	Sample number	Pair	p-value
Cross-sectional area	MN18-12, MN18-27	MBG ic 3m and ic 6.5 m	***
Vascular bundle area	MN18-11, MN18-12	MBG ic 5 m and ic 3m	*
	MN18-11, MN18-27	MBG ic 5m and ic 6.5 m	*
	MN18-10, MN18-27	MBG oc 5m and ic 6.5 m	***
	MN18-12, MN18-27	MBG ic 3m and ic 6.5 m	***
	MN18-13, MN18-27	MBG oc 3m and ic 6.5 m	**
Leaf width	MN18-10, MN18-27	MBG oc 5m and ic 6.5 m	***
	MN18-12, MN18-27	MBG ic 3m and ic 6.5 m	***
	MN18-13, MN18-27	MBG oc 3m and ic 6.5 m	*
Leaf thickness	MN18-12, MN18-27	MBG ic 3m and ic 6.5 m	***
	MN18-13, MN18-27	MBG oc 3m and ic 6.5 m	*
	MN18-20, MN18-22	NA oc 1 m and oc 6.5 m	***
	MN18-20, MN18-23	NA oc 1 m and oc 8 m	*

MBG = Matthaei Botanical Garden; NA = Nichols Arboretum; ic = inner canopy; oc = outer canopy.
All pairs are statistically significant using Bonferroni adjustment: * $p<0.05$, ** $p<0.01$, *** $p<0.001$

with increasing height a general trend of increasing cross-sectional area and vascular bundle area, leaf width, and leaf thickness, but no strong correlations ($r<0.5$) were found (fig. 2.5). Instead, I found that leaves from Matthaei at 6.5 m (highest) were the most statistically different from other canopy heights in all traits but resin canal area ($p<0.05$). However, samples at both 3m (lowest) and 5m were not statistically different from each other (table 2.7). I was able to sample only within ∼8 m from the ground with available equipment, and the trees I sampled from (∼15–20 m tall) are less than half the maximum height of *Metasequoia* (∼45 m; Farjon, 2005).

My data capture only a small fraction of height but show that leaf anatomy varies at different canopy heights in both trees. The PCA (fig. 2.9) morphospace overlap is strongly correlated with leaf thickness, vascular bundle area, and cross-sectional area, which may be explained by similarities in physiology such as general hydraulic conductivity (vascular bundle area) or photosynthesis (leaf thickness), while non-overlapping regions reflect differences of habitats such as shade (leaf width).

While angiosperms have shown a tendency for shade leaves to be thin, with lower

stomatal density and thinner leaf cuticle (Ashton and Berlyn, 1994), not all species respond in this way. Some responses are species specific and depend on leaf position and climatic seasonal variation (Sperlich et al., 2015). Studies on Pinaceae found that leaf shape and angle influence plant physiology (Jordan and Smith, 1993; Smith et al., 1997; Sperlich et al., 2015). Relatively flat and thin leaves such as those of *Abies nordmanniana* (Steven) Spach (Pinaceae) had higher light interception at higher angles than thicker leaves (Jordan and Smith, 1993). Leaf angle and thickness combined with the varying habitat and habit of *Metasequoia*—branches that are either horizontal or curve upward (Farjon, 2005)—may explain the differences I found between Matthaei and Nichols. Matthaei was exposed to full sun in a habitat that is flat and seasonally waterlogged and had branches that curved upward, while Nichols grew in more shaded conditions on a slope, very close to another *Metasequoia* with horizontal branches. The tree habit and leaf thickness of Matthaei may reflect a high amount of light received, with thinner leaves and branches that curved upward. Leaf anatomy of *Sequoia sempervirens* (Cupressaceae), a taxon closely related to *M. glyptostroboides*, was investigated along a height gradient to study differences in leaf morphology (Oldham et al., 2010). Leaves at the top of the *S. sempervirens* crown are more scale-like and thicker than the leaves at the bottom; this leaf dimorphism has been interpreted as reflecting differences in sun and shade leaves (Ellsworth and Reich, 1993; Niinemets et al., 1998; Koch et al., 2004; Ishii et al., 2008; Mullin et al., 2009). Oldham et al. (2010) sampled leaves at the OC and IC at 10-m intervals on trees as tall as 113 m and showed that hydrostatic gradient was responsible for the variation of leaf shape and leaf thickness, not solar radiation. Investment of water transport tissue in high canopy leaves of *S. sempervirens* also supports investment in photosynthesis, regardless of limited photosynthetic capacity (Jennings, 2002; Oldham et al., 2010). Whether *Metasequoia* similarly invests in water transport tissue remains to be tested; my data show a trend similar to *Sequoia*, with increased leaf thickness with height, though sampling from higher branches is needed to test this further. Leaves from the same site and tree, even branchlet,

do not overlap in PCA or CCA, which is expected from these results of variation in leaf anatomy at different heights. This plasticity of traits is most likely caused by varying microclimate and habit, demonstrated in my results of variation within a tree. While increased sampling will provide stronger and clearer relationships between leaf anatomy and canopy height, both PCA and sensitivity analysis suggest that sampling at the lowest canopy captures sufficient variation across climate gradients and within a tree. Combined with the results from the sensitivity analysis of the predictive model, I consider that the random sampling of leaves from fossils—where I do not know their canopy position—is not likely to be a major bias in this study.

2.4.2 Leaf Anatomy over Geologic Time

While gross morphology of *Metasequoia* leaves has remained relatively static (Liu et al., 1999; Stockey et al., 2001; LePage et al., 2005), the data show that leaf anatomy has not. Comparing leaf anatomy of *M. glyptostroboides* with that of *M. milleri* showed that each species occupied a separate morphospace, with absolutely no overlap (fig. 2.11). This may be a reflection of the overall shape of the leaf cross-sectional area, with leaves of*M. milleri* appearing more triangular than the oblong-shaped leaves of *M. glyptostroboides* (fig. 2.8). Leaves of *M. milleri* are statistically ($p<0.05$) smaller in cross-sectional area, vascular bundle area, and leaf width and statistically larger in resin canal area and leaf thickness than leaves of *M. glyptostroboides*. Overall, the data suggest that the genus had a broader morphospace in the past. *Metasequoia* also includes the extinct species *M. foxii* and *M. occidentalis* (Chaney, 1950; Liu et al., 1999; Stockey et al., 2001), which are predominantly preserved as compression/impression fossils. Additional data from other fossil taxa would clarify how morphospace has shifted or contracted over time and ultimately provide insights into how strong and universal the climate-trait relationships observed here are.

2.4.3 Leaf Anatomy–Climate Links

Since the rediscovery of living *Metasequoia* in the 1940s, seeds and seedlings were sent to numerous institutions worldwide and grown (Hendricks and Søndergaard, 1998; LePage et al., 2005). Institutions that successfully grew these trees helped calibrate my understanding of climatic tolerance in *M. glyptostroboides*, which is much larger than its natural habitat. My analysis shows that extant samples fall primarily in seasonally hot and wet climates. By combining anatomy with climate, I created a trait-climate model of *M. glyptostroboides*, which I applied to fossils to predict past climates.

Investigating leaf anatomy in *Metasequoia* across climate gradients has shown how anatomy responds to a variety of climate and environmental variables within a species. Individual anatomical traits did not correlate ($r>0.5$) with any individual climate variables (Appendix table A.2). For simplification in my analysis, climate vectors were grouped based on clustering of vector into sets of six climate groupings (table 2.3.2). These climate groupings (daily temperature fluctuations, mild cold-season temperatures, high mean annual temperature, high warm-season precipitation, high temperature seasonality, and high cold-season precipitation) reflect the growing environments sampled. While individual anatomical variables did not correlate with any single climate vectors, they appear to correlate with climate groupings: resin canal area and leaf thickness correlated with mild cold-season temperatures, vascular bundle area correlated with high warm-season precipitation, and leaf width and cross-sectional area correlated with high cold-season precipitation (fig. 2.10).

Comparing climate variables from my sampling sites illustrates the similarity between different localities. CCA shows no grouping of samples by continent, suggesting that there is not a geographical bias within the data. Temperature range (Bio 7) is part of the high temperature seasonality climate grouping, and my data set shows a range of 18.4° to 42.1°C. The largest fluctuations are seen in coastal and continental China; in Beijing,for example, maximum temperatures reach 32.1°C, and minimum temperatures reach 210.0°C.

The lowest temperature range is recorded in Liverpool (UK), where maximum temperatures reach 19.2°C and minimum temperatures reach 0.8°C. Isothermality (Bio 3), or daily temperature fluctuations, range from 22.54% to 39.63% across my samples. Maximum isothermality was recorded in Kunming (Yunnan, China) at 39.63%, followed by Bordeaux (France) at 39.55%. Lowest isothermality was recorded in Shanghai (China) at 22.54%, followed by Copenhagen (Denmark) at 25%.

I used CCA to predict climate variables for *M. milleri* (table 2.3.3). Predicted climate was similar to *M. glyptostroboides* for temperature and precipitation variables; however, more seasonal climate variables, such as precipitation seasonality (Bio 15), mean diurnal (temperature) range (Bio 2), temperature seasonality (Bio 4), and temperature range (Bio 7), were lower. Overall, predicted climate for *M. milleri* is a warmer and less seasonal climate, which is in line with other data about *M. milleri*'s habitat based on depositional environment, modern analogs, and nearby reconstructed climates (Basinger, 1981; Cevallos-Ferriz et al., 1991; Wing and Greenwood, 1993; Wolfe, 1994; Greenwood and Wing, 1995; Wolfe et al., 1998; Greenwood et al., 2005). My data support a shift in climatic niche within the genus, as the realized climatic tolerance of *M. milleri* does not match the fundamental climatic tolerance of *M. glyptostroboides*.

The Princeton Chert has been interpreted as a near-shore/shallow lacustrine deposit, suggesting that plants grew in a swamp-like, flooded environment (Basinger, 1981; Cevallos-Ferriz et al., 1991), not dissimilar to other occurrences of extinct *Metasequoia* that are interpreted as growing in floodplain wetland habitats from the Eocene to Miocene (Momohara, 2005).

These forest-dominated floodplains have been similarly described as comparable in biomass and annual productivity to modern *Taxodium* (Cupressaceae) forests, which occupy swamps and riparian habitats in southeastern North America (Williams et al., 2003); however, this remains to be explicitly tested. Sampling more species of conifers, especially the closely related *Taxodium distichum*, will potentially improve our characterization and

modeling of leaf anatomy–climate relationships.

Paleoclimate estimates for nearby early Eocene fossil sites in the Okanagan Highlands (Quilchena and One Mile Creek, Allenby Formation; 16 km north of Princeton Chert) show climates similar to estimated climate. LMA-based estimates for MAT reconstructed a warmer Quilchena (15.0º ± 0.6º C) than One Mile Creek (13.1º C ± 3.1º C; Greenwood et al., 2005) and closely matched my estimated MAT of 11.8º ± 0.3º C based on leaf anatomy–climate model. However, MAP estimate was lower than previous paleoclimate estimates at nearby sites. Using the CLAMP method, MAP was estimated at 1140 ± 20 mm yr^{-1} for One Mile Creek and at 1260 ± 280 mm yr^{-1} for Quilchena, both higher than my estimate of 836 ± 29 mm yr^{-1} (Greenwood et al., 2005, table 2.3 and 2.4). Bioclimatic analysis used in Greenwood et al. (2005) estimated a CMMT of 5.3º ± 2.8º C at One Mile Creek and 5.8º ± 2.0º C at Quilchena. This is comparable to the equivalent of both Bioclim variables minimum temperature of the coldest month (Bio 6) and mean temperature of the coldest quarter (Bio 11), calculated at 3.5°C and estimated at 6.6º ± 0.4º C model for *M. milleri*. My estimates overall are on the lower end of the range of the estimates from other approaches. This predicted climate for the extinct *M. milleri* is similar to climate reconstructed in previous studies using linear regression and multivariate analysis of eudicot leaves. I performed a sensitivity analysis by increasing the size of a trait of *M. milleri* by 25%, which did not change climate estimates significantly. Finding additional anatomically preserved *Metasequoia* fossils will permit further testing and validation of my findings here.

2.5 Conclusions

Conifers have been used in bioclimatic analyses to infer past climates, yet this generally assumes that the climatic niche of closely related species is the same. This is a necessary assumption in one sense, but in order to refine our understanding of paleoenvironments

and interactions between plants and climate on a geologic timescale, we need to test this assumption. Quantifying relationships between morpho-anatomy and environment provides one approach to do this. Little is understood or known about intraspecific variation of conifer leaf anatomy and how conifer leaf anatomy responds to and reflects climate, let alone environment.How anatomical variation corresponds to climatic differences, and whether this relationship applies to all conifers or, more generally, all plants, is virtually unknown. However, future research into leaf anatomy–climate relationships could provide insights into evolutionary and ecological processes, such as how plants track habitats, and selection processes at an ecophysiological level. Here, I aim to understand and unravel how leaf anatomy within individual trees and across climatic gradients of *M. glyptostroboides* varies and the link to climate.

Within a tree, the highest variability was found within cross-sectional area (223,529.8–562,210.5 μm^2) and resin canal area, and across a climatic gradient, the highest variability was found within cross-sectional area (140,944.4–970,908.3 μm^2) and leaf width.

Leaf anatomy is integral to gross leaf morphology, which in *Metasequoia* has been considered to be in evolutionary stasis over geologic time (Liu et al., 1999; Stockey et al., 2001; LePage et al., 2005). With anatomically preserved fossils, I tested whether this stasis extended to leaf anatomy and showed that this group is not in anatomical stasis. *Metasequoia milleri* occupies a distinct leaf-anatomical morphospace from *M. glyptostroboides*, with smaller cross-sectional area, vascular bundle area, and leaf thickness than *M. glyptostroboides* but larger resin canal area and leaf width. Preservation bias of fossils prevents us from testing other *Metasequoia* species, since the majority of *Metasequoia* fossils are compressions/impressions. Regardless of whether these other species occupy a morphospace that overlaps in part with that of *M. glyptostroboides*, the fact remains that the *Metasequoia milleri* morphospace no longer exists. The fossil record of *Metasequoia* throughout the Cenozoic has shown a shift with global climate.

My paleoclimate interpretations based on anatomy and modern climate suggest that *M. milleri* inhabited a warmer, less seasonal climate than extant *Metasequoia*, which grows in a seasonal temperate climate today, and thus support previous interpretations of environmental and habitat shifts in *Metasequoia* (LePage et al., 2005; Tang et al., 2011).

I also show that variation of leaf anatomy across climate gradients in *M. glyptostroboides* correlates with climate in a multidimensional analysis. Specifically, vascular bundle area correlates with high warm-season precipitation, leaf width and cross-sectional area correlate with high cold-season precipitation, leaf thickness correlates with mild cold-season temperatures and high mean annual temperatures, and resin canal area correlates with daily temperature fluctuations and mild cold-season temperatures. While the relationship between anatomical features and climate needs further refinement, this study demonstrates the potential utility of investigating the anatomy of conifers and other plants on broad spatial and temporal scales to better characterize climatic niche.

CHAPTER 3

Distinct anatomy but convergent physiology in leaves of three closely related Cupressaceae trees

Abstract

Ideally, a deep understanding of plant response to climate should cover all plant groups broadly. Our understanding of plant-climate links in conifers is continuously developing. Previous research has connected leaf anatomical and physiological response to their growing environment, providing a foundation to investigate leaf anatomy and physiology across broad climatic gradients. I explicitly test how inter- and intraspecific variation of leaf anatomy and physiology relate to climate across a wide climatic gradient with three species of Cupressaceae: *Metasequoia glyptostroboides*, *Sequoia sempervirens*, and *Taxodium distichum*. Leaf samples were collected from Asia, Europe, and North America (39 sites, 149 trees sampled). Five anatomical traits were measured from leaf cross sections: cross-sectional area, resin canal area, vascular bundle area, leaf width, and leaf thickness. Physiological traits that are proxies for photosynthesis were also collected and analyzed: carbon and nitrogen content, and isotopic photosynthetic discrimination of carbon (Δ_{leaf}). Bivariate correlations, principal components analysis (PCA), and canonical correspondence analysis (CCA) were used to determine trait links to climate. PCA showed that each taxon occupied a mostly separate anatomical morphospace, but overlapped in physiological traits. Across taxa, strong associations exist between cross-sectional area

with temperature seasonality and precipitation of coldest quarter, leaf width with MAP, and leaf thickness with isothermality. These relationships did not hold in individual species trait-climate relationships except for cross-sectional area with precipitation of coldest quarter in *Metasequoia* and *Sequoia*. *Metasequoia* and *Sequoia* show climatic niche conservatism and partitioning compared to their more distant relative (*Taxodium*). No correlations were found in vascular bundle area nor Δ_{leaf}. By investigating more species, we can further refine the relationships found in this study and ultimately test how leaf anatomy and physiology of conifers broadly reflect climate.

3.1 Introduction

Climatic links to leaf physiognomy have provided significant insights to and important implications of ecological and evolutionary processes, *e.g.* increased leaf vein and stomatal density over the Cenozoic has improved angiosperm photosynthetic efficiency (Boyce et al., 2009, 2010; Beerling and Franks, 2010). Reconstruction of past climatic variables have relied on the relationships observed between woody non-monocot angiosperm leaves and modern climate (Bailey and Sinnott, 1915; Wolfe, 1994; Wilf et al., 1998; Huff et al., 2003; Royer et al., 2005; Peppe et al., 2011). The focus on angiosperm plant response means our analytical scope of past climates is restricted to their evolution and ecological dominance, $\sim$140 Ma and 125 Ma respectively (Crane and Lidgard, 1989), which is short compared to the 425 million year evolutionary history of terrestrial plants. Conifers, which have a longer evolutionary history that dates back to $\sim$300 Ma (Clayton, 1996; Taylor et al., 2009; Leslie et al., 2012), dominated terrestrial landscapes prior to angiosperms yet their relationship to climate is not as well understood. By extending our studies to conifers, we can expand our spatial and temporal analytical scope and deepen our knowledge of how conifers broadly respond to their climate.

Conifer leaves show variations within their anatomy that reflect physiological

differences within and between individuals, such as increases or decreases in mesophyll mass which in turn affects photosynthetic capacity (Niinemets et al., 2007; Wyka et al., 2012). Most conifers are known for their needle-like (*e.g.* *Pinus* spp. L.; pine trees) and scale-like (*e.g.* *Cupressus* spp. L.; cypress trees) leaves. These leaves often maintain a more-or-less cylindrical to flattened-cylindrical form undergoing physiological trade-offs of different leaf anatomical layers; a vascular system surrounded by an endodermis, then mesophyll, all encased by an often sclerotic hypodermis and an epidermis. In contrast, typically most angiosperm leaves are flat and broad and a reticulate vascular system within the mesophyll layers, all enclosed by the outermost epidermis. Compared to the physiologically constrained conifer leaves, this planar, sheet-like construction, allows angiosperms to modify their leaf size and shape in response to environmental conditions.

Research conducted on select species within Pinaceae (pine family) and Cupressaceae (cypress and redwood family) have demonstrated conifer leaf anatomy and physiological links to their growing environment or climate (Niinemets and Kull, 1995; Wyka et al., 2012; Laforest-Lapointe et al., 2014; Ng and Smith, 2020). Anatomical traits have been linked to climate in *Metasequoia glyptostroboides* H. H. Hu & W. C. Cheng (Cupressaceae; Chapter 2, Ng and Smith, 2020), providing a foundation to test closely related conifers. These traits were strongly associated to climatic variables: increased leaf width and cross-sectional area strongly associated with high cold-season precipitation, increased vascular bundle area with high warm-season precipitation, increased leaf thickness with mild cold-season temperatures and high mean annual temperatures, and increased resin canal area with daily temperature fluctuations and mild cold-season temperatures. Adding physiological traits, such as photosynthetic proxies using carbon/nitrogen content and stable carbon isotopes, provides another layer with which we can better quantify conifer response to climate. Understanding intraspecific variability of leaf anatomical and physiological response across closely related conifers is a start to understand trait-climate relationships across all conifers.

Cupressaceae are a family in which testing anatomical and physiological relationships

to climate has interesting evolutionary implications. These conifers are found predominately in the Northern Hemisphere, and include well-known trees such as juniper, cypress, and redwoods. They are diverse in vegetative morphology and habitat, found from arid regions to deep-shaded swamps (Farjon, 2005). Focusing on Cupressaceae provides insights and opportunity to link leaf anatomy of diverse leaf morphologies across distinct environments.

In this chapter, I test these relationships across three closely related Cupressaceae taxa: *Metasequoia glyptostroboides*, *Taxodium distichum* (L.) Rich. and *Sequoia sempervirens* (D. Don) Endl (Gadek et al., 2000; Farjon, 2005). These taxa occurred in forests across the Northern Hemisphere during the Cretaceous and Paleogene, demonstrating an overlap in climatic tolerance, in contrast to their present-day non-overlapping distributions (LePage et al., 2005). *Taxodium* is found in lowland swamps of south eastern North America and Central America, *Sequoia sempervirens* occupies lowland coastal summer dry winter wet northern California, and *Metasequoia* occurs in the temperate deciduous forest of a small valley in the Hubei Province of central China (although often grown horticulturally worldwide; Farjon, 2005; Tang et al., 2011). Here I answer how the leaf anatomy and physiology of *Metasequoia*, *Sequoia*, and *Taxodium* respond to their environment across climatic gradients. These results build upon previous research and aims to characterize plant-climate links in closely related conifers, ultimately to aid in our understanding of whether variation in leaf anatomical and physiological links to climate is uniform across all conifers.

3.2 Methods

3.2.1 Collection

Samples of *Taxodium distichum*, *Sequoia sempervirens*, and *Metasequoia glyptostroboides* were collected from natural and cultivated trees across North America,

Asia, and Europe during 2016 and 2017 (fig. 3.1; Appendix table A.1, B.1). These sites were determined by both natural distribution and climatic gradient and where permission was obtained from national parks, state parks, and botanical gardens. Latitude and longitude locations were taken with a Garmin eTrex Venture HC (WGS84) GPS. Five to ten branchlets (about 1–3 m from ground) from up to three trees per site were collected for a total of 39 sites and 149 trees sampled. Samples were split, with three branchlets fixed in formalin propionic acid (FPA) or 100% ethanol (when travel restricted the use of FPA) for anatomy (115 of 149 samples), and the rest dried in silica for elemental and isotopic analysis (n=149). Samples kept in FPA or ethanol were transferred after at least 24 hours to 70% ethanol for long term storage. Samples stayed in 70% ethanol for at least one week prior to paraffin processing. Vouchers from each site are deposited at the University of Michigan Herbarium (MICH).

3.2.2 Anatomy

For each sample, three leaves from the middle of each branchlet (n=9 per sample) were embedded into paraffin (after Johansen et al., 1940) using an automated paraffin tissue processor (Leica ASP 300) and tissue embedding station (Tissue-Tek) at the University of Michigan Microscope and Imaging analysis Laboratory (MIL), now Orthopedic Research Laboratory (ORL). Once embedded, these samples were sectioned at 10 μm thick at MIL/ORL using a Leica 2215 and Leica 2235 rotary microtome then adhered to slides with Mayer's Albumen Adhesive (one part egg white, one part glycerin, and 1g sodium benzoate) or Haupts Adhesive (Dorn & Hart Microedge Inc., USA). Slides were then stained with 0.1% toluidine blue O solution in 0.1 M benzoate buffer, pH 4.4 (Yeung, 1998) in a xylene and ethanol series (after Johansen et al., 1940), and finally mounted with Eukitt mounting medium (O. Kindler, Germany). Photographs of each leaf were taken on Nikon Eclipse LV100ND microscope with a Nikon DS-Fi2/DS-U3 camera unit. Five anatomical features were measured: cross-sectional area, vascular bundle area, resin

canal area, leaf thickness, and leaf width (after Ng and Smith, 2020) using Nikon Imaging Software Elements v4.30.

3.2.3 Physiology

Once leaves were dried for each accession, samples were ground to a fine powder using a mortar and pestle, then stored in vials. To prepare for elemental analysis of carbon (%C) and nitrogen (%N) content within leaves, two replicate aliquots (∼0.625 mg) of each sample were loaded into tin capsules. These were analyzed with a Costech ECS 4010 Elemental Analyzer (EA) at the University of Michigan Earth System Science lab, calibrated using acetanilide (71.09% C, 10.36% N) and atropine (70.56% C, 4.84% N) standards, then averaged for each sample. For isotopic analyses, two replicate aliquots (∼0.750 mg) of each sample were loaded into tin capsules. These were analyzed with a Picarro Cavity Ring-Down Spectrometer (CRDS) G2201-i at the University of Michigan Earth System Science lab, reported in standard delta-notation as δ^{13}C values relative to the PDB scale and calibrated against acetanilide (-28.17‰; Costech code 031040), IAEA-600 caffeine (-27.77‰), and IAEA-CH-6 sucrose (-10.45‰), then averaged for each sample. To calculate the carbon isotopic composition (δ^{13}C), the output from the CRDS was corrected with the standards (measured vs. expected) using linear regression. The resulting δ^{13}C was then used to derive photosynthetic discrimination (Δ_{leaf}; equation 1), the difference of carbon fractionation between the leaf and atmosphere (Farquhar, 1989; Diefendorf et al., 2010). $\delta^{13}C_{atm}$ was determined from NOAA (Trolier et al., 1996), ranging from -8.0‰ to -8.5‰.

$$(1) \qquad \Delta_{leaf} = \frac{\delta^{13}C_{atm} - \delta^{13}C_{plant}}{1 + (\delta^{13}C_{plant})/1000}$$

The linear relationship between Δ_{leaf} and the ratio of internal concentration (c_i) to atmospheric concentration (c_a) of CO_2 is expressed using equation (2) (Farquhar et al.,

1982; Seibt et al., 2008; Llorens et al., 2009).

$$(2) \qquad \Delta_{leaf} = a + (b - a)(c_i/c_a)$$

The isotopic fractionation of carbon in the air (a) is 4.4‰ (O'Leary, 1988) and by Ribulose-1,5-biphosphate carboxylase/oxygenase and phosphoenolpyruvate carboxylase (b) is 27‰ (Farquhar and Richards, 1984). By measuring δ^{13}C, I can then calculate Δ_{leaf} and c_i/c_a, in order to calculate the intrinsic water use efficiency (WUE), expressed in equation (3) (Farquhar, 1989; Llorens et al., 2009).

$$(3) \qquad WUE = \frac{[\mathrm{CO_2}](1 - c_i/c_a)}{1.6D}$$

Leaf-to-air vapor mole fraction deficit (D) was calculated using average vapor pressure deficit (VPD) extracted from WorldClim climate layers (after Seager et al., 2015). The present day ambient [CO_2] was obtained from the Scripps Institute of Oceanography for each collection month, August 2016–August 2018 (Keeling and Whorf, 2005).

3.2.4 Climate

Nineteen WorldClim Bioclim variables (Fick and Hijmans, 2017) at 30s resolution from all sample locations were extracted from sampling locations using Matlab R2015 (Matlab, 2015). Samples from urban or cultivated collections were considered unaffected by an added watering regime due to the nature of how these trees access water; *Sequoia* obtains an isotopically significant amount of foliar water from coastal fog in the summer months (Dawson, 1993) and xylem water isotopes in *Taxodium* demonstrates its access to ground water (White et al., 1985). Bioclim variables 5, 6, 13, and 14 were excluded from analysis, as they are similar to variables Bio 10, 11, 16, and 17. Maximum temperature of coldest and warmest month (Bio 5 and Bio 6) are similar to mean temperature of the warmest and coldest quarter (Bio 10 and Bio 11), and precipitation of wettest/driest month (Bio 13/14)

Table 3.1: Bioclim variables used in this study and their abbreviation

Bio 1	Annual Mean Temperature	MAT
Bio 2	Mean Diurnal Temperature Range	MDiR
Bio 3	Isothermality	Isoth
Bio 4	Temperature seasonality	Tseason
Bio 7	Temperature range	Trange
Bio 8	Mean Temperature of Wettest Quarter	MTWeQ
Bio 9	Mean Temperature of Driest Quarter	MTDrQ
Bio 10	Mean Temperature of Warmest Quarter	MTWaQ
Bio 11	Mean Temperature of Coldest Quarter	MTCoQ
Bio 12	Annual Precipitation	MAP
Bio 15	Precipitation seasonality	Pseason
Bio 16	Precipitation of Wettest Quarter	PWeQ
Bio 17	Precipitation of Driest Quarter	PDrQ
Bio 18	Precipitation of Warmest Quarter	PWaQ
Bio 19	Precipitation of Coldest Quarter	PCoQ

were similar to wettest/driest quarter (Bio 16/17). The Bioclim variables were given 3-7 letter codes for simplicity (M = mean, T= temperature, P= precipitation, We = wettest, Wa = warmest, Dr= driest, Co= coldest, Q= quarter; table 3.1).

3.2.5 Analysis and statistics

Anatomy and physiology measurements were standardized using z-score $[(x - mean(x)) \times [stddev(x)^{-1}]$. These measurements were then analyzed in both a principal components analysis (PCA) and then combined with climate data and analyzed in a canonical correspondence analysis (CCA) in PAST v3.19 (Hammer et al., 2001). Correlation and statistical (p-values and pairwise t-test) analyses were conducted in R Studio (Team et al., 2015).

Table 3.2: Leaf anatomical summary of measurements and statistics for *Metasequoia glyptostroboides*, *Taxodium distichum*, and *Sequoia sempervirens*.

		Metasequoia glyptostroboides	*Sequoia sempervirens*	*Taxodium distichum*
Cross- sectional area (μm^2)	mean $\pm$ sd,	413539.4 $\pm$ 98278.8,	797997.6 $\pm$ 210517.4	181496.1 $\pm$ 38390.9
	min–max	235749.1–648417.2	478764.5–1336646.8	107075–291283.6
Vascular bundle area (μm^2)	mean $\pm$ sd,	12747.0 $\pm$ 5597.5	9970.9 $\pm$ 2103.3	3713.7 $\pm$ 865.6
	min–max	4908.8–29482.7	7214.9–17292	1982.6–5885.5
Resin canal area (μm^2)	mean $\pm$ sd,	1353.3 $\pm$ 611.6	6406.3 $\pm$ 2302.6	1807.3 $\pm$ 1028.5
	min–max	433.5–3605.5	1936.5–9990.3	357.1–4259.3
Leaf width (mm)	mean $\pm$ sd,	1.95 $\pm$ 0.18	2.20 $\pm$ 0.35	1.03 $\pm$ 0.14
	min–max	1.43–2.31	1.63–2.80	0.71–1.32
Leaf thickness (mm)	mean $\pm$ sd,	0.26 $\pm$ 0.05	0.49 $\pm$ 0.08	0.23 $\pm$ 0.05
	min–max	0.17–0.41	0.38–0.68	0.14–0.35

Table 3.3: Leaf physiological summary of measurements and statistics for *Metasequoia glyptostroboides, Taxodium distichum,* and *Sequoia sempervirens.*

	Metasequoia glyptostroboides		*Sequoia sempervirens*		*Taxodium distichum*	
Traits	mean ± sd,	min - max	mean ± sd,	min - max	mean ± sd,	min - max
Δleaf (‰)	19.96 ± 1.13	17.14–22.87	21.00 ± 1.19	19.32–23.74	20.30 ±1.18	16.67–22.97
WUE (mmol CO_2 mol^{-1} H_2O)	2.01 ± 0.73	0.64–3.81	1.27 ± 0.63	0.51–3.39	1.29 ± 0.59	0.64–3.45
%C	45.92 ±2.11	42.13–49.45	46.31 ±1.42	44.36–50.28	48.25 ± 1.84	43.06–51.64
%N	1.87 ± 0.43	1.1–2.91	1.1 ±0.34	0.67–2.03	1.57 ± 0.45	0.75–2.41
C:N	25.9 ± 6.46	15.53–43.72	45.57 ±12.48	23.65–68.66	34.05 ± 12.54	19.06–67.61
ci/ca	0.69 ± 0.05	0.56–0.82	0.73 ± 0.05	0.66–0.86	0.7 ± 0.05	0.54–0.82

3.3 Results

3.3.1 Traits

In total, 992 leaf measurements were collected and averaged for 115 trees sampled. Averages were used in data analyses for *Metasequoia* (n=59 trees), *Sequoia* (n=25), and *Taxodium* (n=31).

3.3.1.1 Anatomy

Anatomical trait measurements and statistics (table 3.2, fig. 3.2) generally show *Sequoia* had the largest and *Taxodium* the smallest measurements for all traits, except *Taxodium* had a larger mean resin canal area than *Metasequoia*, and *Metasequoia* had a larger vascular bundle area than *Sequoia*. Mean resin canal area in *Metasequoia* measured 1353.3 $\pm$ 611.6 μm^2 (range: 433.5–3605.5 μm^2), in *Sequoia* measured 6406.3 $\pm$ 2302.6 μm^2 (1936.5–9990.3 μm^2), and in *Taxodium* measured 1807.3 $\pm$ 1028.5 μm^2 (357.1–4259.3 μm^2). Average vascular bundle area in *Metasequoia* measured 12747.0 $\pm$ 5597.5 μm^2 (4908.8–29482.7 μm^2), in *Sequoia* measured 9970.9 $\pm$ 2103.3 μm^2 (7214.9–17292.0 μm^2), *Taxodium* measured 3713.7 $\pm$ 865.6 μm^2 (1982.6–5885.5 μm^2). All anatomical traits were statistically different between species in an ANOVA ($p<0.001$) yet pairwise t-test using Bonferroni method showed resin canal area and leaf thickness in both *Metasequoia* and *Taxodium*, and vascular bundle area in both *Metasequoia* and *Sequoia*, were not statistically different from one another ($p>0.05$).

3.3.1.2 Physiology

Physiological traits had low variability between species for Δ_{leaf}, c_i/c_a, and %C, and modest variability for %N and WUE (table 3.3; fig. 3.3). Δ_{leaf} is highest in *Sequoia* at 21.00 $\pm$ 1.19‰ and *Metasquoia* has the smallest average at 19.96 $\pm$ 1.13‰. A reverse trend in WUE shows the highest average in *Metasequoia* at 2.01 $\pm$ 0.73 mmol CO_2 mol^{-1}

H_2O and *Sequoia* the smallest average at 1.27 $\pm$ 0.63 mmol CO_2 mol^{-1} H_2O. *Metasequoia* has the largest range and highest average of %N at 1.87 $\pm$ 0.43%, with the lowest average found in *Sequoia* at 1.57 $\pm$ 0.45%. However *Taxodium* had the highest average %C at 48.25 $\pm$ 1.84% instead of *Sequoia* which is at 46.31 $\pm$ 1.42%. All physiological traits were statistically different between species ($p<0.001$) in ANOVA while pairwise t-test using Bonferroni method showed Δ_{leaf} and c_i/c_a values in *Taxodium* were not statistically different from both *Metasequoia* and *Sequoia*, and WUE in *Sequoia* and *Taxodium* were not statistically different from one another.

3.3.2 Bivariate correlations between traits and climate

Both between and within taxa, correlations between anatomical traits and climate were stronger ($r>0.5$) and statistically significant using (ANOVA, $p<0.001$) than for physiological traits and climate (table 3.4). Cross-sectional area showed the strongest correlation ($r>0.60$) with PDrQ and PWaQ; resin canal area with Isoth, Tseason, and Pseason; leaf width with MTWeQ, MTWaQ, PDrQ; and leaf thickness with Isoth, Pseason, and PDrQ (table 3.4). Among physiological traits, correlations with temperature variables ($r>0.5$; MAT and MTWaQ, and Isoth, respectively) were found only for %C and %N and were statistically significant (ANOVA, $p<0.001$; table 3.4).

3.3.2.1 *Metasequoia glyptostroboides*

WUE of *Metasequoia glyptostroboides* was positively correlated with climate variables MAT, Pseason, PWeQ, PWaQ, and no strong correlations ($r>0.5$) were found between anatomy and climate (table 3.5). Other bivariate correlations were found between traits: cross-sectional area was correlated with all anatomical traits ($r>0.5$), vascular bundle area correlated moderately with resin canal area ($r= 0.57$) and strongly with leaf thickness ($r= 0.81$), and leaf thickness correlated strongly with resin canal area ($r= 0.72$) and moderately with leaf width ($r= 0.53$).

3.3.2.2 *Sequoia sempervirens*

Anatomy and climate in *Sequoia sempervirens* were correlated in both cross-sectional and vascular bundle area with MDiR, leaf thickness with MDiR, Pseason, and PDrQ, and WUE with MTWeQ and PWaQ (table 3.6), %N with MAT and MTWeQ, and both %N and %C correlated with PWaQ (table 3.6). Trait-trait correlations were found between: cross-sectional area moderately correlated with all anatomical traits (r>0.5), and leaf thickness strongly with both vascular bundle (r=0.84) and resin canal area (r=0.61). WUE is moderately correlated with both Δ_{leaf} (r= -0.62) and %C (r = 0.66). Leaf width moderately correlated with both Δ_{leaf} (r= 0.58) and WUE (r= -0.56).

3.3.2.3 *Taxodium distichum*

Cross-sectional and vascular bundle area within *Taxodium distichum* were moderately correlated with PDrQ (r=-0.68 and -0.66, respectively) and PCoQ (r=-0.66 and r= -0.61), and resin canal area strongly correlated with Pseason (r=0.71) and PDrQ (r=-0.54; table 3.7). Δ_{leaf} was moderately correlated with MAT (r=0.57) and MTCoQ (r=0.57), and %N was moderately correlated with Tseason (r=0.57; table 3.7. In addition, cross-sectional area was strongly correlated with leaf thickness (r=0.77). Cross-sectional area and leaf thickness were correlated with both vascular bundle (r= 0.74, r=0.56, respectively) and resin canal area (r= 0.50, r=0.68). Leaf width was moderately correlated with %C (r=-0.62). WUE was moderately correlated with Δ_{leaf} (r= -0.65).

3.3.3 Variation in anatomy and physiology across climatic gradients

3.3.3.1 Principal components analyses

Five principal components (PC) analyses were used to test relationships between different traits within and between taxa. In PCA of all anatomical traits (PCA$_anat$), PC 1 (68.3%) was strongly correlated with cross-sectional area and PC 2 (22.7%) with vascular

bundle area (Appendix table B.2). Each taxon occupied its own morphospace; *Metasequoia* and *Sequoia* occupied similarly large morphospaces while *Taxodium* occupied the smallest (fig. 3.4). To test redundancy in my variables, I repeated the analysis excluding one trait at a time. I found by excluding vascular bundle area (PCA$_{anat-vb}$), the variation explained by the first two axes increased to 96.5% from 91.0% in the data (Appendix table B.2). PC 1 (79.3%) was strongly correlated with cross-sectional area and PC 2 (17.2%) with leaf width (Appendix table B.2). *Sequoia* increased in morphospace size and overlapped *Metasequoia* sample MN17-18, while *Taxodium* increased its morphospace size with be similar to that of *Metasequoia* (fig. 3.4). PCA with only directly measured physiological traits (PCA$_{phys}$; *i.e.*, using only Δ_{leaf}, %C, and %N since WUE and c_i/c_a are linearly derived from Δ_{leaf}) showed PC 1 (43.1%) most strongly correlated with %N and PC 2 (37.4%) with %C (Appendix table B.2). Morphospace of all taxa overlapped. *Taxodium* had the largest morphospace and *Sequoia* the smallest (fig. 3.5). Each vector was correlated with one taxon: %N with *Metasequoia*, %C with *Taxodium*, and Δ_{leaf} with *Sequoia*. In PCA of both anatomical and physiological traits (PCA$_{anat+phys}$), PC 1 (45.7%) was highly correlated with cross-sectional area, and PC 2 (21.8%) with %N (fig. 3.6; Appendix table B.2). In this analysis, each taxon occupied its own morphospace, *Metasequoia* showed highest variation in %N, vascular bundle area, and leaf width, *Sequoia* in Δ_{leaf}, resin canal area, and leaf thickness, and *Taxodium* in %N and %C. Finally, I modified the analysis and omitted both vascular bundle area and Δ_{leaf} to reduce redundancy, decreasing the variation within the data. PCA$_{anat+phys-vb-\Delta leaf}$ increased the variation explained by the first two axes from 67.5% to 81.4%, where PC 1 (52.8%) is correlated with resin canal area and PC2 (24.5%) with %C (Appendix table B.2). *Metasequoia* overlapped both *Sequoia* and *Taxodium* in morphospace (fig. 3.6). *Taxodium* showed strongest variation with %N and %C, *Sequoia* with cross-sectional area, leaf thickness, and resin canal area, and *Metasequoia* with %N and leaf width.

3.3.3.2 Canonical correspondence analyses

Six different canonical correspondence analyses (CCA) were done for various combinations of traits to test for relationships between anatomical and physiological traits to climate variables (table 3.8). CCA$_{anat}$ combined all anatomical traits, and the first two axes explained 93.9% of the data (Appendix table B.3). *Metasequoia* occupied its own morphospace while *Sequoia* is nested in the large morphospace of *Taxodium* (fig. 3.7A). Axis 1 (84.8%) was most correlated with resin canal area and MDiR and Axis 2 (9.3%) with vascular bundle area and MTWaQ (table 3.9; Appendix tables B.5–B.7). CCA$_{anat-vb}$, similar to PCA$_{anat-vb}$ where vascular bundle area was omitted from the analysis to decrease redundancy, increasing the explained percent variance of the data from 93.9% to 97.3% (Appendix table B.3). Here, *Taxodium* occupied the largest morphospace and both *Metasequoia* and *Sequoia* had similar sized morphospaces, and *Metasequoia* overlapped both *Taxodium* and *Sequoia* (Appendix fig. B.4A). Axis 1 (88.8%) was most strongly correlated with resin canal area and MDiR, and Axis 2 with cross-sectional area and PDrQ (table 3.9, Appendix tables B.5–B.7). CCA$_{phys}$ combined physiological traits, Δ_{leaf}, %C, and %N. Axis 1 (74.1%) was most correlated with %N and Isoth, and Axis 2 (25.9%) with %C and MTWaQ (Appendix tables B.3, B.5–B.7). Morphospace of all taxa overlap (fig. 3.7) and are similar in size, with *Sequoia* slightly smaller. CCA$_{anat+phys}$ combined all anatomical and physiological traits, and the first two axes explained 90.5% of the variation in the data. Axis 1 (59.6%) was most correlated with resin canal area and Isoth, while Axis 2 was most correlated with vascular bundle area and MAT. CCA$_{anat+phys-vb}$ was similar to CCA$_{anat+phys}$ except vascular bundle area was again omitted. In CCA$_{anat+phys-vb}$ the first two axes explained 93.8% of the variation in the data with *Metasequoia* overlapping *Sequoia* and *Taxodium* (Appendix fig. B.4). Axis 1 (67.4%) was most correlated with resin canal area and PrDrQ and Axis 2 (26.4%) with leaf width and MAT (Appendix tables B.5–B.7). CCA$_{anat+phys-vb-\Delta_{leaf}}$ was similar to CCA$_{anat+phys}$ but both vascular bundle area and Δ_{leaf} were omitted. The first two axes of CCA$_{anat+phys-vb-\Delta leaf}$ explained 96.5%

of variance in the data. Axis 1 (69.6%) was most correlated with resin canal area and PDrQ. Axis 2 was most correlated with %C and MAT (Appendix fig. B.4C; Appendix tables B.5–B.7).

I repeated CCA analyses of anatomical traits with climate variables for *Sequoia* and *Taxodium* separately ($\text{CCA}_{Sequoia}$, $\text{CCA}_{Taxodium}$), using results from Chapter 2 (Ng and Smith, 2020) for *Metasequoia* as the data were unchanged. I used CCA scores to determine intraspecies associations for Axis 1 and 2 (Appendix tables B.8–B.10). *Sequoia* showed trait-climate associations between cross-sectional area and PCoQ, leaf width with MAP and PDrQ (fig. 3.8, Appendix table B.8). In *Taxodium*, cross-sectional area associated with MAP and MDiR, leaf width with PCoQ, resin canal area with PrWaQ, and leaf thickness with MTWaQ (fig. 3.8, Appendix table B.9).

In an attempt to have a deeper understanding of trait-climate links, I looked for repeated associations of trait and climate in each analysis using CCA scores for the first two axes to find most variation within the data (table 3.9, Appendix tables B.5-B.7). I found cross-sectional area was associated with Tseason in $\text{CCA}_{anat+phys}$ (Axis 1) and CCA of *Metasequoia* ($\text{CCA}_{Metasequoia}$) and $\text{CCA}_{Taxodium}$ (Axis 2), and PCoQ in $\text{CCA}_{Metasequoia}$ and $\text{CCA}_{Sequoia}$ (Axis 1) and CCA_{anat} (Axis 2). Leaf width showed an association with MAP for $\text{CCA}_{anat-vb}$ and $\text{CCA}_{Sequoia}$ (both Axis 2). Leaf thickness was associated with Isoth for $\text{CCA}_{anat+phys-vb-\Delta_{leaf}}$ (Axis 1) and $\text{CCA}_{anat+phys}$, $\text{CCA}_{anat+phys-vb-\Delta_{leaf}}$, and $\text{CCA}_{Metasequoia}$ (Axis 2).

3.4 Discussion

Overall, my findings highlight the importance of leaf anatomy and physiology within conifers, evolutionary implications of climatic niche, and a start in conifer leaf-climate links. Specifically, I found most leaf anatomical traits of *Sequoia* measured the largest and *Taxodium* the smallest, consistent with gross morphological observations. However,

I found insignificant statistical differences between vascular bundle area and leaf width, where *Sequoia* was not statistically different from *Metasequoia*, and resin canal area and leaf thickness, where *Taxodium* was not statistically different from *Metasequoia*. Leaf physiology was more nuanced, I found the highest and significantly different (from the other taxa; $p<0.05$) measurements of Δ_{leaf} and c_i/c_a for *Sequoia*, WUE and %N for *Metasequoia*, and %C for *Taxodium*. There was less differentiation between the lowest and second lowest physiological measurement, such that no statistical differences ($p>0.05$) were found. Across all sampled species, bivariate correlations between climate and anatomical traits were stronger and overall statistically significant than between climate and physiological traits. In PCA and CCA using anatomical traits, taxa occupied distinct to slightly overlapping morphospaces, while significant overlap between species was observed when physiological traits were incorporated. Repeated associations of traits and climate (table 3.9) were found for cross-sectional area with Tseason and PCoQ, leaf width with MAP, and leaf thickness with Isoth. Our bivariate correlations and ordination analyses (PCA and CCA) reflect the links between leaf anatomy and physiology to climate, discussed in the following sections.

3.4.1 Trait analysis

Metasequoia, *Sequoia*, and *Taxodium* once inhabited the same forests in the Cretaceous and Paleogene and therefore once had overlapping climatic and environmental niches (Chaney, 1950; LePage et al., 2005). Published growth experiments suggest these species have similar physiological responses to photosynthesis, *e.g.* photosynthetic light saturation and dry mass of leaf, and soluble starch between *Taxodium* and *Metasequoia* (Equiza et al., 2006), and transpiration, whole plant WUE between *Metasequoia*, *Sequoia*, and *Taxodium* (Osborne and Beerling, 2003). Similar photosynthesis response of these closely related species may be an evolutionary artifact of shared past habitats, which is supported by PCA of physiological traits in this study.

Vascular bundle area in leaves has been suggested to reflect water transport efficiency in *Pseudotsuga menzeisii* (Mirb.) Franco (Pinaceae; Apple et al., 2002). In *P. menzeisii*, vascular bundle area reaches maximum efficiency with increased age and height, but within an individual does not change significantly with height (Apple et al., 2002). Data from Oldham et al. (2010) supports these findings by demonstrating insignificant changes in vascular bundle area with increased height in *S. sempervirens*. My dataset did not test for changes in vascular bundle size with increased height or age. If vascular bundle area does not change with height, my data suggests vascular bundle size reflects interspecific variation since this trait, when included in analyses, lowered the variance in the data for both PCA and CCA. Correlation of vascular bundle area with MDiR was found in *Sequoia*, and with both PCoQ and PDrQ in *Taxodium*, which suggests these are the climatic variables that influence the bundle sizes for each taxon. No climatic links to vascular bundle area were found in *Metasequoia*.

Resin canals of conifers are not well understood yet previous research demonstrates that the development of resin canal area in *P. menzeisii* leaves was related to defense against herbivory (Apple et al., 2002). In my data, resin canal area was significantly larger in *Sequoia* than both *Metasequoia* and *Taxodium*, which is most likely explained by differences in habit (evergreen *Sequoia* versus deciduous *Metasequoia* and *Taxodium*), and an economic balance between protection and productivity. I suggest that as a sapling, *Sequoia* invest in larger resin canals that would increase the amount of terpenes ingested during browsing, deterring herbivory (Coley, 1983; Coley et al., 1985; Reich et al., 1992; Givnish, 2002). Over time, this investment in resin canal area decreases as it transitions from defense to growth and reproduction when browsing is less likely to affect survival. Especially since *Sequoia* leaves are retained year after year, initial investment pays off whereas *Metasequoia* and *Taxodium* leaves are built to last one growing season (to maximize photosynthesis during the growing season), thus the investment is minimal (Reich et al., 1992).

Nitrogen content (%N) in plants is a marker of productivity and photosynthesis activity, where nitrogen uptake is used in synthesizing photosynthetic proteins. Generally, %N is lower in conifers than angiosperms, with deciduous conifers having slightly higher %N than evergreens (Reich and Oleksyn, 2004). This is reflected in my data, where *Metasequoia* and *Taxodium* had higher %N (mean 1.87 $\pm$ 0.43% and 1.57 $\pm$ 0.45%, respectively) than *Sequoia* (1.10 $\pm$ 0.34%). Leaf economics studies have compared short and long lifespan leaves and found higher photosynthetic activity in short lifespan leaves (Field and Mooney, 1986; Loomis, 1997). A short-leaf-lifespan strategy and generally higher photosynthetic activity has been suggested to increase the competitiveness of *Taxodium* and *Metasequoia* against angiosperms at high latitudes in past warmer climates (Chaney, 1950; LePage et al., 2005).

The highest average Δ_{leaf} was measured in *Sequoia*, most likely because summer coastal fog makes up approximately 30% of total annual water intake (Dawson, 1998; Burgess and Dawson, 2004). Canopy leaves within *Sequoia* are able to uptake water from coastal fog to recharge and repair potential embolisms (Burgess and Dawson, 2004) and in this case, discriminate against δD. In *Taxodium*, δD has shown that these trees access ground water for growth, not from its wetland habitat (Dawson, 1993; White et al., 1985). This strange life strategy benefits *Taxodium* by allowing it to inhabit and tolerate environments prone to flooding and saline influxes (Anderson and Pezeshki, 2000).

WUE is linked with stomatal conductance, and is a metric of the amount of CO_2 exchanged for water (Farquhar and Richards, 1984). Controlled growth experiments showed *Taxodium* had a higher WUE than both *Sequoia* and *Metasequoia* (Llorens et al., 2009), however my data shows *Metasequoia* had a higher mean WUE and range than both *Sequoia* and *Taxodium*. *Metasequoia* samples most likely measured high WUE since many samples grew away from buildings and other trees, exposed to abiotic stress, *i.e.* wind and sunlight, which most likely increased regulation of stomata in order to minimize water loss (Adams and Kolb, 2004). A previous study that investigated sun and shade leaves of *Betula*

pendula Roth, showed higher WUE in sun than shade leaves (Sellin et al., 2010). But was contradicted by another study that demonstrated thinning stands of *Pinus ponderosa* P. Lawson and C. Lawson, essentially increasing sun exposure, decreased WUE. How stand density and exposure to sun affects WUE is likely driven by and dependent on species- or lineage-specific responses (Forrester, 2015).

Across all taxa, cross-sectional area correlated with PDrQ and PWaQ, suggesting that total leaf area is sensitive to warm and dry periods. Resin canal area increased with increasing Isoth and Pseason, and decreased with increasing Tseason. Resin canals in conifers have different functional roles ranging from anti-herbivory defense to fire defense. Species alter their resin canal shape and density in response to fire or anti-herbivory/parasitic damage (Nagy et al., 2000; Arbellay et al., 2014). This response is species-specific, increasing or decreasing in size, and a means to recover in order to continue to defend itself and grow (Arbellay et al., 2014). Thus, different size resin canals in Cupressaceae may point to a defense strategy we have not yet uncovered, and whether these defense strategies are related to trends or correlations in climate. Whether they increase their size in drier areas prone to fire or with seasonal herbivory/parasitic damage can be tested by investigating more conifers.

Leaf width decreased with increased MTWeQ, MTWaQ, and PDrQ. Leaf width in angiosperms affects the boundary layer which regulates leaf temperature (Perez-Harguindeguy et al., 2016). Narrow leaves tend to have a smaller boundary layer and were more effective in losing heat (Leuzinger and Körner, 2007; Perez-Harguindeguy et al., 2016). This relationship is seen within my samples, where *Taxodium* has the narrowest leaves and inhabit warmer temperatures, while *Sequoia* has the widest leaves in cooler environments.

Δ_{leaf} had been widely accepted to reflect global mean annual precipitation (MAP; Diefendorf et al., 2010; Kohn, 2010), however, recent studies have challenged this relationship and instead suggest isotope fractionation is lineage specific (Jagels and Equiza,

2007; Franks et al., 2014; Sheldon et al., 2020). Recently, Δ_{leaf} in conifers across North America and Asia have demonstrated no relationship with either growing environment or climate, and in fact is taxon dependent (Stein et al., 2019; Sheldon et al., 2020). Δ_{leaf} has a narrow range of ca. 7‰ across a wide precipitation regime, from 427–1952 mm yr^{-1}, yet very weak relationships were found with MAP across taxa and within each taxon ($r<0.5$; table 3.4–3.7). This supports other findings that Δ_{leaf} does not reflect climate, and is lineage specific.

%C in plants has been shown to vary based on their growth and reproduction strategy, not climate (Osborne and Beerling, 2003). Through meta-analyses, differences in %C are observed between plant functional types (e.g. herbaceous versus woody) but not deciduous and evergreen plants (Ma et al., 2018; Thomas and Martin, 2012). Although relationships were weak between %C and MTWaQ when examined for individual taxa, a slightly stronger relationship appeared when all taxa were analyzed together. %C was only correlated with PWaQ in *Sequoia* ($r= 0.53$; table 3.4, 3.6). %C in this case shows correlation with MTWaQ, coinciding with the productive season.

Many studies have found that herbaceous and deciduous plants have increasing %N with decreasing MAT and increasing latitude (Körner, 1989; Reich et al., 1996; Reich and Oleksyn, 2004). This is, in part, influenced by decreased microbial activity, controlled by colder MAT with increasing latitude. My analysis of %N was strongly associated with Isoth and PCoQ, partially supporting previous research that reflects decreased temperature evenness with increasing latitudes (Isoth), but needs to be further tested with PCoQ. I suspect, however, this is an artifact related with decreasing cold season precipitation with increasing latitudes.

3.4.2 Links between climate and leaf traits

While the taxa studied here are anatomically distinct, they are similar in photosynthesis-related physiology. Climate variable vectors and scores in CCA showed

repeated associations between cross-sectional area with both Tseason and PCoQ, leaf width and MAP, and leaf thickness and Isoth. Resin canal area did not have strong associations with climate. A strong positive correlation in the bivariate analysis was also found between leaf thickness and Isoth. A positive correlation with Isoth would suggest an effect related to high temperature changes throughout the day and year. The data shows most samples of *Metasequoia* and *Taxodium* have a similar Isoth, which was about half that of *Sequoia*. Outliers within *Taxodium* show similar Isoth values to *Sequoia*, although its leaf thickness is much thinner than *Sequoia* (fig. 3.2).

Despite some of these repeated associations, each species showed different relationships between climate and traits. Only one similarity was found in sister species *Metasequoia* and *Sequoia*, where in each analysis cross-sectional area was strongly correlated with PCoQ. Similarity of plant responses in *Metasequoia* and *Sequoia* may be worth exploring further to provide insights into the evolution of climatic niches within closely related coniferous taxa, as these species once inhabited the same forests (Chaney, 1950; LePage et al., 2005). Further, these findings raise questions about whether other closely related species share anatomy-climate associations in CCA and whether species-specific responses are informative of climatic niche partitioning.

3.5 Conclusions

Previous research on intraspecific variation of leaf anatomy in *Metasequoia* showed how leaf anatomy respond to climate, with some predictive value (Chapter 2; Ng and Smith, 2020). This study expands on previous research by adding data from the closely related species *Sequoia* and *Taxodium* to increase our understanding of the relationships within and between conifer leaf anatomy and physiology with climate. PCA of anatomical traits showed each taxon occupies its own morphospace, but overlap when physiological traits were incorporated. While taxa are anatomically distinct, they achieve a similar

photosynthetic function. This analysis also showed that the traits I measured highlights our current understanding of plant- and conifer-climate links. Overall, I improved our understanding of climatic links across taxa and within each taxon, showing that these responses are different. Similarities in responses suggest broad climatic responses across all sampled taxa and species-specific responses reflect climatic partitioning. From CCA of all traits and climatic variables, repeated associations were found between cross-sectional area and both Tseason and PCoQ, leaf width and MAP, leaf thickness and Isoth. These relationships were also seen within species, *Metasequoia* showed strong associations in cross-sectional area with PCoQ and Tseason and leaf width with MAT and Trange. *Sequoia* also showed strong associations between cross-sectional area with PCoQ, but leaf width with MAP. Finally, *Taxodium* showed strong associations between cross-sectional area with MDiR and MAP, and leaf thickness with MTWaQ. The similarities between strong associations in cross-sectional area and PCoQ in *Metasequoia* and *Sequoia* might reflect climatic niche conservatism between closely related species. Further testing of trait-climate links by incorporating even more conifers will strengthen our understanding of the universality of these findings as well as general anatomy-climate relationships.

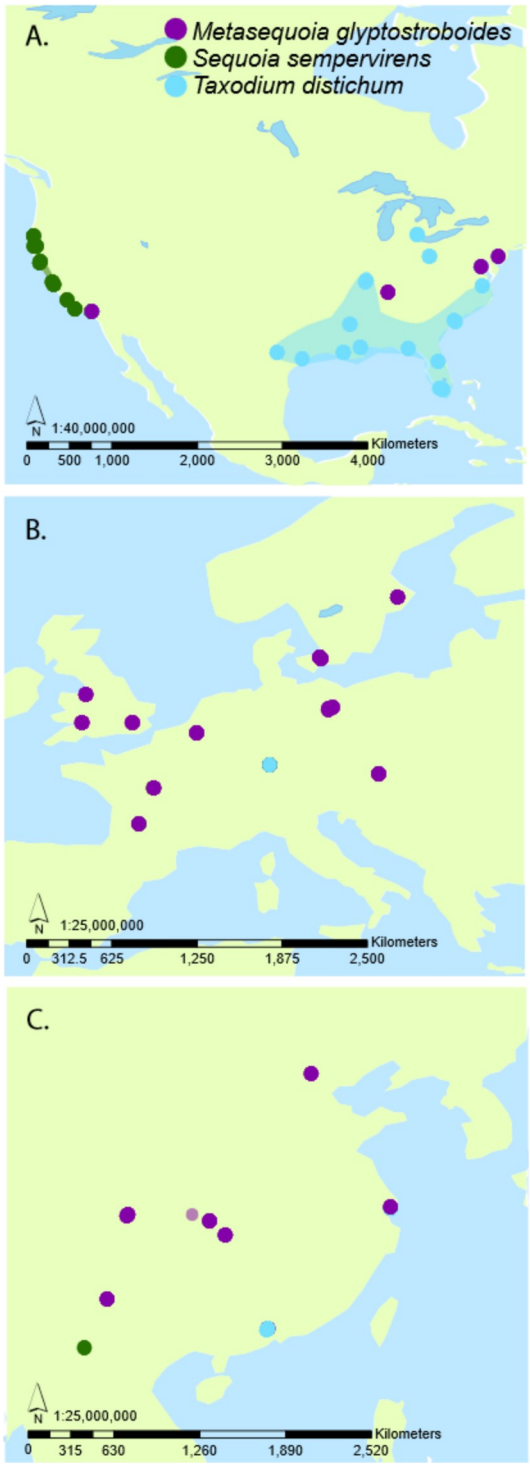

Figure 3.1: Map of sampling sites for *Metasequoia glyptostroboides* (purple dots), *Sequoia sempervirens* (green dots), and *Taxodium distichum* (blue dots) across North America (A), Europe (B), and Asia (C) in 2016 and 2017. Natural distributions for each species are mapped as transparent polygons: coastal North America for *S. sempervirens*, southeast United States for *T. distichum*, and central China (star) for *M. glyptostroboides*.

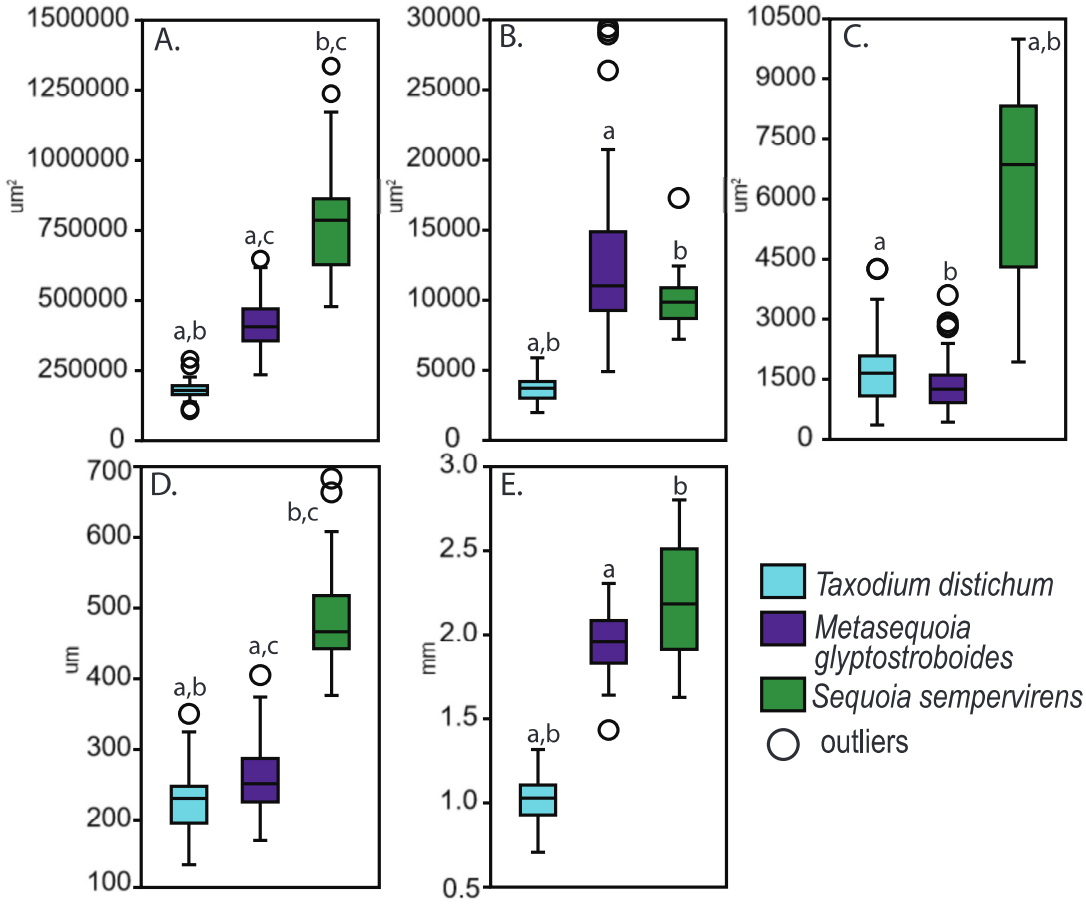

Figure 3.2: Boxplot of anatomical leaf measurements for *Metasequoia glyptostroboides* (purple), *Sequoia sempervirens* (green), and *Taxodium distichum* (blue). A, cross-sectional area. B, vascular bundle area. C, resin canal area. D, leaf thickness. E, leaf width. Significant pairs are indicated with letters (a, b, and c) above each boxplot p-value$<$0.05.

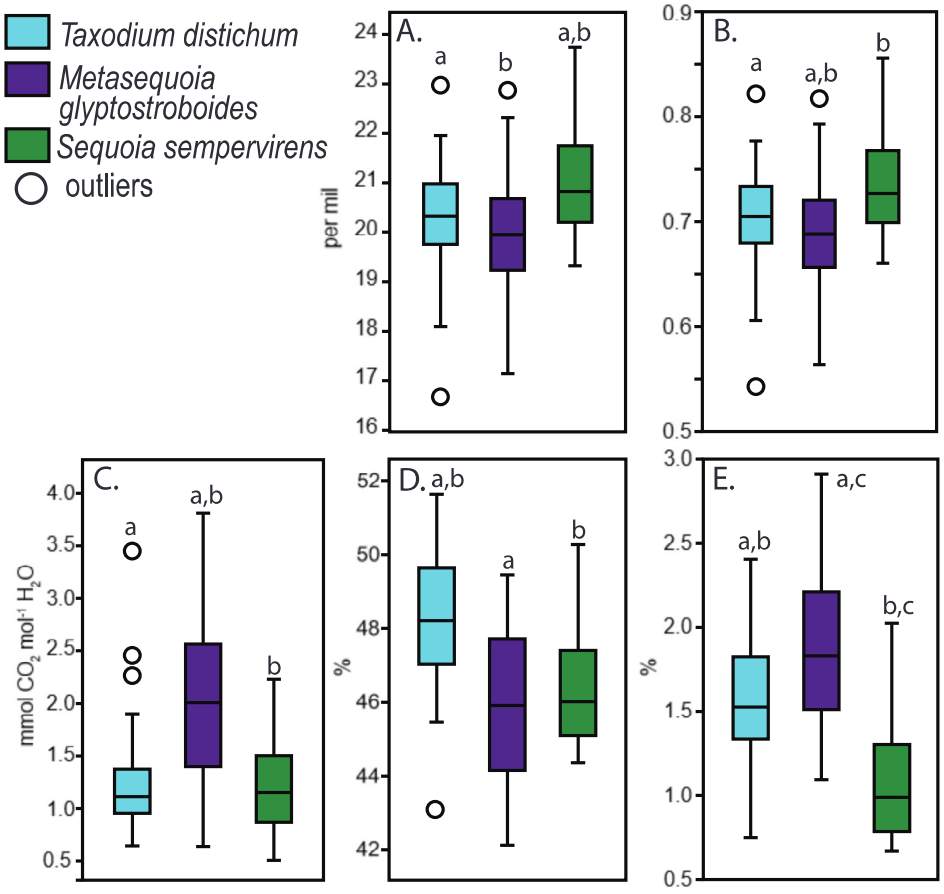

Figure 3.3: Boxplot of physiological leaf measurements for *Metasequoia glyptostroboides* (purple), *Sequoia sempervirens* (green), and *Taxodium distichum* (blue). A, Δ_{leaf}. B, c_i/c_a. C, WUE, D, %C. E, %N. Significant pairs are indicated with letters (a, b, and c) above each boxplot p-value$<$0.05.

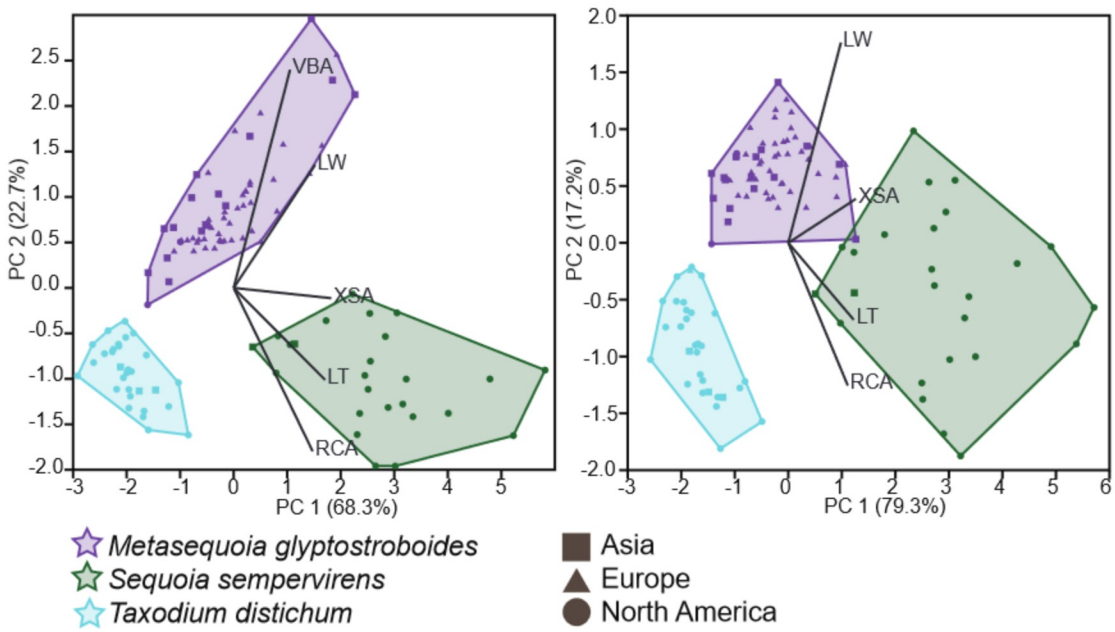

Figure 3.4: Principal components analysis (PCA) of leaf anatomical traits. A, all leaf anatomical traits: cross-sectional area (XSA), vascular bundle area (VBA), resin canal area (RCA), leaf width (LW), and leaf thickness (LT). PC1 (68.3%) shows high variability with XSA and PC2 (22.7%) with VBA. Note relatively smaller morphospace of *Taxodium* (blue) compared with *Sequoia* (green) and *Metasequoia* (purple). All taxa occupy their own morphospace. B, with VBA omitted from analysis. PC1 (79.3%) shows high variability with XSA and PC2 (17.2%) with LW. One *Metasequoia* sample from China (MN17-18) overlaps between *Metasequoia* and *Sequoia* morphospaces; *Taxodium* occupies its own morphospace.

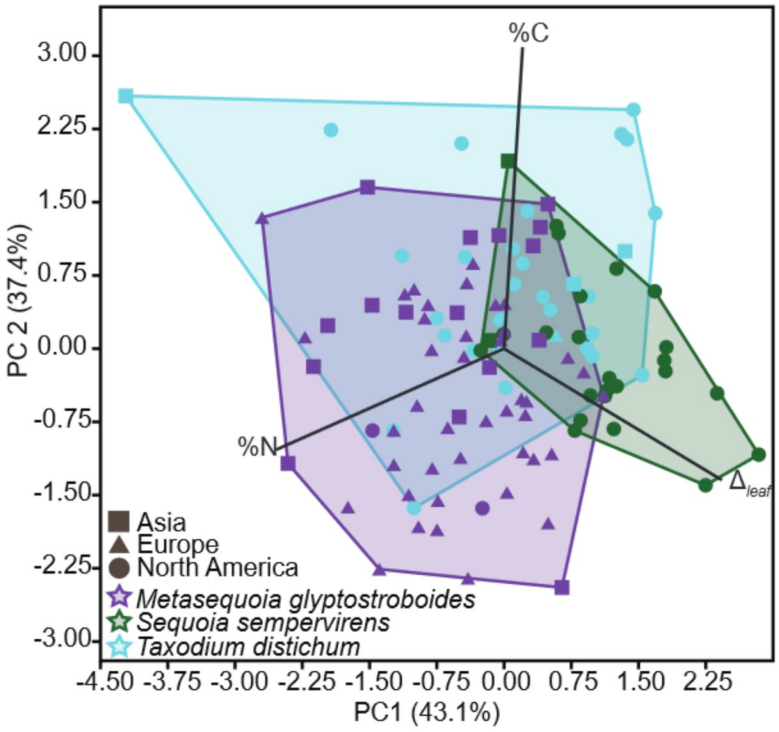

Figure 3.5: Principal components (PC) analysis of leaf physiological traits (%C, %N, and Δ_{leaf}) measured across climatic gradients. PC1 (43.1%) shows high variability with %N and PC2 (37.4%) with %C. All taxa overlap, suggesting lack of variance in our data between groups.

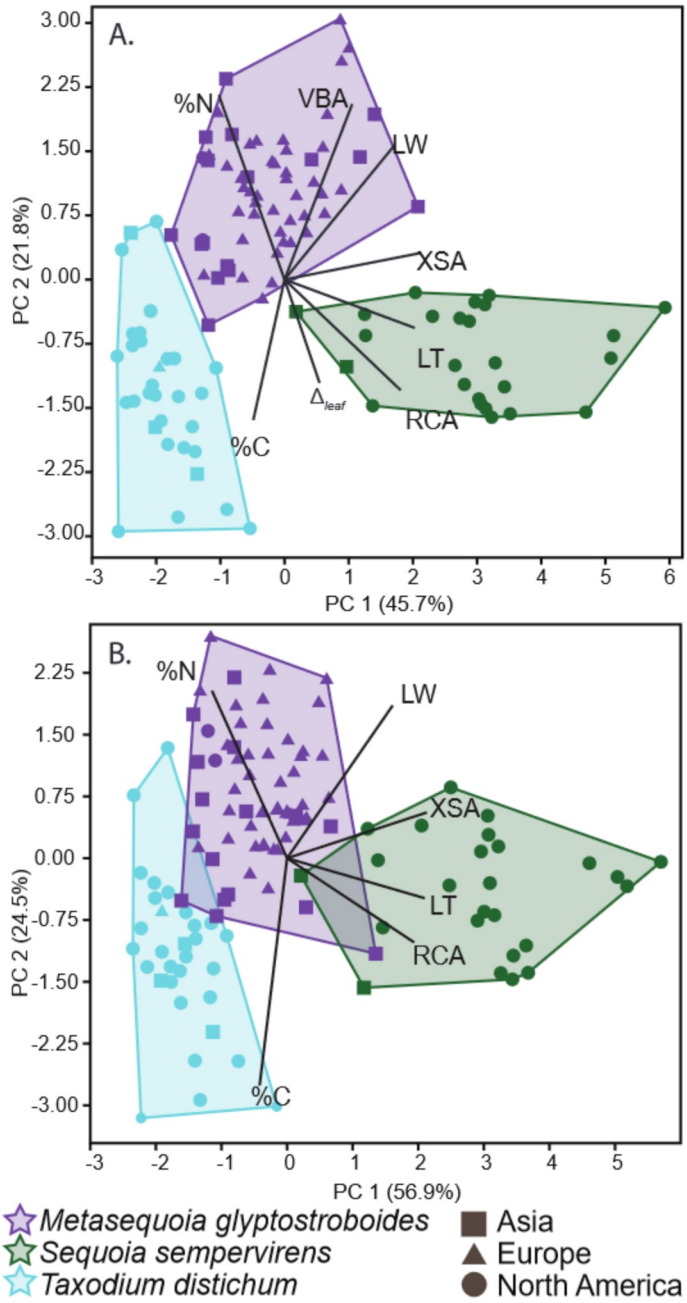

Figure 3.6: Principal components analysis (PCA) of anatomical and physiological traits. A. PC1 (52.8%) shows high variability with RCA and PC2 (24.1%) with %C. Morphospaces are similar in size for each taxon. B. As in A but excluding Δ_{leaf}. PC1 (56.9%) shows high variability with XSA and PC2 (24.5%) with %C. Note morphospace of *Metasequoia* (purple) overlaps slightly with *Sequoia* (green) and *Taxodium* (light blue).

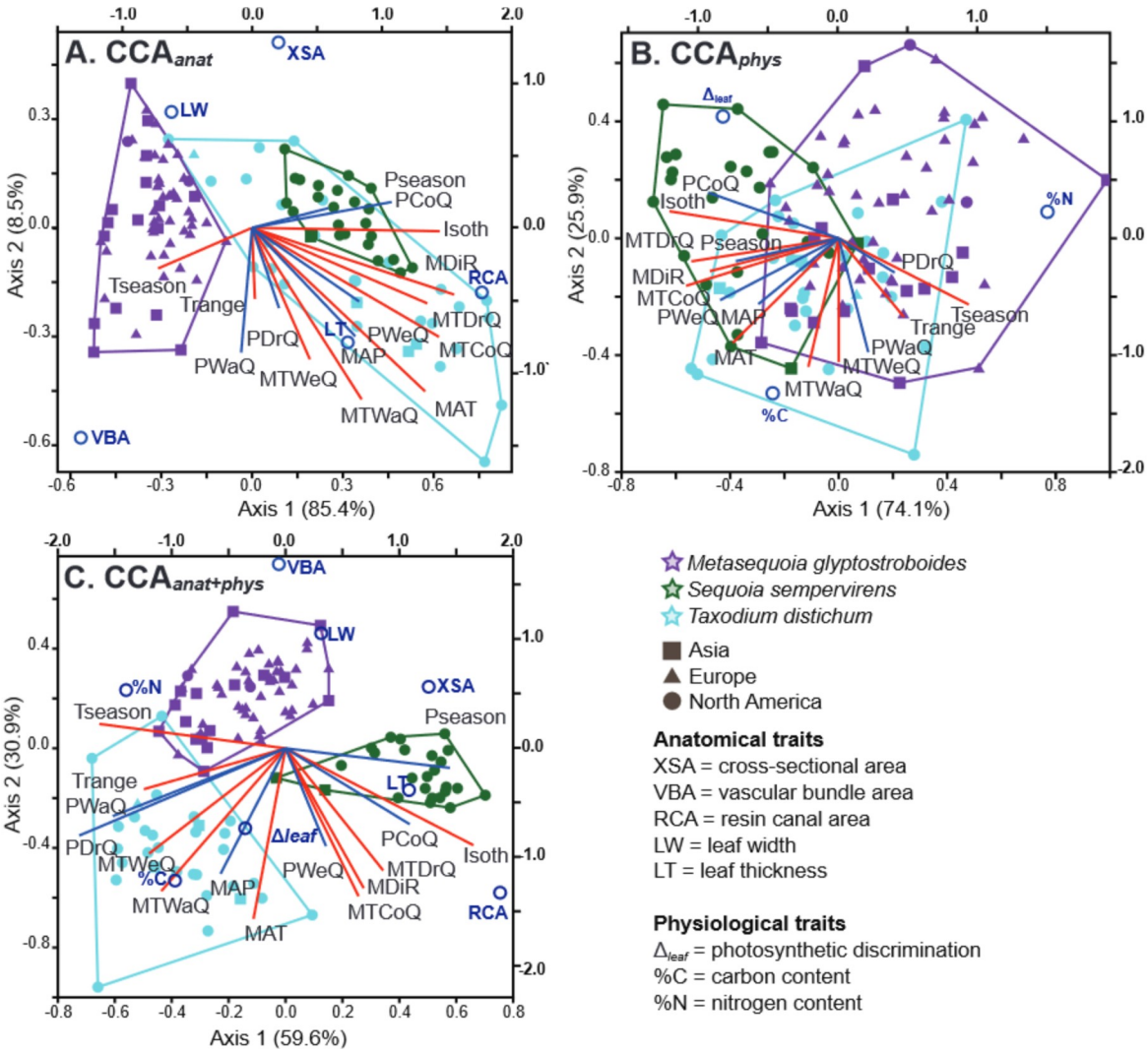

Figure 3.7: Canonical correspondence analysis (CCA) of *Metasequoia glyptostroboides* (purple), *Sequoia sempervirens* (green), and *Taxodium distichum* (light blue) across Bioclim variables (temperature = red, precipitation = dark blue). **A,** With anatomical traits Axis 1 (85.4%) shows high association with RCA and mean diurnal temperature range (MDiR), Axis 2 (8.5%) with vascular bundle area (VBA), temperature range (Trange), precipitation of warmest quarter (PWaQ), and precipitation of driest quarter (PDrQ) but most strongly with mean temperature of the warmest quarter (MTWaQ). **B,** CCA_{phys} Axis 1 (74.1%) shows high association with isothermality (Isoth) and %N and Axis 2 (25.9%) with mean temperature of wettest quarter (MTWeQ) and %C. **C,** $CCA_{anat+phys}$ Axis 1 (59.6%) highly associated with PDrQ and resin canal area (RCA) and Axis 2 (30.9%) with mean annual temperature (MAT) and VBA.

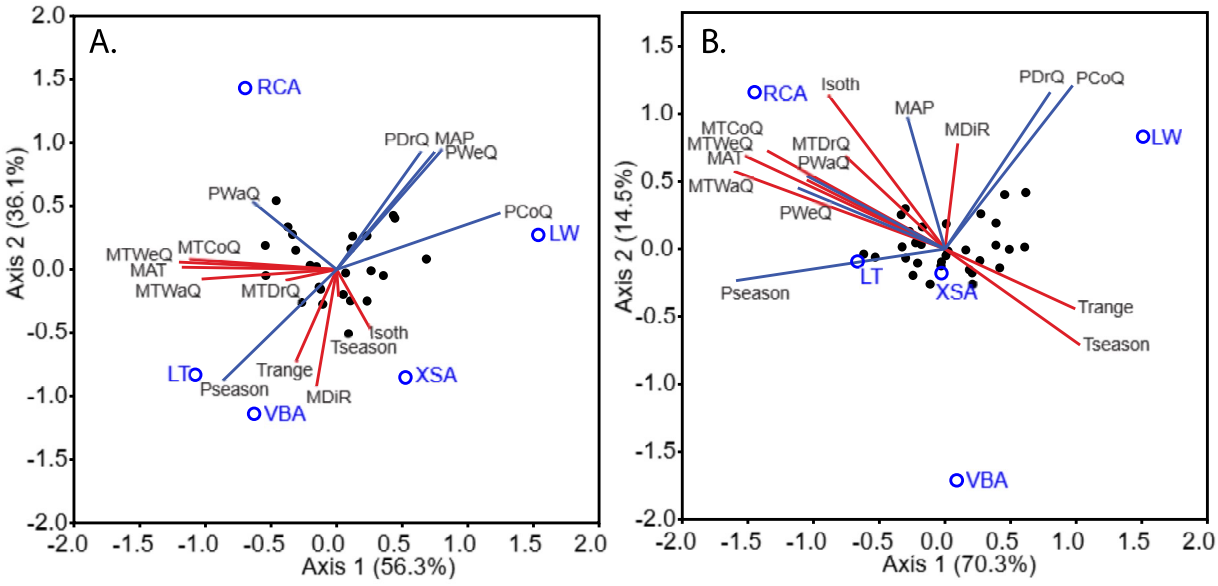

Figure 3.8: Canonical correspondence analysis for A, *Sequoia sempervirens* and B, *Taxodium distichum* of all leaf anatomical traits. A, Axis 1 (56.3%) showed strongest association with precipitation of coldest quarter (PCoQ) and leaf width (LW), and Axis 2 (36.1%) with precipitation of wettest quarter (PWeQ) and resin canal area (RCA). B, Axis 1 (70.3%) showed strongest association with mean temperature of warmest quarter (MTWaQ) and LW, and Axis 2 (14.5%) with PCoQ and vascular bundle area (VBA).

Table 3.4: Correlation (r-value) between traits and climate variables for all species

	Cross-sectional area	Vascular bundle area	Resin canal area	Leaf width	Leaf thickness	Δ_{leaf}	WUE	%C	%N	C:N	c_i/c_a
Vascular bundle area	**0.48**	-	-	-	-	-	-	-	-	-	-
Resin canal area	**0.75**	0.08	-	-	-	-	-	-	-	-	-
Leaf width	**0.82**	**0.64**	**0.39**	-	-	-	-	-	-	-	-
Leaf thickness	**0.90**	**0.34**	**0.88**	**0.55**	-	-	-	-	-	-	-
Δ_{leaf}	0.18	**-0.21**	**0.22**	0.14	0.13	-	-	-	-	-	-
WUE	-0.14	**0.29**	**-0.27**	0.06	**-0.20**	**-0.67**	-	-	-	-	-
%C	**-0.23**	-0.12	0.04	**-0.43**	-0.04	-0.15	0.10	-	-	-	-
%N	**-0.33**	0.10	**-0.54**	-0.05	**-0.48**	**-0.29**	**0.41**	-0.17	-	-	-
C:N	**0.34**	-0.12	**0.58**	0.05	**0.49**	**0.27**	**-0.38**	**0.26**	**-0.92**	-	-
c_i/c_a	**0.19**	**-0.20**	**0.23**	0.16	0.14	**1.00**	**-0.66**	-0.15	**-0.29**	**0.27**	-
MAT	**-0.22**	**-0.34**	0.17	**-0.52**	0.04	0.13	-0.08	**0.51**	**-0.30**	**0.34**	0.13
MDiR	**0.22**	**-0.35**	**0.53**	**-0.20**	**0.43**	**0.20**	**-0.46**	**0.18**	**-0.45**	**0.46**	**0.20**
Isoth	**0.57**	-0.17	**0.78**	**0.19**	**0.71**	**0.42**	**-0.47**	0.02	**-0.57**	**0.59**	**0.41**
Tseason	**-0.58**	-0.04	**-0.61**	**-0.38**	**-0.60**	**-0.44**	**0.29**	0.12	**0.42**	**-0.43**	**-0.44**
Trange	**-0.46**	**-0.20**	**-0.34**	**-0.46**	**-0.37**	**-0.34**	0.08	**0.20**	**0.19**	**-0.20**	**-0.34**
MTWeQ	**-0.54**	**-0.28**	**-0.30**	**-0.60**	**-0.38**	**-0.21**	0.14	**0.44**	-0.01	**0.01**	**-0.21**
MTDrQ	**0.29**	-0.17	**0.53**	-0.06	**0.45**	**0.35**	**-0.35**	**0.24**	**-0.43**	**0.47**	**0.35**
MTWaQ	**-0.49**	**-0.33**	-0.16	**-0.67**	**-0.26**	-0.11	0.06	**0.52**	-0.06	0.09	-0.11
MTCoQ	0.13	**-0.24**	**0.46**	**-0.21**	**0.35**	**0.33**	**-0.22**	**0.34**	**-0.46**	**0.50**	**0.34**
MAP	**-0.29**	**-0.26**	-0.01	**-0.42**	-0.15	**0.19**	-0.09	**0.37**	**-0.20**	**0.24**	**0.19**
Pseason	**0.54**	0.08	**0.62**	**0.36**	**0.60**	0.07	0.11	0.09	**-0.37**	**0.43**	0.10
PWeQ	0.07	-0.11	**0.30**	-0.10	**0.19**	**0.20**	0.02	**0.34**	**-0.35**	**0.41**	**0.22**
PDrQ	**-0.71**	**-0.39**	**-0.55**	**-0.70**	**-0.64**	-0.02	-0.16	0.18	**0.24**	**-0.24**	-0.05
PWaQ	**-0.64**	-0.13	**-0.48**	**-0.55**	**-0.55**	-0.15	**0.35**	**0.44**	0.15	-0.12	-0.14
PCoQ	**0.40**	**-0.20**	**0.56**	0.14	**0.46**	**0.37**	**-0.47**	-0.05	**-0.42**	**0.46**	**0.36**

Note: bold indicates statistically significant p-value ($p<0.05$)

Table 3.5: Correlation (r-value) between traits and climate values for *M. glyptostroboides*

	Cross-sectional area	Vascular bundle area	Resin canal area	Leaf width	Leaf thickness	Δ_{leaf}	WUE	%C	%N	C:N	c_i/c_a
Vascular bundle area	**0.66**	-	-	-	-	-	-	-	-	-	-
Resin canal area	**0.59**	**0.57**	-	-	-	-	-	-	-	-	-
Leaf width	**0.75**	**0.45**	**0.35**	-	-	-	-	-	-	-	-
Leaf thickness	**0.85**	**0.81**	**0.72**	**0.53**	-	-	-	-	-	-	-
Δ_{leaf}	**-0.30**	**-0.33**	0.00	-0.05	**-0.30**	-	-	-	-	-	-
WUE	-0.11	0.12	-0.03	-0.13	-0.06	**-0.47**	-	-	-	-	-
%C	0.03	**0.37**	0.12	0.13	0.09	-0.21	**0.34**	-	-	-	-
%N	0.04	-0.16	-0.09	0.08	-0.11	-0.07	0.13	-0.09	-	-	-
C:N	-0.01	**0.26**	0.14	-0.02	0.16	0.01	-0.03	**0.28**	**-0.95**	-	-
c_i/c_a	**-0.30**	**-0.33**	0.00	-0.05	**-0.30**	**1.00**	**-0.47**	-0.21	-0.07	0.01	-
MAT	**-0.41**	0.16	-0.06	**-0.33**	-0.13	-0.11	**0.59**	**0.34**	-0.08	0.20	-0.11
MDiR	-0.14	0.07	-0.11	-0.01	-0.07	-0.19	0.00	-0.05	0.00	0.02	-0.19
Isoth	-0.04	-0.04	-0.01	-0.02	-0.09	0.19	-0.05	**-0.27**	0.12	-0.19	0.19
Tseason	-0.10	0.08	-0.07	-0.01	0.01	**-0.33**	0.07	0.20	-0.09	0.19	**-0.33**
Trange	-0.13	0.10	-0.09	-0.03	-0.02	**-0.33**	0.08	0.15	-0.08	0.16	**-0.33**
MTWeQ	**-0.29**	0.07	-0.19	-0.21	-0.13	**-0.29**	**0.31**	**0.30**	-0.15	0.25	**-0.29**
MTDrQ	0.05	0.20	0.05	0.03	0.12	0.12	0.14	0.07	0.05	-0.04	0.12
MTWaQ	**-0.35**	0.17	-0.07	**-0.26**	-0.08	-0.24	**0.47**	**0.35**	-0.11	0.25	-0.24
MTCoQ	**-0.32**	0.11	0.00	**-0.31**	-0.11	0.12	**0.52**	0.20	-0.02	0.07	0.12
MAP	-0.23	**0.33**	0.00	-0.25	0.04	-0.05	**0.47**	**0.30**	-0.10	0.21	-0.05
Pseason	**-0.29**	-0.02	-0.17	-0.11	-0.24	**-0.27**	**0.62**	**0.32**	0.10	0.03	**-0.27**
PWeQ	**-0.33**	0.23	-0.08	-0.24	-0.10	-0.16	**0.66**	**0.40**	-0.06	0.21	-0.16
PDrQ	0.09	-0.01	0.07	-0.09	0.12	0.20	**-0.39**	**-0.32**	0.07	-0.16	0.20
PWaQ	**-0.34**	0.21	-0.07	-0.23	-0.10	-0.17	**0.61**	**0.40**	-0.10	0.24	-0.17
PCoQ	0.14	-0.01	0.04	-0.04	0.08	0.19	**-0.26**	**-0.28**	0.18	-0.25	0.19

Note: bold indicates statistically significant p-value ($p<0.05$)

Table 3.6: Correlation (r-value) between traits and climate values for *Sequoia sempervirens*

	Cross-sectional area	Vascular bundle area	Resin canal area	Leaf width	Leaf thickness	Δ_{leaf}	WUE	%C	%N	C:N	c_i/c_a
Vascular bundle area	**0.80**	-	-	-	-	-	-	-	-	-	-
Resin canal area	**0.52**	**0.49**	-	-	-	-	-	-	-	-	-
Leaf width	**0.74**	0.35	0.36	-	-	-	-	-	-	-	-
Leaf thickness	**0.78**	**0.84**	**0.61**	0.23	-	-	-	-	-	-	-
Δ_{leaf}	0.25	-0.18	0.00	**0.58**	-0.24	-	-	-	-	-	-
WUE	-0.33	0.01	-0.18	**-0.56**	0.00	**-0.62**	-	-	-	-	-
%C	0.02	0.19	0.11	-0.25	0.24	-0.45	0.66	-	-	-	-
%N	-0.16	0.04	-0.23	-0.26	-0.03	-0.11	**0.43**	0.23	-	-	-
C:N	0.05	-0.15	0.23	0.17	-0.07	0.09	-0.34	-0.12	**-0.95**	-	-
c_i/c_a	0.25	-0.18	0.00	**0.58**	-0.24	**1.00**	**-0.62**	**-0.45**	-0.11	0.09	-
MAT	0.00	0.26	-0.08	-0.29	0.20	-0.27	**0.48**	0.27	**0.51**	**-0.41**	-0.27
MDiR	**0.61**	**0.59**	**0.43**	0.31	**0.67**	-0.04	-0.25	-0.13	-0.25	0.13	-0.04
Isoth	**0.49**	0.37	**0.40**	**0.43**	**0.43**	0.11	**-0.43**	-0.26	-0.15	0.03	0.11
Tseason	0.08	0.13	-0.05	-0.04	0.08	-0.02	0.21	0.18	-0.05	0.05	-0.02
Trange	0.34	**0.41**	0.19	0.05	**0.44**	-0.12	0.03	0.05	-0.19	0.13	-0.12
MTWeQ	-0.20	0.06	-0.28	**-0.41**	-0.02	-0.32	**0.76**	**0.50**	**0.59**	**-0.46**	-0.32
MTDrQ	0.34	**0.43**	0.26	0.09	**0.43**	-0.01	-0.28	-0.26	0.06	-0.09	-0.01
MTWaQ	0.07	0.31	-0.06	-0.24	0.25	-0.24	**0.44**	0.25	**0.42**	-0.34	-0.24
MTCoQ	0.01	0.25	-0.04	-0.24	0.21	-0.25	0.35	0.17	**0.49**	**-0.41**	-0.25
MAP	-0.24	-0.34	-0.21	0.03	**-0.44**	0.32	-0.07	0.02	0.14	-0.06	0.32
Pseason	0.33	**0.47**	0.34	0.00	**0.57**	-0.36	0.02	-0.05	-0.13	0.03	-0.36
PWeQ	-0.22	-0.31	-0.20	0.02	**-0.41**	0.29	-0.02	0.05	0.16	-0.08	0.29
PDrQ	-0.32	-0.33	-0.36	-0.07	**-0.51**	0.26	0.11	0.15	0.35	-0.24	0.26
PWaQ	-0.39	-0.25	**-0.43**	-0.39	-0.34	-0.12	**0.77**	**0.53**	**0.55**	-0.38	-0.12
PCoQ	0.06	-0.14	0.11	0.31	-0.17	0.37	**-0.57**	-0.31	-0.28	0.22	0.37

Note: bold indicates statistically significant p-value ($p<0.05$)

Table 3.7: Correlation (r-value) between traits and climate for *Taxodium distichum*

	Cross-sectional area	Vascular bundle area	Resin canal area	Leaf width	Leaf thickness	Δ_{leaf}	WUE	%C	%N	C:N	c_i/c_a
Vascular bundle area	**0.74**	-	-	-	-	-	-	-	-	-	-
Resin canal area	**0.50**	0.34	-	-	-	-	-	-	-	-	-
Leaf width	0.25	0.28	-0.16	-	-	-	-	-	-	-	-
Leaf thickness	0.77	**0.56**	**0.68**	-0.30	-	-	-	-	-	-	-
Δ_{leaf}	-0.09	-0.21	0.06	-0.02	-0.06	-	-	-	-	-	-
WUE	0.00	0.29	-0.06	0.11	-0.13	**-0.65**	-	-	-	-	-
%C	0.11	-0.05	**0.43**	**-0.62**	**0.38**	-0.06	0.02	-	-	-	-
%N	-0.16	0.09	-0.22	0.21	-0.23	-0.27	**0.37**	**-0.40**	-	-	-
C:N	0.15	-0.12	0.25	-0.28	0.27	0.21	-0.32	**0.52**	**-0.93**	-	-
c_i/c_a	-0.09	-0.21	0.06	-0.02	-0.06	**1.00**	**-0.65**	-0.06	-0.27	0.21	-
MAT	0.10	-0.04	**0.50**	-0.32	0.29	**0.57**	**-0.48**	**0.39**	**-0.51**	**0.51**	**0.57**
MDiR	-0.12	-0.27	-0.07	-0.02	0.08	0.17	**-0.57**	-0.18	-0.01	-0.10	0.17
Isoth	0.23	-0.13	**0.44**	-0.02	0.25	**0.52**	**-0.68**	0.23	**-0.53**	**0.47**	**0.52**
Tseason	-0.25	0.02	**-0.45**	0.09	-0.20	**-0.54**	**0.47**	-0.33	**0.57**	**-0.55**	**-0.54**
Trange	-0.27	-0.05	**-0.43**	0.08	-0.16	**-0.45**	0.27	-0.35	**0.53**	**-0.53**	**-0.45**
MTWeQ	-0.03	-0.05	0.32	-0.26	0.16	0.27	-0.15	0.14	**-0.41**	**0.40**	0.27
MTDrQ	-0.12	-0.18	0.20	-0.23	-0.03	**0.43**	**-0.39**	**0.40**	-0.27	0.30	**0.43**
MTWaQ	-0.06	-0.05	**0.44**	**-0.45**	0.30	**0.49**	**-0.41**	**0.36**	-0.35	**0.38**	**0.49**
MTCoQ	0.16	-0.03	**0.49**	-0.24	0.26	**0.57**	**-0.49**	**0.37**	**-0.54**	**0.54**	**0.57**
MAP	**-0.43**	**-0.46**	-0.10	-0.26	-0.31	**0.47**	-0.27	0.19	**-0.37**	**0.39**	**0.47**
Pseason	**0.48**	**0.37**	**0.71**	-0.10	**0.49**	0.29	-0.01	0.35	**-0.44**	**0.44**	0.29
PWeQ	-0.01	-0.12	0.31	-0.24	0.06	**0.49**	-0.19	0.33	**-0.53**	**0.55**	**0.49**
PDrQ	**-0.68**	**-0.66**	**-0.54**	-0.13	**-0.56**	0.10	-0.27	-0.08	0.01	0.01	0.10
PWaQ	-0.07	-0.17	0.27	-0.24	0.01	**0.45**	-0.15	0.26	**-0.54**	**0.54**	**0.45**
PCoQ	**-0.66**	**-0.61**	**-0.51**	-0.07	**-0.59**	0.15	-0.25	-0.09	0.04	-0.04	0.15

Note: bold indicates statistically significant p-value ($p<0.05$)

Table 3.8: CCA and traits included in each analysis

CCA	Cross-sectional area	Vascular bundle area	Resin canal area	Leaf width	Leaf thickness	Δ_{leaf}	%Carbon	%Nitrogen
CCA_{anat}	x	x	x	x	x			
$CCA_{anat-vb}$	x		x	x	x			
CCA_{phys}						x	x	x
$CCA_{anat+phys}$	x	x	x	x	x	x	x	x
$CCA_{anat+phys-vb}$	x		x	x	x	x	x	x
$CCA_{anat+phys-vb-\Delta leaf}$	x		x	x	x		x	x

Table 3.9: Trait-climate association matrix based on CCA score proximity for each taxon, *Metasequoia* (M), *Taxodium* (T), *Sequoia* (S), and CCA analyses renamed A–E (A = CCA_{anat}, B = $CCA_{anat-vb}$, C = $CCA_{anat+phys}$, D = $CCA_{anat+phys-vb}$, E = $CCA_{anat+phys-vb-\Delta leaf}$. Numbers in the matrix indicate whether these associations were on Axis 1 or Axis 2.

	cross-sectional area						resin canal area			leaf width							leaf thickness						
Code	M	T	S	A	B	C	M	A	B	M	T	S	B	C	D	E	M	T	A	B	C	D	E
MAT								2		1										1			
MDiR		1													1				1				
Isoth																	2				2		1,2
Tseason	2	2				1							2										
Trange										2								2					
MTWeQ				1																			
MTDrQ									2					1						1			
MTWaQ																		1					
MTCoQ															1								
MAP		1										2	2				1						
Pseason			2	1														2					
PWeQ																1							
PDrQ							1					2								2			
PCoQ	1		1	2							2											2	

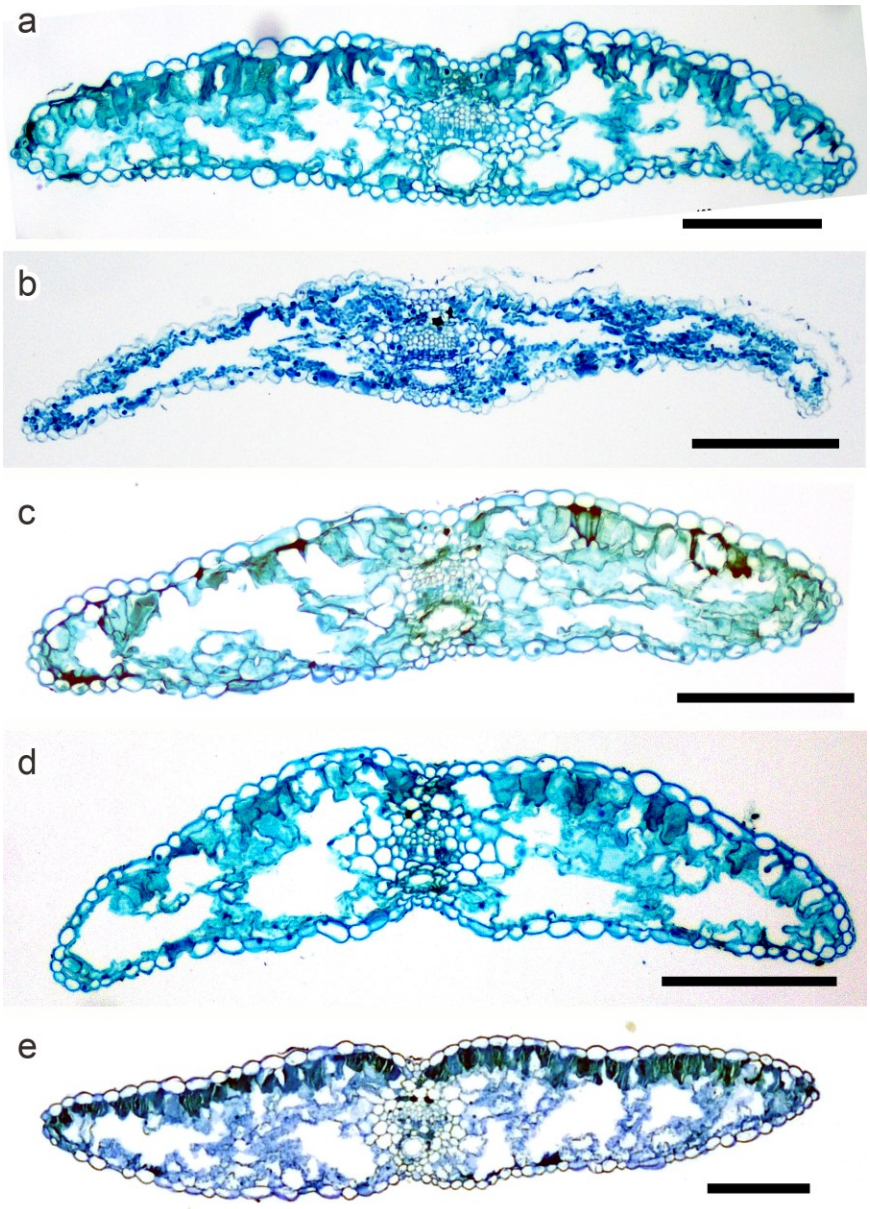

Figure 3.9: Leaf anatomical sections of *Taxodium distichum* collected from its natural distribution throughout south east USA (A–D) and cultivated in garden (E). A, Big Cypress National Preserve (Florida), MN16-13. B, Pearl River Wildlife Management Area (WMA; Louisiana), MN16-19. C, Attakapas Island WMA (Louisiana), MN16-24. D, Delta National Forest (Mississippi), MN16-30. E, Dawes Arboretum (Ohio), MN16-37. Scale bars = 200 µm.

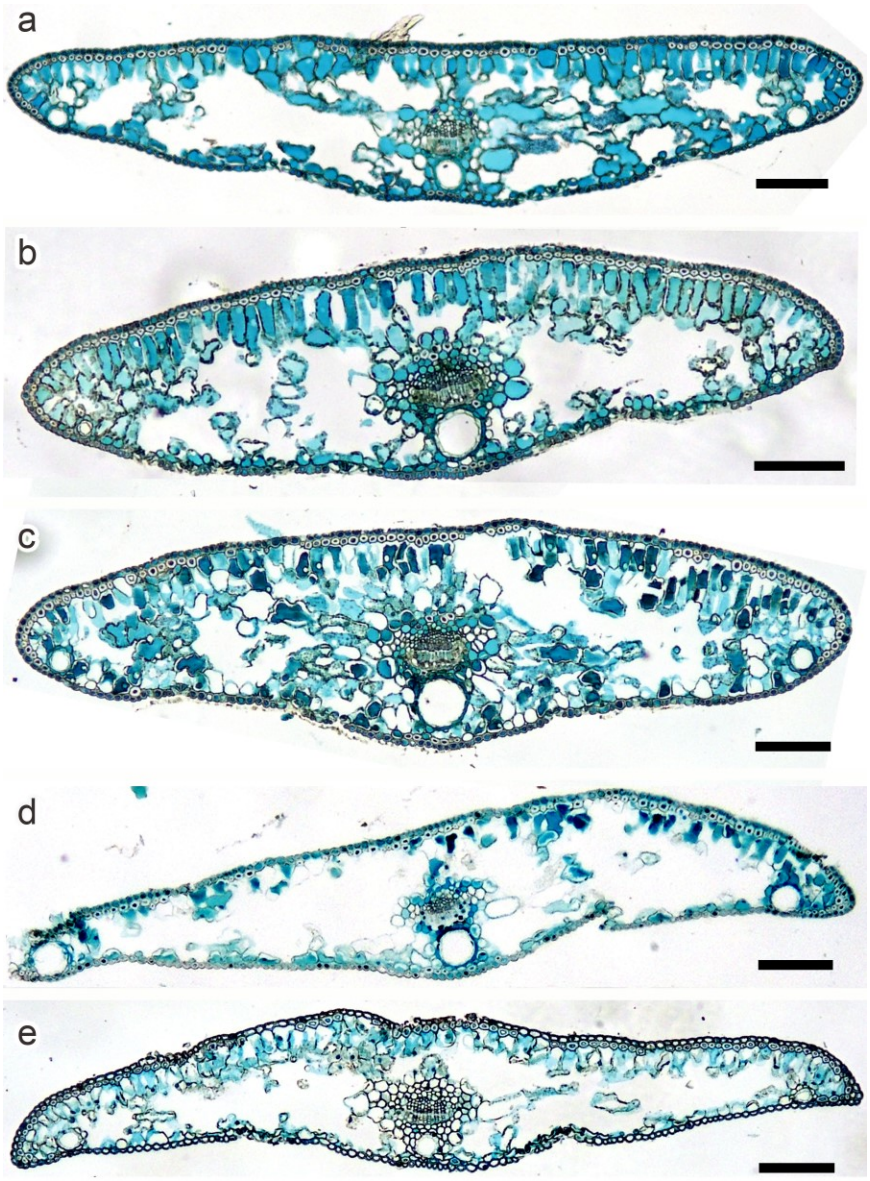

Figure 3.10: Leaf anatomical sections of *Sequoia sempervirens* collected from its natural distribution throughout coastal Calfironia (A–D) and cultivated in garden (E). A, Portola Redwood State Park (La Honda, CA), MN16-41. B, Jackson State Forest (Willits, CA), MN16-50. C, University of California (Santa Cruz), MN16-56. D, Green Diamond Logging Company (Trinidad, CA), MN16-45. E, Shanghai Botanical Garden (Shanghai, China), MN17-27. Scale bars = 200 µm.

CHAPTER 4

Can present-day trait-climate relationships be used to model leaf anatomical traits? A case study using early Eocene *Metasequoia*

Abstract

How has climate shaped plant evolution? While climate plays an important role in determining the geographic distributions of plants, our understanding of the extent to which climate acts as a selecting filter on plant traits is limited. By examining how plant traits change with climatic variation over time, we can better understand the effects of climate on plant evolutionary history. In order to study the effects of climate on plant evolution, we need to understand how plant traits change with climate. Here, I reconstruct leaf traits for early Eocene *Metasequoia* under two different CO_2 scenarios to test the climatic effects on traits, which affect leaf function. I used modern trait and climate data from *Metasequoia*, *Sequoia*, and *Taxodium* (Cupressaceae) to generate species-specific generalized linear models for four leaf anatomical traits (cross-sectional area, resin canal area, leaf thickness, and leaf width). The models were tested for fit and compared to models constructed with different climate variables for model performance. I applied the models to the early Eocene using published fossil locality data and early Eocene climate simulations with 3x and 6x pre-industrial atmospheric CO_2, then compared these estimates to modern traits in order to

assess plant response. The models suggest that sets of climate variable are more important than individual climate variables for inferring climate-trait correlations. I found that leaf width, leaf thickness, and cross-sectional area decreased with increased CO_2, most likely as a result of regulating heat stress. Resin canal area did not show any significant differences with increased CO_2, consistent with previous findings of taxonomic constraints in resin canals. Leaf thickness for *Metasequoia*-only models showed no significant changes with increasing CO_2, yet all-species models resulted in a significantly lower leaf thickness, suggesting a taxonomic influence in the model by thinner-leaved species such as *Taxodium*. This aspect of my results needs to be further investigated. Lastly, I validated early Eocene leaf width model estimates with measurements from fossil *Metasequoia occidentalis* and showed that these measurements matched modelled data. These results demonstrate the promise of this approach and could be expanded throughout the Cenozoic to better understand how climate-trait links might have influenced plant response of and evolution of *Metasequoia*.

4.1 Introduction

Over large temporal and spatial scales, the effects of climate on plants have shaped plant evolutionary history. This is often recorded in the plant fossil record by the expansion and contraction of geographic ranges in response to shifts in climate (Uemura, 1997; Tiffney and Manchester, 2001; Falcon-Lang and DiMichele, 2010; Huang et al., 2015). Plants must adapt or migrate at the same rate climate shifts in order to stay within their climatic envelope. One way to adapt is to develop new anatomies and morphologies, such as Kranz anatomy or syndrome within the leaf, which is physiologically tied to C_4 photosynthetic pathway (Brown and Smith, 1972; Ehleringer et al., 1991). This anatomical arrangement and photosynthetic pathway concentrates and stores CO_2, and has been suggested to have evolved in response to high temperature and low CO_2 conditions (Ehleringer et al., 1991).

Established methods permit us to estimate some plant morphological responses based on climate variables, such as leaf area to increase with higher mean annual precipitation (Wilf et al., 1998). Studying how anatomical and physiological traits within lineages have been affected over geologic time is important in understanding temporal implications on plant function and evolutionary history.

Species distribution models have provided valuable insights into plant biogeography and evolutionary patterns (Saupe et al., 2011; Varela et al., 2011; Huang et al., 2015), although accounts for neither evolutionary nor ecological processes. This is seen in *Metasequoia* (Cupressaceae), one of many "relict species" that were once widespread across the Northern Hemisphere but is now naturally constricted to central China (Wen, 1999; Huang et al., 2015). Species distribution models suggest *Metasequoia* has tracked their habitat, retaining a constant climatic envelope throughout the Cenozoic (Huang et al., 2015). These findings rely on presence/absence in the fossil record and assume maintaining climatic suitability in high preservation environments throughout the Cenozoic, during which global climate transitioned from warm and wet to cool and arid (Zachos et al., 2001). By shifting from species-based to trait-based approaches, we can improve on species distribution modelling by moving our focus away from climatic suitability and learning how climate affects traits and therefore function (Lavorel and Garnier, 2002; Regos et al., 2019; Zakharova et al., 2019). Climate-induced pressure to adapt or migrate is diverse and varies in magnitude, which ultimately affects a plant's access to resources, and thus how it grows and reproduces. Cooling climate over the Cenozoic, for example, initiated polar glaciation (Shackleton et al., 1988; Zachos et al., 2001), which blocked migratory routes. Glaciers not only separated species that once inhabited the same forest (*e.g.*, *Sequoia*, *Metasequoia*, and *Taxodium* (Cupressaceae; LePage et al., 2005)), but also impeded gene flow between species causing disjunct distributions across the Northern Hemisphere (*e.g.*, *Liriodendron tulipifera* and *L. chinensis* (Magnoliaceae), Chaney, 1947; Axelrod, 1983; Wen, 1999).

Whether traits have been selected against in response to climatic shifts during range contractions or expansions remain unknown. Plants respond to climatic variables in order to mitigate stress and optimize resources. Leaves, the most abundant and accessible plant organ, reflect their growing environment, interacting with the atmosphere to access light and carbon, which results in changes in leaf physiognomy (Givnish, 1986; Gurevitch, 1988; Dudley, 1996; Ackerly et al., 2000). Leaf traits such as leaf width and thickness, if preserved, may collectively offer insights to global climatic and environmental conditions. In paleobotanical and paleoecological studies, leaf traits have been important in understanding mechanisms behind selection in plant evolution (McElwain, 2018). By measuring and analyzing traits preserved throughout the fossil record, over spatial and temporal scales, we can begin to understand how traits have shifted with climate, and overall, how this has affected plant evolutionary history.

Metasequoia is an ideal species to test how traits have shifted over time in response to climate because of how well it has been studied (*e.g.*, morphology, physiology, growth experiments, population genetics, and germination rates). These studies emphasize *Metasequoia*'s physiology in paleo-Arctic conditions, where plants are subject to continuous light and dark regimes (Beerling and Royer, 2002; Osborne and Beerling, 2003; Equiza et al., 2007; Llorens et al., 2009), and addresses its current restricted distributions through germination and population genetics studies (Jagels and Equiza, 2007; Tang et al., 2011; Li et al., 2012). The gross morphology of *Metasequoia* is hypothesized to have remained static over geological time (Liu et al., 1999). Yet recent study by Ng and Smith (2020) has shown that it has not remained in anatomical stasis. The extensive Cenozoic fossil record of *Metasequoia* across the Northern Hemisphere demonstrates range expansion with globally warm climates, and contraction with cooling climate (Liu et al., 1999; LePage et al., 2005). These expansions and contractions are suggested to be a result of global climate, changes in environment, and competition with other plant groups (LePage et al., 2005). However, the degree of influence from these different factors on

the lineage over time has not been studied. By incorporating traits and understanding how traits have changed over the Cenozoic, I test how climate has influenced *Metasequoia*.

This study aims to investigate how climatic models and modern traits can be used to estimate past traits, with the ultimate goal of investigating how climate affects plant traits in *Metasequoia*. Here, I used anatomical links to climate (as leaf anatomy has been shown to reflect physiology and function) I found in Chapter 2 (Ng and Smith, 2020) as a foundation to build and test models of trait-climate relationships for *Metasequoia*. I focus on the following trait-climate links within *Metasequoia*: leaf width and cross-sectional area with cold-season precipitation, vascular bundle area with warm-season precipitation, leaf thickness with mild cold-season temperatures and mean annual temperature, and resin canal area with daily temperature fluctuations and mild cold-season temperatures (Chapter 2; Ng and Smith, 2020). Once these models are established, I answer how early Eocene traits are estimated using paleoclimate model data then validated with fossil data. Ultimately, data from this model will be used in a trait-based distribution modelling approach to deepen our understanding of plant-climate links through time.

4.2 Methods

I approached the research in a series of six steps (fig. 4.1): gathering climate data for fossils, modern model inputs and creation, models using "random" climate sets, model application, and model validation. Generalized linear models (GLMs) were created based on modern trait-climate relationships from previously collected data (Chapter 2 and 3) and Worldclim Bioclim (Hijmans et al., 2005) climate variables. Climate data for fossils were extracted from early Eocene climate models, for 3x and 6x pre-industrial CO_2 scenarios, based on locality paleo-latitude and longitude, and converted to Bioclim climate variables (Hijmans et al., 2005). These Eocene climate variables were employed in modern trait-climate models to reconstruct early Eocene traits. I assume that climate-trait links

have remained the same through time, based on previous findings between *Metasequoia glyptostroboides* and *M. milleri* (Ng and Smith, 2020). Inferred early Eocene traits were then validated by comparing them with early Eocene fossils from published literature. These steps are described in more detail below.

4.2.1 Climate data for early Eocene fossils

Early Eocene *Metasequoia* fossil occurrences were compiled from literature (LePage et al., 2005; Xing et al., 2016, n=41). Present-day locations were translated to paleo-latitude and -longitudes (table C.1) using the 50 Ma calibration on Gplates Web Service (www.gws.gplates.org; Müller et al., 2018). These paleo-coordinates were combined with early Eocene climate models to extract respective climate data for each location.

Early Eocene climate data was derived from the simulation models of Zhu et al. (2019), created using both Community Earth System Models v1.2 and Community Atmospheric Models v5, following the Deep-Time Model Intercomparison Project, simulating pre-industrial CO_2 scenarios at 1x, 3x, 6x, and 9x. Cloud microphysical processes for these early Eocene simulations are comparable to modern satellite data, which simulates cloud water content, particle size, and droplet concentration. I chose to use 3x and 6x pre-industrial CO_2 climate scenarios (from here, referred to as 3x and 6x) because they fit within previous estimates of CO_2 (Sloan and Rea, 1996; Smith et al., 2010a; Hyland and Sheldon, 2013; Anagnostou et al., 2016; Hollis et al., 2019). Monthly minimum and maximum estimates for temperatures, and "convective precipitation rate" and "large scale precipitation rate" estimates for precipitation, were extracted from Zhu et al. (2019) 3x and 6x climate simulations into R using package "ncdf4" version 1.17 and converted into standard units (º C and mm mo^{-1}, respectively). Convective precipitation and large scale precipitation rates were summed for mean precipitation rate. Bioclim variables were created from mean precipitation rate and monthly minimum and maximum temperature

variables using function biovars() from R package "dismo" version 1.1-4 (Hijmans et al., 2005).

4.2.2 Model inputs and creation

To create modern trait-climate models, I combined traits and respective climate (table 4.2). I used modern quantitative leaf anatomical traits of *Metasequoia glyptostroboides* (n=59) and closely related species, *Sequoia sempervirens* (n=25) and *Taxodium distichum* (n=31), collected across a climatic gradient during 2016–2018. Leaf anatomical trait measurements were used to generate models for the following: cross-sectional area, resin canal area, leaf width, and leaf thickness. *Sequoia* and *Taxodium* were included to develop a combined model in addition to species-specific models and test how well each of these models performed.

Bioclim climate variables at 2.5 minutes resolution (WorldClim v1.4; Hijmans et al., 2005) were extracted for each present-day sample collection location for the three taxa. I chose six Bioclim variables that can be reconstructed in the past using independent methods: Bio 1, mean annual temperature (MAT); Bio 10, mean temperature of the warmest quarter (MTWQ); Bio 11, mean temperature of coldest quarter (MTCQ); B12, annual precipitation (MAP); Bio 16, precipitation of wettest quarter (PWeQ); and Bio 17, precipitation of driest quarter (PDrQ). MTWQ and MTCQ are variables that closely represent warm month mean temperature and cold month mean temperature, and PWeQ and PDrQ represent precipitation during the three wettest and driest months that can be estimated in CLAMP (Climate Leaf Analysis Multivariate Program; Wolfe, 1994).

Generalized linear models (GLM) were implemented in the Biodiversity Climate Change Visual Laboratory (BCCVL), an online platform (Hallgren et al., 2016), using the "Species Trait Modelling" experiment. For each trait, four climate sets of 2–4 climate variables (A–D) were created, except for cross-sectional area which has five climate sets (A–E). These climate variables were determined by correlation coefficients between traits

and climate from Chapter 3 (r>0.5; table 4.2). Four sub-models were created based on taxon input: all-species, *Metasequoia*-only, *Sequoia*-only, and *Taxodium*-only.

GLMs were tested for fit and compared to measured data using unpaired two-sample Wilcoxon test, where a p-value<0.05 indicates that the mean of the sample was statistically different from measured modern data and therefore were not considered a good fit. This was implemented in RStudio using wilcox.test() function with a two sided adjustment.

4.2.3 Model sensitivity to climate data inputs

To test the construct of my models, I performed two separate tests. First, in R I generated "random" climate sets of two to three variables from the same six variables, removing models that matched any of my current models (referred to as "random models", table 4.3). These were tested for fit and compared to measured modern trait data, using unpaired two-sample Wilcoxon test. Next, I ran a second set of models, where climate variables were expanded to all 19 Bioclim variables and based on correlations found previously (Ng and Smith, 2020, referred to as "all-bioclim models" table 4.5).

4.2.4 Model application

Once models were tested for fit, all-species and *Metasequoia*-only datasets were used with past climate simulations to estimate Eocene traits. I used these two datasets to increase our understanding of plant response to climate. Early Eocene fossil climate variables (see section Climate data for early Eocene fossils) were input into models to estimate anatomical traits for each CO_2 scenario. Each fossil trait estimate had four models (A–D) per trait except for cross-sectional area which has five models (A–E). In Chapter 2 and 3, I found cross-sectional area explained most variation in the data and included an extra model. Each fossil trait estimate was tested for differences in mean (p<0.05) with modern measured dataset using unpaired two-sample Wilcoxon test.

Table 4.1: Summary of each climate set

	all-species	*Metasequoia*-only	3x	6x
MAT (°C)	13.7 ± 4.2	11.4 ± 3.1	9.4 ± 7.0	17.0 ± 6.9
MTWQ (°C)	21.1 ± 4.3	19.6 ± 3.4	23.2 ± 7.3	31.4 ± 8.3
MTCQ (°C)	6.3 ± 5.0	3.4 ± 3.0	-2.9 ± 9.1	3.9 ± 8.7
MAP (mm)	977 ± 383	820 ± 279	923 ± 349	1132 ± 413
PWeQ (mm)	393 ± 192	313 ± 165	342 ± 147	405 ± 157
PDrQ (mm)	125 ± 85	117 ± 50	140 ± 63	175 ± 92

4.2.5 Model validation

I compared models with leaf width measurements from fossils (n=5; table 4.8). Figures of *Metasequoia* leaf compressions from literature were compiled from two early Eocene localities: Falkland site from Okanagan Highlands, B.C., Canada (50.61 ± 0.16 Ma; fig. C from Greenwood et al. (2005); and fig. C, D from Smith et al. (2009)); and Quilchena, B.C., Canada (51.5 ± 0.4 Ma; fig. 4G, 4I; Mathewes et al., 2016). Leaf images were measured at the middle using ImageJ v1.49 (Schneider et al., 2012); for each branchlet, 5–8 measurements were made. Measurements were averaged per branchlet and compared to estimated Eocene traits, using the unpaired two-sample Wilcoxon test.

4.3 Results

4.3.1 Modern and early Eocene climate

The modern dataset has a latitudinal range from 23.15–59.85º N. Overall, the mean climate of the all-species dataset was similar to *Metasequoia*-only (table 4.1). Early Eocene *Metasequoia* localities had a paleo-latitude ranging from 43.39 to 81.93ºN, reported across Japan, USA (Alaska, North Dakota, and Washington), Canada (British Columbia, Nunavut, and Ellesmere Island), Greenland, Russia, and Spitsbergen. Based on fossil localities, early Eocene climate for *Metasequoia* spp. estimate 6x climate was a warmer and wetter climate than 3x (table 4.1).

4.3.2 Trait-climate models

Trait-climate models, with standard error, were generated on BCCVL are listed in table 4.2. I tested model fit by using modern climate to compare estimated traits to measured modern traits and found all models estimated traits within the modern range. Trait estimates for *Metasequoia*- and *Sequoia*-only datasets had a smaller range than all-species and *Taxodium*-only models (fig. 4.2). Two-sample Wilcoxon test showed a significantly different median in only one instance, between measured resin canal area and model rca_C ($p<0.001$; table 4.2).

4.3.3 Trait estimates for early Eocene *Metasequoia*

Trait-climate models of all-species and *Metasequoia*-only datasets were used to estimate traits based on input of early Eocene climate simulations data at 3x and 6x [CO_2] (table 4.6, 4.7). I omitted *Sequoia*- and *Taxodium*-only models because my focus is on the better-studied *Metasequoia*. I compared modern measured trait data (referred to as modern traits) to modelled early Eocene estimated trait data (Eocene traits; fig. 4.6) and found that the largest cross-sectional area was estimated at 739162.8 μm^2 in *Metasequoia* model xsa_E (table 4.2) at 3x, while the smallest was estimated at 19607.1 μm^2 in all-species model xsa_D at 3x (table 4.2). Largest and smallest resin canal area, 4418.2 and 113.5 μm^2 respectively, were estimated in 3x all-species model rca_B. The widest and narrowest leaf width were estimated in 3x all-species model lw_B and lw_D, 2643.6 and 697.3 µm respectively. Leaf thickness minimum and maximum were estimated in 3x all-species model lt_A at 71.3 µm and lt_C at 394.6 µm. Wilcoxon test comparing estimated Eocene traits to measured modern traits show significant differences ($p<0.05$) for a subset of models in each trait except in *Metasequoia*-only resin canal area (3x and 6x) and leaf width (3x; table 4.9).

4.3.4 General trends in all-species datasets

For cross-sectional area, most models using 3x and 6x resulted in trait values with a lower mean than for modern measured (Table ModelSummary; fig. 4.6). Generally, 6x models estimated a lower median and mean than 3x models. I tested the models by comparing modern traits to both 3x and 6x Eocene traits and found all but three 3x models (xsa_B, xsa_C, and xsa_E) had significantly different medians ($p<0.05$) from modern traits.

Resin canal area models (rca_A–C) mean and median were highest in 6x models and lowest in 3x models. However, these 6x estimates were not statistically different than modern. Model rca_D show the opposite relationship: a decrease in mean area from 3x to 6x CO_2 (table ModelSummary). Both 3x models rca_A and rca_B, and 6x rca_D had a significantly different mean from modern trait ($p<0.05$).

Leaf width estimates show 3x models lw_A and lw_D have lower, and lw_B and lw_C have higher, mean and median values compared to modern trait (table ModelSummary; fig. 4.6). All 6x models show a decrease in mean and median from modern and 3x. A Wilcoxon test between modern and 3x estimates of Eocene traits show only lw_B and lw_C were statistically different $p<0.05$, whereas all 6x models were statistically different ($p<0.05$) from modern traits.

All estimated leaf thickness Eocene traits have a lower mean than modern traits (table ModelSummary), however only 6x lt_C and 3x lt_D were not statistically different.

4.3.5 General trends in *Metasequoia*-only datasets

Model xsa_B at 3x had a lower mean and median than modern traits compared to the other 3x models. Models xsa_C and xsa_D at 3x had a significantly different mean than modern traits ($p<0.05$). All 6x Eocene trait estimates were significantly lower ($p<0.05$) than modern and 3x estimates. Resin canal area showed no significant differences between means of modern and Eocene traits. Leaf width showed smaller leaf widths in 6x climate scenario than 3x, and 6x were significantly different from modern in lw_A, lw_B, and lw_D.

No significant differences ($p>0.05$) were found between modern and 3x Eocene traits. Leaf thickness for Eocene traits are approximately the same or higher than modern. Only two significant differences in mean were found, in 6x model lt_A and 3x lt_B.

4.3.6 Models created using random climate sets

Our random models performed well, with significant differences in all-species datasets for resin canal models rca_01, rca_02, and leaf thickness models lt_01, lt_02 (table 4.4, fig. 4.3). All-bioclim models for all cross-sectional and resin canal area models and only some leaf thickness and width models were significantly different from modern traits ($p<0.001$; table 4.5, fig. 4.4).

4.3.7 Fossil leaf widths

Fossil leaf width measurements from published literature (n=5) ranged from 1126.1–2360.0 µm, with a mean of 1784.6 $\pm$ 333.2 µm (table 4.8). I compared measured fossil to estimated Eocene leaf width and found fossil measurements were only statistically different for 6x all-species model lw_A, lw_C, and lw_D (table 4.8).

4.4 Discussion

The natural modern habitat of *Metasequoia glyptostroboides* has a MAT of 13° C, with coldest recorded temperatures between -6.1 and 1.7° C, warm summer months between 23.3 and 32.3° C, and a MAP $\sim$1300 mm yr^{-1} (Bartholomew et al., 1983; Fu et al., 1992; LePage et al., 2005). The all-species dataset including *Metasequoia*, *S. sempervirens* and *T. distichum* reflect climate that is within the natural habitat of *M. glyptostroboides* climatic range, with a similar MAT (13.7 $\pm$ 4.2° C) and MTWQ (21.1 $\pm$ 4.3° C). MTCQ at 6.3° C is much warmer than recorded temperatures for *Metasequoia*'s natural habitat, because the dataset range was $\sim$30° of latitude, which is broader than *Metasequoia*'s natural range that

is limited to ∼31° N. The *Metasequoia*-only dataset was a bit cooler and drier than either the natural habitat or the all-species dataset, with a mean MAT at 11.4 ± 3.1° C and a MAP of 820 ± 279 mm yr^{-1}, a result of excluding the sub-tropical habitat of *T.distichum* and cool coastal climate of *S. sempervirens*.

Both 3x and 6x early Eocene climate scenarios fit within published reconstructed estimates of CO_2, yet previous environmental and climatic niche estimates derived from proxies suggest climatic reconstructions of *Metasequoia* fell somewhere in between 3x and 6x (Cevallos-Ferriz et al., 1991; Wing et al., 1991; Wilf, 2000; Ng and Smith, 2020). Early Eocene estimate of atmospheric CO_2 is between ∼200 and 1700 ppm, based on methods such as stomatal index and paleosol proxies, and climate simulations (Sloan and Rea, 1996; Smith et al., 2010a; Hyland and Sheldon, 2013; Anagnostou et al., 2016; Hollis et al., 2019). The early Eocene climate model from Zhu et al. (2019) simulated a climate that infers *Metasequoia* either inhabited a climatic niche that was either warmer and wetter climate (6x) or cooler and drier (3x) relative to published findings (Cevallos-Ferriz et al., 1991; Wing et al., 1991; Wilf, 2000; Ng and Smith, 2020). Climate estimates for *M. milleri*, an early Eocene Princeton Chert fossil from the Allenby Formation in British Columbia, Canada, were warmer and less seasonal than modern *Metasequoia*, similar to the climatic and environmental niche of modern *Taxodium* (Cevallos-Ferriz et al., 1991; Ng and Smith, 2020). Early Eocene climate estimates in Wyoming (USA) found *Metasequoia occidentalis* inhabiting climate closer to 6x simulations. MAT estimated using leaf margin analysis from plant fossils in the Willwood Formation (early Eocene, Wyoming) was 16–18° C (Wing et al., 1991), with a CMMT above freezing (based on nearest living relatives of frost intolerant tree ferns, palms, and cycads; Wing et al., 1991). While 3x climate reconstruction of *Metasequoia* is more similar to current climate, 6x climate matches qualitative descriptions and quantitative analyses of early Eocene conditions *Metasequoia* inhabited in the past. The difference between previous and present climatic conditions suggests a change in *Metasequoia*'s climatic niche through time. Further modelling may

show whether this was a constriction or a shift.

4.4.1 Trait-climate model accuracy

The trait-climate models that were generated reflected and fit the data well. Model rca_C for all-species dataset was the only model statistically different ($p<0.05$) from the measured data, yet was still within range of modern resin canal area. The test models, random and all-bioclim, emphasized the importance of climate variable sets over individual climate variables for inferring climate-trait correlations. Random models all used the same six-variable suite of climate data (MAT, MTWQ, MTCQ, MAP, PWeQ, PDrQ) and each estimated the tested trait that was not significantly different than modern trait data (table 4.4), whereas all-bioclim models used a set of correlated variables from all 19 bioclim climate variables and showed significant differences in all resin canal and cross-sectional area estimates (table 4.5. While bioclim climate variables may each correlate to the traits tested, when combined together, overall do not predict traits well.

4.4.2 Trait estimates for the early Eocene

Investigating plant response to climate through trait-climate models is an important step in understanding how climate has shaped plant evolutionary history. Species distribution models show accuracy in predicting a species' geographic range in the past and present for short time scales (*i.e.,* hundreds of years), investigating immediate response (Marini et al., 2010; Godsoe, 2010). When applied to longer time scales (*i.e.*, thousands of years), many non-climatic predictive factors, such as species' ecology and response to environmental changes, are not accounted for (Worth et al., 2014; Morin and Lechowicz, 2008). Unlike species distribution models that rely solely on presence and absences (shown to be inherently biased; Daru et al., 2018) and climatic variables, trait-based approaches are valuable in that they have the potential to account for variations in physiology, morphology, and growth (Lavorel and Garnier, 2002; Regos et al., 2019; Zakharova et al., 2019).

Estimating early Eocene conifer traits, while preliminary, will help us understand the extent of these variations in traits linked to physiology and growth and thus, provide a foundation in which we can model traits across spatial and temporal scales in order to understand the evolutionary influences of climate on physiology and growth.

In this chapter, I reconstructed early Eocene traits for this once-widespread conifer with the ultimate goal of understanding how Cenozoic climate change has affected leaf traits, and therefore anatomy and physiology. It is important to note that my models do not account for actual changes in CO_2, *i.e.* no growth experiments were conducted, but instead use changes in temperature that rely on modelled CO_2. The majority of my trait models show that warmer climates correspond to smaller-than-average traits, except for resin canal area where 6x scenario estimated larger resin canals. The all-species and *Metasequoia*-only datasets have different ranges of estimated trait responses, all-species exhibit a wide range compared to highly constrained *Metasequoia*-only. This may suggests that different species have different trait optima for a given climate, based on the hypothesis that a species' environment act as a filter and therefore, all species should converge on a single trait optimum (Parker and Smith, 1990; Makela et al., 2002). However, this hypothesis is highly contested within the scientific community, where some have argued in support of multiple trait optima, countering the idealized organism with an idealized response (Marks and Lechowicz, 2006; Marks, 2007; Pistón et al., 2019). Insignificant differences between measured modern and estimated early Eocene traits could suggest species persist through time by inhabiting favorable habitat maintaining a range of trait optima, or alternatively that climate has less predictive value for traits when using generalized linear models. Trait variation across time within *Metasequoia* has not been explicitly studied in part because of the inherent nature of fossil preservation. Collecting leaf width measurements across spatial and temporal scales, while the record is imperfect and biased, will help determine whether climate, using generalized linear models, can accurately reflect trait variation through time.

I found that most models responded linearly with increased CO_2 (fig. 4.6). These

responses varied within each trait, suggesting a link to climate, however that is outside the scope of this paper. Non-linear responses increase then decrease median and mean with increasing CO_2, most notably for cross-sectional area (xsa_C) and leaf width (lw_B and lw_C) in both all-species and *Metasequoia*-only models. Non-linear responses are, in part, the result of increased temperature and precipitation seasonality at higher latitudes which results in a median trait shift (fig. 4.5). Previous growth experiments in elevated CO_2 conditions of ambient (340), 520, 718, and 910 ppm, reported pine needle leaf thickness had a similar non-linear response (Thomas and Harvey, 1983). Thomas and Harvey (1983) and this study had an overall leaf thickness increase with increased CO_2 conditions, except at CO_2 levels 520 ppm (Thomas and Harvey, 1983) and 3x ($\sim$840ppm, this study), where leaves were less thick than leaves at ambient or elevated. Why these non-linear responses occur at these CO_2 levels remain a mystery.

Changes in leaf thickness and width affects cross-sectional area. Growth experiments by Lin et al. (2001) on *Pinus sylvestris* (Pinaceae) showed that with increased CO_2, cross-sectional area increased by 10%, however most of that change was due to an increase in leaf thickness from increased mesophyll tissue. The model suggests changes in cross-sectional area is from leaf width, not leaf thickness. Leaf width estimates are more variable than leaf thickness and are thought to reflect temperature regulation, changing the boundary layer of the leaf. A wider leaf has a higher boundary layer that affects heat offloading (Gurevitch, 1988; Hatfield and Burke, 1991; Schuepp, 1993; Vogel, 2009). Temperature regulation is important in order to maintain physiological processes such as photosynthesis. At high temperatures, oxygen molecules compete with CO_2 for binding sites on Rubisco, decreasing photosynthetic activity and form hydrogen peroxide, damaging photosynthetic cells beyond repair (Hueve et al., 2011). Early Eocene estimates show both all-species and *Metasequoia*-only models exhibit slight shifts in leaf width, where it increased in 3x lw_B–C and decreased for the remainder.

Across modern ecosystems, thick leaves are found in plants that have longer life spans

and occupy drier, sunnier, and less fertile habitats (Perez-Harguindeguy et al., 2016). Leaf thickness is hypothesized to correlate with relative growth rates and photosynthesis (Perez-Harguindeguy et al., 2016). From experimental studies, leaf thickness was expected to increase in a warmer, wetter world, because of an increased access to resources such as CO_2 and water, which would lead to increased investment in photosynthetic tissue and thus higher photosynthetic rate (Thomas and Harvey, 1983; Sims et al., 1998; Lin et al., 2001). The *Metasequoia*-only models show minimal and insignificant shifts with increasing CO_2, while all-species models showed significant decreases with increasing CO_2. This similarity between early Eocene leaf thickness estimates from *Metasequoia*-only models and present-day values suggested that thickness is limited by physiological constraints. The all-species model estimates significantly thinner leaves which may suggest a shift in physiological optimum based on leaf thickness, such as *Taxodium*. *Taxodium* has the narrowest, thinnest leaves of the three species examined, and when its environmental preferences are considered, inhabits a much warmer climate today than both *Metasequoia* and *Sequoia*. Although, if climate was more optimal for thin leaved species, most likely *Metasequoia* was able to out compete *Taxodium* because it is especially adapted to live in seasonal continuous light and dark conditions and unlike *Taxodium* does not undergo photosynthetic inhibition (Jagels and Day, 2004; Equiza et al., 2006; Jagels and Equiza, 2007).

4.4.3 Fossil validation

Fossil leaf width measurements were based on two fossil localities and show *Metasequoia occidentalis* fossils were narrower than modern leaves, in agreement and most closely reflects the model trait estimate means of 6x *Metasequoia*-only models (table 4.7, 4.6). In addition, previous quantification of traits of permineralized *Metasequoia milleri* Rothwell and Basinger show this taxon had narrow leaves (1133.1 $\pm$ 401.5 µm), and slightly thicker leaves (mean 332.7 $\pm$ 67 µm, Ng and Smith, 2020) comparable to

results from 6x all-species models. The early Eocene 3x all-species and *Metasequoia*-only and 6x *Metasequoia*-only models were not statistically different from empirical leaf width measurements from early Eocene fossils (table 4.9). These statistically insignificant p-values suggests although the means of fossil are within 6x *Metasequoia*-only estimates, there are models (3x all-species and *Metasquoia*-only) which still need to be considered, especially with my current sample size. *Metasequoia* compression/impression fossils are known across the Northern Hemisphere in the early Eocene, however many studies have not published images of these fossils with their findings (McIver and Basinger, 1999; Wing, 1987; Akhmetiev, 2010; Williams et al., 2010). By accessing collections to expand the range of early Eocene sites with *Metasequoia occidentalis* and adding even more time intervals, we can improve my model validation and deepen our understanding of how climate affects traits in *Metasequoia*.

4.5 Conclusions

In order to better understand how climate affects plant traits, I created and tested trait-climate models from modern data to estimate leaf traits of fossils. I found that the six-variable suite of climate variables used in my models are more important than which variables are highly correlated to traits in a model. These six climate variables are: MAT, MTWQ, MTCQ, MAP, PWeQ, and PDrQ.

Based on model fit with modern data, I estimated traits for fossils in the early Eocene using 3x and 6x pre-industrial CO_2 climate scenarios and found increased CO_2 corresponded to decreased leaf width and leaf thickness and thus, cross-sectional area. However, resin canal area was constant, likely due to phylogenetic conservatism. Overall plant response to a warmer climate shows a shift to smaller and thinner leaves, which is a response to mitigate heat stress.

Leaf width, the only trait I could reliably measure from compression/impression fossils

and use to validate my models, was not significantly different from all 3x and 6x models for *Metasequoia*-only dataset, and all 3x models for all-species dataset. This statistical result may suggest 3x climate models more accurately reflect climatic stressors than 6x reconstructions, however, more leaf measurements from fossils beyond western North America, are needed to more confidently assess these trait-climate models.

My results from projecting traits in the past show promise as a first step in trying to understand the evolutionary and ecological adaptations of plant leaves in response to climate. We can further deepen our understanding of how climate affects traits in *Metasequoia* by applying these models to more time intervals, such as middle and late Eocene, and early and middle Miocene, which encompass other Cenozoic warm intervals. By adding these time intervals, results can be combined with species distribution modelling to mechanistically model how leaf traits and therefore leaf economics and physiology of *Metasequoia* has changed over time.

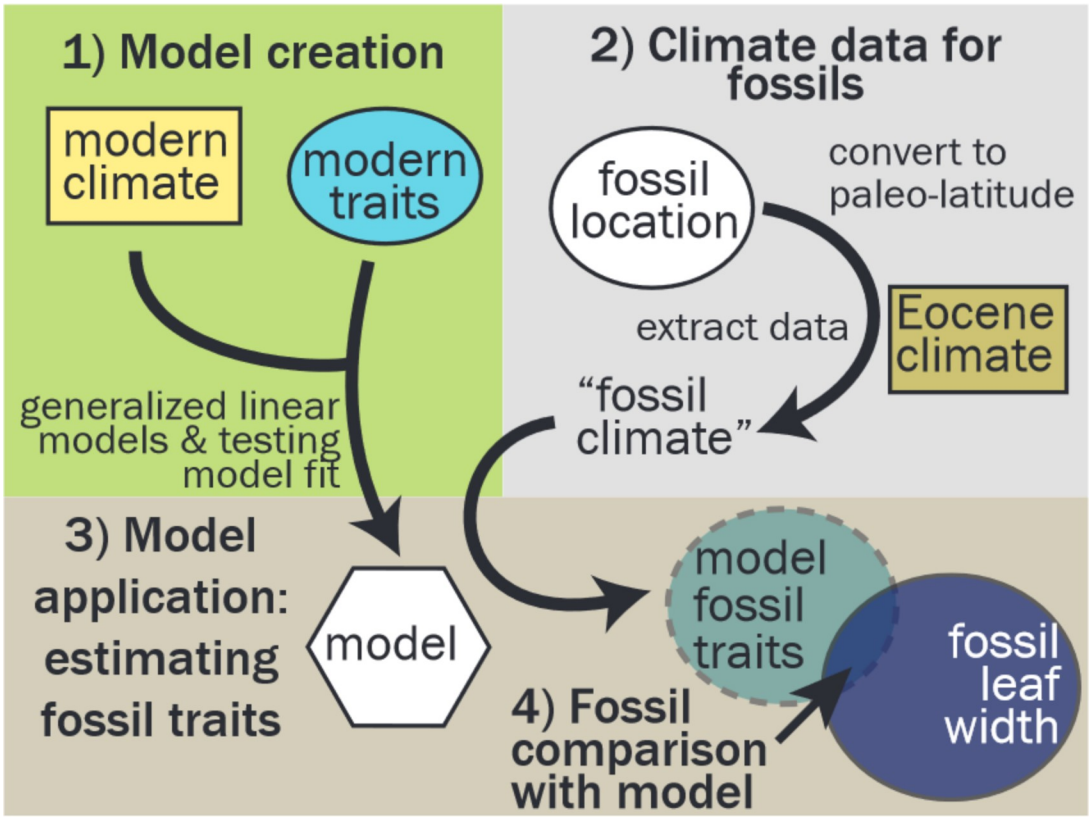

Figure 4.1: Workflow of study broken down into five parts: 1) Modern trait-climate models were created using generalized linear models and 2) tested for fit and sensitivity using “random climate” sets. 3) climate data for fossils were collected from literature and climate simulations. 4) 1 & 3 were combined to estimate traits in the early Eocene. 5) Fossil leaves were compared to fossil estimates.

Table 4.2: Trait-climate model matrix and standard error

Model	B01	B10	B11	B12	B16	B17	Model std. error All-species	*Metasequoia*	*Sequoia*	*Taxodium*
Transverse area										
xsa_A	x	x		x		x	0.21	0.42	0.29	0.98
xsa_B		x				x	0.17	0.33	0.23	0.39
xsa_C	x			x			0.19	0.17	0.17	0.13
xsa_D	x	x		x			0.26	0.48	0.21	0.64
xsa_E	x			x		x	0.16	0.17	0.17	0.86
Resin canal area										
rca_A			x		x	x	0.18	0.37	0.32	1.15
rca_B			x			x	0.15	0.34	0.19	0.41
rca_C			x		x		0.22*	0.32	0.16	0.67
rca_D					x	x	0.16	0.43	0.43	0.28
Leaf width										
lw_A	x	x				x	0.09	0.40	0.10	0.35
lw_B	x			x			0.09	0.13	0.05	0.29
lw_C	x			x		x	0.07	0.14	0.07	0.53
lw_D		x		x		x	0.08	0.28	0.10	0.49
Leaf thickness										
lt_A		x	x		x	x	0.12	0.51	0.23	0.52
lt_B		x	x			x	0.11	0.56	0.20	0.27
lt_C			x			x	0.06	0.12	0.08	0.15
lt_D		x				x	0.13	0.36	0.19	0.22

* Wilcoxon p-value <0.05

Table 4.3: Trait-climate matrix for each random model

Model	B01	B10	B11	B12	B16	B17
trait_01	x			x	x	
trait_02			x	x	x	
trait_03				x	x	x
trait_04	x	x			x	
trait_05		x			x	x
trait_06		x	x	x		

Table 4.4: Random climate set model standard error and significance

Model	All-species	*Metasequoia*-only	*Sequoia*-only	*Taxodium*-only
Cross-sectional area				
xsa_01	0.18	0.16	0.54	0.18
xsa_02	0.13	0.13	0.53	0.14
xsa_03	0.08	0.14	0.30	0.14
xsa_04	0.27	0.25	0.65	0.61
xsa_05	0.18	0.26	0.76	0.35
xsa_06	0.23	0.19	0.59	0.46
Resin canal area				
rca_01	0.31*	0.35	0.84	0.58
rca_02	0.19*	0.26	0.78	0.38
rca_03	0.14	0.28	0.38	0.41
rca_04	0.40	0.52	0.99	2.12
rca_05	0.40	0.50	1.02	1.35
rca_06	0.31	0.38	0.88	1.66
Leaf width				
lw_01	0.07	0.06	0.32	0.15
lw_02	0.06	0.05	0.31	0.13
lw_03	0.05	0.05	0.19	0.13
lw_04	0.12	0.10	0.41	0.40
lw_05	0.08	0.10	0.49	0.28
lw_06	0.11	0.07	0.37	0.38
Leaf thickness				
lt_01	0.12*	0.15	0.29	0.18
lt_02	0.08*	0.07	0.24	0.12
lt_03	0.07	0.22	0.37	0.72
lt_04	0.17	0.11	0.16	0.15
lt_05	0.13	0.21	0.42	0.36
lt_06	0.14	0.16	0.33	0.54

* Wilcoxon p-value$<$0.05

Table 4.5: All-bioclim models with p-values

Model	B01	B03	B04	B08	B09	B10	B15	B17	B18	B19	All-species	*Metasequoia*-only	*Sequoia*-only	*Taxodium*-only
Cross-sectional area														
xsa_01		x				x			x	-	-	-	-	
xsa_02							x	x		x	-	-	-	-
xsa_03		x						x		x	-	-	-	-
Resin canal area														
rca_01		x						x	x		-	-	-	-
rca_02		x			x			x			-	-	-	-
rca_03		x					x				-	-	-	-
Leaf width														
lw_01	x					x		x			0.61	0.75	-	0.77
lw_02	x			x		x					0.64	0.74	0.97	0.74
lw_03	x					x			x		-	0.22	-	0.75
Leaf thickness														
lt_01		x	x				x				-	0.22	-	-
lt_02								x	x		0.26	0.19	0.36	0.68
lt_03			x				x				-	-	-	-

"-" represents significant p-values, when $p<0.05$

Table 4.6: Fossil trait estimates for all-species dataset

Model	3x		6x	
	mean ± sd	min–max	mean ± sd	min–max
Cross-sectional area (μm^2)				
xsa_A[3,6]	307625 ± 182715	112850–591656	200742 ± 143231	60622–436885
xsa_B[6]	353490 ± 178786	118743–628509	213601 ± 138208	72172–445727
xsa_C	436032 ±98780	215146–685002	406464 ± 108327	166462–655083
xsa_D[3,6]	244125 ± 214823	26209–585962	160347 ± 148309	19607–395079
xsa_E[6]	421163 ± 126962	128946–5723467	287793 ± 118060	87428–474658
Resin canal area (μm^2)				
rca_A[3]	1366.0 ± 793.7	137.1–3165.6	1814.7 ± 1255.6	113.5–4410.6
rca_B[3]	1367.8 ± 795.4	137.1–3174.1	1817.2 ± 1258.0	113.5–4418.2
rca_C	1583.7 ± 822.0	402.4–3492.9	2487.9 ± 1190.0	660.1–4321.4
rca_D[6]	1798.9 ± 730.5	230.0–3185.0	1502.8 ± 915.3	129.3–3132.1
Leaf width (μm)				
lw_A[6]	1719.3 ± 438.6	979.9–2323.0	1218.1 ± 371.0	765.2–1804.7
lw_B[3,6]	2018.0 ± 414.3	1317.1–2643.6	1566.9 ± 299.0	1057.2–1961.7
lw_C[3,6]	1934.9 ± 429.6	1199.9–2514.0	1385.6 ± 307.0	915.3–1833.2
lw_D[6]	1598.8 ± 456.1	878.0–2280.6	1155.4 ± 396.2	697.3–1785.4
Leaf width (μm)				
lt_A[3,6]	212.3 ± 90.9	91.6–339.1	199.1 ± 95.6	71.3–338.0
lt_B[3,6]	211.4 ± 87.2	96.9–333.1	196.0 ± 91.2	73.5–328.8
lt_C[3]	241.1 ± 66.8	102.4–352.2	256.4 ± 91.1	92.6–394.6
lt_D[6]	271.9 ± 59.3	135.6–352.1	224.3 ± 67.8	105.2–324.4

Note– [3],[6] refers to Wilcoxon p-value$<$0.05 for respective CO_2 model
Cross-sectional area estimates rounded to nearest whole number.

Table 4.7: Fossil trait estimates for *Metasequoia*-only dataset

Model	3x		6x	
	mean ± sd	min–max	mean ± sd	min–max
Cross-sectional area (μm^2)				
xsa_A[6]	462688 ± 136900	199462–717841	328769 ± 96135	148157–498355
xsa_B[3,6]	377073 ± 69485	224875–473336	303882 ± 63901	189754–393359
xsa_C[3,6]	460766 ± 121774	231015–697588	348812 ± 92625	179101–522927
xsa_D[3,6]	462992 ± 126011	232730–711703	350160 ± 94838	180145–532671
xsa_E[3,6]	468898 ± 142023	204420–739163	333907 ± 98857	151932–512017
Resin canal area (μm^2)				
rca_A	1262.4 ± 157.2	1007.5–1528.2	1330.1± 170.0	1017.1–1543.2
rca_B	1377.4 ± 58.2	1306.4–1556.6	1397.9± 85.1	1301.3–1609.8
rca_C	1264.2 ± 154.2	1012.9–1527.8	1332.0± 165.8	1025.5–1539.5
rca_D	1352.0 ± 49.1	1273.3–1404.7	1336.5± 48.7	1253.5–1389.4
Leaf width (μm)				
lw_A[6]	1969.6 ± 151.6	1671.7–2144.8	1773.7± 128	1540.7–1920.5
lw_B[6]	1989.7 ± 139.4	1692.5–2212.1	1843.1 ± 126.6	1580.0–2037.3
lw_C[6]	2018.2 ± 231.7	1498.3–2359.7	1753.5± 187.8	1336.6–2025.8
lw_D[6]	1871.7 ± 137.9	1593.8–2070.3	1711.9± 147	1498.2–1938.5
Leaf thickness (μm)				
lt_A[6]	266.6 ± 14.9	242.9–331.1	280.2± 18.8	245.4–337.0
lt_B[3]	269.4 ± 15.3	245.1–300.2	260.6± 18.1	236.0–296.0
lt_C	271.5 ± 17.6	251.2–303.9	264.5± 19.4	243.1–302.7
lt_D	259.6 ± 6.4	241.3–275.2	256.3± 8.1	237.4–274.8

Note– [3],[6] Wilcoxon p-value$<$0.05 for respective CO_2 model
Cross-sectional area estimates are rounded to the nearest whole number.

Table 4.8: Summary of *Metasequoia occidentalis* fossil leaf width measurements from literature

Authority	Locality	Age	Leaves measured	Mean ± std. dev., min–max (µm)
Mathewes et al. 2016, fig. 4G	Quilchena	51.5 ±0.4	7	1980.33 ±185.72, 1766.47–2215.57
Mathewes et al. 2016, fig. 4I	Quilchena	51.5 ±0.4	7	1533.53 ±166.39, 1387.76–1795.92
Smith et al. 2009, fig. C	Falkland site, Okanagan Highlands	50.61 ±0.16	8	2150.00 ±108.50, 2000.00–2360.00
Smith et al. 2009, fig. D	Falkland site, Okanagan Highlands	50.61 ±0.16	8	1345.72 ±135.00, 1126.13–1531.53
Greenwood et al. 2005, fig. C	Falkland site, Okanagan Highlands	50.61 ±0.16	5	1913.67 ±158.53, 1774.58–2182.25

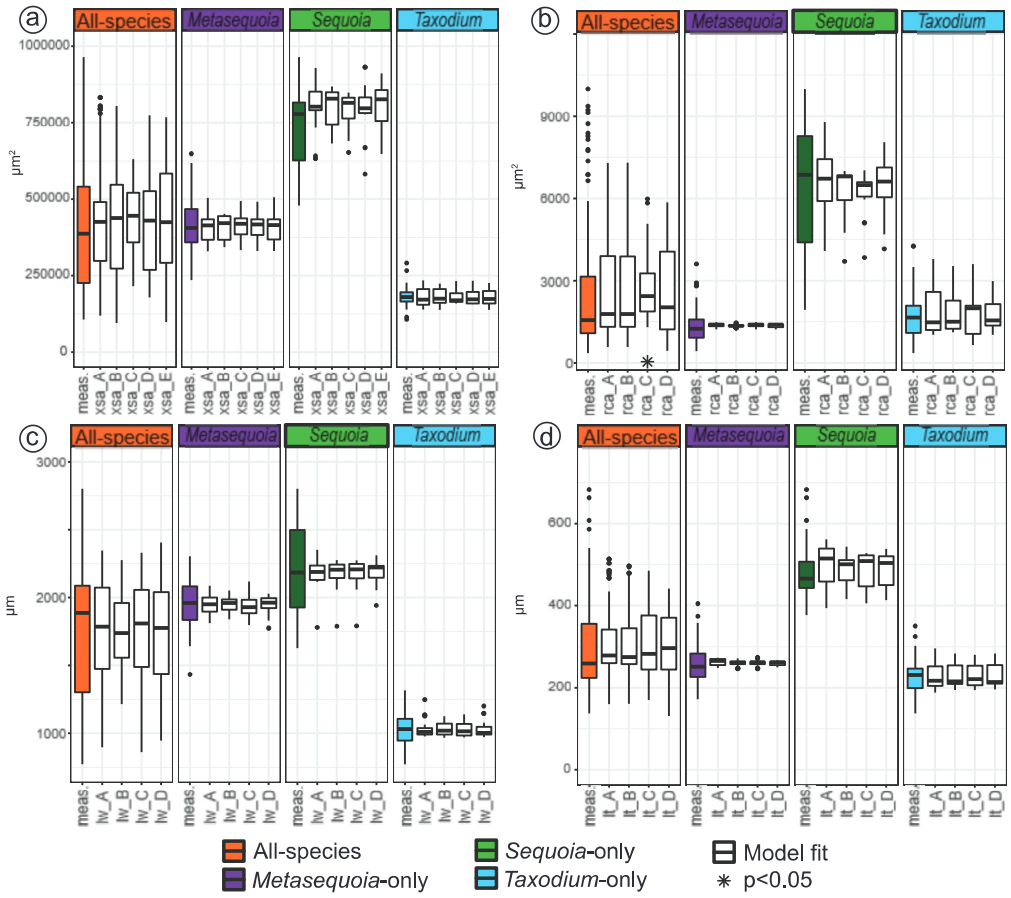

Figure 4.2: Boxplot of trait-climate models (white) compared with measured data (meas.; green) organized by traits: a) cross-sectional area, b) resin canal area, c) leaf width, and d) leaf thickness. For each trait, four datasets were tested: all-species, *Metasequoia*-only, *Sequoia*-only, *Taxodium*-only. Asterisk by model name indicates models are statistically different from modern measured data using two-sample Wilcoxon test ($p<0.05$).

Table 4.9: Two-sample Wilcoxon test for fossil estimates for 3x and 6x CO_2 scenarios

		3x		6x	
Model dataset	Model	W	p-val	W	p-val
Metasequoia-only	lw _A	74	0.322	120	0.547
	lw _B	64	0.178	105	0.944
	lw _C	63	0.167	119	0.571
	lw _D	99	0.915	113	0.723
all-species	lw _A	114	0.697	181	**0.006**
	lw _B	63	0.167	150	0.096
	lw _C	71	0.272	171	**0.016**
‘	lw _D	132	0.305	181	**0.006**

W - *W* - Wilcoxon coefficient

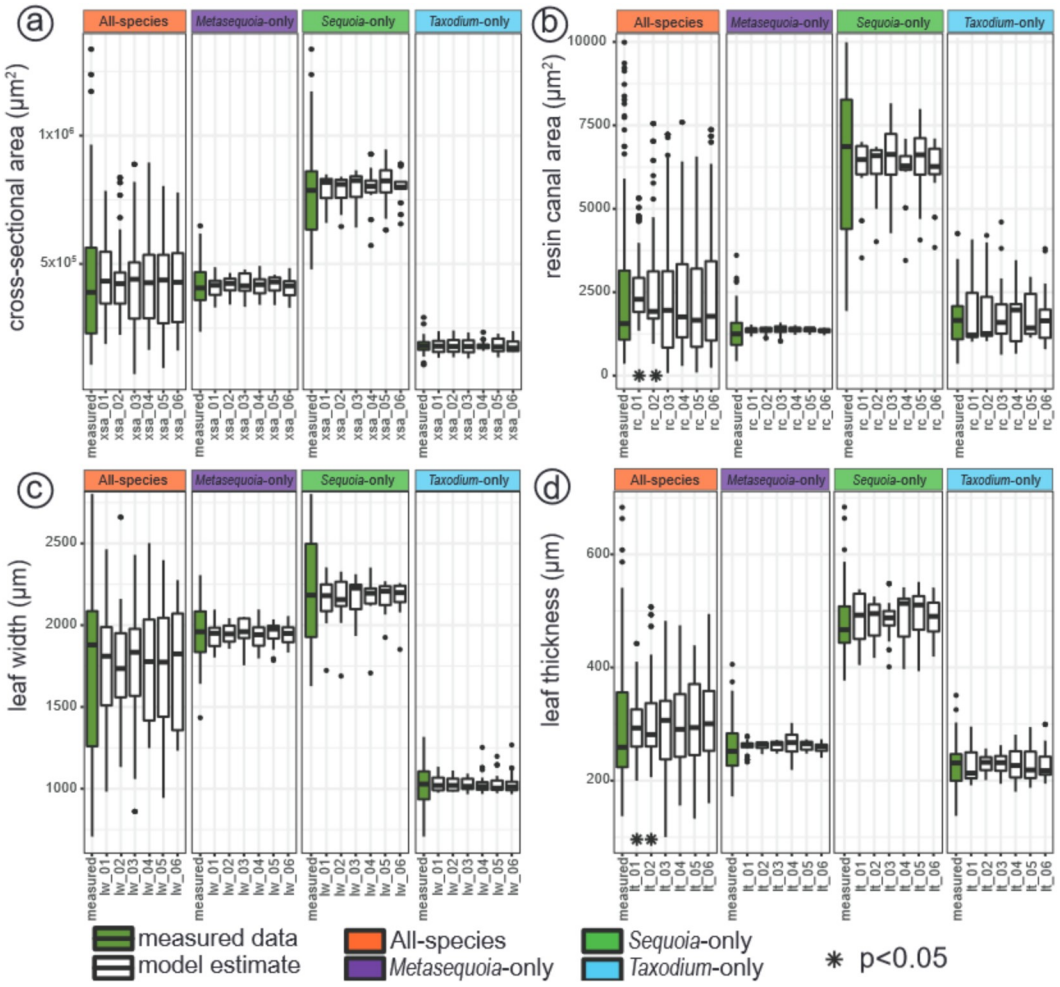

Figure 4.3: Boxplot of model sensitivity results of random models (white) compared with measured data (green) organized by traits: a) cross-sectional area, b) resin canal area, c) leaf width, and d) leaf thickness. For each trait, four datasets were tested: all-species, *Metasequoia*-only, *Sequoia*-only, *Taxodium*-only. Asterisk by model name indicates models are statistically different from modern measured data using two-sample Wilcoxon test ($p<0.05$

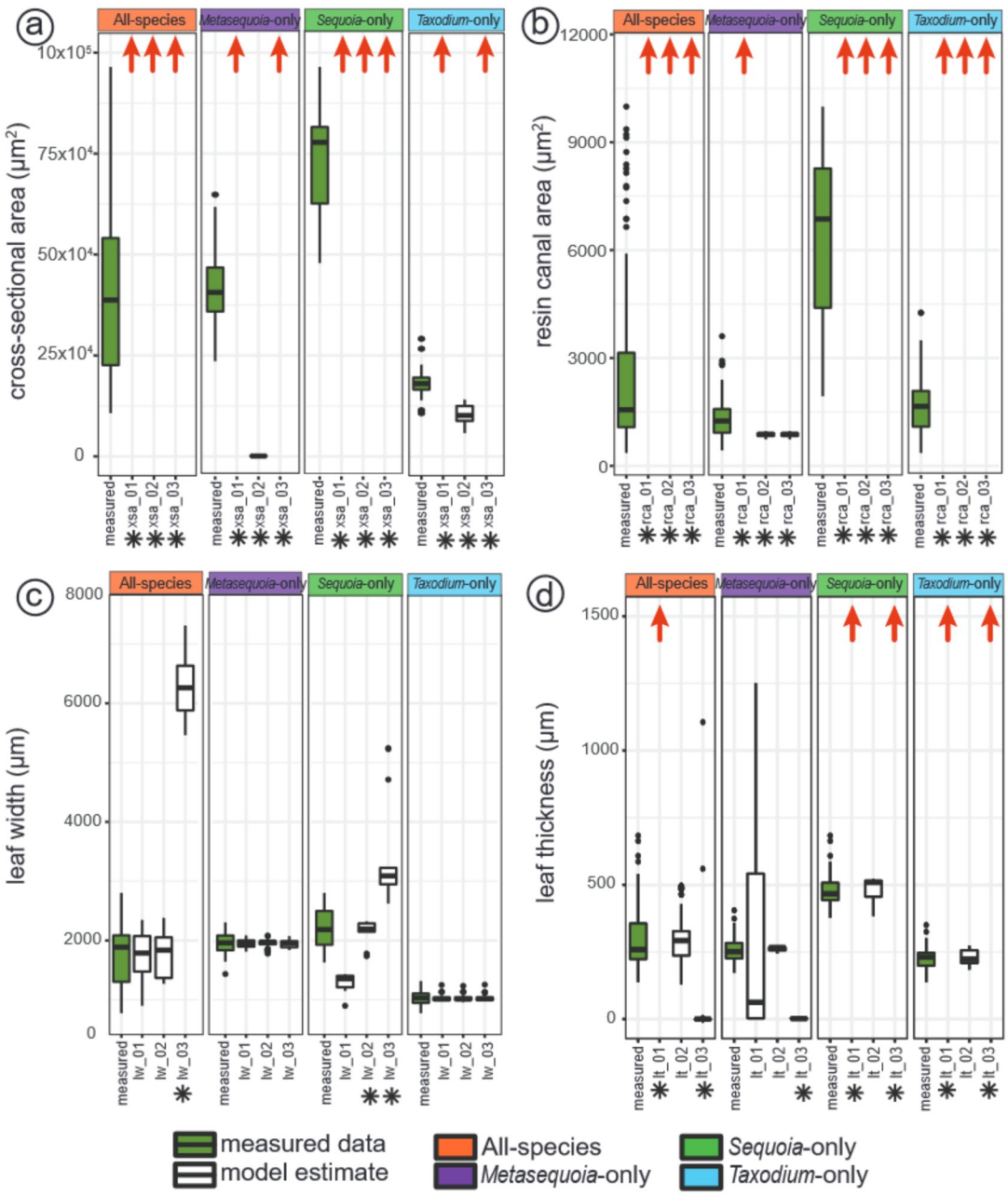

Figure 4.4: Boxplot of model sensitivity results of all-bioclim models (white) compared with measured data (green) organized by traits: a) cross-sectional area, b) resin canal area, c) leaf width, and d) leaf thickness. For each trait, four datasets were tested: all-species, *Metasequoia*-only, *Sequoia*-only, *Taxodium*-only. Red arrow indicates direction of estimates that were out of modern range. Asterisk by model name indicates models are statistically different from modern measured data using two-sample Wilcoxon test ($p<0.05$)

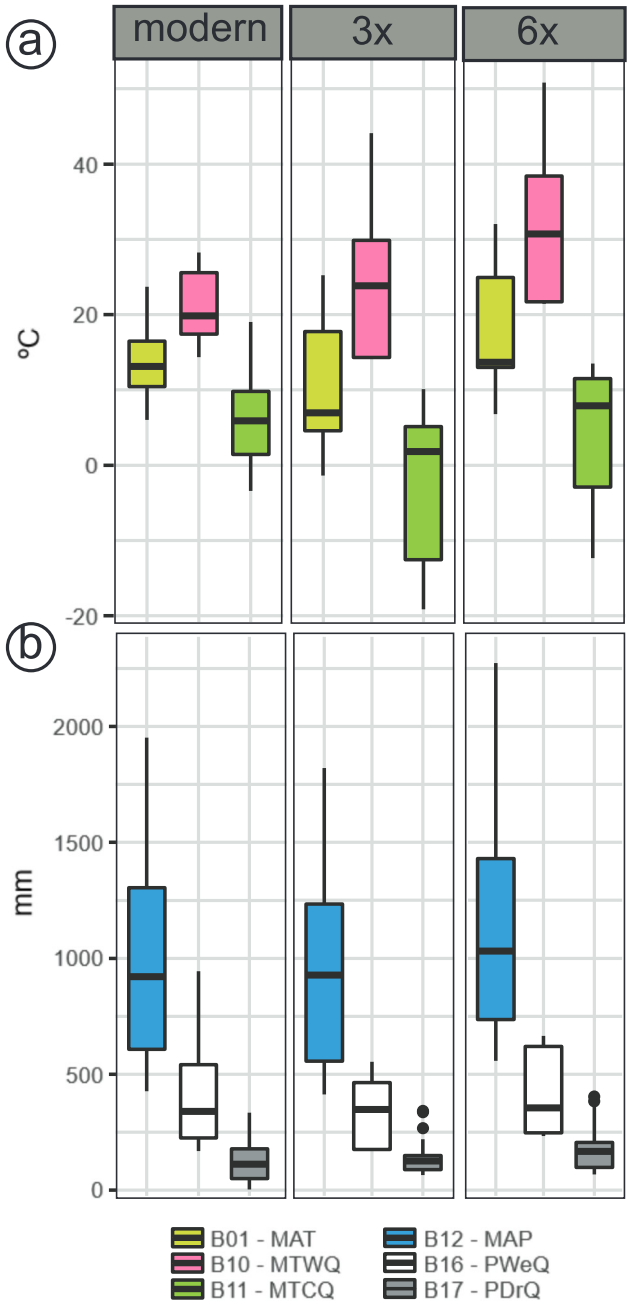

Figure 4.5: Boxplot of climatic data used in this study for modern, 3x CO_2, and 6x CO_2 scenarios. a) temperature data: mean annual temperature (dark yellow-green), mean temperature of warmest quarter (pink), and mean temperature of coldest quarter (green), and b) precipitation data: mean annual precipitation (blue), precipitation wettest quarter (white), and precipitation driest quarter (grey).

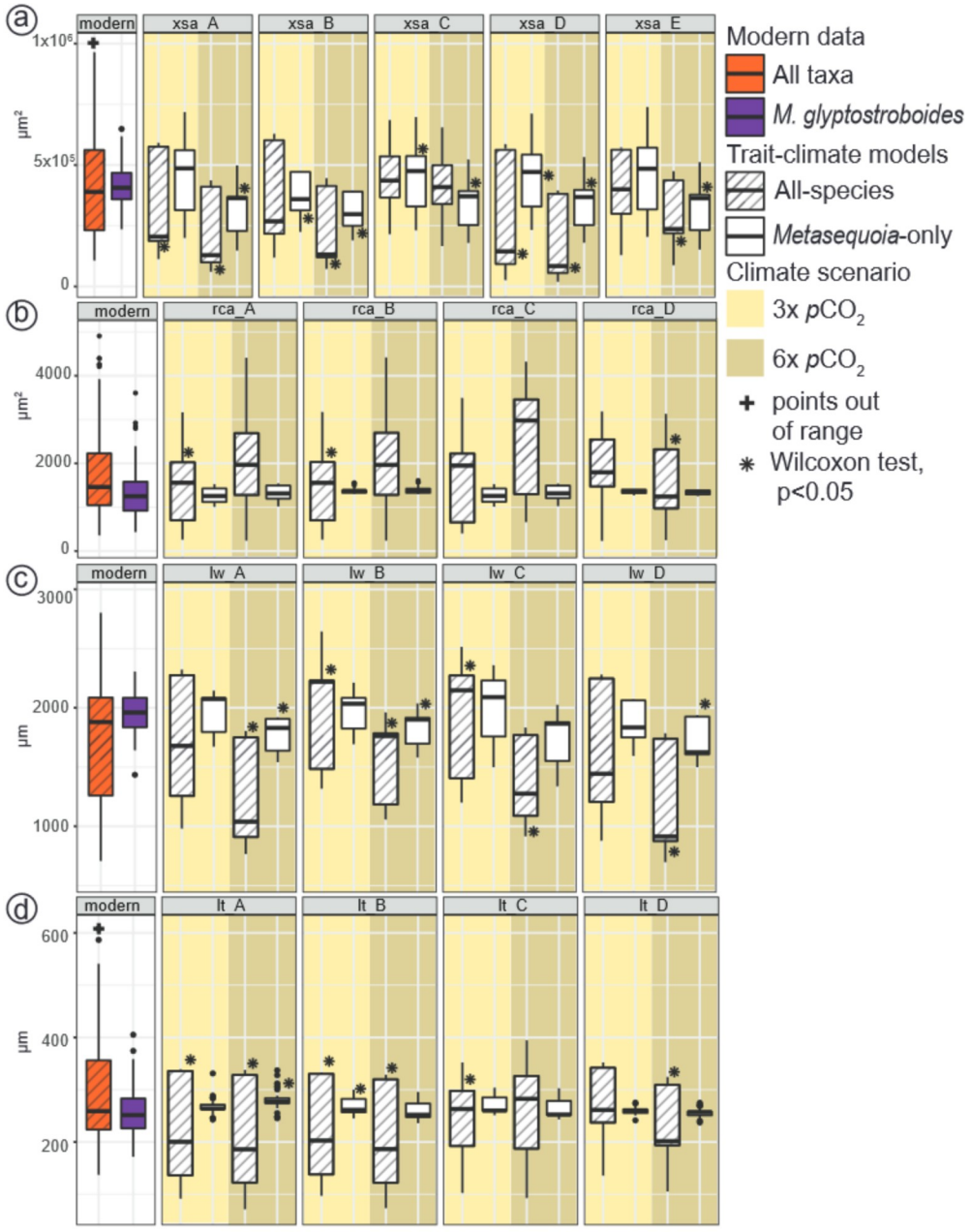

Figure 4.6: Early Eocene trait estimates for a) cross-sectional area, b) resin canal area, c) leaf width, and d) leaf thickness. For each trait, measured modern traits (white background) of all-species (orange and diagonal pattern boxes) and *Metasequoia glyptostroboides* (purple boxes) were compared to different model estimates at 3x (light yellow background) and 6x (dark yellow background), Asterisk indicates model was statisticaly different from modern measured traits using a two-sample Wilcoxon test ($p<0.05$)

CHAPTER 5

Conclusion

Correlations between plant traits and climate are valuable in testing ecological and evolutionary hypotheses, offering insights into past climate and environments, evolution of traits, and plant ecology. Heretofore approaches to understanding plant response to climate over long time scales were predominately based on woody eudicots. These approaches limit our analytical scope to the origin and ecological dominance of angiosperms, covering only ∼125-140 of ∼450 million years of plant evolution. Non-angiosperm based methods rely on modern climatic tolerances, and while semi-quantitative, the implications that are derived from these variables are limited. Studying and applying quantitative conifer links to climate is important in developing and applying models to study environments, ecology, and evolution.

By linking plant response to climate in conifers, we can expand our analytical scope. I chose to work on the conifer family Cupressaceae because of its morphological diversity in cones, leaf, and habit, and the wide range of habitats they occupy from floodplains to arid deserts (Farjon, 2005). In particular, I focused on *Metasequoia* because of its extensive fossil record across the Northern Hemisphere from mid- to high-latitudes, extending back to ca. 100 Ma (summarized in LePage et al., 2005). Over the Cenozoic, the range of this conifer has contracted substantially, now found naturally only in a small valley in Hubei Province in central China. Because *Metasequoia* has a long evolutionary history and once occupied high-latitude environments, it has been well studied, which provides an

opportunity to test hypotheses of plant-climate links in conifers over geologic time. This will deepen our knowledge of conifer evolution and ecology, which will ultimately help us understand how this once widespread conifer underwent extreme range contraction.

In this thesis, I sought to establish leaf anatomical response to climate within *Metasequoia*. I focus on the link between leaf anatomy and climate in *Metasequoia glyptostroboides*, and closely related taxa *Sequoia sempervirens* and *Taxodium distichum*. I collected leaves across North America, Asia, and Europe to measure and determine leaf anatomical links to climate. General anatomical features were collected: cross-sectional area, resin canal area, vascular bundle area, leaf width, and leaf thickness.

In Chapter 2, I found links between leaf anatomy and climate in *Metasequoia glyptostroboides*. Leaf width and cross-sectional area were associated with cold-season precipitation, vascular bundle area with warm-season precipitation, leaf thickness with mild cold-season temperatures and mean annual temperature, and resin canal area with daily temperature fluctuations and mild cold-season temperatures. These relationships were tested with the fossil *Metasequoia milleri*, an early Eocene Princeton Chert anatomically preserved from the Allenby Formation (British Columbia, Canada), to estimate past climate variables that are commonly used by paleoclimatologists. When results were compared with independent climate estimates, climatic estimates for *M. milleri* matched. This demonstrated that these trait-climate relationships held through time. Further, I discovered that *M. milleri* did not occupy or overlap the same anatomical morphospace and therefore further supported a shift in climatic niche.

Building on the results from Chapter 2, in Chapter 3 I tested how universal these trait-climate relationships were in closely related taxa, *Sequoia sempervirens* and *Taxodium distichum*. Anatomical traits (following Chapter 2) and physiological proxies for photosynthesis (carbon/nitrogen content; δ^{13}C to calculate photosynthetic discrimination (Δ_{leaf}), water use efficiency (WUE), and internal cellular:atmospheric pCO_2 (c_i/c_a)) were analyzed with 19 climate variables to look for relationships. I found strong

associations in cross-sectional area with temperature seasonality, leaf width with mean annual precipitation, and leaf thickness with temperature evenness. Trait response to climate variables varied across taxa, however, in closely-related *Metasequoia* and *Sequoia*, cross-sectional area was strongly associated with precipitation of coldest quarter. This similarity of trait-climate association between closely related taxa suggests conservation of a shared climatic niche. Further, my analyses showed that while leaf anatomy was quite distinct between taxa (reflected in inferred morphospaces), there was convergence in physiological traits related to photosynthesis. This suggests that different forms are achieving a similar function, perhaps reinforcing conservation in climatic niche therefore influencing anatomical response to climate.

The relationships between leaf traits and climate that I established in Chapter 3 were applied in Chapter 4 to test whether climate could be used to infer past plant traits, which would complement findings from Chapter 2. Generalized linear models of modern trait-climate relationships were developed and used to estimate traits of *Metasequoia* in the early Eocene using climate variables extracted from climate simulations at two CO_2 levels: 3x and 6x pre-industrial CO_2 at the known early Eocene fossil occurrences of *Metasequoia*. Models were validated by comparison with known leaf widths measured from compression fossils, which closely matched predicted values. Inferred past traits for early Eocene *Metasequoia* suggest that cross-sectional area, leaf width, and leaf thickness decrease with increased CO_2, while resin canal area increases. These trends most likely reflect cooling strategies to offload heat. My early Eocene fossil estimates show promising potential in understanding how traits and thus function, have changed over time. Increasing the support for these models can help us project and understand gaps in the fossil record. Also, by incorporating physiological characters, these models could offer exciting insights into photosynthesis of *Metasequoia*, challenging or supporting previous research of *Metasequoia*'s past in the Arctic Circle.

5.1 Trait-climate relationships through time: next steps

Quantitative means of characterizing the relationships between conifers and climate were based previously on modern climatic tolerances. Here, I demonstrated the promise of using a multi-variate approach to link anatomical trait data collected over broad climatic gradients with climate. I was able to estimate Bioclim variables of climate and quantitative climatic variables for fossils with known anatomy, and conversely use broad distributions of a fossil taxon with paleoclimate model estimates to infer traits where fossils are not anatomically preserved.

However, results in Chapter 3 show that there are species-specific differences in trait responses to climate, and when data from multiple species are analyzed together different trait-climate relationships are inferred. This suggests that there is more work needed to fully understand how and why climate and leaf traits vary across conifers. For example, the addition of more coniferous taxa from Cupressaceae, such as *Glyptostrobus pensilis* (Staunton ex D. Don) K. Koch and *Cunninghamia lanceolata* (Lamb.) Hook, will refine my models. Ultimately, expanding these models to the arid inhabiting Cupressaceae species, such as juniper (*Juniperus* spp.) and cypress (*Cupressus*, *Chamaecyparis*), and eventually to another diverse, Northern Hemisphere conifer family – Pinaceae, the pine family – would accomplish and contribute to overall knowledge of conifer links to climate.

Conifers are found across the world, inhabiting diverse, often considered harsh environments. Conifer leaves are reflective of adaptations to grow and reproduce in these environments. By studying these adaptations, or traits, we can deepen our understanding of conifer evolution and their link to their growing environment. This thesis demonstrated methods in how conifer leaves can be linked to climate. I applied these links to answer interesting questions about the evolution and ecology of conifers, in hopes of igniting interest in others so we can ask these questions together.

LITERATURE CITED

Ackerly, D. D. (2003), Community assembly, niche conservatism, and adaptive evolution in changing environments, International Journal of Plant Sciences, 164(S3), S165–S184.

Ackerly, D. D., S. A. Dudley, S. E. Sultan, J. Schmitt, J. S. Coleman, C. R. Linder, D. R. Sandquist, M. A. Geber, A. S. Evans, T. E. Dawson, et al. (2000), The evolution of plant ecophysiological traits: recent advances and future directions: new research addresses natural selection, genetic constraints, and the adaptive evolution of plant ecophysiological traits, Bioscience, 50(11), 979–995.

Adams, H. D., and T. E. Kolb (2004), Drought responses of conifers in ecotone forests of northern Arizona: tree ring growth and leaf δ^{13}C, Oecologia, 140(2), 217–225.

Akhmetiev, M. A. (2010), Paleocene and Eocene floristic and climatic change in Russia and Northern Kazakhstan, Bulletin of Geosciences, 85(1), 77–94.

Alvin, K., and M. C. Boulter (1974), A controlled method of comparative study for taxodiaceous leaf cuticles, Botanical Journal of the Linnean Society, 69(4), 277–286.

Anagnostou, E., E. H. John, K. M. Edgar, G. L. Foster, A. Ridgwell, G. N. Inglis, R. D. Pancost, D. J. Lunt, and P. N. Pearson (2016), Changing atmospheric co_2 concentration was the primary driver of early Cenozoic climate, Nature, 533(7603), 380–384.

Anderson, P., and S. Pezeshki (2000), The effects of intermittent flooding on seedlings of three forest species, Photosynthetica, 37(4), 543–552.

Apple, M., K. Tiekotter, M. Snow, J. Young, A. Soeldner, D. Phillips, D. Tingey, and B. J. Bond (2002), Needle anatomy changes with increasing tree age in Douglas-fir, Tree Physiology, 22(2-3), 129–136.

Arbellay, E., M. Stoffel, E. K. Sutherland, K. T. Smith, and D. A. Falk (2014), Resin duct size and density as ecophysiological traits in fire scars of *Pseudotsuga menziesii* and *Larix occidentalis*, Annals of botany, 114(5), 973–980.

Ashton, P. M. S., and G. P. Berlyn (1994), A comparison of leaf physiology and anatomy of *Quercus* (section Erythrobalanus-Fagaceae) species in different light environments, American Journal of Botany, 81(5), 589–597.

Axelrod, D. I. (1966), Origin of deciduous and evergreen habits in temperate forests, Evolution, pp. 1–15.

Axelrod, D. I. (1983), Biogeography of oaks in the Arcto-Tertiary province, Annals of the Missouri Botanical Garden, pp. 629–657.

Bailey, I. W., and E. W. Sinnott (1915), A botanical index of Cretaceous and Tertiary climates, Science, 41(1066), 831–834.

Barclay, R. S., and S. L. Wing (2016), Improving the *Ginkgo* co_2 barometer: implications for the early Cenozoic atmosphere, Earth and Planetary Science Letters, 439, 158–171.

Bartholomew, B., D. E. Boufford, and S. A. Spongberg (1983), *Metasequoia glyptostroboides*-its present status in central China, Journal of the Arnold Arboretum, 64(1), 105–128.

Basinger, J., D. Greenwood, and T. Sweda (1994), Early Tertiary vegetation of Arctic Canada and its relevance to paleoclimatic interpretation, in Cenozoic plants and climates of the Arctic, pp. 175–198, Springer.

Basinger, J. F. (1981), The vegetative body of *Metasequoia milleri* from the Middle Eocene of southern British Columbia, Canadian Journal of Botany, 59(12), 2379–2410.

Basinger, J. F. (1984), Seed cones of *Metasequoia milleri* from the Middle Eocene of southern British Columbia, Canadian Journal of Botany, 62(2), 281–289.

Beerling, D., and D. Royer (2002), Reading a CO_2 signal from fossil stomata, New Phytologist, 153(3), 387–397.

Beerling, D., J. McElwain, and C. Osborne (1998), Stomatal responses of the 'living fossil' *Ginkgo biloba* L. to changes in atmospheric CO_2 concentrations, Journal of Experimental Botany, 49(326), 1603–1607.

Beerling, D. J., and P. J. Franks (2010), The hidden cost of transpiration, Nature, 464(7288), 495–496.

Bettarini, I., F. P. Vaccari, and F. Miglietta (1998), Elevated CO_2 concentrations and stomatal density: observations from 17 plant species growing in a CO_2 spring in central Italy, Global Change Biology, 4(1), 17–22.

Boyce, C. K., T. J. Brodribb, T. S. Feild, and M. A. Zwieniecki (2009), Angiosperm leaf vein evolution was physiologically and environmentally transformative, Proceedings of the Royal Society B: Biological Sciences, 276(1663), 1771–1776.

Boyce, C. K., J.-E. Lee, T. S. Feild, T. J. Brodribb, and M. A. Zwieniecki (2010), Angiosperms Helped Put the Rain in the Rainforests: The Impact of Plant Physiological Evolution on Tropical Biodiversity, Annals of the Missouri Botanical Garden, 97(4), 527–540.

Brown, W., and B. Smith (1972), Grass evolution, the Kranz syndrome, $^{13}C/^{12}C$ ratios and continental drift, Nature, 239(5371), 345–346.

Burgess, S., and T. Dawson (2004), The contribution of fog to the water relations of *Sequoia sempervirens* (D. Don): foliar uptake and prevention of dehydration, Plant, Cell & Environment, 27(8), 1023–1034.

Cevallos-Ferriz, S. R., R. A. Stockey, and K. B. Pigg (1991), The Princeton chert: evidence for *in situ* aquatic plants, Review of Palaeobotany and Palynology, 70(1-2), 173–185.

Chaney, R. W. (1947), Tertiary centers and migration routes, Ecological Monographs, 17(2), 139–148.

Chaney, R. W. (1950), A revision of fossil *Sequoia* and *Taxodium* in western North America based on the recent discovery of *Metasequoia*, Transactions of the American Philosophical Society, 40(3), 171–263.

Chartzoulakis, K., A. Patakas, G. Kofidis, A. Bosabalidis, and A. Nastou (2002), Water stress affects leaf anatomy, gas exchange, water relations and growth of two avocado cultivars, Scientia horticulturae, 95(1-2), 39–50.

Clayton, G. (1996), Mississippian miospores, Palynology: Principles and applications, 2, 589–596.

Coleman, J. S. (1986), Leaf development and leaf stress: increased susceptibility associated with sink-source transition, Tree Physiology, 2(1-2-3), 289–299.

Coley, P. D. (1983), Herbivory and defensive characteristics of tree species in a lowland tropical forest, Ecological monographs, 53(2), 209–234.

Coley, P. D., J. P. Bryant, and F. S. Chapin (1985), Resource availability and plant antiherbivore defense, Science, 230(4728), 895–899.

Cope, J. S., D. Corney, J. Y. Clark, P. Remagnino, and P. Wilkin (2012), Plant species identification using digital morphometrics: A review, Expert Systems with Applications, 39(8), 7562–7573.

Corney, D. P., H. L. Tang, J. Y. Clark, Y. Hu, and J. Jin (2012), Automating digital leaf measurement: the tooth, the whole tooth, and nothing but the tooth, PloS one, 7(8).

Crane, P. R., and S. Lidgard (1989), Angiosperm diversification and paleolatitudinal gradients in Cretaceous floristic diversity, Science, 246(4930), 675–678.

Daru, B. H., D. S. Park, R. B. Primack, C. G. Willis, D. S. Barrington, T. J. Whitfeld, T. G. Seidler, P. W. Sweeney, D. R. Foster, A. M. Ellison, et al. (2018), Widespread sampling biases in herbaria revealed from large-scale digitization, New Phytologist, 217(2), 939–955.

Dawson, T. E. (1993), Water sources of plants as determined from xylem-water isotopic composition: perspectives on plant competition, distribution, and water relations, in Stable isotopes and plant carbon-water relations, pp. 465–496, Elsevier.

Dawson, T. E. (1998), Fog in the California redwood forest: ecosystem inputs and use by plants, Oecologia, 117(4), 476–485.

De Boer, H. J., M. B. Eppinga, M. J. Wassen, and S. C. Dekker (2012), A critical transition in leaf evolution facilitated the Cretaceous angiosperm revolution, Nature Communications, 3, 1221.

Diefendorf, A. F., K. E. Mueller, S. L. Wing, P. L. Koch, and K. H. Freeman (2010), Global patterns in leaf ^{13}c discrimination and implications for studies of past and future climate, Proceedings of the National Academy of Sciences, 107(13), 5738–5743.

Dörken, V. M. (2013), Leaf dimorphism in Thuja plicata and *Platycladus orientalis* (thujoid Cupressaceae s. str., Coniferales): the changes in morphology and anatomy from juvenile needle leaves to mature scale leaves, Plant systematics and evolution, 299(10), 1991–2001.

Dudley, S. A. (1996), The response to differing selection on plant physiological traits: evidence for local adaptation, Evolution, 50(1), 103–110.

Ehleringer, J. R., R. F. Sage, L. B. Flanagan, and R. W. Pearcy (1991), Climate change and the evolution of C_4 photosynthesis, Trends in ecology & evolution, 6(3), 95–99.

Ellsworth, D., and P. B. Reich (1993), Canopy structure and vertical patterns of photosynthesis and related leaf traits in a deciduous forest, Oecologia, 96(2), 169–178.

Equiza, M. A., M. E. Day, and R. Jagels (2006), Physiological responses of three deciduous conifers (*Metasequoia glyptostroboides, Taxodium distichum* and *Larix laricina*) to continuous light: adaptive implications for the early Tertiary polar summer, Tree Physiology, 26(3), 353–364.

Equiza, M. A., R. Jagels, and D. Cirelli (2007), Differential carbon allocation in *Metasequoia glyptostroboides, Taxodium distichum* and *Sequoia sempervirens* growing under continuous light, Bulletin of the Peabody Museum of Natural History, 48(2), 269–280.

Falcon-Lang, H. J., and W. A. DiMichele (2010), What happened to the coal forests during Pennsylvanian glacial phases?, Palaios, 25(9), 611–617.

Falder, A. B., R. A. Stockey, and G. W. Rothwell (1999), *In situ* fossil seedlings of a *Metasequoia*-like taxodiaceous conifer from Paleocene river floodplain deposits of central Alberta, Canada, American Journal of Botany, 86(6), 900–902.

Farjon, A. (2005), Monograph of Cupressaceae and *Sciadopitys*, Royal Botanic Gardens, Kew.

Farquhar, G., and R. Richards (1984), Isotopic composition of plant carbon correlates with water-use efficiency of wheat genotypes, Functional Plant Biology, 11(6), 539–552.

Farquhar, G. D. (1989), Models of integrated photosynthesis of cells and leaves, Philosophical Transactions of the Royal Society of London. B, Biological Sciences, 323(1216), 357–367.

Farquhar, G. D., M. H. O'Leary, and J. A. Berry (1982), On the relationship between carbon isotope discrimination and the intercellular carbon dioxide concentration in leaves, Functional Plant Biology, 9(2), 121–137.

Fernández-de Uña, L., S. Rossi, I. Aranda, P. Fonti, B. D. González-González, I. Cañellas, and G. Gea-Izquierdo (2017), Xylem and leaf functional adjustments to drought in *Pinus sylvestris* and *Quercus pyrenaica* at their elevational boundary, Frontiers in plant science, 8, 1200.

Fick, S. E., and R. J. Hijmans (2017), WorldClim 2: new 1-km spatial resolution climate surfaces for global land areas, International journal of climatology, 37(12), 4302–4315.

Field, C., and H. Mooney (1986), The photosynthesis-nitrogen relationship in wild plants., In TJ Givnish (ed.) On the economy of form and function. Cambridge Univ. Press, Cambridge, UK.

Florin, R. (1963), The distribution of conifer and taxad genera in time and space, Acta Horti Bergiani, 20(4), 121–312.

Forrester, D. I. (2015), Transpiration and water-use efficiency in mixed-species forests versus monocultures: effects of tree size, stand density and season, Tree Physiology, 35(3), 289–304.

Franks, P. J., D. L. Royer, D. J. Beerling, P. K. Van de Water, D. J. Cantrill, M. M. Barbour, and J. A. Berry (2014), New constraints on atmospheric CO_2 concentration for the Phanerozoic, Geophysical Research Letters, 41(13), 4685–4694.

Fu, L., C.-m. Chin, et al. (1992), China plant red data book, Science press.

Gadek, P. A., D. L. Alpers, M. M. Heslewood, and C. J. Quinn (2000), Relationships within Cupressaceae *sensu lato*: a combined morphological and molecular approach, American journal of botany, 87(7), 1044–1057.

Gebauer, R., D. Volařík, J. Urban, I. Børja, N. E. Nagy, T. D. Eldhuset, and P. Krokene (2011), Effect of thinning on anatomical adaptations of Norway spruce needles, Tree Physiology, 31(10), 1103–1113.

Givnish, T. J. (1986), On the economy of plant form and function: Proceedings of the Sixth Maria Moors Cabot Symposium, vol. 6, Cambridge University Press.

Givnish, T. J. (2002), Adaptive significance of evergreen vs. deciduous leaves: solving the triple paradox, Silva fennica, 36(3), 703–743.

Godsoe, W. (2010), I can't define the niche but i know it when i see it: a formal link between statistical theory and the ecological niche, Oikos, 119(1), 53–60.

Gotoh, E., N. Suetsugu, T. Higa, T. Matsushita, H. Tsukaya, and M. Wada (2018), Palisade cell shape affects the light-induced chloroplast movements and leaf photosynthesis, Scientific reports, 8(1), 1–9.

Greenwood, D. R., and J. F. Basinger (1994), The paleoecology of high-latitude Eocene swamp forests from Axel Heiberg Island, Canadian High Arctic, Review of Palaeobotany and Palynology, 81(1), 83–97.

Greenwood, D. R., and S. L. Wing (1995), Eocene continental climates and latitudinal temperature gradients, Geology, 23(11), 1044–1048.

Greenwood, D. R., P. T. Moss, A. I. Rowett, A. J. Vadala, and R. L. Keefe (2003), Plant communities and climate change in southeastern Australia during the early Paleogene, in Causes and consequences of globally warm climates in the early Paleogene, Geological Society of America, doi:10.1130/0-8137-2369-8.365.

Greenwood, D. R., S. B. Archibald, R. W. Mathewes, and P. T. Moss (2005), Fossil biotas from the Okanagan Highlands, southern British Columbia and northeastern Washington State: climates and ecosystems across an Eocene landscape, Canadian Journal of Earth Sciences, 42(2), 167–185.

Gurevitch, J. (1988), Variation in leaf dissection and leaf energy budgets among populations of *Achillea* from an altitudinal gradient, American Journal of Botany, 75(9), 1298–1306.

Hallgren, W., L. Beaumont, A. Bowness, L. Chambers, E. Graham, H. Holewa, S. Laffan, B. Mackey, H. Nix, J. Price, et al. (2016), The biodiversity and climate change virtual laboratory: where ecology meets big data, Environmental Modelling & Software, 76, 182–186.

Hammer, Ø., D. A. Harper, P. D. Ryan, et al. (2001), PAST: Paleontological statistics software package for education and data analysis, Palaeontologia electronica, 4(1), 9.

Harris, A., J. Dee, and M. W. Palmer (2017), The effects of taxonomic rank on climatic calibrations: A test using extant floras of united states counties, Review of palaeobotany and palynology, 244, 316–324.

Hatfield, J., and J. Burke (1991), Energy exchange and leaf temperature behavior of three plant species, Environmental and experimental botany, 31(3), 295–302.

Hendricks, D. R., and P. Søndergaard (1998), *Metasequoia glyptostroboides* 50 years out of China. Observations from the United States and Denmark, Dansk Dendrologisk Arsskrift, 16, 6–24.

Hijmans, R. J., S. E. Cameron, J. L. Parra, P. G. Jones, and A. Jarvis (2005), Very high resolution interpolated climate surfaces for global land areas, International Journal of Climatology: A Journal of the Royal Meteorological Society, 25(15), 1965–1978.

Hollis, C. J., T. Dunkley Jones, E. Anagnostou, P. K. Bijl, M. J. Cramwinckel, Y. Cui, G. R. Dickens, K. M. Edgar, Y. Eley, D. Evans, et al. (2019), The Deep MIP contribution to PMIP4: methodologies for selection, compilation and analysis of latest Paleocene and early Eocene climate proxy data, incorporating version 0.1 of the DeepMIP database, Geoscientific Model Development, 12(7), 3149–3206.

Huang, Y., F. M. Jacques, T. Su, D. K. Ferguson, H. Tang, W. Chen, and Z. Zhou (2015), Distribution of Cenozoic plant relicts in China explained by drought in dry season, Scientific Reports, 5, 14,212.

Hueve, K., I. Bichele, B. Rasulov, and Ü. Niinemets (2011), When it is too hot for photosynthesis: heat-induced instability of photosynthesis in relation to respiratory burst, cell permeability changes and H_2O_2 formation, Plant, Cell & Environment, 34(1), 113–126.

Huff, P. M., P. Wilf, and E. J. Azumah (2003), Digital future for paleoclimate estimation from fossil leaves? preliminary results, Palaios, 18(3), 266–274.

Hyland, E. G., and N. D. Sheldon (2013), Coupled CO_2-climate response during the early Eocene climatic optimum, Palaeogeography, Palaeoclimatology, Palaeoecology, 369, 125–135.

Irving, E., P. Wynne, R. Christie, and N. McMillan (1991), The paleolatitude of the Eocene fossil forests of Arctic Canada, Geological Survey of Canada Bulletin, 403, 209–211.

Ishii, H. T., G. M. Jennings, S. C. Sillett, and G. W. Koch (2008), Hydrostatic constraints on morphological exploitation of light in tall *Sequoia sempervirens* trees, Oecologia, 156(4), 751–763.

Jacques, F. M., T. Su, R. A. Spicer, Y. Xing, Y. Huang, W. Wang, and Z. Zhou (2011), Leaf physiognomy and climate: are monsoon systems different?, Global and Planetary Change, 76(1-2), 56–62.

Jagels, R., and M. E. Day (2004), The adaptive physiology of *Metasequoia* to Eocene high-latitude environments, in The evolution of plant physiology, pp. 401–425, Elsevier.

Jagels, R., and M. A. Equiza (2007), Why did *Metasequoia* disappear from North America but not from China, Bulletin of the Peabody Museum of Natural History, 48(2), 281–290.

Jennings, G. M. (2002), Vertical hydraulic gradients and the cause of foliar variation in tall redwood trees (*Sequoia sempervirens*), Ph.D. thesis, Humboldt State University.

Johansen, D. A., et al. (1940), Plant microtechnique., Plant microtechnique.

Jordan, D., and W. Smith (1993), Simulated influence of leaf geometry on sunlight interception and photosynthesis in conifer needles, Tree Physiology, 13(1), 29–39.

Jordan, G. J., T. J. Brodribb, C. J. Blackman, and P. H. Weston (2013), Climate drives vein anatomy in Proteaceae, American Journal of Botany, 100(8), 1483–1493.

Keeling, C. D., and T. Whorf (2005), Atmospheric carbon dioxide record from Mauna Loa, Carbon Dioxide Research Group, Scripps Institution of Oceanography, University of California La Jolla, California, pp. 92,093–0444.

Kennedy, E. M., N. C. Arens, T. Reichgelt, R. A. Spicer, T. E. Spicer, L. Stranks, and J. Yang (2014), Deriving temperature estimates from Southern Hemisphere leaves, Palaeogeography, Palaeoclimatology, Palaeoecology, 412, 80–90.

Khan, M. A., R. A. Spicer, S. Bera, R. Ghosh, J. Yang, T. E. Spicer, S.-x. Guo, T. Su, F. Jacques, and P. J. Grote (2014), Miocene to Pleistocene floras and climate of the Eastern Himalayan Siwaliks, and new palaeoelevation estimates for the Namling–Oiyug Basin, Tibet, Global and Planetary Change, 113, 1–10.

Koch, G. W., S. C. Sillett, G. M. Jennings, and S. D. Davis (2004), The limits to tree height, Nature, 428(6985), 851–854.

Kohn, M. J. (2010), Carbon isotope compositions of terrestrial C3 plants as indicators of (paleo) ecology and (paleo) climate, Proceedings of the National Academy of Sciences, 107(46), 19,691–19,695.

Körner, C. (1989), The nutritional status of plants from high altitudes, Oecologia, 81(3), 379–391.

Laforest-Lapointe, I., J. Martínez-Vilalta, and J. Retana (2014), Intraspecific variability in functional traits matters: case study of Scots pine, Oecologia, 175(4), 1337–1348.

Larcher, W., and A. Winter (1981), Frost susceptibility of palms: experimental data and their interpretation., Principes.

Lavorel, S., and E. Garnier (2002), Predicting changes in community composition and ecosystem functioning from plant traits: revisiting the Holy Grail, Functional ecology, 16(5), 545–556.

LePage, B. A. (2007), The taxonomy and biogeographic history of *Glyptostrobus* endlicher (cupressaceae), Bulletin of the Peabody Museum of Natural History, 48(2), 359–426.

LePage, B. A., H. Yang, and M. Matsumoto (2005), The evolution and biogeographic history of *Metasequoia*, in The geobiology and ecology of Metasequoia, pp. 3–114, Springer.

Leslie, A. B., J. M. Beaulieu, H. S. Rai, P. R. Crane, M. J. Donoghue, and S. Mathews (2012), Hemisphere-scale differences in conifer evolutionary dynamics, Proceedings of the National Academy of Sciences, 109(40), 16,217–16,221.

Leslie, A. B., J. Beaulieu, G. Holman, C. S. Campbell, W. Mei, L. R. Raubeson, and S. Mathews (2018), An overview of extant conifer evolution from the perspective of the fossil record, American journal of botany, 105(9), 1531–1544.

Leuzinger, S., and C. Körner (2007), Tree species diversity affects canopy leaf temperatures in a mature temperate forest, Agricultural and forest meteorology, 146(1-2), 29–37.

Li, Y.-Y., E. P. K. Tsang, M.-Y. Cui, and X.-Y. Chen (2012), Too early to call it success: an evaluation of the natural regeneration of the endangered *Metasequoia glyptostroboides*, Biological conservation, 150(1), 1–4.

Lin, J., M. Jach, and R. Ceulemans (2001), Stomatal density and needle anatomy of scots pine (*Pinus sylvestris*) are affected by elevated CO_2, New phytologist, 150(3), 665–674.

Little, S. A., S. W. Kembel, and P. Wilf (2010), Paleotemperature proxies from leaf fossils reinterpreted in light of evolutionary history, PLoS One, 5(12).

Liu, Y.-J., C.-S. Li, and Y.-F. Wang (1999), Studies on fossil *Metasequoia* from north-east China and their taxonomic implications, Botanical Journal of the Linnean Society, 130(3), 267–297.

Liu, Y.-J., N. C. Arens, and C.-S. Li (2007), Range change in *Metasequoia*: relationship to palaeoclimate, Botanical Journal of the Linnean Society, 154(1), 115–127.

Llorens, L., C. P. Osborne, and D. J. Beerling (2009), Water-use responses of 'living fossil'conifers to co2 enrichment in a simulated cretaceous polar environment, Annals of botany, 104(1), 179–188.

Loomis, R. (1997), On the utility of nitrogen in leaves, Proceedings of the National Academy of Sciences, 94(25), 13,378–13,379.

Lowe, A. J., D. R. Greenwood, C. K. West, J. M. Galloway, M. Sudermann, and T. Reichgelt (2018), Plant community ecology and climate on an upland volcanic landscape during the Early Eocene Climatic Optimum: McAbee Fossil Beds, British Columbia, Canada, Palaeogeography, Palaeoclimatology, Palaeoecology, 511, 433–448.

Ma, S., F. He, D. Tian, D. Zou, Z. Yan, Y. Yang, T. Zhou, K. Huang, H. Shen, and J. Fang (2018), Variations and determinants of carbon content in plants: a global synthesis, Biogeosciences, 15(3), 693.

MacLeod, N. (2002), Geometric morphometrics and geological shape-classification systems, Earth-Science Reviews, 59(1-4), 27–47.

Macleod, N. (2005), Shape models as a basis for morphological analysis in paleobiological systematics: dicotyledenous leaf physiography, Bulletins of American Paleontology, 369, 219–238.

MacLeod, N., and D. Steart (2015), Automated leaf physiognomic character identification from digital images, Paleobiology, 41(4), 528–553.

Magallón, S., K. W. Hilu, and D. Quandt (2013), Land plant evolutionary timeline: gene effects are secondary to fossil constraints in relaxed clock estimation of age and substitution rates, American Journal of Botany, 100(3), 556–573.

Makela, A., T. J. Givnish, F. Berninger, T. N. Buckley, G. D. Farquhar, and P. Hari (2002), Challenges and opportunities of the optimality approach in plant ecology, Silva Fennica, 36(3), 605–614.

Marini, M. Â., M. Barbet-Massin, J. Martinez, N. P. Prestes, and F. Jiguet (2010), Applying ecological niche modelling to plan conservation actions for the Red-spectacled Amazon (*Amazona pretrei*), Biological Conservation, 143(1), 102–112.

Marks, C. O. (2007), The causes of variation in tree seedling traits: the roles of environmental selection versus chance, Evolution, 61(2), 455–469.

Marks, C. O., and M. J. Lechowicz (2006), Alternative designs and the evolution of functional diversity, The American Naturalist, 167(1), 55–66.

Mathewes, R. W., D. R. Greenwood, and S. B. Archibald (2016), Paleoenvironment of the quilchena flora, british columbia, during the early eocene climatic optimum, Canadian Journal of Earth Sciences, 53(6), 574–590.

Matlab, V. (2015), 8.5. 0.197613 (r2015a), The MathWorks Inc., Natick, Massachusetts.

Maxbauer, D. P., D. L. Royer, and B. A. LePage (2014), High Arctic forests during the middle Eocene supported by moderate levels of atmospheric CO_2, Geology, 42(12), 1027–1030.

McElwain, J. C. (2018), Paleobotany and global change: Important lessons for species to biomes from vegetation responses to past global change, Annual review of plant biology, 69, 761–787.

McElwain, J. C., and W. G. Chaloner (1995), Stomatal density and index of fossil plants track atmospheric carbon dioxide in the Palaeozoic, Annals of Botany, 76(4), 389–395.

McIver, E., and J. Basinger (1999), Early Tertiary floral evolution in the Canadian high Arctic, Annals of the Missouri Botanical Garden, pp. 523–545.

McKenna, M. C. (1980), Eocene paleolatitude, climate, and mammals of Ellesmere Island, Palaeogeography, Palaeoclimatology, Palaeoecology, 30, 349–362.

Miller, C. N. (1977), Mesozoic conifers, The Botanical Review, 43(2), 217–280.

Momohara, A. (2005), Paleoecology and history of *Metasequoia* in Japan, with reference to its extinction and survival in East Asia, in The geobiology and ecology of Metasequoia, pp. 115–136, Springer.

Morin, X., and M. J. Lechowicz (2008), Contemporary perspectives on the niche that can improve models of species range shifts under climate change, Biology Letters, 4(5), 573–576.

Mosbrugger, V. (2009), Nearest-Living-Relative Method, pp. 607–609, Springer Netherlands, Dordrecht, doi:10.1007/978-1-4020-4411-3_149.

Mosbrugger, V., and T. Utescher (1997), The coexistence approach—a method for quantitative reconstructions of Tertiary terrestrial palaeoclimate data using plant fossils, Palaeogeography, Palaeoclimatology, Palaeoecology, 134(1-4), 61–86.

Müller, R. D., J. Cannon, X. Qin, R. J. Watson, M. Gurnis, S. Williams, T. Pfaffelmoser, M. Seton, S. H. Russell, and S. Zahirovic (2018), GPlates: building a virtual Earth through deep time, Geochemistry, Geophysics, Geosystems, 19(7), 2243–2261.

Mullin, L. P., S. C. Sillett, G. W. Koch, K. P. Tu, and M. E. Antoine (2009), Physiological consequences of height-related morphological variation in *Sequoia sempervirens* foliage, Tree Physiology, 29(8), 999–1010.

Nagy, N. E., V. R. Franceschi, H. Solheim, T. Krekling, and E. Christiansen (2000), Wound-induced traumatic resin duct development in stems of Norway spruce (Pinaceae): anatomy and cytochemical traits, American Journal of Botany, 87(3), 302–313.

Ng, M., and S. Y. Smith (2020), Evaluating stasis in *Metasequoia* (Cupressaceae): testing the relationship between leaf traits and climate, International Journal of Plant Sciences, 181(2), 157–174.

Niinemets, Ü., and O. Kull (1995), Effects of light availability and tree size on the architecture of assimilative surface in the canopy of *Picea abies*: variation in needle morphology, Tree physiology, 15(5), 307–315.

Niinemets, Ü., O. Kull, and J. D. Tenhunen (1998), An analysis of light effects on foliar morphology, physiology, and light interception in temperate deciduous woody species of contrasting shade tolerance, Tree physiology, 18(10), 681–696.

Niinemets, Ü., A. Lukjanova, M. H. Turnbull, and A. D. Sparrow (2007), Plasticity in mesophyll volume fraction modulates light-acclimation in needle photosynthesis in two pines, Tree Physiology, 27(8), 1137–1151.

Oksanen, J., F. G. Blanchet, R. Kindt, P. Legendre, P. Minchin, R. O'hara, G. Simpson, P. Solymos, M. H. H. Stevens, and H. Wagner (2018), Package 'vegan'community ecology package, See https://cran. r-project. org/web/packages/vegan/index. html.

Oldham, A. R., S. C. Sillett, A. M. Tomescu, and G. W. Koch (2010), The hydrostatic gradient, not light availability, drives height-related variation in *Sequoia sempervirens* (Cupressaceae) leaf anatomy, American journal of botany, 97(7), 1087–1097.

O'Leary, M. H. (1988), Carbon isotopes in photosynthesis, Bioscience, 38(5), 328–336.

Osborne, C. P., and D. J. Beerling (2003), The penalty of a long, hot summer. Photosynthetic acclimation to high CO_2 and continuous light in "living fossil" conifers, Plant Physiology, 133(2), 803–812.

Parker, G. A., and J. M. Smith (1990), Optimality theory in evolutionary biology, Nature, 348(6296), 27–33.

Pearson, R. G., and T. P. Dawson (2003), Predicting the impacts of climate change on the distribution of species: are bioclimate envelope models useful?, Global ecology and biogeography, 12(5), 361–371.

Peppe, D. J., D. L. Royer, B. Cariglino, S. Y. Oliver, S. Newman, E. Leight, G. Enikolopov, M. Fernandez-Burgos, F. Herrera, J. M. Adams, et al. (2011), Sensitivity of leaf size and shape to climate: global patterns and paleoclimatic applications, New phytologist, 190(3), 724–739.

Perez-Harguindeguy, N., S. Diaz, E. Garnier, S. Lavorel, H. Poorter, P. Jaureguiberry, M. S. Bret-Harte, W. K. Cornwell, J. M. Craine, D. E. Gurvich, et al. (2016), Corrigendum to: new handbook for standardised measurement of plant functional traits worldwide, Australian Journal of botany, 64(8), 715–716.

Pistón, N., F. de Bello, A. T. Dias, L. Götzenberger, B. H. Rosado, E. A. de Mattos, R. Salguero-Gómez, and C. P. Carmona (2019), Multidimensional ecological analyses demonstrate how interactions between functional traits shape fitness and life history strategies, Journal of Ecology, 107(5), 2317–2328.

Pittermann, J., S. A. Stuart, T. E. Dawson, and A. Moreau (2012), Cenozoic climate change shaped the evolutionary ecophysiology of the Cupressaceae conifers, Proceedings of the National Academy of Sciences, 109(24), 9647–9652.

Ranjbar, M., and Z. Hajmoradi (2016), Comparative leaf epidermis and anatomical study in populations of *Trigonella spruneriana* (Fabaceae) from Iran, Webbia, 71(1), 107–115.

Read, J., and J. Francis (1992), Responses of some Southern Hemisphere tree species to a prolonged dark period and their implications for high-latitude Cretaceous and Tertiary floras, Palaeogeography, Palaeoclimatology, Palaeoecology, 99(3-4), 271–290.

Regos, A., L. Gagne, D. Alcaraz-Segura, J. P. Honrado, and J. Domínguez (2019), Effects of species traits and environmental predictors on performance and transferability of ecological niche models, Scientific reports, 9(1), 1–14.

Reich, P. B., and J. Oleksyn (2004), Global patterns of plant leaf N and P in relation to temperature and latitude, Proceedings of the National Academy of Sciences, 101(30), 11,001–11,006.

Reich, P. B., M. Walters, and D. Ellsworth (1992), Leaf life-span in relation to leaf, plant, and stand characteristics among diverse ecosystems, Ecological monographs, 62(3), 365–392.

Reich, P. B., J. Oleksyn, and M. Tjoelker (1996), Needle respiration and nitrogen concentration in Scots pine populations from a broad latitudinal range: a common garden test with field-grown trees, Functional Ecology, pp. 768–776.

Reichgelt, T., E. M. Kennedy, D. C. Mildenhall, J. G. Conran, D. R. Greenwood, and D. E. Lee (2013), Quantitative palaeoclimate estimates for early Miocene southern

New Zealand: evidence from Foulden Maar, Palaeogeography, Palaeoclimatology, Palaeoecology, 378, 36–44.

Reichgelt, T., C. K. West, and D. R. Greenwood (2018), The relation between global palm distribution and climate, Scientific reports, 8(1), 1–11.

Rothwell, G. W., and J. F. Basinger (1979), *Metasequoia milleri n. sp.*, anatomically preserved pollen cones from the Middle Eocene (Allenby Formation) of British Columbia, Canadian Journal of Botany, 57(8), 958–970.

Royer, D. (2001), Stomatal density and stomatal index as indicators of paleoatmospheric CO_2 concentration, Review of Palaeobotany and Palynology, 114(1-2), 1–28.

Royer, D. L., S. L. Wing, D. J. Beerling, D. W. Jolley, P. L. Koch, L. J. Hickey, and R. A. Berner (2001), Paleobotanical evidence for near present-day levels of atmospheric CO_2 during part of the Tertiary, Science, 292(5525), 2310–2313.

Royer, D. L., C. P. Osborne, and D. J. Beerling (2003), Carbon loss by deciduous trees in a CO_2-rich ancient polar environment, Nature, 424(6944), 60–62.

Royer, D. L., P. Wilf, D. A. Janesko, E. A. Kowalski, and D. L. Dilcher (2005), Correlations of climate and plant ecology to leaf size and shape: potential proxies for the fossil record, American journal of botany, 92(7), 1141–1151.

Royer, D. L., J. C. McElwain, J. M. Adams, and P. Wilf (2008), Sensitivity of leaf size and shape to climate within *Acer rubrum* and *Quercus kelloggii*, New Phytologist, 179(3), 808–817.

Sakai, A., and W. Larcher (2012), Frost survival of plants: responses and adaptation to freezing stress, vol. 62, Springer Science & Business Media.

Saupe, E. E., M. Papes, P. A. Selden, and R. S. Vetter (2011), Tracking a medically important spider: climate change, ecological niche modeling, and the brown recluse (*Loxosceles reclusa*), PloS one, 6(3).

Schneider, C. A., W. S. Rasband, and K. W. Eliceiri (2012), NIH Image to ImageJ: 25 years of image analysis, Nature methods, 9(7), 671–675.

Schubert, B. A., A. H. Jahren, J. J. Eberle, L. S. Sternberg, and D. A. Eberth (2012), A summertime rainy season in the Arctic forests of the Eocene, Geology, 40(6), 523–526.

Schuepp, P. (1993), Tansley review no. 59. leaf boundary layers, New Phytologist, pp. 477–507.

Seager, R., A. Hooks, A. P. Williams, B. Cook, J. Nakamura, and N. Henderson (2015), Climatology, variability, and trends in the us vapor pressure deficit, an important fire-related meteorological quantity, Journal of Applied Meteorology and Climatology, 54(6), 1121–1141.

Seibt, U., A. Rajabi, H. Griffiths, and J. A. Berry (2008), Carbon isotopes and water use efficiency: sense and sensitivity, Oecologia, 155(3), 441.

Sellin, A., E. Eensalu, and A. Niglas (2010), Is distribution of hydraulic constraints within tree crowns reflected in photosynthetic water-use efficiency? an example of *Betula pendula*, Ecological Research, 25(1), 173–183.

Shackleton, N. J., J. Imbrie, N. G. Pisias, J. Rose, N. J. Shackleton, R. G. West, and D. Q. Bowen (1988), The evolution of oceanic oxygen-isotope variability in the North Atlantic over the past three million years, Philosophical Transactions of the Royal Society of London. B, Biological Sciences, 318(1191), 679–688, doi:10.1098/rstb.1988.0030.

Sharkey, T. D. (2012), Advances in photosynthesis and respiration.

Sheldon, N. D., S. Y. Smith, R. Stein, and M. Ng (2020), Carbon isotope ecology of gymnosperms and implications for paleoclimatic and paleoecological studies, Global and Planetary Change, 184, 103,060.

Sims, D. A., J. R. Seemann, and Y. Luo (1998), Elevated CO_2 concentration has independent effects on expansion rates and thickness of soybean leaves across light and nitrogen gradients, Journal of Experimental Botany, 49(320), 583–591.

Sloan, L. C., and D. Rea (1996), Atmospheric carbon dioxide and early Eocene climate: A general circulation modeling sensitivity study, Palaeogeography, Palaeoclimatology, Palaeoecology, 119(3-4), 275–292.

Smith, R. Y., J. F. Basinger, and D. R. Greenwood (2009), Depositional setting, fossil flora, and paleoenvironment of the Early Eocene Falkland site, Okanagan Highlands, British Columbia, Canadian Journal of Earth Sciences, 46(11), 811–822.

Smith, R. Y., D. R. Greenwood, and J. F. Basinger (2010a), Estimating paleoatmospheric pCO_2 during the early Eocene climatic optimum from stomatal frequency of ginkgo, Okanagan highlands, British Columbia, Canada, Palaeogeography, Palaeoclimatology, Palaeoecology, 293(1-2), 120–131.

Smith, S. A., J. M. Beaulieu, and M. J. Donoghue (2010b), An uncorrelated relaxed-clock analysis suggests an earlier origin for flowering plants, Proceedings of the National Academy of Sciences, 107(13), 5897–5902.

Smith, W. K., T. C. Vogelmann, E. H. DeLucia, D. T. Bell, and K. A. Shepherd (1997), Leaf form and photosynthesis, Bioscience, 47(11), 785–793.

Sperlich, D., C. Chang, J. Peñuelas, C. Gracia, and S. Sabaté (2015), Seasonal variability of foliar photosynthetic and morphological traits and drought impacts in a Mediterranean mixed forest, Tree physiology, 35(5), 501–520.

Spicer, R., P. Valdes, T. Spicer, H. Craggs, G. Srivastava, R. Mehrotra, and J. Yang (2009), New developments in CLAMP: calibration using global gridded meteorological data, Palaeogeography, Palaeoclimatology, Palaeoecology, 283(1-2), 91–98.

Spicer, R. A., A. B. Herman, and E. M. Kennedy (2004), Foliar physiognomic record of climatic conditions during dormancy: Climate Leaf Analysis Multivariate Program (CLAMP) and the cold month mean temperature, The Journal of Geology, 112(6), 685–702.

Spicer, R. A., S. Bera, S. De Bera, T. E. Spicer, G. Srivastava, R. Mehrotra, N. Mehrotra, and J. Yang (2011), Why do foliar physiognomic climate estimates sometimes differ from those observed? Insights from taphonomic information loss and a CLAMP case study from the Ganges Delta, Palaeogeography, Palaeoclimatology, Palaeoecology, 302(3-4), 381–395.

Stein, R. A., N. D. Sheldon, and S. Smith (2019), Rapid response to anthropogenic climate change by *Thuja occidentalis*: implications for past climate reconstructions and future climate predictions, PeerJ, 7, e7378.

Stockey, R. A., G. W. Rothwell, and A. B. Falder (2001), Diversity among taxodioid conifers: *Metasequoia foxii sp. nov.* from the Paleocene of central Alberta, Canada, International Journal of Plant Sciences, 162(1), 221–234.

Sultan, S. E. (1987), Evolutionary implications of phenotypic plasticity in plants, in Evolutionary biology, pp. 127–178, Springer.

Tang, C. Q., Y. Yang, M. Ohsawa, A. Momohara, M. Hara, S. Cheng, and S. Fan (2011), Population structure of relict *Metasequoia glyptostroboides* and its habitat fragmentation and degradation in south-central China, Biological Conservation, 144(1), 279–289.

Taylor, E. L., T. N. Taylor, and M. Krings (2009), Paleobotany: the biology and evolution of fossil plants, Academic Press.

Team, R., et al. (2015), RStudio: integrated development for R., Inc., Boston, MA, 639, 640.

Terashima, I., and K. Hikosaka (1995), Comparative ecophysiology of leaf and canopy photosynthesis, Plant, Cell & Environment, 18(10), 1111–1128.

Thomas, J. F., and C. N. Harvey (1983), Leaf anatomy of four species grown under continuous CO_2 enrichment, Botanical Gazette, 144(3), 303–309.

Thomas, S. C., and A. R. Martin (2012), Carbon content of tree tissues: a synthesis, Forests, 3(2), 332–352.

Tiffney, B. H., and S. R. Manchester (2001), The Use of Geological and Paleontological Evidence in Evaluating Plant Phylogeographic Hypotheses in the Northern Hemisphere Tertiary, International Journal of Plant Sciences, 162(S6), S3–S17, doi:10.1086/323880.

Trolier, M., J. White, P. Tans, K. Masarie, and P. Gemery (1996), Monitoring the isotopic composition of atmospheric CO_2: Measurements from the NOAA Global Air Sampling Network, Journal of Geophysical Research: Atmospheres, 101(D20), 25,897–25,916.

Uemura, K. (1997), Cenozoic history of *Ginkgo* in east Asia, in Ginkgo Biloba A Global Treasure, pp. 207–221, Springer.

Varela, S., J. M. Lobo, and J. Hortal (2011), Using species distribution models in paleobiogeography: a matter of data, predictors and concepts, Palaeogeography, Palaeoclimatology, Palaeoecology, 310(3-4), 451–463.

Visscher, G. E., and R. Jagels (2003), Separation of *Metasequoia* and *Glyptostrobus* (Cupressaceae) based on wood anatomy, IAWA journal, 24(4), 439–450.

Vogel, S. (2009), Leaves in the lowest and highest winds: temperature, force and shape, New Phytologist, 183(1), 13–26.

Vogelmann, T. C. (1993), Plant tissue optics, Annual review of plant biology, 44(1), 231–251.

Wang, L., L. Kunzmann, T. Su, Y.-W. Xing, S.-T. Zhang, Y.-Q. Wang, and Z.-K. Zhou (2019), The disappearance of *Metasequoia* (Cupressaceae) after the middle Miocene in Yunnan, Southwest China: Evidences for evolutionary stasis and intensification of the Asian monsoon, Review of palaeobotany and palynology, 264, 64–74.

Wang, Y., A. Momohara, L. Wang, J. Lebreton-Anberree, and Z. Zhou (2015), Evolutionary history of atmospheric CO_2 during the late Cenozoic from fossilized *Metasequoia* needles, PloS one, 10(7).

Webb, L. (1968), Environmental relationships of the structural types of Australian rain forest vegetation, Ecology, 49(2), 296–311.

Wen, J. (1999), Evolution of Eastern Asian and Eastern North American Disjunct Distributions in Flowering Plants, Annual Review of Ecology and Systematics, 30(1), 421–455, doi:10.1146/annurev.ecolsys.30.1.421.

White, J. W., E. R. Cook, J. R. Lawrence, et al. (1985), The δH ratios of sap in trees: Implications for water sources and tree ring DH ratios, Geochimica et Cosmochimica Acta, 49(1), 237–246.

Wilf, P. (1997), When are leaves good thermometers? A new case for leaf margin analysis, Paleobiology, 23(3), 373–390.

Wilf, P. (2000), Late Paleocene–early Eocene climate changes in southwestern Wyoming: Paleobotanical analysis, Geological Society of America Bulletin, 112(2), 292–307.

Wilf, P., S. L. Wing, D. R. Greenwood, and C. L. Greenwood (1998), Using fossil leaves as paleoprecipitation indicators: an Eocene example, Geology, 26(3), 203–206.

Williams, C. J., A. H. Johnson, B. A. LePage, D. R. Vann, and T. Sweda (2003), Reconstruction of Tertiary *Metasequoia* forests. II. Structure, biomass, and productivity of Eocene floodplain forests in the Canadian Arctic, Paleobiology, 29(2), 271–292.

Williams, C. J., K. D. Trostle, and D. Sunderlin (2010), Fossil wood in coal-forming environments of the late Paleocene–early Eocene Chickaloon Formation, Palaeogeography, Palaeoclimatology, Palaeoecology, 295(3-4), 363–375.

Wing, S. L. (1987), Eocene and Oligocene floras and vegetation of the Rocky Mountains, Annals of the Missouri Botanical Garden, pp. 748–784.

Wing, S. L., and D. R. Greenwood (1993), Fossils and fossil climate: the case for equable continental interiors in the Eocene, Philosophical Transactions of the Royal Society of London. Series B: Biological Sciences, 341(1297), 243–252.

Wing, S. L., T. M. Bown, and J. D. Obradovich (1991), Early Eocene biotic and climatic change in interior western North America, Geology, 19(12), 1189–1192.

Wolfe, J. A. (1979), Temperature parameters of humid to mesic forests of Eastern Asia and relation to forests of other regions of the Northern Hemisphere and Australasia: analysis of temperature data from more than 400 stations in Eastern Asia, United States. Geological Survey. Professional paper (USA).

Wolfe, J. A. (1985), Distribution of major vegetational types during the Tertiary, The carbon cycle and atmospheric CO2: natural variations Archean to present, 32, 357–375.

Wolfe, J. A. (1994), Tertiary climatic changes at middle latitudes of western North America, Palaeogeography, Palaeoclimatology, Palaeoecology, 108(3-4), 195–205.

Wolfe, J. A., C. E. Forest, and P. Molnar (1998), Paleobotanical evidence of Eocene and Oligocene paleoaltitudes in midlatitude western North America, Geological Society of America Bulletin, 110(5), 664–678.

Woodward, F. I., and F. Woodward (1987), Climate and plant distribution, Cambridge University Press.

Worth, J. R., G. J. Williamson, S. Sakaguchi, P. G. Nevill, and G. J. Jordan (2014), Environmental niche modelling fails to predict Last Glacial Maximum refugia: niche shifts, microrefugia or incorrect palaeoclimate estimates?, Global Ecology and Biogeography, 23(11), 1186–1197.

Wyka, T. P., J. Oleksyn, R. Żytkowiak, P. Karolewski, A. Jagodziński, and P. B. Reich (2012), Responses of leaf structure and photosynthetic properties to intra-canopy light gradients: a common garden test with four broadleaf deciduous angiosperm and seven evergreen conifer tree species, Oecologia, 170(1), 11–24.

Xing, Y., M. A. Gandolfo, R. E. Onstein, D. J. Cantrill, B. F. Jacobs, G. J. Jordan, D. E. Lee, S. Popova, R. Srivastava, T. Su, et al. (2016), Testing the biases in the rich Cenozoic angiosperm macrofossil record, International Journal of Plant Sciences, 177(4), 371–388.

Yamakawa, C., A. Momohara, T. Saito, and T. Nunotani (2017), Composition and paleoenvironment of wetland forests dominated by *Glyptostrobus* and *Metasequoia* in the latest Pliocene (2.6 Ma) in central Japan, Palaeogeography, Palaeoclimatology, Palaeoecology, 467, 191–210.

Yang, H., and J.-H. Jin (2000), Phytogeographic history and evolutionary stasis of *Metasequoia*: geological and genetic information contrasted, Acta Palaeontologica Sinica, 39(SUPP), 288–307.

Yang, J., R. A. Spicer, T. E. Spicer, and C.-S. Li (2011), 'CLAMP Online': a new web-based palaeoclimate tool and its application to the terrestrial Paleogene and Neogene of North America, Palaeobiodiversity and Palaeoenvironments, 91(3), 163.

Yeung, E. C. (1998), A beginner's guide to the study of plant structure, Tested studies for laboratory teaching, 19, 125–141.

Zachos, J., M. Pagani, L. Sloan, E. Thomas, and K. Billups (2001), Trends, rhythms, and aberrations in global climate 65 Ma to present, science, 292(5517), 686–693.

Zakharova, L., K. Meyer, and M. Seifan (2019), Trait-based modelling in ecology: A review of two decades of research, Ecological Modelling, 407, 108,703.

Zhu, J., C. J. Poulsen, and J. E. Tierney (2019), Simulation of Eocene extreme warmth and high climate sensitivity through cloud feedbacks, Science advances, 5(9), eaax1874.

APPENDIX A

Chapter 2 Supplemental Tables

A.1 *Metasequoia glyptostroboides* climatic gradient samples: Samples were collected across North America, Asia, and Europe 2016–2017.

Sample No.	Vouchers	Latitude	Longitude	Location
MN16-02	MN16-02-MICH	39.947251	-75.148861	Rose Garden, PA
MN16-04		38.908682	-76.971053	National Arboretum, D.C.
MN16-07		38.914275	-76.957572	National Arboretum, D.C.
MN17-11		25.1391	102.742317	Kunming Institute of Botany, Kunming, China
MN17-13		25.147433	102.740917	Kunming Institute of Botany, Kunming, China
MN17-14		30.765333	104.124767	Chengdu Botanical Gardens, Chengdu, China
MN17-15		30.767083	104.12115	Chengdu Botanical Gardens, Chengdu, China
MN17-16		30.662483	104.041883	Chengdu Botanical Gardens, Chengdu, China
MN17-17	MN17-17-MICH	30.662733	104.042267	Chengdu Botanical Gardens, Chengdu, China
MN17-18		30.27925	109.50145	Enshi, China
MN17-19		30.278933	109.50225	Enshi, China
MN17-20		30.278483	109.5018	Enshi, China

MN17-21	MN17-21-MICH	29.353283	110.531683	Jiangjiajie, China
MN17-22		29.35325	110.5318	Jiangjiajie, China
MN17-24		29.35325	110.5318	Jiangjiajie, China
MN17-25	MN17-25-MICH	29.35325	110.5318	Jiangjiajie, China
MN17-26	MN17-26-MICH	31.151567	121.44145	Shanghai Botanical Garden, China
MN17-30		31.215367	121.4383	Shanghai, China
MN17-31		31.2189	121.441633	Shanghai, China
MN17-32		39.990533	116.207967	Beijing, China
MN17-33		39.990483	116.207883	Beijing, China
MN17-34	MN17-34-MICH	55.8673	12.50461	Horsholm Arboretum, Copenhagen, Denmark
MN17-35		55.86726	12.50445	Horsholm Arboretum, Copenhagen, Denmark
MN17-36		55.86728	12.50437	Horsholm Arboretum, Copenhagen, Denmark
MN17-37		55.86899	12.50537	Horsholm Arboretum, Copenhagen, Denmark
MN17-38	MN17-38-MICH	55.86894	12.50529	Horsholm Arboretum, Copenhagen, Denmark
MN17-39		55.86907	12.50513	Horsholm Arboretum, Copenhagen, Denmark
MN17-40		55.75109	12.57353	Forestbotanisk Have, Copenhagen, Denmark
MN17-41		55.75087	12.57326	Forestbotanisk Have, Copenhagen, Denmark
MN17-42		55.75087	12.57298	Forestbotanisk Have, Copenhagen, Denmark

MN17-43	MN17-43-MICH	55.74993	12.57392	Forestbotanisk Have, Copenhagen, Denmark
MN17-44		55.74947	12.57132	Forestbotanisk Have, Copenhagen, Denmark
MN17-46		50.84829	4.38446	Ambrioxsquare, Brussels, Belgium
MN17-47		50.84832	4.38462	Ambrioxsquare, Brussels, Belgium
MN17-48		50.84893	4.38492	Ambrioxsquare, Brussels, Belgium
MN17-49	MN17-49-MICH	53.38301	-2.93849	Liverpool, UK
MN17-50		53.38292	-2.93825	Liverpool, UK
MN17-51		53.3772	-2.93853	Liverpool, UK
MN17-52	MN17-52-MICH	51.50539	-3.17446	Roath Park, Cardiff, Wales
MN17-53		51.51193	-3.17616	Roath Park, Cardiff, Wales
MN17-54	MN17-54-MICH	51.49395	-3.19366	Bute Park, Cardiff, Wales
MN17-55		51.49399	-3.19374	Bute Park, Cardiff, Wales
MN17-56		51.50425	0.16005	Hyde Park, London, UK
MN17-57		51.5038	0.15899	Hyde Park, London, UK
MN17-58		51.51504	0.11293	London, UK
MN17-61		44.84475	0.55883	Bordeaux, France
MN17-62		44.84525	0.56042	Bordeaux, France
MN17-63		47.21994	1.54456	Nantes, France
MN17-64		47.2201	1.54406	Nantes, France
MN17-66		47.21624	1.55676	Nantes, France
MN17-67		48.709788	9.207059	Stuttgart, Germany
MN17-68		48.709578	9.208047	Stuttgart, Germany
MN17-71		48.14814	16.39811	Vienna, Austria
MN17-72		48.14811	16.39812	Vienna, Austria
MN17-73		48.14783	16.39841	Vienna, Austria
MN17-74		48.14798	16.3984	Vienna, Austria
MN17-75		52.39547	13.06492	Berlin, Germany
MN17-76		52.41243	13.06889	Berlin, Germany
MN17-77		52.51667	13.34629	Berlin, Germany
MN17-78		52.51648	13.34643	Berlin, Germany

MN17-80	MN17-80-MICH	59.8508	17.62732	Uppsala Botanical Garden, Uppsala, Sweden
MN17-81		59.85017	17.63002	Uppsala Botanical Garden, Uppsala, Sweden
MN18-04		36.1409915	-86.796662	Vanderbilt University, Nashville Tennessee
MN18-05		34.141144	-118.05384	Los Angeles Arboretum
MN18-08		34.141596	-118.05278	Los Angeles Arboretum
MN18-10		42.3004	-83.661402	Matthaei Botanical Garden; 5m outer canopy
MN18-11		42.3004	-83.661402	Matthaei Botanical Garden; 5m inner canopy
MN18-12		42.3004	-83.661402	Matthaei Botanical Garden; 3m inner canopy
MN18-13		42.3004	-83.661402	Matthaei Botanical Garden; 3m outer canopy
MN18-20		42.280150	-83.721361	Nichols Arboretum; 1 m outer canopy
MN18-21		42.280150	-83.721361	Nichols Arboretum; 1 m inner canopy
MN18-22		42.280150	-83.721361	Nichols Arboretum; 6.5 m outer canopy
MN18-23		42.280150	-83.721361	Nichols Arboretum; 8 m outer canopy
MN18-27		42.3004	-83.661402	Matthaei Botanical Garden; 6.5 m inner canopy

A.2 Correlations (r-value) between anatomy and climate

Climate variable	Cross-sectional area	Vascular bundle area	Resin canal area	Leaf width	Leaf thickness
Bio 1	-0.351*	0.123*	-0.063	-0.300*	-0.148*
Bio 2	-0.076	0.118*	-0.014	0.012	-0.063
Bio 3	-0.093*	-0.055	<0.001	-0.064	-0.101*
Bio 4	0.014	0.129*	-0.018	0.061	0.029
Bio 5	-0.248*	0.169*	-0.054	-0.187*	-0.097*
Bio 6	-0.314*	0.001	-0.047	-0.322*	-0.143*
Bio 7	-0.015	0.154*	-0.017	0.046	0.007
Bio 8	-0.188*	0.089	-0.137*	-0.142*	-0.122*
Bio 9	-0.037	0.110*	-0.016	-0.065	0.030
Bio 10	-0.258*	0.166*	-0.049	-0.205*	-0.089
Bio 11	-0.334*	0.045	-0.044	-0.324*	-0.147*
Bio 12	-0.157*	0.318*	0.040	-0.213*	0.038
Bio 13	-0.272*	0.169*	-0.064	-0.238*	-0.124*
Bio 14	0.133*	0.054	0.105*	0.046	0.118*
Bio 15	-0.259*	-0.030	-0.143*	-0.145*	-0.238*
Bio 16	-0.266*	0.196*	-0.049	-0.246*	-0.104*
Bio 17	0.172*	0.068	0.120*	0.066	0.151*
Bio 18	-0.264*	0.182*	-0.042	-0.222*	-0.094*
Bio 19	0.156*	0.027	0.058	0.046	0.091*

Note: Significant values ($p < 0.05$) are denoted by asterisk.

A.3 CCA scores for anatomical traits and Bioclim variables

	Axis 1	Axis 2	Axis 3	Axis 4
Cross-sectional area	-0.67769	-0.57333	-1.14914	-1.21699
Vascular bundle area	2.27422	-1.54665	0.748425	-0.42277
Resin canal area	0.673941	2.16642	0.501253	-1.0475
Leaf width	-0.8627	-0.23103	1.04664	0.422649
Leaf thickness	0.436538	0.358775	-1.10203	1.45018
Bio 1	0.211117	0.008741	0.23253	0.201113
Bio 2	-0.0423	-0.07383	0.108686	0.055852
Bio 3	-0.01746	0.134731	0.065102	-0.07836
Bio 4	0.092323	-0.15819	0.10285	0.093096
Bio 5	0.176792	-0.08213	0.223053	0.194881
Bio 6	0.13718	0.115535	0.112258	0.109583
Bio 7	0.070868	-0.15739	0.13164	0.107027
Bio 8	0.143374	-0.10514	0.18144	0.17909
Bio 9	0.002217	-0.0494	-0.01399	0.073643
Bio 10	0.221893	-0.07103	0.228131	0.203274
Bio 11	0.142005	0.095765	0.140728	0.126826
Bio 12	0.325313	-0.10615	0.16067	0.122781
Bio 13	0.249173	-0.06189	0.261942	0.163042
Bio 14	-0.03172	-0.05534	-0.08969	-0.09562
Bio 15	0.0099	-0.01479	0.239516	0.112561
Bio 16	0.266455	-0.05847	0.250801	0.161681
Bio 19	-0.02886	-0.06581	-0.11556	-0.09707
Bio 18	0.276585	-0.03554	0.249728	0.177744
Bio 19	-0.1246	-0.07868	-0.12981	-0.12224

APPENDIX B

Chapter 3 Supplemental Tables and Figures

B.1 Leaf collection of *Taxodium distichum*, *Sequoia sempervirens*, and *Metasequoia glyptostroboides* used in this study collected across North America, Asia, and Europe between 2016 and 2017

Date	code	Species	Lat, Long	Location
3-Jul-16	MN16-01	*Taxodium distichum*	39.947213, -75.148767	Rose Garden, PA
5-Jul-16	MN16-03	*Taxodium distichum*	38.906058, -76.971796	National Arboretum, D.C.
5-Jul-16	MN16-05	*Taxodium distichum*	38.910335, -76.971265	National Arboretum, D.C.
5-Jul-16	MN16-06	*Taxodium distichum*	38.910156, -76.961893	National Arboretum, D.C.
6-Jul-16	MN16-08	*Taxodium distichum*	36.843387, -76.829121	Zuni, VA
6-Jul-16	MN16-09	*Taxodium distichum*	36.843371, -76.829085	Zuni, VA
30-Jul-16	MN16-10	*Taxodium distichum*	33.162403, -79.829641	Francis Marion National Forest, SC
30-Jul-16	MN16-11	*Taxodium distichum*	33.046995, -79.657732	Francis Marion National Forest, SC
5-Aug-16	MN16-12	*Taxodium distichum*	25.854, -81.01996	Big Cypress National Preserve, FL
5-Aug-16	MN16-13	*Taxodium distichum*	25.85513, -81.01982	Big Cypress National Preserve, FL
6-Aug-16	MN16-14	*Taxodium distichum*	25.96495, -81.33611	Big Cypress National Preserve, FL
6-Aug-16	MN16-15	*Taxodium distichum*	28.87487, -81.48874	Seminole State Forest, FL

6-Aug-16	MN16-16	*Taxodium distichum*	28.87489, -81.48871	Seminole State Forest, FL
7-Aug-16	MN16-17	*Taxodium distichum*	30.16731, -84.65559	Apalachicola National Forest, FL
7-Aug-16	MN16-18	*Taxodium distichum*	30.16759, -84.65544	Apalachicola National Forest, FL
8-Aug-16	MN16-19	*Taxodium distichum*	30.39229, -89.72487	Pearl River WMA, LA
8-Aug-16	MN16-20	*Taxodium distichum*	30.39498, -89.71277	Pearl River WMA, LA
8-Aug-16	MN16-21	*Taxodium distichum*	30.39686, -89.69938	Pearl River WMA, LA
11-Aug-16	MN16-22	*Taxodium distichum*	29.87936, -91.4713	Attakapas Island WMA, LA
11-Aug-16	MN16-23	*Taxodium distichum*	29.87951, -91.47157	Attakapas Island WMA, LA
11-Aug-16	MN16-24	*Taxodium distichum*	29.87826, -91.47115	Attakapas Island WMA, LA
12-Aug-16	MN16-25	*Taxodium distichum*	29.17749, -95.84204	San Bernard NWR, TX
12-Aug-16	MN16-26	*Taxodium distichum*	29.87601, -98.48644	Guadalupe River State Park, TX
12-Aug-16	MN16-27	*Taxodium distichum*	29.87596, -98.48687	Guadalupe River State Park, TX
12-Aug-16	MN16-28	*Taxodium distichum*	29.8758, -98.48716	Guadalupe River State Park, TX
14-Aug-16	MN16-29	*Taxodium distichum*	32.76935, -90.7953	Delta National Forest, MS
14-Aug-16	MN16-30	*Taxodium distichum*	32.76945, -90.79974	Delta National Forest, MS
14-Aug-16	MN16-31	*Taxodium distichum*	32.76945, -90.79973	Delta National Forest, MS
15-Aug-16	MN16-32	*Taxodium distichum*	37.33851, -89.07297	Cypress Creek NWR, IL
15-Aug-16	MN16-33	*Taxodium distichum*	37.33839, -89.07283	Cypress Creek NWR, IL

15-Aug-16	MN16-34	*Taxodium distichum*	37.28552, -89.15553	Cypress Creek NWR, IL
26-Aug-16	MN16-35	*Taxodium distichum*	39.97853, -82.41219	Dawes Arboretum Newark, OH
26-Aug-16	MN16-36	*Taxodium distichum*	39.97847, -82.41206	Dawes Arboretum Newark, OH
26-Aug-16	MN16-37	*Taxodium distichum*	39.97829, -82.41213	Dawes Arboretum Newark, OH
11-Sep-16	MN16-38	*Taxodium distichum*	42.3004, -83.6614023	MBGNA Ann Arbor, MI
13-Sep-16	MN16-39	*Taxodium distichum*	42.2787368, -83.7397456	Panera Bread Ann Arbor, MI
20-Dec-16	MN16-40	*Sequoia sempervirens*	37.25625, -122.21931	Portola Redwood State Park
20-Dec-16	MN16-41	*Sequoia sempervirens*	37.25355, -122.21803	Portola Redwood State Park
20-Dec-16	MN16-42	*Sequoia sempervirens*	37.25362, -122.21835	Portola Redwood State Park
21-Dec-16	MN16-43	*Sequoia sempervirens*	41.10152, -124.15422	Trinidad, CA
21-Dec-16	MN16-44	*Sequoia sempervirens*	41.10152, -124.15422	Trinidad, CA
21-Dec-16	MN16-45	*Sequoia sempervirens*	41.05508, -123.88755	Logging company
21-Dec-16	MN16-46	*Sequoia sempervirens*	41.05508, -123.88755	Logging company
21-Dec-16	MN16-47	*Sequoia sempervirens*	42.11937, -124.19595	Oregon
21-Dec-16	MN16-48	*Sequoia sempervirens*	42.12092, -124.19652	Oregon
21-Dec-16	MN16-49	*Sequoia sempervirens*	42.12194, -124.19668	Oregon
22-Dec-16	MN16-50	*Sequoia sempervirens*	39.39301, -123.46055	Jackson State Forest, Willits
22-Dec-16	MN16-51	*Sequoia sempervirens*	39.38271, -123.4797	Jackson State Forest, Willits
22-Dec-16	MN16-52	*Sequoia sempervirens*	39.34858, -123.54216	Jackson State Forest, Willits

22-Dec-16	MN16-53	*Sequoia sempervirens*	39.34855, -123.54221	Jackson State Forest, Willits
23-Dec-16	MN16-54	*Sequoia sempervirens*	36.99752, -122.05316	UC Santa Cruz
23-Dec-16	MN16-55	*Sequoia sempervirens*	36.9996, -122.05296	UC Santa Cruz
23-Dec-16	MN16-56	*Sequoia sempervirens*	37.00082, -122.06189	UC Santa Cruz
23-Dec-16	MN16-57	*Sequoia sempervirens*	35.27982, -120.66468	San Louis Obispo
23-Dec-16	MN16-58	*Sequoia sempervirens*	35.27985, -120.66453	San Louis Obispo
26-Dec-16	MN16-59	*Sequoia sempervirens*	34.132312, -118.11209	Huntington Library
26-Dec-16	MN16-60	*Sequoia sempervirens*	34.132312, -118.11209	Huntington Library
26-Dec-16	MN16-61	*Sequoia sempervirens*	34.132312, -118.11209	Huntington Library
29-Dec-16	MN16-62	*Sequoia sempervirens*	34.44948, -119.8462	Santa Barbara
29-Dec-16	MN16-63	*Sequoia sempervirens*	34.4496, -119.84623	Santa Barbara
29-Dec-16	MN16-64	*Sequoia sempervirens*	34.44949, -119.84607	Santa Barbara
Jul-17	MN17-07	*Taxodium distichum*	23.148783, 113.27745	XTBG, China
Jul-17	MN17-08	*Taxodium distichum*	23.148783, 113.27745	XTBG, China
Jul-17	MN17-10	*Sequoia sempervirens*	21.931117, 101.253833	Kunming Institute of Botany, Kunming, China
Jul-17	MN17-12	*Sequoia sempervirens*	25.14605, 102.74145	Kunming Institute of Botany, Kunming, China
Jul-17	MN17-28	*Taxodium distichum*	31.150583, 121.441567	Shanghai Botanical Garden, China
Aug-17	MN17-59	*Taxodium distichum*	44.85021, -0.57973	Bordeaux, France

XTBG- Xishuangbanna Tropical Botanical Garden

B.2 PCA Eigenvalue

	Axes	Eigenvalue	% variance
PCA_{anat}	1	3.41482	68.296
	2	1.134	22.68
	3	0.325887	6.5177
	4	0.105601	2.112
	5	0.019692	0.39384
$PCA_{anat-vb}$	1	3.17172	79.293
	2	0.688885	17.222
	3	0.116916	2.9229
	4	0.022482	0.56204
PCA_{phys}	1	0.060879	43.125
	2	0.0458	37.431
	3	0.013995	19.445
$PCA_{anat+phys}$	1	3.65645	45.706
	2	1.74228	21.778
	3	1.18454	14.807
	4	0.610839	7.6355
	5	0.480169	6.0021
	6	0.20228	2.5285
	7	0.104249	1.3031
	8	0.019195	0.23994
$PCA_{anat+phys-vb-\Delta leaf}$	1	3.41626	56.938
	2	1.4709	24.515
	3	0.614537	10.242
	4	0.359721	5.9953
	5	0.116114	1.9352
	6	0.02247	0.37451

B.3 CCA Eigenvalues

	Axis	Eigenvalue	% variance
CCA_{anat}	1	0.088372	85.4
	2	0.008828	8.5
	3	0.004934	4.8
	4	0.001344	1.3
$\text{CCA}_{anat-vb}$	1	0.069472	88.8
	2	0.006652	8.5
	3	0.002136	2.7
CCA_{phys}	1	0.050838	74.1
	2	0.01779	25.9
$\text{CCA}_{anat+phys}$	1	0.10369	59.6
	2	0.053797	30.9
	3	0.009774	5.6
	4	0.004505	2.6
	5	0.001664	0.9
	6	0.000426	0.2
	7	0.000161	0.1
$\text{CCA}_{anat+phys-vb}$	1	0.11084	67.4
	2	0.043337	26.4
	3	0.005064	3.1
	4	0.004026	2.4
	5	0.000768	0.5
	6	0.000365	0.2
$\text{CCA}_{anat+phys-vb-\Delta_{leaf}}$	1	0.13227	69.6
	2	0.051178	26.9
	3	0.005041	2.7
	4	0.001127	0.6
	5	0.000513	0.3

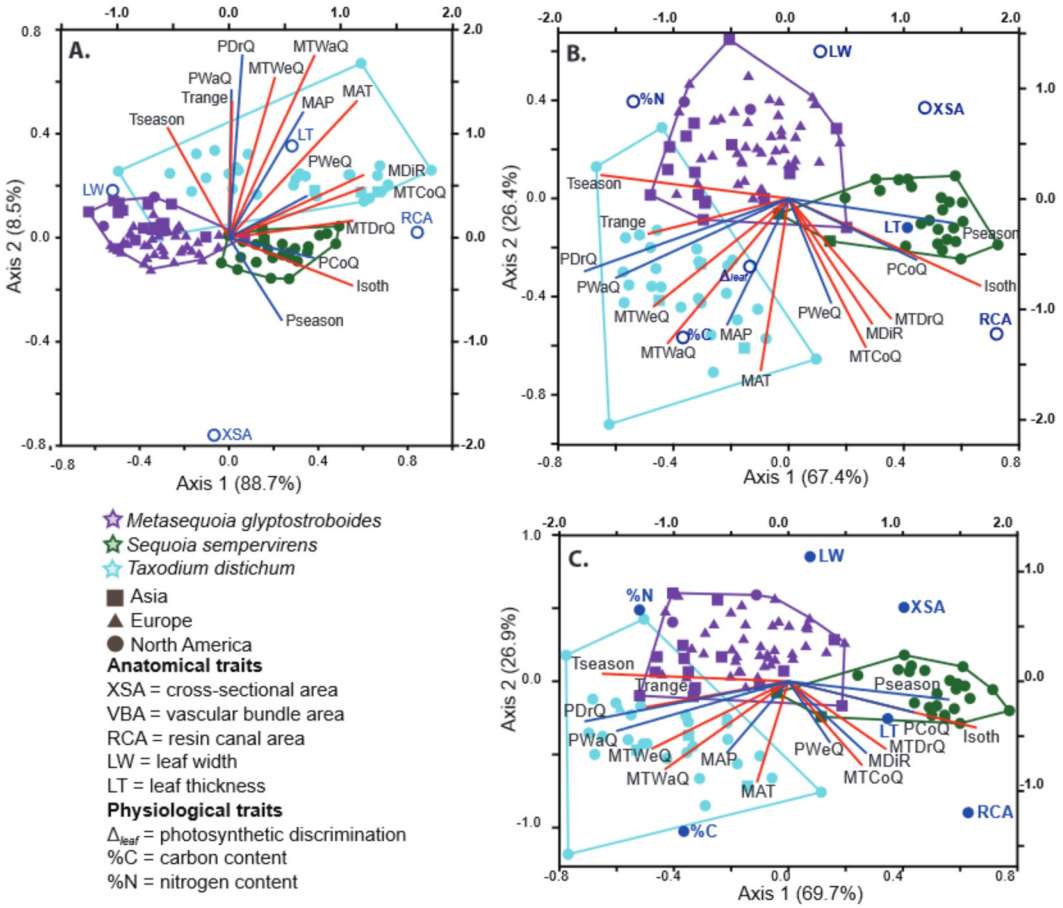

B.4 CCA plot for each taxon

Canonical correspondence analyses (CCA) for *Metasequoia glyptostroboides* (purple), *Sequoia sempervirens* (green), and *Taxodium distichum* (light blue) of traits and Bioclim variables (temperature = red, precipitation = dark blue). **A,** CCA$_{anat}$ but with VBA omitted. Axis 1 (88.7%) shows strongest variation with RCA and mean temperature driest quarter, Axis 2 (8.5%) with XSA, temperature range (Trange), precipitation of warmest quarter (PWaQ), and precipitation of driest quarter (PDrQ). **B,** CCA$_{anat+phys-vb}$ uses the same traits as CCA$_{anat+phys}$ but omits VBA. Axis 1 (67.4%) shows high variability with PDrQ and Axis 2 (26.4%) with mean annual temperature (MAT). In traits, Axis 1 was highly variable with RCA and Axis 2 with LW. **C,** CCA$_{anat+phys-vb-\Delta_{leaf}}$ also uses the same traits as CCA$_{anat+phys}$ but omits both VBA and Δ_{leaf}. Axis 1 (69.7%) shows high variability with PDrQ and Axis 2 (26.9%) with MAT. In traits, Axis 1 was highly variable with RCA and Axis 2 with %C.

B.5 CCA$_{anat}$ scores

CCA$_{anat}$	Axis 1	Axis 2	Axis 3	Axis 4
MAT	0.5718	-0.4515	0.2781	-0.0039
MDiR	0.6678	-0.1843	0.1673	-0.0577
Isoth	0.6201	-0.0094	-0.1555	0.0273
Tseason	-0.3106	-0.1122	0.3393	-0.0625
Trange	0.0093	-0.1965	0.4053	-0.0898
MTWeQ	0.1911	-0.3629	0.4073	-0.0426
MTDrQ	0.5791	-0.2086	-0.0277	0.0237
MTWaQ	0.3621	-0.4738	0.4278	-0.0346
MTCoQ	0.6178	-0.3011	0.0399	0.0309
MAP	0.3412	-0.2995	0.3255	-0.0243
Pseason	0.2524	0.0544	-0.2940	0.1080
PWeQ	0.3542	-0.2035	0.0440	0.0525
PDrQ	0.0890	-0.2216	0.6103	-0.1635
PWaQ	-0.0360	-0.3446	0.3563	0.0006
PCoQ	0.4612	0.0714	0.0051	-0.0186
Cross-sectional area	0.2024	1.2831	-1.7421	-0.4567
Vascular bundle area	-1.3208	-1.4446	-0.7632	0.4569
Leaf thickness	0.7366	-0.7867	0.5201	-1.6782
Resin canal area	1.7702	-0.4423	0.0367	1.5916
Leaf width	-0.6224	0.8034	1.0243	0.2635
MN16-01	-0.1358	0.1287	0.3463	0.0948
MN16-02	-0.2089	0.1287	0.2163	-0.1506
MN16-03	0.0033	-0.1079	0.1254	-0.0956
MN16-04	-0.4111	0.2383	0.1578	-0.0772
MN16-05	0.1385	0.2398	0.4281	0.1433
MN16-06	-0.2763	0.2451	0.3868	-0.2618
MN16-10	0.0560	-0.0401	0.2438	-0.0235
MN16-11	0.1067	-0.1554	0.2470	-0.1598
MN16-13	0.6239	-0.1698	0.1219	0.3706
MN16-14	0.6843	-0.2177	0.0844	0.0803
MN16-15	0.7749	-0.2006	0.1491	0.2505
MN16-16	0.2071	-0.0210	0.1747	-0.0480
MN16-17	0.5568	-0.2571	0.1481	-0.0168
MN16-18	0.7810	-0.2481	0.1484	0.2123
MN16-19	0.4518	-0.0946	0.2423	0.0519
MN16-20	0.0238	0.2217	0.5626	0.6768
MN16-21	0.0635	-0.1128	0.2020	-0.1275
MN16-22	0.5955	-0.2635	0.1360	-0.1521
MN16-23	0.7683	-0.6456	0.3594	-1.4087
MN16-24	0.2334	0.0762	0.3595	-0.1203

MN16-26	0.8245	-0.4893	0.0429	-0.0324
MN16-27	0.3461	-0.2718	-0.0024	-0.3294
MN16-28	0.6761	-0.3338	0.0992	-0.0987
MN16-31	0.0980	0.0638	0.4277	0.0201
MN16-32	0.3427	-0.1471	0.1773	-0.0601
MN16-33	0.6216	-0.3828	0.1119	-0.0359
MN16-35	0.3463	-0.2057	0.1464	-0.2359
MN16-36	-0.0191	0.1348	0.2673	-0.0528
MN16-39	0.3380	-0.1447	0.1398	-0.1545
MN16-40	0.1139	0.0687	0.0113	-0.3582
MN16-41	0.3387	0.0717	-0.0261	0.0370
MN16-42	0.2892	-0.0203	-0.0442	-0.1138
MN16-43	0.2193	0.1170	-0.0375	0.0074
MN16-44	0.1080	0.2174	0.0100	0.0020
MN16-45	0.3182	0.1443	0.0461	0.1143
MN16-46	0.1578	0.1328	-0.0128	-0.0308
MN16-48	0.3842	-0.0458	-0.0490	0.0553
MN16-49	0.2183	0.0851	0.0211	-0.0088
MN16-50	0.4900	-0.1238	-0.0850	-0.0194
MN16-51	0.2694	0.0571	-0.0517	-0.0145
MN16-53	0.3934	0.1093	-0.0002	0.1841
MN16-54	0.3858	0.0521	0.0057	0.1567
MN16-55	0.3758	0.0127	-0.0933	-0.0527
MN16-56	0.3942	-0.0227	-0.0595	0.0581
MN16-57	0.3066	-0.0167	-0.0687	-0.0301
MN16-58	0.1422	0.1369	-0.0746	-0.1363
MN16-59	0.2820	0.1034	-0.1241	-0.0805
MN16-60	0.2852	0.0081	-0.1661	-0.0314
MN16-61	0.1358	0.0446	-0.0077	-0.1657
MN16-62	0.5295	-0.1100	0.0189	0.1500
MN16-63	0.4161	-0.0907	-0.0198	0.0960
MN16-64	0.4673	-0.0877	-0.0065	0.1178
MN17-07	0.5167	-0.3410	0.0013	-0.1606
MN17-08	0.3460	-0.2067	0.0967	0.0360
MN17-10	0.1981	-0.0182	0.0142	-0.1315
MN17-11	-0.4000	0.3984	0.3259	0.0890
MN17-12	0.1933	-0.0247	-0.0379	-0.1672
MN17-13	-0.3771	0.0218	0.0440	0.0527
MN17-14	-0.3056	0.0608	0.0695	0.0465
MN17-15	-0.4883	-0.0227	0.1099	0.1248
MN17-16	-0.3487	0.1994	0.2163	0.0699
MN17-17	-0.3105	-0.0013	0.0192	0.0085
MN17-18	-0.2349	-0.3369	-0.1789	0.0552
MN17-19	-0.4496	-0.2219	-0.0941	-0.0484
MN17-20	-0.5226	-0.3430	-0.1583	-0.0223

MN17-21	-0.4618	0.0505	0.1557	0.0508
MN17-22	-0.4760	0.0144	0.0955	0.0984
MN17-24	-0.5210	-0.2642	-0.0474	0.0588
MN17-25	-0.3158	-0.2407	-0.1269	0.0745
MN17-26	-0.1896	0.0867	0.1852	0.0790
MN17-28	0.5427	-0.3210	0.0575	0.2759
MN17-32	-0.3499	0.1254	0.0467	-0.0432
MN17-33	-0.3443	0.2958	0.1130	0.0388
MN17-34	-0.3174	0.2912	0.0776	-0.1526
MN17-35	-0.2940	0.0888	-0.0281	-0.1018
MN17-36	-0.2940	0.1925	-0.0010	-0.0137
MN17-37	-0.3254	-0.0082	-0.0723	-0.0110
MN17-38	-0.3213	0.2043	0.1224	0.0204
MN17-39	-0.2911	-0.0717	-0.0809	0.0254
MN17-40	-0.2917	-0.1318	-0.1208	-0.0108
MN17-41	-0.1824	0.0943	0.0538	-0.0428
MN17-42	-0.2770	0.2341	0.1630	-0.0836
MN17-43	-0.3058	0.1265	-0.0617	-0.0500
MN17-44	-0.2455	0.2060	0.0757	-0.0458
MN17-46	-0.0854	-0.0342	0.0013	0.0715
MN17-47	-0.2716	0.0228	0.0381	0.0512
MN17-48	-0.1828	-0.1404	-0.1096	0.0148
MN17-49	-0.3124	0.1177	-0.0275	-0.0933
MN17-50	-0.3088	0.1374	0.0407	-0.0108
MN17-51	-0.1501	0.0176	-0.0033	0.0392
MN17-52	-0.3554	0.1983	0.0856	0.0646
MN17-53	-0.2094	0.0477	0.0510	-0.0267
MN17-54	-0.3484	0.3286	0.1355	0.0407
MN17-55	-0.3961	0.2465	0.0987	-0.0007
MN17-56	-0.1988	0.0102	0.0116	-0.0013
MN17-57	-0.3234	0.0196	0.0989	0.0500
MN17-58	-0.2481	0.0845	0.0711	0.0273
MN17-59	-0.1919	0.2058	0.1104	-0.0214
MN17-61	-0.3340	-0.0740	-0.1302	-0.0165
MN17-62	-0.3830	-0.2903	-0.2143	-0.0149
MN17-63	-0.3082	0.0291	0.0208	0.0054
MN17-64	-0.4807	-0.0608	-0.0233	0.0221
MN17-66	-0.1990	0.0300	0.0543	-0.0625
MN17-67	-0.4995	-0.0347	-0.0339	0.0662
MN17-68	-0.4870	-0.1919	-0.0799	0.1059
MN17-71	-0.2680	0.0922	0.1108	0.0916
MN17-72	-0.2739	0.0920	0.0982	0.0948
MN17-73	-0.2591	0.0994	0.0085	0.0434
MN17-74	-0.2248	0.1405	0.1018	-0.0268
MN17-75	-0.2705	-0.0397	-0.0791	-0.0354

MN17-76	-0.2046	-0.0149	-0.0578	-0.1489
MN17-77	-0.3295	0.0004	-0.0342	0.0182
MN17-78	-0.2239	-0.0051	0.0290	-0.0446
MN17-80	-0.3238	0.0488	0.0167	-0.0172
MN17-81	-0.2376	-0.1084	-0.1418	-0.0179

B.6 $CCA_{anat-vb}$ scores

	Axis 1	Axis 2	Axis 3
Cross-sectional area	-0.1334	-1.8984	0.5042
Leaf thickness	0.5640	0.8827	1.4892
Leaf width	-1.0419	0.4548	-0.5465
Resin canal area	1.6859	0.0521	-1.3408
MAT	0.5754	0.5277	0.0217
MDiR	0.6054	0.2426	0.0479
Isoth	0.5561	-0.1846	-0.0153
Tseason	-0.2766	0.4255	0.0362
Trange	0.0143	0.5265	0.0606
MTWeQ	0.2060	0.6184	0.0314
MTDrQ	0.5576	0.0660	0.0060
MTWaQ	0.3840	0.7025	0.0384
MTCoQ	0.6035	0.1934	-0.0019
MAP	0.3339	0.4853	0.0155
Pseason	0.2381	-0.3193	-0.0765
PWeQ	0.3521	0.1621	-0.0322
PDrQ	0.0602	0.7051	0.0902
PWaQ	0.0109	0.5709	0.0009
PCoQ	0.3839	-0.0782	-0.0093
MN16-01	-0.2648	0.2475	-0.1933
MN16-02	-0.3338	0.1566	0.0851
MN16-03	0.0156	0.1879	0.0952
MN16-04	-0.5617	0.0446	0.0037
MN16-05	-0.1030	0.2302	-0.2554
MN16-06	-0.4954	0.2557	0.1328
MN16-10	-0.0008	0.2461	-0.0217
MN16-11	0.0852	0.3217	0.1385
MN16-13	0.6034	0.1395	-0.3560
MN16-14	0.6293	0.1523	-0.0614
MN16-15	0.6829	0.1781	-0.2326
MN16-16	0.1243	0.1659	0.0118
MN16-17	0.5357	0.2421	0.0260
MN16-18	0.7125	0.2040	-0.1907
MN16-19	0.3424	0.2366	-0.0854
MN16-20	-0.1462	0.3226	-0.8073
MN16-21	0.0425	0.2585	0.1086
MN16-22	0.5428	0.2422	0.1561
MN16-23	0.5916	0.6708	1.2602
MN16-24	0.0308	0.2709	0.0238
MN16-26	0.9057	0.2595	0.1029

MN16-27	0.3913	0.1597	0.3825
MN16-28	0.6652	0.2391	0.1260
MN16-31	-0.0639	0.3360	-0.1183
MN16-32	0.2989	0.2273	0.0449
MN16-33	0.6759	0.2769	0.0758
MN16-35	0.3170	0.2461	0.2347
MN16-36	-0.1670	0.1779	-0.0289
MN16-39	0.2889	0.2016	0.1440
MN16-40	-0.0029	0.0091	0.3313
MN16-41	0.2389	-0.0664	-0.0475
MN16-42	0.2385	-0.0242	0.1210
MN16-43	0.1221	-0.0941	-0.0240
MN16-44	-0.0341	-0.0970	-0.0455
MN16-45	0.1737	-0.0439	-0.1461
MN16-46	0.0526	-0.0754	0.0058
MN16-48	0.3553	-0.0343	-0.0404
MN16-49	0.1207	-0.0255	-0.0145
MN16-50	0.4782	-0.0234	0.0532
MN16-51	0.1957	-0.0771	0.0106
MN16-53	0.2724	-0.0753	-0.1976
MN16-54	0.2955	-0.0416	-0.1650
MN16-55	0.3064	-0.0900	0.0627
MN16-56	0.3512	-0.0550	-0.0451
MN16-57	0.2712	-0.0567	0.0433
MN16-58	0.0384	-0.1221	0.1213
MN16-59	0.1875	-0.1558	0.0802
MN16-60	0.2695	-0.1578	0.0613
MN16-61	0.0626	-0.0153	0.1558
MN16-62	0.4930	0.0444	-0.1343
MN16-63	0.4055	0.0089	-0.0787
MN16-64	0.4386	0.0160	-0.1027
MN17-07	0.5914	0.1757	0.2194
MN17-08	0.3839	0.1820	-0.0218
MN17-10	0.1479	0.0308	0.1286
MN17-11	-0.6281	0.0995	-0.2304
MN17-12	0.1573	-0.0096	0.1779
MN17-13	-0.3828	0.0371	-0.0720
MN17-14	-0.3347	0.0392	-0.0778
MN17-15	-0.4915	0.1340	-0.1694
MN17-16	-0.4760	0.1052	-0.1598
MN17-17	-0.2994	0.0272	-0.0095
MN17-18	0.0701	0.0037	0.0677
MN17-19	-0.3039	0.0504	0.1567
MN17-20	-0.2913	0.0559	0.1895
MN17-21	-0.5172	0.1417	-0.1025

MN17-22	-0.4961	0.0965	-0.1395
MN17-24	-0.3622	0.1290	0.0125
MN17-25	-0.1037	0.0030	0.0037
MN17-26	-0.2575	0.1296	-0.1410
MN17-28	0.6663	0.1767	-0.2391
MN17-32	-0.4196	-0.0091	0.0155
MN17-33	-0.4964	-0.0423	-0.1207
MN17-34	-0.4821	-0.0535	0.0871
MN17-35	-0.3339	-0.0598	0.1057
MN17-36	-0.3805	-0.0963	-0.0206
MN17-37	-0.2903	-0.0643	0.0383
MN17-38	-0.4365	0.0160	-0.0870
MN17-39	-0.2088	-0.0422	0.0113
MN17-40	-0.1668	-0.0470	0.0813
MN17-41	-0.2392	0.0110	0.0169
MN17-42	-0.4274	0.0478	0.0080
MN17-43	-0.3501	-0.1205	0.0482
MN17-44	-0.3607	-0.0246	-0.0069
MN17-46	-0.0446	0.0140	-0.0708
MN17-47	-0.2712	0.0271	-0.0684
MN17-48	-0.0475	-0.0338	0.0454
MN17-49	-0.3664	-0.0754	0.0899
MN17-50	-0.3776	-0.0261	-0.0221
MN17-51	-0.1395	-0.0139	-0.0441
MN17-52	-0.4551	-0.0211	-0.1271
MN17-53	-0.2374	0.0325	0.0104
MN17-54	-0.5188	-0.0374	-0.1327
MN17-55	-0.5295	-0.0259	-0.0673
MN17-56	-0.1924	0.0108	-0.0006
MN17-57	-0.3383	0.0938	-0.0807
MN17-58	-0.2921	0.0278	-0.0608
MN17-59	-0.3146	0.0049	-0.0401
MN17-61	-0.2463	-0.0907	0.0773
MN17-62	-0.1335	-0.0590	0.1678
MN17-63	-0.3143	0.0117	-0.0130
MN17-64	-0.4439	0.0204	0.0012
MN17-66	-0.2238	0.0490	0.0524
MN17-67	-0.4716	-0.0131	-0.0580
MN17-68	-0.3472	0.0290	-0.0622
MN17-71	-0.3167	0.0569	-0.1426
MN17-72	-0.3190	0.0444	-0.1435
MN17-73	-0.2931	-0.0450	-0.0675
MN17-74	-0.3126	0.0322	-0.0199
MN17-75	-0.2165	-0.0512	0.0747
MN17-76	-0.1877	-0.0298	0.1877

MN17-77	-0.3051	-0.0313	-0.0078
MN17-78	-0.2196	0.0424	0.0476
MN17-80	-0.3432	-0.0009	0.0099
MN17-81	-0.1196	-0.0835	0.0871

B.7 CCA$_{phys}$ scores

	Axis 1	Axis 2
%Carbon	-0.4651	-1.3260
Δ_{leaf}	-0.8216	1.0424
%Nitrogen	1.5044	0.2265
MAT	-0.3903	-0.3578
MDiR	-0.4753	-0.1126
Isoth	-0.6240	0.0927
Tseason	0.4795	-0.2268
Trange	0.2403	-0.2692
MTWeQ	0.0002	-0.4238
MTDrQ	-0.5430	-0.0788
MTWaQ	-0.1119	-0.4402
MTCoQ	-0.5624	-0.1627
MAP	-0.2963	-0.2255
Pseason	-0.3794	-0.0783
PWeQ	-0.4371	-0.2117
PDrQ	0.2067	-0.1174
PWaQ	0.1092	-0.3901
PCoQ	-0.4813	0.1566
MN16-01	0.4694	0.4058
MN16-02	0.2631	0.6619
MN16-03	0.1623	-0.1332
MN16-04	0.4719	0.1234
MN16-05	0.0706	0.0865
MN16-06	0.3799	0.1245
MN16-10	-0.4321	0.0101
MN16-11	-0.1273	-0.0948
MN16-13	-0.4014	-0.1859
MN16-14	-0.5435	-0.4457
MN16-15	-0.1740	-0.0727
MN16-16	-0.2228	0.0750
MN16-17	-0.2336	0.1300
MN16-18	0.0322	-0.2411
MN16-19	0.1642	-0.0503
MN16-20	-0.1670	0.0508
MN16-21	-0.1207	-0.2494
MN16-22	-0.4648	-0.4144
MN16-23	-0.5209	-0.4654
MN16-24	-0.1323	-0.2046
MN16-26	-0.0370	-0.4482
MN16-27	0.0167	-0.0597

MN16-28	-0.2414	-0.0674
MN16-31	0.1024	-0.0112
MN16-32	-0.1612	-0.2981
MN16-33	0.1941	-0.2010
MN16-35	-0.0028	-0.0166
MN16-36	-0.1272	-0.1866
MN16-39	0.2778	-0.7404
MN16-40	-0.3981	0.2449
MN16-41	-0.6835	0.1251
MN16-42	-0.6184	0.2014
MN16-43	-0.2557	0.2950
MN16-44	-0.3725	0.4427
MN16-45	-0.6338	0.2775
MN16-46	-0.6128	0.2260
MN16-48	-0.4888	-0.1589
MN16-49	-0.0943	0.2419
MN16-50	-0.3736	-0.1153
MN16-51	-0.3393	0.2291
MN16-53	-0.6468	0.4580
MN16-54	-0.5697	-0.0599
MN16-55	-0.1147	-0.0120
MN16-56	-0.3971	-0.3702
MN16-57	-0.3729	-0.3299
MN16-58	-0.2810	0.0152
MN16-59	-0.4656	0.1392
MN16-60	-0.2915	0.1735
MN16-61	-0.2433	0.2954
MN16-62	-0.0359	-0.0496
MN16-63	0.0525	-0.0217
MN16-64	-0.6004	0.2871
MN17-07	-0.4387	-0.1707
MN17-08	-0.1374	-0.0773
MN17-10	0.0695	-0.0171
MN17-11	0.0950	0.5892
MN17-12	-0.1751	-0.4455
MN17-13	0.2508	-0.1801
MN17-14	0.0196	-0.2495
MN17-15	0.2245	-0.4948
MN17-16	-0.1773	-0.2407
MN17-17	0.4570	-0.0489
MN17-18	-0.2851	-0.3569
MN17-19	-0.0629	0.0350
MN17-20	-0.1730	-0.2486
MN17-21	-0.0897	0.0016
MN17-22	-0.0911	-0.2881

MN17-24	0.3160	-0.1723
MN17-25	0.1117	-0.1035
MN17-26	0.2000	0.1329
MN17-28	0.3212	-0.3725
MN17-32	0.9897	0.1997
MN17-33	0.4181	-0.1326
MN17-34	0.4953	0.2652
MN17-35	0.2382	-0.2563
MN17-36	0.3434	0.0989
MN17-37	0.0143	-0.0957
MN17-38	0.1480	0.1261
MN17-39	0.2152	-0.0624
MN17-40	0.0141	-0.2259
MN17-41	0.0784	-0.1362
MN17-42	0.3235	0.2461
MN17-43	-0.0663	0.3539
MN17-44	0.1987	-0.1446
MN17-46	0.0716	0.4282
MN17-47	0.1942	-0.1378
MN17-48	0.6817	0.3446
MN17-49	0.2495	0.2858
MN17-50	0.4067	0.1365
MN17-51	-0.0400	0.2239
MN17-52	0.0493	-0.0104
MN17-53	0.1341	0.4437
MN17-54	0.5294	0.4192
MN17-55	0.3913	0.3410
MN17-56	0.3872	0.4169
MN17-57	0.0172	0.3286
MN17-58	0.3583	0.6157
MN17-59	0.0659	-0.1896
MN17-61	0.1734	-0.1844
MN17-62	0.5165	-0.4417
MN17-63	0.0655	0.1524
MN17-64	-0.1821	0.0643
MN17-66	-0.0351	0.1649
MN17-67	0.1267	-0.0079
MN17-68	0.0916	-0.0680
MN17-71	-0.2526	0.1919
MN17-72	-0.1947	0.1103
MN17-73	-0.1054	-0.1587
MN17-74	-0.0926	-0.0816
MN17-75	-0.0792	0.1863
MN17-76	0.5011	0.3950
MN17-77	0.3896	0.4359

MN17-78	0.2410	0.1547
MN17-80	0.0213	0.3396
MN17-81	0.5376	-0.1536

B.8 CCA$_{anat+phys}$ scores

	Axis 1	Axis 2	Axis 3	Axis 4	Axis 5	Axis 6	Axis 7
Cross-sectional area	1.2582	0.5608	0.4770	0.4725	0.7567	2.2773	-1.4545
Vascular bundle area	-0.0585	1.6864	-2.1772	-0.1728	-1.1106	-0.4500	-0.7657
Resin canal area	1.8856	-1.3289	0.3807	0.3770	-0.2229	-2.1113	-1.3682
Leaf width	0.3135	1.0521	0.3551	-0.3022	1.4184	-0.7060	1.0152
Leaf thickness	1.0849	-0.3874	0.0307	0.7645	-1.5878	0.6984	2.0025
Δ_{leaf}	-0.3540	-0.7378	0.1576	-1.9810	-0.3057	0.3736	-0.0691
%Carbon	-0.9710	-1.2177	-1.0669	0.9397	0.9032	0.1888	0.0990
%Nitrogen	-1.4005	0.5304	1.4930	0.7598	-0.8073	-0.3072	-0.4840
MN16-01	-0.4350	0.1289	0.5144	-0.1604	-0.2094	-0.1330	-0.0500
MN16-02	-0.1237	0.2467	0.3594	-0.3187	-0.1661	0.0140	0.1076
MN16-03	-0.4529	-0.1871	0.0869	0.1229	-0.0539	-0.0050	-0.0101
MN16-04	-0.3440	0.2910	0.2746	0.0351	0.0067	-0.0038	0.0344
MN16-05	-0.5873	-0.3138	0.2535	-0.1603	-0.0336	-0.0090	-0.0608
MN16-06	-0.6803	-0.0401	0.4290	0.0019	-0.1514	0.0049	-0.0308
MN16-10	-0.2175	-0.4061	-0.1468	-0.3016	0.0938	0.0571	0.0996
MN16-11	-0.4836	-0.4188	-0.0324	-0.0851	0.0088	0.0602	0.0345
MN16-13	-0.0825	-0.6018	-0.1554	-0.0877	0.1012	-0.1156	-0.0672
MN16-14	0.0939	-0.6691	-0.2716	0.0994	0.1015	-0.0503	0.0420
MN16-15	-0.1113	-0.5421	0.0354	-0.0323	-0.0411	-0.1238	-0.0684
MN16-16	-0.2131	-0.3413	0.0197	-0.2141	-0.0053	0.0389	0.0434
MN16-17	-0.3126	-0.5073	0.0430	-0.2986	-0.1068	0.0412	-0.0204
MN16-18	-0.3237	-0.5053	0.0555	0.1869	-0.0336	-0.1144	-0.0828
MN16-19	-0.4933	-0.3304	0.2167	0.0702	-0.0927	-0.0553	-0.0650
MN16-20	-0.5736	-0.4595	0.0594	-0.3199	0.0941	-0.0315	-0.0707
MN16-21	-0.4471	-0.3987	-0.1072	0.0561	0.0793	0.0480	0.0512
MN16-22	-0.2727	-0.7330	-0.3377	0.0468	0.1616	0.0954	0.0912
MN16-23	-0.6594	-0.9589	-0.5246	-0.0162	0.3249	0.2584	0.1168
MN16-24	-0.5953	-0.5286	-0.0478	-0.0092	0.1175	0.0756	0.0131
MN16-26	-0.2771	-0.5915	-0.1184	0.3459	-0.0619	-0.0599	-0.0235
MN16-27	-0.1940	-0.2916	0.0394	0.0775	-0.1944	0.0859	0.0512
MN16-28	-0.1837	-0.5536	-0.0464	-0.0710	-0.1000	0.0200	0.0197
MN16-31	-0.5307	-0.2756	0.1918	-0.0344	-0.0232	-0.0382	-0.0005
MN16-32	-0.3824	-0.4949	-0.1219	0.0952	0.0860	0.0265	0.0333
MN16-33	-0.5902	-0.4029	0.1372	0.2365	-0.1119	-0.0396	-0.0890
MN16-35	-0.3155	-0.3364	0.0874	-0.0118	-0.1303	0.0387	0.0399
MN16-36	-0.3214	-0.2749	-0.0359	-0.0039	0.1512	0.0260	0.0891
MN16-39	-0.4673	-0.3488	-0.0670	0.6867	0.1015	-0.0496	0.0317
MN16-40	0.3132	-0.0178	0.0096	-0.0950	-0.0496	0.2523	0.2368

MN16-41	0.5649	-0.1555	-0.0168	-0.0524	0.0728	-0.0030	0.0074
MN16-42	0.3959	-0.1990	-0.0697	-0.1441	-0.0392	0.1087	0.0735
MN16-43	0.4190	-0.0063	0.0852	-0.0686	0.0361	0.0272	-0.0094
MN16-44	0.3021	0.0014	0.1049	-0.2510	0.1008	0.0734	0.0245
MN16-45	0.4912	-0.1611	0.0454	-0.1668	0.1338	-0.0539	0.0052
MN16-46	0.5597	0.0584	-0.0041	-0.0452	0.1154	0.0542	0.0732
MN16-48	0.5153	-0.1997	-0.0793	0.0821	0.0034	-0.0572	-0.0229
MN16-49	0.1961	-0.0687	0.1300	-0.0941	-0.0193	0.0079	0.0059
MN16-50	0.5791	-0.2384	-0.0398	0.1483	-0.1318	-0.0341	-0.0209
MN16-51	0.5148	-0.0294	0.0406	-0.0077	-0.0007	0.0221	0.0039
MN16-53	0.6042	-0.1605	0.0854	-0.1652	0.0833	-0.1137	-0.0797
MN16-54	0.5428	-0.1984	-0.0231	0.0096	0.1084	-0.1219	-0.0444
MN16-55	0.5238	-0.0878	0.0620	0.1489	-0.0631	0.0298	-0.0205
MN16-56	0.5618	-0.1728	-0.0685	0.1859	0.0287	-0.0689	-0.0348
MN16-57	0.4982	-0.1136	-0.0896	0.1695	0.0179	0.0126	0.0176
MN16-58	0.4039	0.0372	0.0087	0.0427	0.0709	0.1555	0.0661
MN16-59	0.5466	-0.0542	0.0191	0.0164	0.0278	0.1331	-0.0057
MN16-60	0.5714	-0.0082	-0.0009	0.0642	-0.0646	0.0728	-0.0735
MN16-61	0.3697	0.0444	0.0387	-0.0574	-0.0488	0.1116	0.1204
MN16-62	0.5088	-0.2182	0.0781	0.1610	-0.1057	-0.2255	-0.0713
MN16-63	0.4445	-0.1194	0.0676	0.1567	-0.1076	-0.1568	-0.0657
MN16-64	0.7020	-0.1883	0.0069	0.0044	-0.0910	-0.1722	-0.0405
MN17-07	-0.1584	-0.6044	-0.2336	-0.0995	-0.0136	0.1001	0.0491
MN17-08	-0.4591	-0.4775	-0.0218	-0.0991	-0.0086	0.0396	-0.0453
MN17-10	-0.0323	-0.1188	0.0916	0.0686	-0.0753	0.0400	0.0280
MN17-11	-0.3508	0.1070	0.4016	-0.5223	-0.0501	-0.0021	-0.0029
MN17-12	0.1388	-0.1674	-0.1369	0.2296	0.0522	0.0960	0.0892
MN17-13	-0.1791	0.2548	-0.0636	0.1118	0.0853	-0.0529	0.0150
MN17-14	-0.2753	0.0025	-0.1035	0.0822	0.1472	-0.0041	0.0197
MN17-15	-0.4451	0.0683	-0.1572	0.3117	0.1775	-0.0877	0.0040
MN17-16	-0.2873	-0.0925	-0.1401	-0.0331	0.2713	0.0073	0.0889
MN17-17	-0.3881	0.1741	0.1610	0.1634	-0.0700	-0.0468	-0.0627
MN17-18	0.1519	0.1914	-0.4796	0.0766	-0.0908	-0.0348	-0.0490
MN17-19	0.1229	0.4931	-0.3766	-0.0366	-0.0919	0.0200	0.0686
MN17-20	-0.0761	0.2936	-0.4888	0.0094	-0.0684	0.0326	0.0142
MN17-21	-0.2944	0.0418	-0.0866	-0.1556	0.1096	-0.0008	0.0587
MN17-22	-0.2657	0.0709	-0.2305	0.0247	0.1999	-0.0278	0.0494
MN17-24	-0.3689	0.2294	-0.1265	0.1464	-0.0815	-0.0715	-0.0501
MN17-25	-0.0029	0.2850	-0.2584	0.0544	-0.0896	-0.0593	-0.0641
MN17-26	-0.3149	0.0363	0.1882	-0.0827	-0.0250	-0.0651	-0.0123
MN17-28	-0.3042	-0.3098	0.0817	0.4186	-0.0926	-0.2203	-0.1432
MN17-32	-0.1841	0.5491	0.3215	0.1831	-0.0892	-0.0620	-0.0126
MN17-33	-0.3132	0.2201	0.1770	0.1644	0.1466	-0.0279	-0.0070
MN17-34	-0.1276	0.3861	0.2859	-0.0038	0.0336	0.0822	0.0733
MN17-35	-0.0546	0.2736	-0.0653	0.1702	0.0998	0.0743	0.0601

MN17-36	-0.0269	0.3563	0.1000	0.0248	0.0945	0.0321	0.0082
MN17-37	-0.1407	0.1407	-0.1253	0.0053	0.0524	0.0528	-0.0114
MN17-38	-0.2909	0.1018	0.1479	-0.1086	0.0526	0.0087	0.0035
MN17-39	-0.0417	0.2789	-0.1049	0.0688	-0.0188	-0.0138	-0.0354
MN17-40	-0.1132	0.1275	-0.2179	0.0893	0.0088	0.0364	-0.0254
MN17-41	-0.1668	0.0453	-0.0058	0.0653	0.0882	0.0275	0.0391
MN17-42	-0.2243	0.2225	0.2700	-0.0807	-0.0001	0.0141	0.0564
MN17-43	0.0228	0.2602	0.0057	-0.2222	0.0366	0.1150	0.0098
MN17-44	-0.1397	0.1670	0.0532	0.1014	0.1476	0.0302	0.0567
MN17-46	0.0171	0.1355	0.1052	-0.2122	-0.1158	-0.0459	-0.0475
MN17-47	-0.2984	0.0648	0.0104	0.0973	0.0448	-0.0294	-0.0267
MN17-48	0.0768	0.4294	0.0697	0.0697	-0.2302	-0.0681	-0.0888
MN17-49	-0.1296	0.2769	0.1406	-0.1049	-0.0444	0.0801	0.0011
MN17-50	-0.2409	0.2596	0.1999	0.0179	-0.0218	-0.0084	-0.0252
MN17-51	0.0970	0.1828	-0.0246	-0.1205	0.0094	-0.0137	0.0051
MN17-52	-0.3770	-0.0209	0.0556	-0.0786	0.1009	0.0271	-0.0248
MN17-53	-0.0212	0.2335	0.1330	-0.2071	-0.0778	0.0048	0.0282
MN17-54	-0.3302	0.3219	0.4590	-0.1321	-0.0667	-0.0353	-0.0605
MN17-55	-0.3640	0.2463	0.3505	-0.1490	-0.0735	0.0018	-0.0498
MN17-56	-0.0314	0.3133	0.1789	-0.0931	-0.1303	-0.0363	-0.0206
MN17-57	-0.1514	0.1599	0.0593	-0.2611	-0.0321	-0.0241	0.0199
MN17-58	-0.0582	0.3433	0.2664	-0.2313	-0.1225	-0.0465	-0.0132
MN17-59	-0.5198	-0.2183	0.0440	0.0849	0.1100	0.0487	-0.0269
MN17-61	-0.0165	0.3134	-0.1862	0.1102	0.0063	0.0382	-0.0276
MN17-62	-0.0953	0.4000	-0.2793	0.3250	-0.1387	-0.0198	-0.0857
MN17-63	-0.0868	0.2133	-0.0124	-0.1081	0.0137	0.0083	0.0205
MN17-64	-0.0533	0.2852	-0.2467	-0.1605	0.0629	0.0275	0.0452
MN17-66	-0.0005	0.1512	-0.0133	-0.1155	0.0084	0.0328	0.0796
MN17-67	-0.2367	0.2494	-0.1006	-0.0396	0.0318	-0.0077	-0.0305
MN17-68	-0.1403	0.3125	-0.2467	-0.0124	-0.0211	-0.0584	-0.0464
MN17-71	-0.0861	0.0316	-0.0593	-0.2882	0.1084	-0.0009	0.0421
MN17-72	-0.0927	0.0554	-0.0685	-0.2137	0.1232	-0.0108	0.0358
MN17-73	-0.0875	0.0767	-0.1262	-0.0100	0.1668	0.0274	0.0187
MN17-74	0.0232	0.1576	-0.0649	-0.0254	0.1724	0.0204	0.1167
MN17-75	0.1518	0.3241	-0.1561	-0.0850	-0.0113	0.0556	0.0283
MN17-76	0.0754	0.4048	0.1166	0.0077	-0.1666	0.0674	0.0374
MN17-77	-0.1714	0.3321	0.1995	-0.1497	-0.1608	-0.0165	-0.0720
MN17-78	-0.1656	0.1727	0.1018	-0.0355	-0.0786	-0.0011	0.0043
MN17-80	0.0372	0.3228	-0.0182	-0.1780	0.0127	0.0264	0.0517
MN17-81	-0.0246	0.3509	-0.0539	0.2278	-0.0991	-0.0110	-0.0717
MAT	-0.1126	-0.6850	-0.2525	0.0633	0.0231	-0.0469	-0.0283
MDiR	0.2751	-0.5620	0.0132	0.0950	-0.0678	-0.0014	0.0123
Isoth	0.6605	-0.3891	0.0040	-0.0455	-0.0120	0.0216	-0.0155
Tseason	-0.6543	0.0980	0.0214	0.1811	-0.0211	-0.0822	0.0193
Trange	-0.4984	-0.1643	0.0276	0.2203	-0.0646	-0.0854	0.0310

MTWeQ	-0.4800	-0.4229	-0.2144	0.1215	0.0955	-0.0453	0.0592
MTDrQ	0.3434	-0.4905	-0.1438	-0.0123	0.0117	0.0533	-0.0777
MTWaQ	-0.4366	-0.5735	-0.2218	0.1510	0.0063	-0.0873	-0.0196
MTCoQ	0.2568	-0.5941	-0.2128	-0.0452	0.0271	0.0063	-0.0376
MAP	-0.2284	-0.5039	-0.1927	-0.0758	0.0906	0.0091	-0.0362
Pseason	0.5779	-0.0787	-0.0989	0.1830	0.1110	-0.1090	0.0135
PWeQ	0.1422	-0.3933	-0.2382	0.0160	0.1528	-0.0479	-0.0090
PDrQ	-0.7254	-0.3505	0.0603	-0.1323	-0.0375	0.0904	-0.0398
PWaQ	-0.6072	-0.2722	-0.2760	0.0244	0.1181	-0.0446	0.0113
PCoQ	0.4367	-0.3051	0.0923	-0.1029	0.0330	0.0499	-0.0434

B.9 CCA$_{anat+phys-vb}$ scores

	Axis 1	Axis 2	Axis 3	Axis 4	Axis 5	Axis 6
%Carbon	-0.9164	-1.2541	1.2704	-0.7994	-0.1615	0.1546
Cross-sectional area	1.1830	0.8262	0.4974	-0.1697	0.2975	2.5925
Δ_{leaf}	-0.3353	-0.6116	-1.8662	-0.3912	0.3450	0.2550
Leaf thickness	1.0308	-0.2588	0.5508	0.6931	2.2138	-1.0879
Leaf width	0.2750	1.3364	0.0559	-1.1465	-0.5501	-0.9598
%Nitrogen	-1.3480	0.8829	0.1095	1.6438	-0.2326	0.0613
Resin canal area	1.8049	-1.2213	-0.0970	1.2630	-2.0442	-0.4842
MAT	-0.0970	-0.7035	0.0980	-0.0599	-0.0356	-0.0440
MDiR	0.2918	-0.5133	0.0487	0.1288	0.0090	-0.0112
Isoth	0.6688	-0.3567	-0.0617	0.0343	-0.0084	0.0616
Tseason	-0.6534	0.0959	0.1581	0.0770	-0.0332	-0.1428
Trange	-0.4896	-0.1448	0.1751	0.1407	-0.0207	-0.1625
MTWeQ	-0.4707	-0.4423	0.1658	-0.0918	-0.0391	-0.1107
MTDrQ	0.3574	-0.4916	0.0071	-0.0371	0.0043	0.1559
MTWaQ	-0.4215	-0.5926	0.1707	-0.0139	-0.0491	-0.1145
MTCoQ	0.2690	-0.6084	-0.0057	-0.0871	-0.0106	0.0450
MAP	-0.2144	-0.5171	-0.0186	-0.1375	-0.0395	0.0580
Pseason	0.5743	-0.1007	0.2043	-0.0244	-0.1256	-0.1339
PWeQ	0.1487	-0.4284	0.0886	-0.1666	-0.0941	-0.0336
PDrQ	-0.7104	-0.2977	-0.1540	0.0352	0.0404	0.1672
PWaQ	-0.6022	-0.3249	0.1061	-0.1839	-0.0454	-0.0760
PCoQ	0.4468	-0.2514	-0.1239	0.0314	-0.0400	0.1508
MN16-01	-0.4399	0.2887	-0.3284	0.3680	-0.0625	-0.0707
MN16-02	-0.1327	0.3629	-0.4138	0.1347	0.1265	-0.0828
MN16-03	-0.4565	-0.1297	0.0769	0.1354	0.0044	0.0006
MN16-04	-0.3623	0.3935	-0.0195	0.1164	-0.0085	-0.0196
MN16-05	-0.5661	-0.1600	-0.2207	0.1139	-0.0467	0.0395
MN16-06	-0.6676	0.1292	-0.1331	0.3111	0.0170	0.0176
MN16-10	-0.2159	-0.3862	-0.2203	-0.2647	0.0642	-0.0211
MN16-11	-0.4755	-0.3581	-0.0707	-0.0538	0.0547	0.0194
MN16-13	-0.0784	-0.5712	-0.0496	-0.1079	-0.1518	-0.0202
MN16-14	0.0957	-0.6545	0.1626	-0.1380	-0.0412	-0.0541
MN16-15	-0.1071	-0.4511	-0.0733	0.0980	-0.1081	-0.0380
MN16-16	-0.2109	-0.2741	-0.2039	-0.0668	0.0502	-0.0026
MN16-17	-0.3037	-0.4255	-0.3168	0.0136	0.0593	0.0306
MN16-18	-0.3130	-0.4075	0.1221	0.1768	-0.1177	-0.0195
MN16-19	-0.4794	-0.2000	-0.0235	0.2284	-0.0533	0.0036
MN16-20	-0.5547	-0.3529	-0.2995	-0.1029	-0.1069	0.0428
MN16-21	-0.4428	-0.3610	0.0948	-0.0946	0.0285	0.0072
MN16-22	-0.2615	-0.7081	0.1548	-0.2645	0.0603	0.0173

MN16-23	-0.6231	-0.9206	0.1815	-0.5027	0.1194	0.1242
MN16-24	-0.5712	-0.4246	0.0238	-0.1025	0.0020	0.0583
MN16-26	-0.2695	-0.5566	0.3105	0.1519	-0.0255	-0.0320
MN16-27	-0.1944	-0.2513	0.0217	0.1697	0.1703	-0.0001
MN16-28	-0.1779	-0.4947	-0.0866	0.0399	0.0687	-0.0121
MN16-31	-0.5177	-0.1485	-0.0879	0.1091	-0.0339	-0.0212
MN16-32	-0.3737	-0.4434	0.1290	-0.0786	0.0006	0.0059
MN16-33	-0.5748	-0.2997	0.1379	0.2716	-0.0440	0.0268
MN16-35	-0.3114	-0.2572	-0.0621	0.1250	0.0965	-0.0144
MN16-36	-0.3189	-0.2059	0.0451	-0.1472	-0.0023	-0.0234
MN16-39	-0.4606	-0.2861	0.6633	0.1463	-0.0699	-0.0398
MN16-40	0.3172	0.0322	-0.0626	-0.1122	0.3338	0.0008
MN16-41	0.5730	-0.1201	-0.0310	-0.0765	-0.0319	0.0026
MN16-42	0.4065	-0.1942	-0.1204	-0.0901	0.1427	0.0168
MN16-43	0.4269	0.0482	-0.0761	-0.0140	-0.0109	0.0334
MN16-44	0.3026	0.0782	-0.2299	-0.1364	0.0107	0.0502
MN16-45	0.4887	-0.0891	-0.1408	-0.1209	-0.0991	-0.0212
MN16-46	0.5785	0.0921	-0.0011	-0.1427	0.0267	0.0010
MN16-48	0.5336	-0.2107	0.0880	0.0153	-0.0511	-0.0251
MN16-49	0.1960	0.0027	-0.1241	0.0409	0.0066	0.0027
MN16-50	0.5982	-0.2463	0.1099	0.1566	0.0260	-0.0274
MN16-51	0.5300	0.0032	-0.0158	0.0123	0.0138	0.0141
MN16-53	0.6054	-0.0940	-0.1743	-0.0286	-0.1683	-0.0085
MN16-54	0.5502	-0.1670	0.0234	-0.0440	-0.1603	-0.0386
MN16-55	0.5346	-0.0468	0.1103	0.1334	0.0296	0.0299
MN16-56	0.5804	-0.1756	0.1901	0.0433	-0.0806	-0.0207
MN16-57	0.5193	-0.1259	0.1911	0.0013	0.0148	-0.0031
MN16-58	0.4142	0.0785	0.0753	-0.0865	0.1112	0.0731
MN16-59	0.5582	-0.0144	0.0253	-0.0278	0.0724	0.1032
MN16-60	0.6034	-0.0159	0.0441	0.0821	0.0385	0.0987
MN16-61	0.3825	0.0765	-0.0550	-0.0266	0.1703	-0.0143
MN16-62	0.5178	-0.1851	0.0815	0.2454	-0.1575	-0.1186
MN16-63	0.4599	-0.1028	0.0883	0.2254	-0.1059	-0.0765
MN16-64	0.7266	-0.1886	-0.0402	0.1267	-0.1026	-0.1058
MN17-07	-0.1536	-0.6092	-0.0441	-0.1393	0.1166	0.0285
MN17-08	-0.4494	-0.4154	-0.1007	-0.0114	0.0031	0.0589
MN17-10	-0.0341	-0.0624	0.0285	0.1118	0.0681	0.0014
MN17-11	-0.3556	0.2539	-0.5885	0.0363	-0.0068	0.0037
MN17-12	0.1436	-0.1740	0.2786	-0.0608	0.1006	0.0084
MN17-13	-0.1975	0.2192	0.1584	-0.0641	-0.0662	-0.0424
MN17-14	-0.2906	-0.0189	0.1453	-0.1396	-0.0550	0.0007
MN17-15	-0.4798	0.0142	0.3955	-0.0879	-0.1398	-0.0467
MN17-16	-0.2963	-0.0868	0.0759	-0.3081	-0.0609	-0.0251
MN17-17	-0.4132	0.2103	0.0987	0.2154	-0.0523	0.0074
MN17-18	0.2015	-0.1180	0.1952	-0.1416	0.0442	-0.0218

MN17-19	0.1660	0.2851	0.0636	-0.2080	0.1724	-0.0785
MN17-20	-0.0839	-0.0006	0.1449	-0.2442	0.1378	-0.0169
MN17-21	-0.3134	0.0151	-0.0985	-0.2063	-0.0083	-0.0323
MN17-22	-0.2885	-0.0123	0.1408	-0.2808	-0.0686	-0.0373
MN17-24	-0.4194	0.1178	0.1624	0.0827	-0.0306	-0.0343
MN17-25	0.0040	0.1017	0.1014	-0.0186	-0.0105	-0.0209
MN17-26	-0.3253	0.1064	-0.1346	0.0929	-0.0557	-0.0353
MN17-28	-0.3049	-0.2670	0.3152	0.3502	-0.2043	-0.0587
MN17-32	-0.2059	0.6481	0.0903	0.2939	-0.0358	-0.0422
MN17-33	-0.3282	0.3066	0.1552	0.0304	-0.1106	0.0110
MN17-34	-0.1393	0.5027	-0.0410	0.0544	0.0622	0.0172
MN17-35	-0.0604	0.2574	0.2357	-0.0954	0.0481	0.0218
MN17-36	-0.0322	0.3989	0.0364	-0.0410	-0.0251	0.0331
MN17-37	-0.1531	0.0756	0.0569	-0.1171	0.0193	0.0521
MN17-38	-0.3032	0.1670	-0.1236	-0.0156	-0.0280	0.0149
MN17-39	-0.0448	0.1993	0.0973	-0.0098	-0.0102	0.0096
MN17-40	-0.1235	0.0043	0.1561	-0.0900	0.0291	0.0422
MN17-41	-0.1755	0.0622	0.0944	-0.0661	-0.0004	0.0036
MN17-42	-0.2354	0.3290	-0.1289	0.0691	0.0214	-0.0238
MN17-43	0.0242	0.2536	-0.2029	-0.1493	0.0782	0.0827
MN17-44	-0.1490	0.2146	0.1351	-0.0815	-0.0218	0.0024
MN17-46	0.0183	0.1357	-0.2744	0.0824	-0.0091	-0.0133
MN17-47	-0.3163	0.0652	0.1014	0.0179	-0.0607	0.0054
MN17-48	0.0912	0.3881	-0.0117	0.2867	0.0102	-0.0186
MN17-49	-0.1414	0.3147	-0.1388	0.0367	0.0722	0.0549
MN17-50	-0.2581	0.3213	-0.0336	0.1193	-0.0266	0.0147
MN17-51	0.1065	0.1535	-0.1104	-0.0731	-0.0051	-0.0153
MN17-52	-0.3889	0.0220	-0.0653	-0.0741	-0.0481	0.0532
MN17-53	-0.0245	0.2605	-0.2514	0.0290	0.0529	-0.0270
MN17-54	-0.3443	0.4705	-0.2516	0.2306	-0.0639	0.0216
MN17-55	-0.3806	0.3578	-0.2444	0.1733	-0.0198	0.0365
MN17-56	-0.0359	0.3429	-0.1707	0.1583	0.0147	-0.0272
MN17-57	-0.1633	0.1591	-0.2812	-0.0518	0.0112	-0.0377
MN17-58	-0.0658	0.4082	-0.3259	0.1399	0.0018	-0.0367
MN17-59	-0.5174	-0.1423	0.0901	-0.0221	-0.0410	0.0703
MN17-61	-0.0153	0.2043	0.1786	-0.0736	0.0300	0.0463
MN17-62	-0.1095	0.2083	0.4128	0.1238	0.0343	0.0226
MN17-63	-0.0947	0.1909	-0.0956	-0.0764	0.0174	-0.0096
MN17-64	-0.0576	0.1567	-0.0761	-0.2862	0.0497	-0.0162
MN17-66	-0.0009	0.1414	-0.0956	-0.0957	0.0730	-0.0366
MN17-67	-0.2645	0.1780	-0.0052	-0.0933	-0.0279	0.0181
MN17-68	-0.1611	0.1500	0.0456	-0.1076	-0.0355	-0.0237
MN17-71	-0.0912	0.0161	-0.2384	-0.2344	-0.0183	-0.0196
MN17-72	-0.0985	0.0362	-0.1601	-0.2209	-0.0366	-0.0202
MN17-73	-0.0933	0.0420	0.0697	-0.2123	-0.0390	0.0261

MN17-74	0.0233	0.1604	0.0526	-0.2244	0.0079	-0.0506
MN17-75	0.1782	0.2321	-0.0373	-0.1447	0.0897	0.0116
MN17-76	0.0829	0.4170	-0.0466	0.1539	0.1539	-0.0013
MN17-77	-0.1893	0.3580	-0.2473	0.1852	0.0123	0.0233
MN17-78	-0.1782	0.1883	-0.0760	0.0899	0.0339	-0.0133
MN17-80	0.0415	0.2990	-0.1612	-0.1266	0.0547	-0.0217
MN17-81	-0.0257	0.2815	0.2316	0.1574	0.0042	0.0308

B.10 CCA$_{anat+phys-vb-\Delta_{leaf}}$ scores

	Axis 1	Axis 2	Axis 3	Axis 4	Axis 5
%Carbon	-0.9138	-1.3671	0.1403	-0.1484	-0.0251
Cross-sectional area	1.0090	0.6740	-0.2800	0.7663	2.2613
Leaf thickness	0.8672	-0.3402	0.0753	0.0592	-0.0439
Leaf width	0.1893	1.1361	-1.0115	-0.6738	-0.7622
%Nitrogen	-1.3005	0.6504	1.4224	-0.0906	0.1510
Resin canal area	1.5702	-1.1965	0.1687	-0.0967	0.0207
MAT	-0.1097	-0.6902	0.2684	-0.0520	0.0205
MDiR	0.2736	-0.4933	-0.0290	0.0051	-0.0448
Isoth	0.6580	-0.3174	0.0621	-0.0224	0.0749
Tseason	-0.6520	0.0520	0.0363	0.0305	-0.0657
Trange	-0.4969	-0.1764	0.0909	0.0515	-0.0825
MTWeQ	-0.4785	-0.4621	0.0142	-0.0113	0.0584
MTDrQ	0.3422	-0.4649	0.1641	0.1011	-0.0448
MTWaQ	-0.4327	-0.6034	-0.1295	0.0039	-0.0488
MTCoQ	0.2578	-0.5753	-0.0474	0.0477	-0.0029
MAP	-0.2164	-0.4925	-0.0001	-0.0388	-0.0065
Pseason	0.5631	-0.1252	-0.0723	-0.0358	0.0075
PWeQ	0.1461	-0.4201	-0.9351	0.0568	0.2380
PDrQ	-0.7127	-0.2741	-0.6990	0.1850	0.1230
PWaQ	-0.6013	-0.3401	-0.3479	0.0875	0.0081
PCoQ	0.4403	-0.2127	0.0546	-0.0729	0.1213
MN16-01	-0.5052	0.4251	0.5225	-0.1402	-0.0898
MN16-02	-0.1120	0.5905	0.2739	0.0476	-0.1752
MN16-03	-0.5159	-0.1685	0.1306	0.0280	0.0103
MN16-04	-0.4046	0.4044	0.1237	-0.0079	-0.0154
MN16-05	-0.6838	-0.1220	0.2056	-0.0980	0.0399
MN16-06	-0.7768	0.1781	0.3914	0.0131	0.0130
MN16-10	-0.2118	-0.3969	-0.1967	-0.0362	-0.0407
MN16-11	-0.5603	-0.3987	0.0075	0.0514	0.0324
MN16-13	-0.0573	-0.6608	0.2325	-0.1478	-0.0705
MN16-14	0.1144	-0.7580	0.2776	-0.1288	0.0204
MN16-15	-0.0995	-0.5099	-0.1302	0.0462	0.0052
MN16-16	-0.2131	-0.2571	-0.1293	0.0108	0.0656
MN16-17	-0.3337	-0.4455	0.5023	1.8694	-1.2991
MN16-18	-0.3548	-0.4876	-0.1615	0.1269	-0.0090
MN16-19	-0.5496	-0.2295	0.0432	-0.0274	0.0423
MN16-20	-0.6978	-0.3531	-0.2915	-0.0005	-0.0867
MN16-21	-0.5073	-0.4267	-0.0859	-0.0248	0.0354
MN16-22	-0.2906	-0.8500	-0.0524	-0.2297	0.0457
MN16-23	-0.7695	-1.1821	-0.0582	0.0055	-0.0390

MN16-24	-0.6770	-0.4995	0.2649	0.0011	0.0590
MN16-26	-0.3105	-0.6640	-0.1846	-0.0336	-0.0420
MN16-27	-0.2141	-0.2844	0.1378	0.0502	-0.0186
MN16-28	-0.1784	-0.5640	1.1672	-1.8136	-0.0272
MN16-31	-0.6024	-0.1479	0.1526	-0.0592	-0.0238
MN16-32	-0.4250	-0.5269	-0.1174	0.0221	0.0140
MN16-33	-0.6493	-0.3760	0.1057	0.0345	0.0021
MN16-35	-0.3497	-0.2767	-0.1188	0.1495	0.0098
MN16-36	-0.3587	-0.2339	-0.1239	-0.0668	0.0484
MN16-39	-0.4939	-0.4268	0.0933	0.0351	0.0030
MN16-40	0.3837	0.0793	-0.1153	0.3500	-0.0867
MN16-41	0.6344	-0.1167	-0.0730	-0.0443	0.0047
MN16-42	0.5180	-0.1678	-0.0752	0.1337	-0.0313
MN16-43	0.4765	0.0740	0.0023	-0.0209	0.0315
MN16-44	0.4050	0.1794	-0.1048	-0.0371	0.0282
MN16-45	0.5858	-0.0533	-0.0996	-0.1529	-0.0187
MN16-46	0.6096	0.1002	-0.1484	0.0203	-0.0081
MN16-48	0.5465	-0.2451	0.0063	-0.0432	0.0141
MN16-49	0.2423	0.0407	0.0758	-0.0164	-0.0093
MN16-50	0.5997	-0.2874	0.1862	0.2030	-0.0338
MN16-51	0.5641	0.0057	0.0169	0.0151	0.0114
MN16-53	0.7140	-0.0568	0.0133	-0.2269	0.0117
MN16-54	0.5795	-0.1874	-0.0465	-0.1705	-0.0046
MN16-55	0.5192	-0.0853	0.1100	0.0634	0.0379
MN16-56	0.5460	-0.2312	-0.0458	0.0099	0.1451
MN16-57	0.4923	-0.1782	-0.0369	0.0501	0.0109
MN16-58	0.4223	0.0667	-0.1076	0.1378	0.0563
MN16-59	0.5909	-0.0167	-0.0360	0.0987	0.0941
MN16-60	0.6163	-0.0317	0.0737	0.0714	0.0997
MN16-61	0.4295	0.1063	-0.0180	0.1666	-0.0592
MN16-62	0.5008	-0.2312	-0.0848	-0.0119	-0.0047
MN16-63	0.4402	-0.1477	0.2090	-0.0886	-0.0390
MN16-64	0.7721	-0.2004	0.1467	-0.1276	-0.0875
MN17-07	-0.1428	-0.7162	-0.1110	-0.2089	0.0012
MN17-08	-0.5295	-0.4692	-0.1769	-0.0085	-0.0281
MN17-10	-0.0408	-0.0775	0.1138	0.0848	-0.0078
MN17-11	-0.4042	0.6031	0.2274	-0.1680	-0.0656
MN17-12	0.1144	-0.2423	0.1152	0.0010	-0.0171
MN17-13	-0.2334	0.1672	-0.0981	-0.0449	-0.0155
MN17-14	-0.3283	-0.0576	-0.1794	-0.0358	0.0215
MN17-15	-0.5197	-0.0983	-0.1618	-0.0711	0.0140
MN17-16	-0.3321	-0.1030	-0.3593	-0.0752	-0.0174
MN17-17	-0.4590	0.1678	0.1968	-0.0188	0.0347
MN17-18	0.1874	-0.1672	-0.1849	0.0702	-0.0183
MN17-19	0.1603	0.2843	-0.2310	0.1628	-0.1167

MN17-20	-0.1008	-0.0246	-0.2930	0.1561	-0.0424
MN17-21	-0.3495	0.0651	-0.2192	-0.0530	-0.0542
MN17-22	-0.3252	-0.0439	-0.3300	-0.0670	-0.0205
MN17-24	-0.4656	0.0635	0.0485	-0.0002	-0.0109
MN17-25	-0.0163	0.0709	-0.0413	0.0052	-0.0099
MN17-26	-0.3645	0.1562	0.1390	-0.0943	-0.0375
MN17-28	-0.3491	-0.3686	-0.1751	-0.0760	0.0258
MN17-32	-0.2476	0.5565	0.2565	-0.0057	-0.0140
MN17-33	-0.3686	0.2463	-0.0040	-0.0730	0.0493
MN17-34	-0.1629	0.5253	0.0608	0.0649	0.0045
MN17-35	-0.1001	0.1847	-0.1434	0.0905	0.0301
MN17-36	-0.0553	0.3878	-0.0527	-0.0117	0.0428
MN17-37	-0.1734	0.0721	-0.1409	0.0362	0.0534
MN17-38	-0.3377	0.2305	0.0103	-0.0562	0.0110
MN17-39	-0.0698	0.1695	-0.0325	0.0114	0.0214
MN17-40	-0.1494	-0.0346	-0.1290	0.0642	0.0489
MN17-41	-0.2023	0.0397	-0.0916	0.0160	0.0108
MN17-42	-0.2603	0.3958	0.1041	-0.0033	-0.0404
MN17-43	0.0620	0.3775	-0.1293	0.0545	0.0524
MN17-44	-0.1805	0.1763	-0.1131	0.0019	0.0176
MN17-46	0.0608	0.2475	0.1667	-0.0708	-0.0391
MN17-47	-0.3563	0.0333	-0.0041	-0.0400	0.0288
MN17-48	0.0671	0.3668	0.2873	0.0224	-0.0111
MN17-49	-0.1500	0.3950	0.0697	0.0651	0.0333
MN17-50	-0.2907	0.3370	0.1314	-0.0232	0.0232
MN17-51	0.1328	0.2054	-0.0560	-0.0359	-0.0283
MN17-52	-0.4410	0.0534	-0.0709	-0.0630	0.0630
MN17-53	0.0023	0.3849	0.0939	0.0015	-0.0684
MN17-54	-0.3850	0.5908	0.3185	-0.1054	0.0239
MN17-55	-0.4297	0.4830	0.2587	-0.0572	0.0292
MN17-56	-0.0339	0.4140	0.2115	-0.0144	-0.0430
MN17-57	-0.1567	0.2956	0.0082	-0.0646	-0.0812
MN17-58	-0.0472	0.5693	0.2419	-0.0684	-0.0705
MN17-59	-0.5882	-0.1792	-0.0462	-0.0137	0.0942
MN17-61	-0.0471	0.1530	-0.1130	0.0695	0.0542
MN17-62	-0.1666	0.0704	0.0307	0.1133	0.0513
MN17-63	-0.0969	0.2457	-0.0646	-0.0071	-0.0260
MN17-64	-0.0486	0.2192	-0.3085	0.0186	-0.0469
MN17-66	0.0134	0.1951	-0.0862	0.0473	-0.0702
MN17-67	-0.2959	0.1974	-0.1024	-0.0321	0.0229
MN17-68	-0.1846	0.1456	-0.1251	-0.0379	-0.0158
MN17-71	-0.0615	0.1211	-0.2285	-0.1004	-0.0550
MN17-72	-0.0840	0.1100	-0.2223	-0.0986	-0.0399
MN17-73	-0.1075	0.0338	-0.2442	-0.0338	0.0365
MN17-74	0.0160	0.1602	-0.2489	-0.0029	-0.0563

MN17-75	0.1966	0.2679	-0.1498	0.0826	-0.0145
MN17-76	0.0740	0.4348	0.1651	0.1588	-0.0319
MN17-77	-0.2009	0.4769	0.2696	-0.0225	0.0064
MN17-78	-0.1970	0.2240	0.1148	0.0242	-0.0262
MN17-80	0.0660	0.3928	-0.1071	0.0151	-0.0562
MN17-81	-0.0738	0.1883	0.0999	0.0614	0.0534

B.11 CCA scores for only *Sequoia sempervirens*

	Axis 1	Axis 2	Axis 3	Axis 4
Cross-sectional area	0.524556	-0.8526	-0.77834	-1.69983
Vascular bundle area	-0.62772	-1.13882	2.18799	-0.03607
Resin canal area	-0.69617	1.43133	0.081916	-0.38198
Leaf width	1.5372	0.27128	0.139395	0.862765
Leaf thickness	-1.07753	-0.83162	-1.17903	1.21277
MN16-40	0.090729	-0.50795	-0.65599	0.408549
MN16-41	0.108195	0.16309	-0.10024	-0.04178
MN16-42	-0.54353	0.188021	-0.12459	-0.22964
MN16-43	0.262583	-0.01018	0.063415	-0.01503
MN16-44	0.684476	0.081475	0.100274	0.012695
MN16-45	0.443911	0.404461	-0.11885	0.019217
MN16-46	0.355962	-0.04861	0.095675	0.045606
MN16-48	-0.20206	0.031512	0.073243	-0.01392
MN16-49	0.431997	0.427005	0.099229	-0.05146
MN16-50	-0.53952	-0.04933	-0.12798	-0.01493
MN16-51	0.068652	-0.02877	0.034649	-0.02805
MN16-53	0.231067	0.26486	-0.04992	-0.02812
MN16-54	0.122503	0.261251	0.015759	-0.00923
MN16-55	-0.12197	-0.15606	-0.12528	0.026891
MN16-56	-0.15322	0.022034	0.018921	-0.02461
MN16-57	-0.13311	-0.13954	0.064646	0.020092
MN16-58	0.233006	-0.24945	-0.0078	0.019449
MN16-59	0.050551	-0.19841	-0.10756	-0.03816
MN16-60	-0.1057	-0.27441	0.106278	-0.05292
MN16-61	0.105566	-0.24821	0.093713	0.160675
MN16-62	-0.37115	0.335498	-0.04383	0.04928
MN16-63	-0.31134	0.151532	0.143092	0.00156
MN16-64	-0.3365	0.275588	0.034466	-0.00503
MN17-10	-0.45975	0.541563	0.4361	-0.02491
MN17-12	-0.26597	-0.26159	0.156907	0.055629
MAT	-0.47168	0.007217	0.393504	0.022892
MDiR	-0.0612	-0.3699	-0.19052	-0.01092
Isoth	0.102595	-0.18796	-0.19722	-0.03778

Tseason	0.00566	-0.08606	0.143942	-0.02115
Trange	-0.12517	-0.29413	-0.06963	0.015192
MTWeQ	-0.48071	0.023458	0.469842	0.043992
MTDrQ	-0.15529	-0.0344	0.027509	-0.0238
MTWaQ	-0.41158	-0.03097	0.383583	0.0174
MTCoQ	-0.44882	0.031608	0.337019	0.02483
MAP	0.323806	0.380713	0.271164	-0.15103
Pseason	-0.34661	-0.35193	-0.20993	0.095302
PWeQ	0.299759	0.371061	0.302044	-0.1554
PDrQ	0.258273	0.37323	0.443972	-0.11264
PWaQ	-0.25768	0.215262	0.531057	-0.01659
PCoQ	0.499332	0.178963	-0.1214	-0.13478

B.12 CCA scores for only *Taxodium distichum*

	Axis 1	Axis 2	Axis 3	Axis 4
Cross-sectional area	-0.0260	-0.1782	0.1247	-2.0866
Vascular bundle area	0.0900	-1.7116	-0.8067	0.5761
Resin canal area	-1.4493	1.1600	-1.1478	0.3296
Leaf width	1.5098	0.8324	-0.0835	0.3844
Leaf thickness	-0.6657	-0.0924	1.7915	0.6025
MN16-01	0.4905	-0.0025	-0.1258	0.1027
MN16-03	0.2099	-0.2602	-0.0596	0.0085
MN16-05	0.4554	0.4037	-0.0199	0.0027
MN16-06	0.6088	0.0155	0.1076	-0.0370
MN16-10	0.2675	-0.0859	-0.0496	0.0701
MN16-11	0.1863	-0.1528	0.0316	0.1361
MN16-13	-0.1707	0.1640	-0.2107	0.0135
MN16-14	-0.2699	0.1303	0.0117	-0.0996
MN16-15	-0.3015	0.2996	-0.0674	-0.0163
MN16-16	0.1595	-0.0073	0.0091	-0.0813
MN16-17	-0.1788	0.0334	0.0413	0.0349
MN16-18	-0.3330	0.2541	-0.0493	0.0248
MN16-19	0.0108	0.1866	0.0216	0.0219
MN16-20	0.6166	0.4184	-0.4451	0.4092
MN16-21	0.2088	-0.1759	-0.0045	0.0651
MN16-22	-0.2236	0.0467	0.1569	-0.0335
MN16-23	-0.6190	-0.0371	1.4027	0.2150
MN16-24	0.2743	0.2615	0.1512	-0.0163
MN16-26	-0.5310	-0.0598	0.0608	0.0777
MN16-27	-0.1122	-0.2602	0.1410	-0.1412
MN16-28	-0.3259	0.0159	0.1164	-0.0066
MN16-31	0.3898	0.1927	0.0051	0.1732

MN16-32	0.0245	-0.0149	0.0317	0.0053
MN16-33	-0.2980	-0.0666	0.0335	0.1070
MN16-35	-0.0259	-0.0949	0.1360	-0.0243
MN16-36	0.3887	0.0283	-0.0019	-0.0694
MN16-39	0.0079	-0.0478	0.0894	-0.0680
MN17-07	-0.2430	-0.1949	0.0688	-0.0726
MN17-08	-0.0293	-0.1251	-0.0712	0.0100
MN17-28	-0.2077	-0.1039	-0.2197	0.1023
MN17-59	0.4180	-0.1395	-0.0882	-0.2178
MAT	-0.4368	0.1980	0.0473	0.1213
MDiR	0.0278	0.2236	0.0137	0.1545
Isoth	-0.2535	0.3253	-0.0222	-0.0716
Tseason	0.2940	-0.2030	0.0006	0.1075
Trange	0.2835	-0.1264	0.0040	0.1469
MTWeQ	-0.3007	0.1461	0.0729	0.1675
MTDrQ	-0.2178	0.1975	-0.0100	0.2257
MTWaQ	-0.4597	0.1643	0.0766	0.3155
MTCoQ	-0.3873	0.2077	0.0280	0.0408
MAP	-0.0821	0.2810	0.1616	0.3348
Pseason	-0.4547	-0.0666	-0.1408	-0.2155
PWeQ	-0.3199	0.1295	0.0605	0.0501
PDrQ	0.2294	0.3317	0.2766	0.4597
PWaQ	-0.3006	0.1552	0.0868	0.0871
PCoQ	0.2780	0.3457	0.1598	0.4741

B.13 CCA scores (un-averaged) for only *Metasequoia glyptostroboides* used in Ng & Smith (2020).

	Axis 1	Axis 2	Axis 3	Axis 4
Cross-sectional area	-0.71555	-0.59191	-1.13316	-1.2013
Vascular bundle area	2.20954	-1.64386	0.754926	-0.38581
Resin canal area	0.78917	2.12203	0.42994	-1.08877
Leaf width	-0.85954	-0.15473	1.06621	0.414917
Leaf thickness	0.430989	0.338279	-1.10684	1.4531
16-02	-0.155	0.016628	-0.00366	0.226909
16-04	-0.2517	-0.12753	0.065456	0.174887
16-07	-0.32905	-0.45872	0.530335	-0.07984
17-11	-0.48624	0.02505	0.519151	0.00449
17-11	-0.26405	0.22224	0.176844	0.124762
17-11	-0.412	0.291914	0.506765	-0.01978
17-11	-0.56114	0.012424	0.628063	0.021926
17-11	-0.42174	0.158553	0.379766	0.085014
17-11	-0.12281	0.047964	0.139085	0.176241
17-11	-0.26783	0.109631	0.257414	0.117865
17-12	0.100546	0.321999	-0.24414	-0.06545
17-12	0.036077	0.133877	-0.4482	0.140209
17-12	0.09297	0.312214	-0.4509	0.073495
17-12	0.16167	0.514123	-0.31867	-0.01693
17-12	0.093309	0.298706	-0.45554	0.138313
17-12	0.22606	0.583739	-0.32028	-0.01503
17-13	0.276634	-0.25943	0.016276	0.037136
17-13	0.041285	-0.03564	0.074221	0.012947
17-13	-0.12201	-0.06598	0.080243	0.053855
17-13	0.014864	-0.00315	0.174916	0.047753
17-13	-0.19976	0.014653	0.275916	-0.00456
17-13	-0.15805	0.065645	0.331191	0.126742
17-13	-0.07676	0.023403	0.050956	0.095509
17-13	-0.24631	-0.12789	0.174507	0.08833
17-13	-0.13155	0.235576	0.161945	-0.13175
17-14	0.121279	0.104822	0.045434	-0.05773
17-14	0.072797	0.109997	-0.04096	-0.09095
17-14	-0.00324	0.109562	0.060118	-0.04125
17-14	-0.05716	-0.01903	0.005978	0.064021
17-14	-0.05966	0.028035	-0.00597	0.001236
17-14	0.022281	0.211279	0.140018	0.007607
17-14	-0.14233	-0.00948	0.227037	0.06127
17-15	0.342338	-0.19799	0.134657	0.150812
17-15	0.275065	-0.01273	0.219421	0.048376

17-15	0.2829	-0.21263	0.337534	0.173428
17-15	0.037295	0.102451	0.120705	0.0591
17-15	0.064959	0.397784	0.245859	-0.10755
17-15	0.039162	0.289457	0.231283	-0.0753
17-15	0.482281	-0.29776	0.155347	0.125564
17-15	0.17493	-0.20105	0.674146	0.191388
17-15	0.056028	-0.2598	0.274798	0.093574
17-16	-0.11091	0.302723	0.385307	0.146409
17-16	-0.34099	0.176048	0.531769	-0.02317
17-16	-0.11873	0.027087	0.121952	0.059922
17-16	-0.16246	0.03182	0.082243	0.050623
17-16	-0.04867	0.298786	0.188507	-0.01409
17-16	0.068713	-0.13622	0.128691	0.201861
17-16	-0.08822	0.086779	0.159892	0.047078
17-16	-0.04179	0.179474	0.032965	0.13247
17-17	0.124712	0.118793	-0.07883	-0.02246
17-17	0.043224	0.072113	0.013931	-0.08087
17-17	0.016025	0.240362	-0.1084	-0.01918
17-17	0.174031	-0.06906	-0.09013	0.132537
17-17	0.36606	-0.25139	-0.1803	0.249
17-17	0.168261	0.259606	0.004879	-0.11142
17-17	-0.02836	0.106683	0.082926	-0.03263
17-17	-0.25084	-0.24407	0.254513	0.026186
17-17	-0.15582	-0.11576	0.096286	0.019551
17-18	0.106677	-0.06238	-0.02523	0.033227
17-18	0.052985	-0.02178	0.036138	0.000295
17-18	0.138076	0.351323	0.074682	-0.18949
17-18	0.401623	0.200214	-0.16705	-0.09048
17-18	0.31794	0.004836	-0.13851	-0.04587
17-18	0.336101	0.356178	-0.16235	-0.18661
17-18	0.578413	0.074805	-0.0301	-0.14898
17-18	0.495946	-0.13608	-0.1871	0.045791
17-18	0.477347	-0.05462	-0.12343	0.02118
17-19	0.331226	-0.27996	-0.01566	0.035426
17-19	0.236126	-0.24992	-0.1028	0.151307
17-19	0.269343	-0.14708	-0.0227	0.108565
17-19	0.280348	-0.2515	-0.12948	0.141
17-19	0.085407	-0.08541	-0.11882	0.112132
17-19	-0.2114	-0.13237	-0.04738	0.162071
17-19	0.164594	-0.0234	0.032842	0.350396
17-20	0.453769	-0.43675	-0.01889	0.16994
17-20	0.449984	-0.13774	0.031738	0.021095
17-20	0.277223	-0.38356	-0.00311	0.101422
17-20	0.177856	-0.26942	-0.01283	0.164747
17-20	0.348976	-0.35229	0.022151	0.071735

17-20	0.161774	-0.12429	0.037699	0.029625
17-21	0.30571	-0.21146	0.288088	0.119613
17-21	0.111822	0.037814	0.250764	0.042665
17-21	-0.14896	-0.04904	0.354811	0.050393
17-21	0.302229	-0.14978	-0.09041	0.175351
17-21	0.341508	0.255974	0.106929	-0.06385
17-21	0.113394	0.207132	0.150217	0.119019
17-21	-0.11563	-0.12069	0.150802	0.256452
17-21	-0.26378	-0.22538	0.324467	0.222842
17-21	-0.22287	-0.14149	0.233185	0.186322
17-22	0.114074	0.003325	0.237367	-0.02742
17-22	0.174731	0.189291	0.286321	-0.08862
17-22	-0.04714	0.121087	0.170326	-0.00623
17-22	0.021385	-0.265	0.187115	0.120619
17-22	-0.01699	-0.24509	0.151946	0.168667
17-24	0.691791	-0.29635	0.047241	0.081091
17-24	0.381179	-0.33931	0.080742	0.164156
17-24	0.633065	-0.36635	-0.03885	0.258788
17-24	0.275649	-0.27391	0.000623	0.232546
17-24	0.430046	0.505883	0.279191	-0.30656
17-24	0.120056	-0.0837	0.049591	0.102893
17-24	-0.13122	-0.35816	0.105848	0.108852
17-24	1.02164	0.198282	-0.1712	0.22015
17-25	0.17638	-0.1542	0.069867	-0.0909
17-25	0.271891	0.013577	0.067554	-0.14056
17-25	0.132999	-0.26436	0.08673	-0.07864
17-25	0.297098	-0.01252	-0.12603	0.076704
17-25	0.292852	0.253708	-0.05872	-0.06682
17-25	0.07473	0.132457	0.078486	-0.03094
17-25	0.17059	0.043469	0.027519	-0.12469
17-25	0.239787	0.304685	0.07362	-0.19426
17-25	0.082127	-0.1157	0.084161	-0.08234
17-26	0.333428	0.493557	-0.1526	0.101045
17-26	0.223524	0.370816	-0.02409	0.140172
17-26	0.340007	0.359006	-0.26786	0.084077
17-26	-0.09982	-0.05676	0.130605	0.159831
17-26	-0.17673	-0.05255	0.234831	0.082958
17-26	-0.32052	-0.10285	0.157228	0.205164
17-31	-0.40686	-0.26479	0.017837	0.103851
17-31	-0.30406	-0.16885	-0.0083	0.062014
17-31	-0.50227	-0.26601	0.303815	0.069194
17-31	-0.26803	-0.32782	0.137988	0.01664
17-31	-0.20593	-0.18081	0.180608	-0.06512
17-32	-0.03886	-0.2327	-0.05625	0.067344
17-32	-0.16519	0.036297	0.1115	0.011002

17-32	-0.15527	-0.11966	0.013243	0.03671
17-32	-0.22786	0.005253	0.008436	0.096368
17-32	-0.11726	-0.07786	0.084208	-0.0477
17-32	-0.09079	-0.08295	-0.04551	0.025258
17-32	-0.1512	-0.07508	0.012105	-0.06869
17-33	-0.24722	-0.09845	0.158655	-0.03765
17-33	-0.33739	-0.18772	0.152964	0.004885
17-33	-0.30075	-0.20757	0.213462	-0.0062
17-33	-0.15119	0.138704	0.233354	-0.0958
17-33	-0.25748	-0.00262	0.179456	-0.05309
17-33	-0.31724	-0.02176	0.191192	-0.00979
17-33	-0.43472	-0.11826	0.142479	0.018579
17-33	-0.44082	-0.08343	0.142183	0.055934
17-33	-0.34431	-0.10251	0.164407	-0.01207
17-34	-0.33612	-0.1754	-0.05892	0.130393
17-34	-0.35518	-0.21025	-0.11308	0.008023
17-34	-0.26118	-0.04219	-0.03529	0.005625
17-34	-0.24025	-0.08221	-0.1469	0.237392
17-34	-0.28533	-0.12814	-0.10425	0.195709
17-34	-0.23596	-0.07865	-0.13242	0.196758
17-34	-0.31604	-0.11366	0.020649	0.044166
17-34	-0.35121	-0.2246	-0.03503	0.075642
17-34	-0.36283	-0.25516	-0.01723	0.058314
17-35	-0.16919	-0.14603	-0.06069	0.114866
17-35	-0.157	-0.13895	-0.12144	0.155047
17-35	-0.10885	-0.15288	-0.10141	0.182976
17-35	-0.11565	-0.16465	-0.06848	0.006969
17-35	-0.19396	-0.13443	-0.11547	0.008467
17-35	-0.04894	-0.03582	-0.08077	-0.02448
17-35	-0.0801	0.051	-0.08597	-0.02279
17-36	-0.19204	-0.07658	-0.04601	-0.02882
17-36	-0.20317	-0.06623	0.040965	-0.01193
17-36	-0.23397	-0.00847	-0.06509	-0.01175
17-36	-0.16985	-0.0414	-0.06926	-0.04564
17-36	-0.15697	-0.09488	-0.09371	-0.00402
17-36	-0.24396	-0.13247	0.006744	-0.00094
17-36	-0.11262	-0.07749	0.133285	-0.07436
17-36	-0.27691	-0.1909	0.11844	0.008715
17-36	-0.29208	-0.18773	0.071828	-0.02838
17-36	-0.16115	0.006161	-0.00259	-0.11732
17-36	-0.16548	0.046183	0.015412	-0.081
17-36	-0.26016	-0.08182	0.032403	-0.06365
17-37	0.143876	-0.08358	-0.14996	-0.09589
17-37	0.28005	0.099097	-0.2388	-0.00134
17-37	0.201513	0.04089	-0.12096	-0.12755

17-37	-0.11274	-0.161	-0.01524	0.045265
17-37	-0.10206	-0.01103	0.097252	-0.0314
17-37	-0.17044	-0.07086	-0.08997	-0.02984
17-37	0.012783	-0.1507	-0.02768	-0.07157
17-37	-0.05324	-0.13148	0.008979	-0.07157
17-38	-0.19818	-0.02739	0.103817	0.035502
17-38	-0.20329	0.092555	0.185069	-0.00436
17-38	-0.25951	-0.01101	0.118915	-0.0117
17-38	-0.17593	-0.10796	0.157939	0.083485
17-38	-0.27807	-0.21681	0.318714	0.159981
17-38	-0.27431	0.025327	0.088879	0.011609
17-38	-0.15742	-0.01673	0.08196	0.015145
17-38	-0.16163	0.089965	0.124683	-0.01381
17-38	-0.28692	-0.05006	0.126159	0.119336
17-39	0.145072	-0.15983	0.008173	-0.06687
17-39	0.070537	-0.07831	-0.0172	-0.01878
17-39	0.118407	0.099202	0.008823	-0.11718
17-39	0.128832	0.051277	-0.08109	-0.05923
17-39	0.09964	0.140227	-0.07074	-0.0576
17-39	0.107586	0.287795	-0.13012	-0.09768
17-39	0.091258	-0.11012	-0.07239	-0.03136
17-39	0.037088	0.06357	-0.11095	-0.06979
17-39	-0.0142	-0.12409	-0.09835	0.028436
17-40	0.323595	0.037897	-0.12521	-0.05522
17-40	0.130112	-0.36245	0.13678	-0.06722
17-40	0.228028	0.072984	-0.33303	-0.0303
17-40	0.19776	0.044535	-0.10977	-0.02751
17-40	0.17587	0.089918	-0.13878	-0.03485
17-40	0.10222	0.008742	-0.19592	-0.01158
17-40	0.257224	0.046542	-0.20491	-0.03595
17-40	0.091133	0.077784	-0.2045	-0.03574
17-40	-0.06275	-0.12053	-0.1567	-0.05752
17-41	-0.15376	0.063985	-0.00513	0.051947
17-41	-0.09654	0.043012	0.008072	0.082983
17-41	-0.13911	0.148028	-0.0167	-0.00593
17-41	-0.1081	-0.03014	-0.04127	0.133854
17-41	0.070171	0.148594	-0.03667	0.013059
17-41	-0.11697	0.060375	-0.06387	0.091458
17-41	-0.05908	0.201388	0.016327	-0.04923
17-41	-0.11187	0.006246	0.015205	0.082826
17-41	-0.1424	0.089404	-0.00194	0.039117
17-41	-0.07812	0.068596	-0.04047	0.050115
17-42	-0.28075	0.02486	0.073157	0.179427
17-42	-0.09738	0.058505	-0.00534	0.089146
17-42	-0.35901	-0.09968	0.066783	0.192394

17-43	-0.10328	-0.14454	-0.0584	-0.044
17-43	0.11756	0.255417	-0.20081	-0.00963
17-43	-0.18584	-0.05812	-0.11398	-0.00812
17-43	-0.19639	-0.27799	-0.07453	-0.03568
17-43	-0.25906	-0.17275	0.000268	-0.09314
17-43	-0.15643	-0.11295	-0.02923	-0.06131
17-44	-0.25534	0.076105	0.039976	0.093784
17-44	-0.11745	0.11333	-0.00579	0.019356
17-44	-0.08098	0.156211	-0.03851	-0.00444
17-44	-0.20912	-0.09012	-0.0482	0.150702
17-44	-0.12822	0.011585	0.013277	0.049117
17-44	-0.11846	0.290872	0.0501	-0.0619
17-44	-0.27433	-0.17338	-0.07823	-0.00435
17-44	-0.33127	-0.31083	0.051842	0.050828
17-44	-0.27487	-0.04071	0.049501	0.00185
17-46	0.173435	0.307096	0.045236	-0.11819
17-46	0.067814	0.163712	0.05887	-0.05579
17-46	0.057899	0.236047	0.014111	-0.05117
17-46	0.085103	0.504898	0.12991	-0.24774
17-46	-0.02096	0.097041	0.083906	-0.10234
17-46	0.063436	0.37581	-0.00958	-0.15061
17-47	-0.0952	-0.0189	0.054061	0.041661
17-47	0.041819	-0.04262	0.113569	-0.02849
17-47	-0.00617	-0.00506	0.059994	-0.00264
17-47	0.011528	-0.12293	0.071621	0.048814
17-47	-0.0229	-0.02915	0.067844	0.03298
17-47	0.065263	0.018403	0.057497	-0.00901
17-47	-0.06106	0.209	0.073544	0.003474
17-47	0.087668	0.481807	0.052338	-0.07181
17-47	-0.05965	0.255775	0.091491	-0.03316
17-48	0.176596	0.220786	-0.10778	-0.02932
17-48	0.09185	0.008366	-0.05582	0.001556
17-48	0.091915	0.163833	-0.05091	-0.0835
17-48	0.176947	-0.12402	-0.02664	-0.02042
17-48	0.095596	0.022119	-0.08391	-0.04684
17-48	0.162532	0.117563	-0.04136	-0.05357
17-48	0.191553	0.169142	-0.13495	-0.05818
17-48	0.107426	0.216518	-0.10472	-0.0658
17-48	0.034165	0.061497	-0.13104	-0.07213
17-49	-0.25812	-0.16825	-0.13091	0.05913
17-49	-0.18287	-0.09581	-0.21423	-0.01988
17-49	-0.09692	-0.07033	-0.03165	-0.04198
17-49	-0.14528	-0.14909	-0.1574	-0.05916
17-49	-0.06462	-0.06139	-0.11916	-0.06123
17-49	-0.04274	-0.03199	-0.1479	-0.05166

17-50	-0.05972	0.045191	-0.02739	-0.02944
17-50	-0.04176	0.00048	0.028411	0.037704
17-50	-0.15917	-0.05663	0.021915	0.002634
17-50	-0.14944	-0.02924	-0.01004	0.114782
17-50	-0.02175	0.125222	-0.00673	-0.00953
17-50	-0.22785	-0.09699	0.038131	-0.04443
17-50	-0.11475	0.064729	-0.00791	-0.06569
17-50	-0.11083	-0.14208	-0.04031	0.04181
17-51	0.046538	0.256619	-0.05647	-0.00271
17-51	-0.04542	0.263622	-0.04467	-0.00367
17-51	-0.04718	0.279777	-0.04017	0.02259
17-51	0.059125	0.153988	0.006592	-0.11676
17-51	0.079867	0.098436	0.002505	-0.11296
17-51	0.146043	0.178467	-0.02009	-0.11771
17-51	0.077099	0.122733	0.02754	-0.118
17-51	-0.11214	-0.02069	-0.06504	0.030475
17-51	0.022847	0.204378	-0.01142	-0.10497
17-52	-0.23495	-0.14689	0.232244	0.025928
17-52	-0.28923	-0.14606	0.344061	0.039345
17-52	-0.24996	-0.05192	0.391514	0.01021
17-52	-0.11622	-0.01446	0.117335	-0.11396
17-52	-0.07357	0.141593	0.020056	-0.07952
17-52	0.14679	0.325575	-0.02229	-0.18026
17-52	-0.17885	-0.00844	-0.00462	-0.00775
17-52	-0.2055	0.016401	-0.02672	-0.02869
17-53	-0.00457	0.0204	-0.01684	0.02787
17-53	0.048796	0.31858	0.016197	-0.0995
17-53	-0.12275	0.029188	0.015729	0.083525
17-53	0.197021	0.375633	-0.0679	0.045607
17-53	0.10967	0.397365	-0.06598	0.024426
17-53	-0.14372	-0.11031	-0.08164	0.054532
17-53	-0.01178	0.139105	-0.11702	0.108416
17-53	-0.07563	0.039626	-0.09668	0.036738
17-54	-0.47975	-0.24409	0.109648	0.099876
17-54	-0.55327	-0.22536	0.257358	0.055981
17-54	-0.23072	0.125692	0.16279	-0.03871
17-54	-0.19855	0.00071	0.161415	-0.07776
17-54	-0.2676	0.036425	0.192018	-0.08576
17-55	-0.17821	-0.14659	0.080384	0.013775
17-55	-0.08838	-0.06475	0.043312	-0.03144
17-55	-0.27152	-0.14089	0.199516	-0.06451
17-55	-0.33174	-0.08331	0.298194	-0.17328
17-55	-0.04133	0.008859	0.041266	-0.07006
17-55	-0.1751	-0.20233	0.099854	-0.03321
17-55	-0.17616	-0.00604	0.136524	-0.05328

17-55	-0.31999	-0.1002	0.135283	-0.03155
17-55	-0.40486	-0.17812	0.103717	-0.01097
17-55	-0.26616	-0.03754	-0.06635	0.184055
17-56	0.174407	0.18254	-0.00723	-0.05737
17-56	0.072277	0.138601	-0.10168	0.007251
17-56	0.007118	0.036364	-0.08218	0.085008
17-56	0.082465	0.018542	-0.08574	0.020869
17-56	0.104496	0.161304	-0.0543	-0.01386
17-56	0.086445	0.263826	-0.02723	-0.06597
17-56	-0.1317	0.051037	-0.04906	0.013894
17-56	-0.10942	0.214238	-0.00507	0.037033
17-57	-0.01907	-0.05169	0.138473	0.036481
17-57	-0.01681	-0.11228	0.046087	0.137694
17-57	0.074569	0.24807	0.090957	-0.03739
17-57	-0.03826	0.0797	0.154374	0.032744
17-57	0.04178	0.145833	0.189441	0.026767
17-57	0.060479	0.280749	0.042843	0.056498
17-57	0.212172	0.292032	0.157336	0.052995
17-57	0.096823	0.059234	-0.04452	0.213393
17-57	0.056202	0.04857	0.069343	0.163887
17-58	0.058044	0.219589	0.086668	-0.05864
17-58	-0.07827	0.095539	0.011317	-0.00108
17-58	-0.03571	0.190386	0.052633	0.005119
17-58	-0.06584	0.03337	0.090638	-0.03531
17-58	-0.05438	0.111422	0.049576	0.033708
17-58	-0.14309	0.047607	0.009786	0.036851
17-58	0.014055	0.079094	0.008503	0.037339
17-58	-0.15784	-0.03417	0.115557	0.076351
17-58	-0.16533	-0.1112	0.173049	0.111771
17-61	0.059916	-0.01165	-0.00639	-0.13077
17-61	0.015767	-0.12982	-0.08636	-0.01326
17-61	0.061851	0.149119	0.00538	-0.17681
17-61	0.152314	-0.06365	-0.09369	-0.1162
17-61	0.094968	-0.17512	-0.05643	-0.0856
17-61	-0.17432	-0.19285	-0.01946	0.054746
17-61	-0.20954	-0.21919	-0.03916	0.073212
17-61	0.041738	-0.25739	-0.16002	0.072109
17-62	0.406547	-0.05621	-0.12966	-0.10142
17-62	0.234396	-0.02715	-0.0188	-0.0913
17-62	0.311459	0.11401	-0.07258	-0.09938
17-62	0.253723	-0.20065	-0.06131	-0.06176
17-62	0.129719	-0.23422	-0.08075	0.034803
17-62	0.118215	-0.1446	-0.18456	-0.0056
17-62	0.194071	-0.27185	-0.10366	-0.05933
17-62	0.213903	-0.30541	-0.0874	-0.05418

17-62	0.162111	-0.25646	-0.14267	-0.03862
17-63	-0.13174	-0.01313	0.11594	0.145845
17-63	-0.20787	-0.02806	0.10651	0.158728
17-63	-0.16963	-0.04234	0.074301	0.217472
17-63	-0.01881	-0.01193	0.095126	0.004621
17-63	-0.06835	0.261549	0.085827	-0.01347
17-63	-0.07483	-0.14773	0.130911	-0.0511
17-63	-0.08493	-0.00332	0.077466	-0.00293
17-63	-0.01234	0.139033	0.131373	-0.04419
17-64	-0.04246	-0.22157	0.121615	0.031543
17-64	-0.06609	-0.24334	0.024298	0.075287
17-64	-0.07482	-0.24863	0.031859	0.017386
17-64	0.345536	-0.34361	0.341258	-0.00909
17-64	-0.05327	0.0341	0.174365	0.055994
17-64	-0.21083	-0.21742	0.120232	0.210006
17-66	-0.12494	0.019827	-0.06785	0.11625
17-66	-0.07547	0.073941	-0.14176	0.113292
17-66	0.034891	0.046935	-0.07972	0.134003
17-66	0.108026	0.183436	-0.13199	0.10975
17-66	0.101309	0.199035	-0.04223	-0.00446
17-66	0.230492	0.07533	-0.2653	0.094188
17-66	0.009045	0.164689	-0.08169	0.073586
17-67	0.060463	-0.27106	0.114175	-0.02486
17-67	0.095042	-0.15529	0.139096	-0.08516
17-67	0.009372	-0.25339	0.101316	-0.02979
17-67	0.043378	0.080203	0.125747	0.002329
17-67	0.010684	-0.45234	0.160262	0.107874
17-67	-0.01962	-0.17364	0.105241	0.028623
17-67	-0.10616	-0.2272	0.213586	0.011622
17-67	0.058689	0.06105	0.185775	-0.0884
17-67	0.049381	-0.12285	0.071168	-0.02035
17-67	-0.01395	-0.15394	0.078832	0.045956
17-67	-0.11863	-0.24567	0.188801	0.01895
17-68	0.200974	-0.18428	0.185985	-0.0368
17-68	0.170746	-0.16332	0.166278	-0.04832
17-68	0.254164	0.070283	0.186454	-0.11512
17-68	0.202596	-0.14673	0.139468	0.02144
17-68	0.08512	-0.13675	0.081606	0.058495
17-68	0.161814	-0.22339	0.113344	0.010309
17-68	0.128343	-0.0879	0.12401	-0.00112
17-71	-0.01154	-0.03659	-0.03592	0.038312
17-71	-0.10538	0.132143	0.113801	0.038468
17-71	-0.01553	0.318918	0.096893	0.000501
17-71	-0.1114	-0.13867	0.319916	-0.04958
17-71	0.195969	0.444058	0.151724	-0.11007

17-71	-0.15598	0.14655	0.15878	0.087577
17-71	0.052695	0.347832	0.144573	-0.12217
17-72	-0.03158	-0.03018	0.047623	0.014621
17-72	-0.17884	-0.00904	0.028642	0.078505
17-72	-0.0348	0.424968	0.168573	-0.13252
17-72	-0.03735	0.058747	0.219002	-0.0134
17-72	-0.02329	0.187704	0.279122	-0.09297
17-72	-0.04523	0.220572	0.257779	-0.06528
17-72	-0.0106	0.043594	0.076054	0.046934
17-72	0.304955	0.185374	-0.27254	-0.02141
17-73	-0.23189	-0.00969	-0.00613	0.005161
17-73	-0.01844	0.313412	-0.00558	-0.06858
17-73	0.082581	0.36236	-0.00164	-0.17367
17-73	0.026625	0.154856	-0.00602	-0.10443
17-73	-0.0858	-0.08924	-0.03137	-0.07863
17-73	0.014005	0.13723	0.039133	-0.20067
17-73	0.119858	-0.11271	-0.05582	-0.03062
17-73	-0.09423	0.137424	-0.06565	-0.06883
17-73	0.026513	-0.01658	-0.1117	0.012108
17-74	-0.05411	-0.00444	-0.04081	0.082066
17-74	-0.04127	0.004498	0.014645	-0.00322
17-74	-0.26183	-0.02556	0.063721	0.090289
17-74	-0.14217	0.324415	0.126398	-0.01557
17-74	-0.16232	0.307961	0.1177	-0.00099
17-74	-0.13332	-0.00156	0.046166	0.095532
17-74	-0.08305	0.045559	-0.1012	0.133596
17-74	-0.13109	-0.05793	0.013364	0.150771
17-75	0.001169	-0.09026	-0.13711	0.080468
17-75	0.008525	-0.14352	-0.14857	0.070164
17-75	-0.00462	0.059146	-0.14472	0.049116
17-75	0.035639	0.052075	0.033068	-0.09981
17-75	-0.00403	0.020439	0.029863	-0.11995
17-75	0.019083	-0.03827	-0.07027	-0.00335
17-76	-0.09808	-0.1835	-0.05736	0.033332
17-76	-0.1115	-0.18769	-0.08555	0.058395
17-76	-0.07179	-0.18713	-0.07451	-0.0017
17-76	0.045999	0.067491	-0.29183	0.115277
17-76	0.057999	0.047474	-0.19145	0.050671
17-76	-0.1165	0.09826	-0.19484	0.115601
17-77	0.220911	-0.06597	-0.13752	-0.02162
17-77	0.036929	0.041121	-0.04691	-0.0515
17-77	0.1576	0.067104	-0.06931	-0.12776
17-77	-0.04818	-0.13782	-0.13534	0.050172
17-77	-0.02088	0.007834	0.132408	-0.00284
17-77	-0.13976	-0.16291	-0.12601	0.120257

17-77	-0.11374	-0.0128	0.049706	-0.00095
17-77	0.01853	0.056311	-0.00956	-0.02919
17-77	0.224498	0.187597	0.077641	-0.20297
17-77	-0.02925	-0.07021	0.013937	-0.00437
17-78	0.053138	0.041206	-0.1172	0.082897
17-78	0.035259	0.271463	-0.05236	0.01451
17-78	0.161248	0.178822	-0.08036	0.016934
17-78	0.038424	0.181752	0.004846	0.033292
17-78	-0.04355	-0.06965	-0.04461	0.158572
17-78	-0.00833	0.03068	-0.05251	0.105373
17-78	-0.10823	0.105645	-0.13171	0.149527
17-78	0.003271	0.040261	-0.11988	0.116379
17-78	0.158663	0.066746	-0.07833	0.017631
17-80	-0.04398	0.007963	0.050012	-0.00815
17-80	-0.15788	-0.18116	0.030503	0.058965
17-80	-0.15128	-0.06304	-0.00628	0.189506
17-80	-0.04465	-0.04032	0.070482	0.032074
17-80	-0.09453	-0.07346	0.106961	0.03214
17-80	-0.09485	-0.15925	0.041634	0.008196
17-80	-0.03204	0.026972	-0.05884	0.012233
17-81	0.089498	0.030773	-0.10143	0.007091
17-81	0.118021	0.284399	-0.08718	-0.09347
17-81	-0.08776	0.031035	-0.02394	0.076688
17-81	0.016279	-0.08957	-0.10992	0.040593
17-81	0.017766	-0.01052	-0.08877	0.057838
17-81	-0.10884	-0.16143	-0.0542	0.093884
17-81	-0.15402	-0.14278	0.061245	0.108032
17-81	-0.11995	-0.11024	-0.03247	0.002974
17-81	0.216208	-0.0741	-0.08783	-0.13969
17-81	0.049518	-0.18075	-0.1366	-0.13444
17-81	0.009028	-0.16905	-0.2031	0.048351
17-81	0.050036	-0.04293	-0.08757	-0.1656
17-81	0.137425	0.192368	-0.07212	-0.21384
17-81	0.075827	0.108761	-0.07275	-0.17885
17-81	0.208652	0.023753	-0.11665	-0.16753
17-81	0.118676	-0.05665	-0.17941	-0.12991
18-04	-0.35083	-0.1959	0.047922	0.045318
18-04	-0.37898	-0.18348	0.060914	0.109239
18-04	-0.33596	-0.29066	0.111262	0.082348
18-04	-0.20665	-0.15048	-0.03099	0.116965
18-04	-0.33144	-0.10752	0.08553	0.02818
18-04	-0.01128	-0.11787	-0.30813	0.169091
18-05	-0.09687	-0.07943	-0.04018	0.078502
18-05	-0.11578	-0.10332	-0.06694	0.052827
18-05	0.040692	0.218526	-0.11352	-0.0477

18-05	-0.15986	0.038007	0.007567	-0.01542
18-05	-0.09343	0.27719	-0.02109	-0.1052
18-05	-0.11757	0.097862	-0.12489	0.020145
18-08	-0.2227	-0.08354	0.008489	-0.01134
18-08	-0.27044	-0.1831	0.077014	0.062189
18-08	-0.35403	-0.24045	0.056478	0.110023
MAT	0.211999	0.004168	0.226918	0.198343
MDiR	-0.04421	-0.06993	0.110925	0.056282
Isoth	-0.01063	0.1382	0.060119	-0.08338
Tseason	0.085637	-0.16255	0.105576	0.097867
Trange	0.064637	-0.15987	0.13449	0.111042
MTWeQ	0.13928	-0.10902	0.181112	0.180604
MTDrQ	-0.00025	-0.0498	-0.012	0.074797
MTWaQ	0.219166	-0.07745	0.224925	0.203633
MTCoQ	0.146377	0.093642	0.13421	0.121873
MAP	0.319788	-0.12083	0.157077	0.127337
Pseason	0.011429	-0.00963	0.23783	0.109302
PWeQ	0.26428	-0.06708	0.245985	0.162334
PDrQ	-0.03252	-0.06853	-0.11216	-0.09254
PWaQ	0.275296	-0.0442	0.244077	0.177479
PCoQ	-0.12824	-0.07698	-0.12424	-0.1179

APPENDIX C

Chapter 4 Supplemental Tables

C.1 Modern and paleolatitudes of early Eocene fossil localities

Site	Fm	State, Country	Lat, long	Paleo-lat, long	Ref.
Antelope Creek	Golden Valley	North Dakota, USA	46.75, -102.75	46.8, -85.75	L.J.Hickey 1977
North of Lost Bridge	Golden Valley	North Dakota, USA	47.62, -102.75	47.65, -85.51	L.J.Hickey 1977
Head of Otter Creek	Golden Valley	North Dakota, USA	47.00, -101.55	46.89, -84.5	L.J.Hickey 1977
Watercourse Valley		Canada	81.70, -64.67	75.69, -28.95	R.L.Christie 1964
Norden-skiöldfjellet and Lars Hiertafjellet	Aspelin-toppen Fm	Spitsbergen	78.08, 15.60	74.12, -3.75	Kvaček et al., 1994; Kvaček & Manum, 1997
Coral Corner		Greenland	78.83, 30.83	75.91, 6.19	Seward & Edwards, 1941; Boulter & Kvaček, 1989
Fort Conger	Iceberg Bay Fm	Ellesmere Island, Canada	81.75, 64.75	81.34, 22.86	Heer, 1878a
Mosquito Creek	Iceberg Bay Fm	Ellesmere Island, Canada	79.95, 84.72	81.93, 47.65	McIver & Basinger, 1999
Hot weather Creek	Iceberg Bay Fm	Ellesmere Island, Canada	79.93, 84.75	81.92, 47.75	McIver & Basinger, 1999
Fosheim Peninsula	Iceberg Bay Fm	Ellesmere Island, Canada	79.67, 84.30	81.66, 48.38	LePage- unpublished
Fosheim Peninsula	Iceberg Bay Fm	Ellesmere Island, Canada	79.75, 85.02	81.8, 48.77	McIver & Basinger, 1999
Oxhead Creek	Iceberg Bay Fm	Ellesmere Island, Canada	79.72, 85.08	81.78, 48.98	McIver & Basinger, 1999
Strathcona Fiord	Iceberg Bay Fm	Ellesmere Island, Canada	78.67, 82.67	80.65, 50.26	LePage- unpublished

Strathcona Fiord	Margaret Fm	Ellesmere Island, Canada	78.63, 82.88	80.65, 50.59	McIver & Basinger, 1999
Stenkul Fiord	Margaret Fm	Ellesmere Island, Canada	77.87, 81.63	79.86, 51.57	McIver & Basinger, 1999
Split Lake	Margaret Fm	Ellesmere Island, Canada	77.89, 83.60	80.07, 53.59	McIver & Basinger, 1999
Stenkul Fiord	Iceberg Bay Fm	Ellesmere Island, Canada	77.37, 83.47	79.6, 54.85	Nathorst, 1915; Sveshnikova, 1975a; LePage, unpublished
NW Slave Province		Canada	64.73, 110.59	69.78, 101.82	Wolfe, A.P. et al. (2012)
Elko station	Elko Fm	Nevada, USA	40.83, 115.77	46.23, 112.07	Lesquereux, 1873, 1874; Chaney, 1951; Wing, 1987
Quilchena near Nicola	Kamloops Group	BC, Canada	50.13, 120.52	55.71, 116.52	Penhallow, 1906, 1908; Berry, 1926a; Armentrout, 1981; Mathewes & Brooke, 1971
Clayton Bay	Chuckanut Fm	Washington, USA	48.62, 122.46	54.26, 118.85	Pabst, 1968
Pleasant Bay	Chuckanut Fm	Washington, USA	48.66, 122.49	54.3, 118.89	Pabst, 1968
Birch Bay	Whatcom County	Washington, USA	48.92, 122.73	54.57, 119.14	Newberry, 1863, 1898; Chaney, 1951
Hagimori	Okinoyama	Yamaguchi, Japan	34.00, 131.00	43.39, 128.58	K.Huzioka and E.Takahasi 1970
Hirabara	Okinoyama	Yamaguchi, Japan	34.00, 131.00	43.39, 128.58	K.Huzioka and E.Takahasi 1970
Dan	Okinoyama	Yamaguchi, Japan	34.00, 131.00	43.39, 128.58	K.Huzioka and E.Takahasi 1970
Fujimagari	Okinoyama	Yamaguchi, Japan	34.00, 131.00	43.39, 128.58	K.Huzioka and E.Takahasi 1970

Kami-Umeda	Okinoyama	Yamaguchi, Japan	34.00, 131.00	43.39, 128.58	K.Huzioka and E.Takahasi 1970
Motoyama	Okinoyama	Yamaguchi, Japan	34.00, 131.00	43.39, 128.58	K.Huzioka and E.Takahasi 1970
Okinoyama	Okinoyama	Yamaguchi, Japan	34.00, 131.00	43.39, 128.58	
Sakurayama	Okinoyama	Japan	34.00, 131.00	43.39, 128.58	K.Huzioka and E.Takahasi 1970
Kawakami coal mines	Naibuchi Fm	Sakhalin, Japan	47.22, 142.52	60.16, 130.51	Endo, 1928; Kodrul, 1999
Shimizusawa coal mine	Yubari Fm	Japan	43.33, 142.17	51.45, 142.45	Endo, 1928;Huzioka & Kobayashi, 1961
USGS Locs 5892, 9870 - 7894, 9877, 9881	Chickaloon Fm	Alaska	61.75, 149.25	67.51, 150.45	Martin & Katz, 1912; Hollick, 1936; Wolfe, 1966; Wolfe et al., 1966; Triplehorn et al.,1984
USGS Locs 11411, 11412, 11416	Tolstoi Fm	Alaska	55.83, 159.45	64.65, 154.23	Detterman et al., 1996
Chignik Bay	Tolstoi Fm	Alaska	56.30, 158.45	65.38, 154.24	Knowlton, 1896; Hollick, 1930, 1936; Wolfe et al., 1966; Detterman et al., 1996
Chignik River	Chignik Fm	Alaska	56.27, 158.70	65.25, 154.39	Hollick, 1930, 1936; Detterman et al., 1996
Pavlof Bay	Tolstoi Fm	Alaska	55.48, 161.48	63.55, 155.32	Hollick, 1930; Detterman et al., 1996
Cape Douglas	Copper Lake Fm	Alaska	58.85, 153.30	65.59, 157.85	Knowlton, 1896; Hollick, 1936; Wolfe et al., 1966; Detterman et al., 1996
Penjin Bay	undefined	Russia	63.52, 168.00	70.69, 176.14	Kryshtofovich, 1958b

C.2 Trait-climate model p-values

	All-species		*Metasequoia*-only		*Taxodium*-only		*Sequoia*-only	
Model	*W*	p-value	*W*	p-value	*W*	p-value	*W*	p-value
Cross-sectional area								
xsa_A	6450	0.748	1766	0.893	489	0.910	263	0.342
xsa_B	6506	0.834	1733	0.970	476	0.955	260	0.313
xsa_C	5751	0.088	1725	0.936	498	0.811	278	0.509
xsa_D	6163	0.374	1772	0.868	516	0.622	275	0.473
xsa_E	6249	0.472	1764	0.902	494	0.855	256	0.277
Resin canal area								
rca_A	6013	0.235	1443	0.110	453	0.704	318	0.923
rca_B	6008	0.231	1479	0.160	430	0.481	349	0.485
rca_C	4090	<0.001	1443	0.110	450	0.673	349	0.485
rca_D	6194	0.407	1476	0.155	458	0.757	336	0.655
Leaf width								
lw_A	6873	0.606	1800	0.751	502	0.768	313	1.000
lw_B	7411	0.114	1850	0.557	487	0.933	317	0.938
lw_C	6745	0.511	1841	0.590	499	0.800	317	0.938
lw_D	6904	0.564	1826	0.647	501	0.778	304	0.876
Leaf thickness								
lt_A	5877	0.145	1482	0.165	482	0.989	242	0.174
lt_B	5950	0.190	1543	0.289	480	1.000	262	0.332
lt_C	5969	0.203	1548	0.301	465	0.833	268	0.393
lt_D	5963	0.198	1521	0.238	479	0.989	267	0.382

W - Wilcoxon coefficient

C.3 Random models AIC and standard errors

	All-species		*Metasequoia*-only		*Taxodium*-only		*Sequoia*-only	
Model	SE	AIC	SE	AIC	SE	AIC	SE	AIC
Cross-sectional area								
xsa_01	0.179	3143.2	0.164	1521.9	0.537	691.1	0.177	726.8
xsa_02	0.126	3142	0.129	1523.7	0.527	691.1	0.137	725.9
xsa_03	0.084	3058.7	0.136	1518	0.298	690.0	0.138	727.7
xsa_04	0.270	3125.1	0.254	1522.1	0.649	688.4	0.609	745.7
xsa_05	0.184	3068.9	0.258	1523.3	0.759	688.9	0.352	730.7
xsa_06	0.228	3112.3	0.188	1522.3	0.587	690.3	0.464	733.4
Resin canal area								
rca_01	0.309	2096.9	0.353	931.9	0.842	463.6	0.583	498.1
rca_02	0.194	2064.4	0.255	932.0	0.781	464.4	0.381	499.4
rca_03	0.140	2019	0.282	929.3	0.381	461.7	0.414	504.2
rca_04	0.398	2045.7	0.517	932.3	0.994	464.1	2.119	513.8
rca_05	0.401	2039.2	0.502	932.7	1.021	461.7	1.354	506.9
rca_06	0.307	2028	0.380	933.1	0.877	464.1	1.657	505.0
Leaf width								
lw_01	0.073	1670	0.065	779.3	0.319	369.6	0.150	400.4
lw_02	0.064	1712.8	0.049	782.2	0.309	369.6	0.135	401.8
lw_03	0.054	1672.6	0.055	777.3	0.186	370.3	0.126	402.0
lw_04	0.122	1688.8	0.098	779.6	0.407	369.6	0.402	397.2
lw_05	0.083	1636.7	0.097	779.6	0.486	371.0	0.282	397.6
lw_06	0.110	1687.8	0.072	780.8	0.367	370.9	0.378	396.8
Leaf thickness								
lt_01	0.121	1386.8	0.147	635.2	0.291	291.9	0.176	311.0
lt_02	0.081	1364.1	0.066	635.2	0.236	291.6	0.125	327.0
lt_03	0.067	1316.5	0.218	636.8	0.368	291.7	0.721	327.6
lt_04	0.173	1366.1	0.112	624.4	0.161	290.2	0.150	319.0
lt_05	0.133	1342.7	0.211	636.8	0.416	288.5	0.358	310.8
lt_06	0.142	1351.2	0.159	637.0	0.329	292.3	0.541	314.5

SE = Std error, AIC = Akaike Information Criterion

C.4 Trait-climate models

All-species Models

xsa_A = $e^{1.450\times10^{1}+B01(3.611\times10^{-2})+B10(-7.454\times10^{-2})+B12(-2.165\times10^{-5})+B17(-4.400\times10^{-3})}$

xsa_B= $e^{14.4756483+B10(-0.0475841)+B17(-0.0051241)}$

xsa_C= $e^{13.5178705+B01(0.0080684)+B12(-0.0006887)}$

xsa_D= $e^{14.8849205+B01(0.1292771)+B10(-0.1662239)+B12(-0.0002709)}$

xsa_E= $e^{1.393\times10^{1}+B01(-3.021\times10^{-2})+B12(6.476\times10^{-5})+B17(-5.782\times10^{-3})}$

rca_A= $e^{8.162+B11(5.840\times10^{-2})+B16(1.156\times10^{-5})+B17(-7.467\times10^{-3})}$

rca_B= $e^{8.1655743+B11(0.0584665)+B17(-0.0074561)}$

rca_C= $e^{7.4948177+B11(0.0725743)+B16(-0.0002914)}$

rca_D= $e^{8.6723082+B16(0.0001176)+B17(-0.0096330)}$

lw_A= $e^{8.3289446+B01(-0.0138870)+B10(-0.0218289)+B17(-0.0019713)}$

lw_B= $e^{7.980+B01(-2.956\times10^{-2})+B12(-1.239\times10^{-4})}$

lw_C= $e^{8.146+B01(-3.424\times10^{-2})+B12(5.074\times10^{-5})+B17(-2.356\times10^{-3})}$

lw_D= $e^{8.368+B10(-3.335\times10^{-2})+B12(-1.017\times10^{-5})+B17(-1.768\times10^{-3})}$

lt_A= $e^{6.4060252+B10*-0.0275814+B11*0.0342420+B16*-0.0001306+B17*-0.0025805)}$

lt_B= $e^{6.3795960+B10(-0.0287560)+B11(0.0327842)+B17(-0.0025237)}$

lt_C= $e^{5.9335687+B11(0.0203803)+B17(-0.0031149)}$

lt_D= $e^{6.3250349+B10(-0.0116892)+B17(-0.0033925)}$

Taxodium-only Models

xsa_A= $e^{13.3267282+B01(0.0398346)+B10(-0.0483516)+B12(-0.0002770)+B17(-0.0015294)}$

xsa_B= $e^{12.7314144+B10(-0.0062653)+B17(-0.0021760)}$

xsa_C= $e^{12.2887683+B01(0.0272957)+B12(-0.0005259)}$

xsa_D= $e^{13.3329716+B01(0.0610636)+B10(-0.0630666)+B12(-0.0005355)}$

xsa_E= $e^{12.5577654+B01(0.0127902)+B12(-0.0002496)+B17(-0.0017021)}$

rca_A= $e^{8.1250677+B11(0.0617520)+B16(-0.0008965)+B17(-0.0038611)}$

rca_B= $e^{7.847091+B11(0.040978)+B17(-0.003492)}$

rca_C= $e^{7.0324594+B11(0.0909044)+B16(-0.0009309)}$

rca_D= $e^{8.3200310)+B16(0.0003178)+B17(-0.0046722)}$

lw_A= $e^{7.8035898+B01(0.0103596)+B10(-0.0394028)+B17(-0.0001592)}$

lw_B= $e^{7.1472798+B01(-0.0094326)+B12(-0.0000372)}$

lw_C= $e^{7.183+B01(-1.165\times10^{-2})+B12(1.306\times10^{-5})+B17(-2.807\times10^{-4})}$

lw_D= $e^{7.620)+B10(-2.620\times10^{-2})+B12(3.828\times10^{-5}+B17(-2.676\times10^{-4})}$

lt_A= $e^{5.1361860+B10(0.0335561)+B11(0.0061616)+B16(-0.0005470)+B17(-0.0017693)}$

lt_B= $e^{5.0075038+B10(0.0313259)+B11(-0.0034878)+B17(-0.0016371)}$

lt_C= $e^{5.7198443+B11(0.0064001)+B17(-0.0015818)}$

lt_D= $e^{5.163210+B10(0.023856)+B17(-0.001602)}$

Metasequoia-only Models

xsa_A= $e^{13.3925439+B01(-0.0447649)+B10(-0.0020985)+B12(0.0001667)+B17(-0.0005558)}$

xsa_B= $e^{13.4587267+B10(-0.0251909)+B17(-0.0003720)}$

xsa_C= $e^{1.330\times10^{1}+B01(-3.891\times10^{-2})+B12(7.699\times10^{-5})}$

xsa_D= $e^{1.328\times10^{1}+B01(-4.087\times10^{-2})+B10(1.726\times10^{-3})+B12(7.869\times10^{-5})}$

xsa_E= $e^{13.3723018+B01(-0.0466899)+B12(0.0001640)+B17(-0.0005266)}$

rca_A= $e^{7.322+B11(1.193\times10^{-2})+B16(-4.421\times10^{-4})+B17(-2.401\times10^{-5})}$

rca_B= $e^{7.1435641+B11(-0.0009469)+B17(0.0005783)}$

rca_C= $e^{7.3180945+B11(0.0117804)+B16(-0.0004369)}$

rca_D= $e^{7.2806580+B16(-0.0002894)+B17(0.0001930)}$

lw_A= $e^{7.7640790+B01(-0.0107883+B10(-0.0009917)+B17(-0.0004086)}$

lw_B= $e^{7.688+B01(-1.007\times10^{-2})+B12(-5.253\times10^{-8})}$

lw_C= $e^{7.773+B01(-1.825\times10^{-2})+B12(8.344\times10^{-5})+B17(-5.371\times10^{-4})}$

lw_D= $e^{7.803+B10(-9.087\times10^{-3})+B12(2.949\times10^{-6})+B17(-4.530\times10^{-4})}$

lt_A= $e^{5.516+B10(7.596\times10^{-3})+B11(8.206\times10^{-4})+B16(-3.144\times10^{-4}+B17*1.798\times10^{-5})}$

lt_B= $e^{5.5660746+B10(-0.0011151)+B11(-0.0051338)+B17(0.0002827)}$

lt_C= $e^{5.5425051+B11(-0.0055602)+B17(0.0003104)}$

lt_D= $e^{5.5849266+B10(-0.0025953)+B17(0.0002423)}$

Sequoia-only Models

xsa_A= $e^{13.0483049+B01(-0.0742257)+B10(0.0841257)+B12(0.0001796)+B17(-0.0064777)}$

xsa_B= $e^{13.550975+B10(0.006096)+B17(-0.003294)}$

xsa_C= $e^{13.8890574+B01(-0.0105473)+B12(-0.0001567)}$

xsa_D= $e^{13.4608921+B01(-0.1104000)+B10(0.0995626)+B12(-0.0001678)}$

xsa_E= $e^{13.1209693+B01(0.0222992)+B12(0.0004076)+B17(-0.0106096)}$

rca_A= $e^{7.940983+B11(0.035365)+B16(0.001797)+B17(-0.020016)}$

rca_B= $e^{9.136519+B11(-0.022764)+B17(-0.006880)}$

rca_C= $e^{9.4486253+B11(-0.0355578)+B16(-0.0006600)}$

rca_D= $e^{8.5655257+B16(0.0010242)+B17(-0.0147917)}$

lw_A= $e^{7.833728+B01(-0.042865)+B10(0.025880+B17*-0.000682)}$

lw_B= $e^{8.017+B01(-2.005\times10^{-2})+B12(-4.340\times10^{-5})}$

lw_C= $e^{8.010+B01(-1.975\times10^{-2})+B12(-3.807\times10^{-5})+B17(-9.786\times10^{-5})}$

lw_D= $e^{7.821+B10(-8.932\times10^{-3})+B12(9.254\times10^{-5})+B17(-2.267\times10^{-3})}$

lt_A= $e^{5.5106179+B10(0.0164021)+B11(0.0157235)+B16(0.0008757)+B17(-0.0102192)}$

lt_B= $e^{6.041416+B10(0.019058)+B11(-0.012911)+B17(-0.003554)}$

lt_C= $e^{6.214561+B11(0.005136)+B17(-0.003511)}$

lt_D= $e^{6.094960+B10(0.009111)+B17(-0.003421)}$

C.5 Wilcoxon and p-value for fossils trait estimates

	3x All-species		6x All-species		3x *Meta.*-only		6x *Meta.*-only	
Model	*W*	p-value	*W*	p-value	*W*	p-value	*W*	p-value
Cross-sectional area								
xsa_A	3050	0.005	3899	<0.001	950	0.069	1793	<0.001
xsa_B	2712	0.154	3840	<0.001	1491	0.049	1945	<0.001
xsa_C	2077	0.260	2261	0.699	928	0.049	1649	0.002
xsa_D	3569	<0.001	4021	<0.001	929	0.050	1663	0.001
xsa_E	2195	0.514	3163	0.001	938	0.057	1765	<0.001
Resin canal area								
rca_A	2918	0.024	2590	0.350	1200	0.950	1055	0.280
rca_B	2918	0.024	2585	0.361	979	0.107	942	0.061
rca_C	2669	0.211	2034	0.193	1201	0.955	1053	0.274
rca_D	2309	0.847	2866	0.041	1029	0.207	1051	0.268
Leaf width								
lw_A	2457	0.690	3842	<0.001	1127	0.565	1883	<0.001
lw_B	1594	0.002	3097	0.003	1058	0.290	1665	0.001
lw_C	1769	0.018	3446	<0.001	986	0.118	1833	<0.001
lw_D	2646	0.246	4004	<0.001	1565	0.013	2052	<0.001
Leaf thickness								
lt_A	3450	<0.001	3575	<0.001	963	0.085	734	<0.001
lt_B	3454	<0.001	3605	<0.001	909	0.036	1082	<0.001
lt_C	2838	0.0533	2610	0.310	858	0.014	994	<0.001
lt_D	2441	0.738	3326	<0.001	1074	0.344	1164	<0.001

W - Wilcoxon coefficient, *Metasequoia*-only dataset abbreviated *Meta.*-only